UNIVERSITA' DEGLI STUDI DI GENOVA

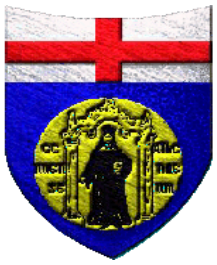

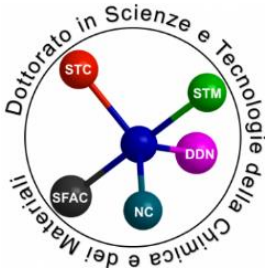

DOCTORATE SCHOOL IN SCIENCES AND TECHNOLOGIES OF CHEMISTRY AND MATERIALS

Curriculum in Pharmaceutical, Food and Cosmetic Sciences

XXXI cycle

PhD THESIS

Synthesis of properly substituted pyridine and pyrimidine derivatives and their biological evaluation as potential antiviral agents

Ilaria Giacchello

Advisor: Prof. Giancarlo Grossi

A tutti quelli che hanno creduto in me
facendo sì che a poco a poco iniziassi a farlo anche io...

TABLE OF CONTENTS

SUMMARY

Influenza A viruses (IAVs) belong to the group of (-)RNA viruses, in particular, to the *Orthomixoviridae*, that is a family of enveloped viruses with a single-stranded (ss) negative-sense (-) and eight-segmented RNA genome. They are the most prevalent pathogens for both humans and animals, causing the so-called seasonal flu, that affects every year approximately 5-10% of the adult and 20-30% of the pediatric population.

IAV virion consists of a lipid envelope out of which two glycoproteins, hemagglutinin (HA or H) and neuraminidase (NA or N), protrude. Embedded within the lipid envelope bilayer, the viral integral membrane protein M2 is present, while M1 protein forms a matrix layer underneath the envelope of the virion. Regarding the genetic material, each segment of the RNA genome is wrapped-up in multiple copies of NP and is associated with the RNA-dependent RNA polymerase, (RdRp). Each NP-encapsidated RNA segment, together with its RdRp, constitutes a viral ribonucleoprotein complex (vRNP). There are several subtypes of IAV, according to the combination of HA and NA expressed on the surface of the virus: to date, eighteen different HA subtypes and eleven different NA subtypes have been identified. Different subtypes of IAV were responsible for widespread pandemics since the 16th century: the most important have been the 1918 Spanish flu (H1N1), the 1957 Asian flu (H2N2), the 1968 Hong Kong flu (H3N2); but also, the 2009 swine-origin pandemic flu (2009 pH1N1) as well as the 1977 Russian flu (H1N1).

The process of viral infection consists of seven steps: adsorption, penetration, uncoating, transcription, translation, assembly and release. A key enzyme for all the infection process is RdRp. It is a heterotrimeric complex of about 250 kDa that is composed of three different subunits: PA (polymerase acidic protein), PB1 and PB2 (polymerase basic proteins 1 and 2). Starting from the ss(-)RNA viral genome, RdRp is responsible for the synthesis of the positive-strand messenger (mRNA), used for viral protein production, and for the synthesis of complementary RNA (cRNA), useful to obtain new viral genome. In particular, the catalytic site is in PB1; PB2 includes the capped-RNA recognition domain, that is necessary for the generation of the primer for the transcription, while PA is responsible for “cap-snatching”, the cleavage of host cell pre-mRNA to utilize its cap for viral generation of the primer for the transcription, and it is also important in the complex assembly.

Vaccination is regarded as the major prophylactic and therapeutic treatment of influenza infections, although the genetic drift in viral genome make it necessary to formulate new vaccines each year and the highly variable nature of the surface glycoproteins HA and NA does not make possible the development of a universal influenza vaccine. A part from the use of vaccines, viral infections can be inhibited at several crucial steps by the use of antiviral agents. It is possible to have an antiviral effect both targeting important proteins for the virus life cycle and targeting host proteins that play crucial roles during influenza virus infection.

Playing a critical role during the life cycle of the virus, RdRp has become a promising target for the development of anti-influenza drugs in recent years. Based on the mechanism of the interactions between inhibitor and polymerase, compounds targeting RdRp can be subdivided into four subtypes: PA endonuclease inhibitors, PB1 inhibitors, PB2 cab-binding (PB2-CBD) inhibitors and RdRp disrupting compounds.

Among these four classes of antiviral compounds, the latest seems to be one of the more promising. These compounds are called protein-protein interaction inhibitors (PPI inhibitors) because of their interference or inhibition of the protein-protein interaction in the RdRp assembly. Among the interactions between the three different subunits of the RdRp, the PA-PB1 is probably the most interesting one for the development of new inhibitors. This interaction has been characterized and is known to occur between the C-terminal region of PA (PA-C) and the N-terminal region of PB1 (PB1-N). The interaction between PA-C and PB1-N is an innovative promising target because it has a high degree of conservation among virus strains that suggests that its inhibitors may be active against many viral subtypes and less prone to drug-resistance. Moreover, this interaction involves few amino acids and so it could be inhibited by small molecules. My research doctorate activity was focused on the synthesis and biological evaluation of novel anti-influenza agents acting as PPI inhibitors, in particular, disrupting the PA-PB1 interaction.

From a high-throughput docking approach used to screen the Asinex database (703,200 molecules), compounds possessing a 4,6-diphenyl-3-cyanopyridinic nucleus were identified as weak inhibitors of the PA-PB1 interaction. Moreover, for a better understanding of the underlying SAR, a series of 4,6-diphenyl-3-cyanopyridine derivatives was synthesized, by performing modification or replacement of molecule portions. Starting from these studies, I decided to synthesize a library of molecules characterized by a hybrid structure constituted by the promising 3-cyano-4,6-diphenylpyridinic core together with an aminoacidic side chain in

C2 (**CHAPTER 4.**, **Paragraph 4.2.**). With the aim to enhance the ability of 3-cyano-diphenylpyridine compounds to completely displace PB1 and increase their affinity toward the target protein PA, I decided to synthesize at first hybrid derivatives combining the cyanopyridine core linked to the last three amino acids of PB1-N (Met-Asp-Val), then to explore better the C2 side chain introducing in this position different L- or D-amino acids as methyl or benzyl esters. The synthesis of these compounds allowed to explore the potential antiviral activity of this new class of hybrid derivatives and to do SAR evaluations. Moreover, some derivatives showed a promising antiviral activity acting as IAV RdRp PPI inhibitors. Since SAR and molecular dynamic simulation studies seem to show that the cyano group is not essential for the antiviral activity, and considering that it is often related to potential cytotoxicity, it was decided to remove the CN group in C3 position of the pyridine core and to include the nitrogen atom in the ring. Following a rational design process, I synthesized a library of phenyl pyrimidine derivatives, maintaining in C2 the 2-mercapto-*N*-(*m*-tolyl)acetamide chain that was present in the promising compound identified in the previous screening study, and I explored the effect of different aromatic substituents in C4 and C6 of the pyrimidine ring (**CHAPTER 4.**, **Paragraph 4.3.**). This new synthesized library of pyrimidine compounds allowed to extend SAR evaluations and to get further insights into this new promising class of antiviral molecules, exploring the effect of different aromatic substituents in C4 and C6 positions of the pyrimidine core. Moreover, it was possible to find promising IAV RdRp PPI inhibitors which will be a good starting point for further development. Since during the previous screening work a representative pyridine derivative showed good biological results, I decided to try to synthesize some pyridine derivatives, maintaining, as done for the pyrimidine library, the 2-mercapto-*N*-(*m*-tolyl)acetamide chain in C2 and exploring the effect of different substituents in C4 and C6 positions (**CHAPTER 4.**, **Paragraph 4.4.**). All modeling studies have been developed in collaboration with the University of Siena, while biological tests have been performed in collaboration with the University of Padua.

Another part of my PhD work was devoted to the synthesis of substituted pyrazolo[3,4-*b*]pyridines as A_1 adenosine antagonists. Adenosine is an endogenous neuromodulator which mediates its effects by interacting with four G-protein-coupled receptor subtypes distributed in a wide variety of tissues, named A_1, A_{2A}, A_{2B} and A_3. In particular, A_1 adenosine receptor (A_1AR) is the more preserved receptor subtype among different species and is widely

expressed in many parts of the body. A_1AR activation inhibits the activity of adenylate cyclase, activates potassium channels, blocks calcium transient (T) channels and increases the intracellular levels of calcium and, due to the phospholipase C (PLC) activation, of inositol-1,4,5-triphosphate (IP3). An excessive stimulation of A_1ARs is related to different pathologies, such as various forms of dementia, including Alzheimer's disease, depression, congestive heart failure, bradyarrhythmias, asystolic arrest, sepsis and cirrhosis of the liver. Because of A_1AR stimulation plays a central role in a lot of pathologies, the discovery of human A_1 selective antagonists is very significant.

In this context, the research group where I worked synthesized a wide library of 4-aminopyrazolo[3,4-*b*]pyridine-5-carboxylic acid esters, introducing various substituents at the N1, C4 and C5 positions of the central scaffold. Many of these compounds turned out to be active as A_1AR antagonists both on bovine and human receptors. Starting from these results, I decided to synthesize two small libraries of 4-aminopyrazolo[3,4-*b*]pyridine-5-carboxylic acid ester derivatives. These two series of compounds have in C5 of the pyrazolo-pyridine scaffold the ethyl ester chain, while in C6 there are different substituents. Some of them have a 2-chloropropyl chain in N1, while others have the bulkier 2-chloro-2-phenylethyl chain (**CHAPTER 5.**). Since previous studies indicated that human A_1AR contains a binding pocket smaller than that of bovine receptors, the aim of my work was that of obtaining more potent and selective antagonists for hA_1AR and evaluating their possible different affinity for bovine and human receptors. With this work it was possible to enrich our library of A_1 antagonists belonging to the class of pyrazolo[3,4-*b*]pyridines, to extend SAR evaluations and, importantly, to confirm that the binding site of the human A_1AR is smaller than that of the bovine A_1AR. In the complex, the synthesized compounds represent a step forward in the research for active compounds on A_1AR, a field that was not so much explored but that could lead to interesting results in therapy thanks to a modulatory effect on target tissues. For this part of my work, docking studies and biological tests have been developed in collaboration with the University of Pisa.

During the third year of my PhD, I spent three months at the Department of Chemistry at the University of Basel, within the research group of Prof. Dr. Olivier Baudoin. The research of this group is focused on the development of step-economical transition-metal-catalyzed methods for the functionalization of non-activated C-H bonds, employing catalysis by Pd(0) complexes. Transition-metal catalysis has emerged as a powerful tool to functionalize

otherwise unreactive C-H bonds and to create a variety of carbon-carbon and carbon-heteroatom bonds. In the context of enantioselective Pd(0)-catalyzed reactions, Baudoin and co-workers are working on the development of a bifunctional molecule that can act as ligand and as base at the same time. The model reaction for the optimization of the catalyst transforms the substrate into a fluoradene derivative. Fluoradenes seem to be key intermediates for the synthesis of buckybowls, interesting compounds having five- and six-membered rings and a curved surface that can be employed, for example, in host-guest chemistry or for light-emitters. In this context, the work that I have done during my three-months internship within Baudoin's group is related to different aspects linked to C-H activation reactions, and could be divided into three main topics: the synthesis of the key intermediate to get the binaphtyl bifunctional ligand, the performing of some enantio and racemic C-H activation reactions and attempts to obtain new substrates for C-H activation reactions (**CHAPTER 6.**).

CHAPTER 1. Introduction

1.1 General features and classification of viruses

Viruses are the smallest infectious agents for humans, and the most common and abundant biological entities on Earth[1]. They can display different morphologies, from rather spherical forms (about 100 nm in diameter) to extended filamentous strains (several micrometers long); the morphological changes are influenced by viral and host cell factors as well as mutations that allow viruses to adapt in different situations. Several studies demonstrate that spherical and filamentous morphologies are linked at least in part to the matrix protein 1 (M1), a bifunctional membrane/RNA-binding protein that mediates the encapsidation of RNA-nucleoprotein cores into the membrane envelope; in particular, different studies reported that mutations in the M1 gene of influenza A viruses (IAVs), in particular, including residues 41, 95, 102, 204, and 218, can affect virion morphology[2-7]. Indeed, it seems that filamentous morphology gives a selective advantage *in vivo*, while viruses with exclusively spherical morphology are more fit in laboratory substrates[8], and that this difference of structure is correlated to functional differences, such as neuraminidase (NA or N) activity[9].

Viruses can contain a single-stranded (ss) or double-stranded (ds) RNA or DNA, either linear or circular, as genome. DNA or RNA viral genome is protected by a proteic membrane, called capsid; the capsid together with the viral nucleic acid is called nucleocapsid. In some viruses the nucleocapsid contains important viral enzymes such as, in the case of the influenza virus, the RNA-dependent RNA polymerase (RdRp). Additional lipidic or carbohydrates layers may be present around the nucleocapsid; they differ according to the type of virus and may contain proteins encoded by viral genes. The complete structure of the virus is called virion.

Viral taxonomy is complex: there are different classifications of viruses based on shape and structure of their capsids, type of genome, chemical-physical properties, structure of the associated proteins, strategy of replication, etc. Classical virology taxonomy is the Baltimore classification that is based on the replication-expression strategies, in particular, on the form of nucleic acid that is incorporated into virions. According to this classification, viruses are divided into six classes: dsDNA viruses (class I) (e.g. *Adenoviruses*, *Herpesviruses*, *Poxviruses*), ssDNA viruses (class II) (e.g. *Parvoviruses*), dsRNA viruses (class III) (e.g. *Reoviruses*), positive (+) ssRNA viruses (class IV) (e.g. *Picornaviruses*, *Togaviruses)*,

negative (-) ssRNA viruses (class V) (e.g. *Orthomyxoviruses*, *Rhabdoviruses*) and RNA tumor viruses and other viruses which have a DNA intermediate in their growth and a ssRNA genome (class VI) (e.g. *Retroviruses*) (**Figure 1.**)[10].

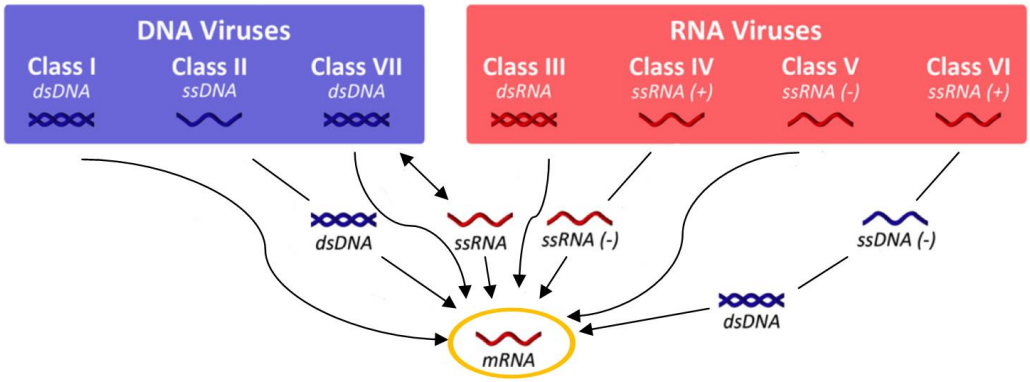

Figure 1. Baltimore classification of viruses. Adapted from: *Chem Soc Rev*., 45(15), 4074-4126.

Today, we refer to the Universal Scheme of Virus Classification of the International Committee on Taxonomy of Viruses (ICTV)[11]. The essential principles of this nomenclature are intended to ensure stability of the naming system by avoiding or rejecting the use of names which might cause error or confusion, and preventing the unnecessary creation of names. Changes in this classification take place every year, as the result of a multi-stage process: proposals submitted to the ICTV Executive Committee (EC) undergo a review process, then are presented for ratification to the full ICTV membership by publication on the ICTV website; the name of a taxon is not official until it has been approved by ICTV. For the ICTV, viruses are divided into orders (*Bunyavirales*, *Caudovirales*, *Herpesvirales*, *Ligamenvirales*, *Mononegavirales*, *Nidovirales*, *Ortevirales*, *Picornavirales*, *Tymovirales*), families and, inside families, in different genera[12].

1.2. Influenza viruses

Influenza viruses belong to the group of (-)RNA viruses, in particular, to the *Orthomixoviridae*, that is a family of enveloped viruses with a single-stranded (ss) negative-sense (-) and eight-segmented (types A and B) or seven-segmented (types C) RNA genome. More recently, in addition to these three types of influenza viruses, a fourth type D was

discovered[13]. In the ICTV taxonomy, *Orthomixoviridae* family is subdivided into seven genera: *Alphainfluenzavirus* (or influenza type A, IAV), *Betainfluenzavirus* (or influenza type B, IBV), *Gammainfluenzavirus* (or influenza type C, ICV), *Deltainfluenzavirus* (or influenza type D, IDV), *Isavirus, Quaranjavirus* and *Thogotovirus*[10]. The most relevant are the first three classes, divided in types A, B, C according to the antigenicity of their nucleoprotein (NP), a structural protein which encapsidates the (-)RNA, and the matrix protein M1[14].

RNA segments of type A and type B viruses encode eleven proteins while RNA segments of type C viruses encode nine proteins. Within the virion, RNA segments form ribonucleoprotein (RNP) complexes. More specifically, the highly conserved 5′ and 3′ *termini* of RNA interact through base-pairing to form a partially double-stranded structure which is bound by the RdRp complex, while the rest of the RNA associates with NPs (one NP for approximately every 24 nucleotides), with high affinity and without sequence specificity, to form a flexible helical filament closed by a loop at the opposite pole to the genomic ends. The interaction between NPs and RNA polymers is *via* the phosphate backbone, so that RNA should be accessible for pairing or genome duplication[15,16]. Influenza virus strains have an identification code according to their antigenic type (A, B, C or D), the host of origin (omitted if human), the geographical origin, strain number, year of isolation and, in the case of IAVs, the hemagglutinin (HA or H) and NA subtype. For example, the code "influenza A/chicken/Hong Kong/220/97(H5N1) virus" refers to IAV, H5N1 subtype, strain number 220, isolated from chickens in Hong Kong in 1997[17].

1.2.1. Influenza A virus and pandemics

Influenza A virus (IAV) is the most prevalent pathogen for both humans and animals (birds, horses, pigs and bats)[18], causing the so-called seasonal flu, that affects every year approximately 5-10% of the adult and 20-30% of the pediatric population[19]. There are several subtypes of IAV, according to the combination of HA and NA proteins that are expressed on the surface of the virus and that are essential for entry into and release from the host cell. To date, eighteen different HA subtypes (HA1-18) and eleven different NA subtypes (NA1-11) have been identified[20]. Aquatic birds are thought to be the primary reservoir for IAV because they can be infected with nearly every subtype of the virus, providing a large pool of virus gene segments that can contribute to novel reassortant viruses. Only the recently discovered subtypes H17N10 and H18N11 have not been found in birds, but in bats[21].

Different subtypes of IAV were responsible for widespread pandemics since the 16th century: the most important have been the 1918 Spanish flu (H1N1), the 1957 Asian flu (H2N2), the 1968 Hong Kong flu (H3N2); but also, the 2009 swine-origin pandemic flu (2009 pH1N1) as well as the 1977 Russian flu (H1N1) (**Figure 2.**).

The Spanish flu has been recorded as the worst pandemic in history; it caused the death of approximately 675,000 people in the USA and more than 50-100 million people worldwide. Most of the deaths resulted from respiratory complications, such as bronchopneumonia with bacterial invasion and progressive cyanosis and collapse. It seems that the pathogenicity of the H1N1 virus was amplified by a concomitant bacterial infection by *S. pneumoniae* and *S. pyogenes*. After the pandemic period, the virus kept accumulating mutations for several years and disappeared in 1957, only to reappear in circulation in 1977. In 1957 another influenza pandemic, the Asian flu, caused by the H2N2 strain of IAV, occurred. The new H2N2 strain was detected in February 1957 in China, and by the summer of 1957 it had spread to the rest of the world. Although the overall impact on mortality was one-tenth of that observed during the 1918 pandemic, in the USA it caused almost 60,000 deaths from September 1957 to March 1958 and about 115,700 worldwide. In 1968, a new influenza virus strain (H3N2) led to the third pandemic. The H3N2 strain was first isolated in Hong Kong in July 1968 and, although it was highly transmissible, caused a milder disease than the Asian flu. The virus mainly spread due to international air travels and it caused an estimated 98,100 deaths in the years 1968-1971. It is important to underline that both H2N2 and H3N2 influenza viruses were avian-human reassortants in which avian gene segments were introduced into a human-adapted virus that was already in circulation. In the spring of 2009 there was the emergence of a novel subtype of IAV (H1N1), which caused the first pandemic of the 21st century, being transmitted very fast worldwide. According to a study done from 15 April 2009 through 23 January 2010 in the USA, the rates of hospitalization were higher in children, with 272 paediatric deaths[22,23].

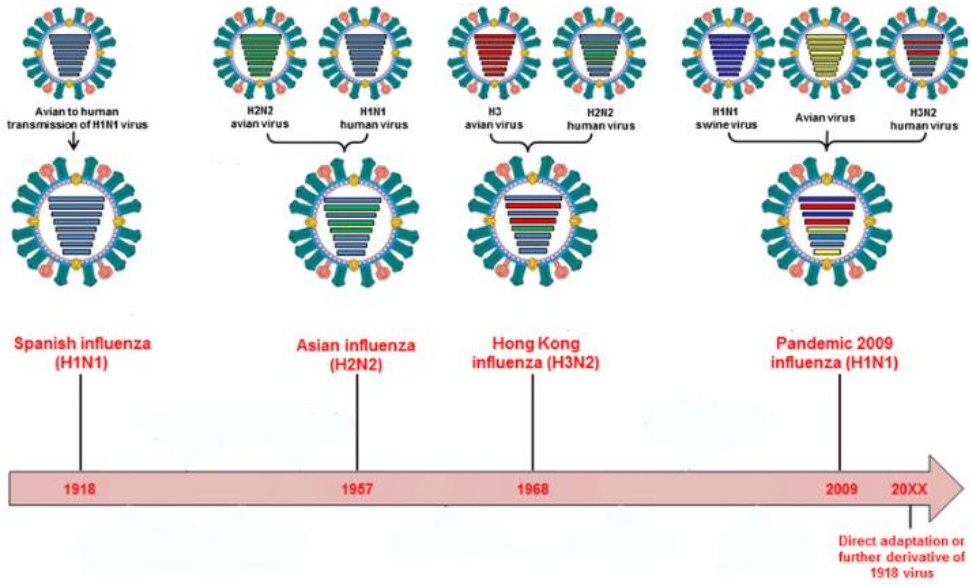

Figure 2. A timeline of major influenza pandemics and the responsible IAV strains. Adapted from: *Arch Virol.*, 163, 831-844 (**2018**).

1.2.2. Influenza B virus

Influenza B viruses (IBVs) are classified into two co-circulating phylogenetically and antigenically distinct lineages, named viruses B/Yamagata/16/88 (Yamagata-lineage) and B/Victoria/2/87 (Victoria-lineage), that diverged in the 1970s. The B/Victoria lineage predominated during the 1980s, while the B/Yamagata lineage during the 1990s. In 2001, the B/Victoria lineage re-emerged in Europe and USA and the two lineages have co-circulated ever since[24]. IBV changes two-three times less rapidly than type A[25] and consequently has less genetic diversity[26]. The lower antigenic mutation rate, combined with a poor range of hosts (which prevents an antigenic displacement between different species) ensures the impossibility of IBV pandemics[27]. It is important to underline that, despite the difference of virus infection frequency between IAV and IVB, an equivalent fatality rate between both viruses has been observed[28].

1.2.3. Influenza C and D viruses

Influenza C virus (ICV) infects humans and pigs. There are many co-circulating ICV variants belonging to different lineages: C/Yamagata/26/81, C/Aichi/1/81, C/Aomori/74 and C/Mississippi/80. Despite the significance of genetic reassortment in ICV epidemiology is

totally unknown, several ICV reassortant strains (C/Yamagata/64, C/Kanagawa/1/76, C/Miyagi/77, C/England/83, C/Nara/1/85, C/Yamagata/9/88 and C/Yamagata/5/92) have been identified[29]. Although seroepidemiological studies revealed that ICVs are widely distributed throughout the world, outbreaks of illness caused by the virus have rarely been detected and clinically appear to cause only minor disorders[30-32].

Influenza D virus (IDV) primarily affects cattle and is not known to infect or cause illness in people[33].

CHAPTER 2. Influenza A virus

2.1 Structure and life cycle

The different types of IAVs are the most dangerous for humans because they are responsible for the seasonal flu, that each year affects millions of people, and for important pandemics that have cyclically hit the world. For this reason, my research has focused on finding new molecules that are potentially active against type A viruses. From now on I will therefore only refer to IAV.

IAV virion consists of a lipid envelope out of which two surface spike-like projections, consisting of HA and NA glycoproteins, protrude. Embedded within the lipid envelope bilayer, the viral integral membrane protein M2 is present, while M1 protein forms a matrix layer underneath the envelope of the virion. The genetic material consists of an eight-stranded, negatively charged RNA. Each strand is wrapped-up in multiple copies of NP and is associated with three proteins responsible for transcription and replication: PB1, PB2, and PA (the viral polymerase complex), creating the distinctive panhandle structure. Each NP-encapsidated RNA segment, together with its heterotrimeric polymerase, constitutes a viral ribonucleoprotein complex (vRNP) (**Figure 3.**)[34].

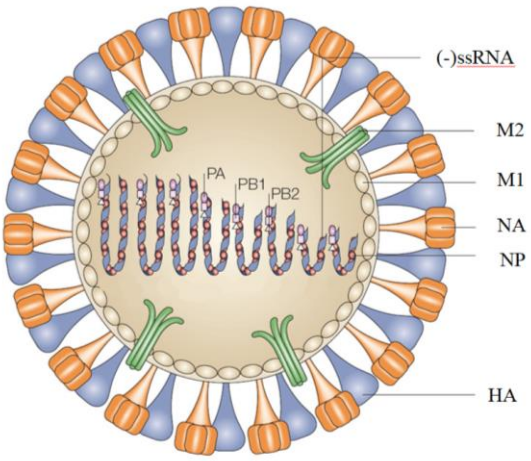

Figure 3. General structure of IAV. Adapted from: *Nature Rev Microbiol*., 3, 591-600 (**2005**).

The process of viral infection consists of seven steps: adsorption, penetration, uncoating, transcription, translation, assembly and release (**Figure 4.**)[16,35].

During the adsorption, the virus attacks to the epithelial cells using a specific bond between HA of the virus and glycoconjugates ending with *N*-acetylneuraminic acid, generally known as sialic acid, located on the surface of the host cell. In particular, HA recognizes glycan structures terminating with sialic acid, linked to galactose in a β-1,4 linkage to glucosamine (GlcNAc). The linkage of the sialic acid to the penultimate galactose is considered to be a determinant of species specificity: avian HA binds to α-2,3 sialic acid while human HA to α-2,6. This specificity normally prevents the transfer of influenza viruses between avian species and humans; however, this restriction can be overcome, as observed in culture where viruses can adapt to their host through mutations in the receptor-binding site of the viral HA gene. Internalization processes could be mediated by different events: the majority seems to be clathrin-coated pits mediated, but internalization *via* caveolae, macropinocytosis, and by non-clathrin, non-caveolae pathways have also been described.

The penetration and the uncoating of the virion occur by fusion between the viral and endosomal membranes, stimulated by acidification of the endosome, that causes a structural change in the viral HA and leads the fusion peptide (FP) of its HA2 subunit to interact with the endosome membrane. The concerted structural change of several HA molecules opens up a pore through which the vRNPs pass into the cytosol of the cell. The virus-associated M2 protein allows the influx of H^+ ions into the endosome; this causes the disruption of the protein-protein interactions and the subsequent release of vRNPs free of the M1 protein. After being released into the cytosol of the cell, vRNPs are transported to the host nucleus. vRNPs are too large to passively diffuse into the nucleus and so they must rely on active transport by the nuclear import machinery. The transport process begins with the recognition of the nuclear localization signal (NLS) by α-karyopherin; then a trimeric complex with β-karyopherin allows vRNP binding with the nuclear pore of the host cell nuclear membrane. Inside the nucleus, the viral RNA (vRNA) is transcribed and replicated. In detail, vRNPs are transcribed to produce viral mRNAs in a process that is called “primary transcription”, independent of *de novo* viral protein synthesis and primer-dependent. The primers used for this purpose, namely 7-methylguanosine-capped pre-mRNAs with 10-13 associated nucleotides, are obtained through “cap-snatching” of cellular mRNAs by the RdRp. This allows polyadenylation of viral mRNAs once the influenza virus has shut down the host cell polyadenylation processing. Once the caps are acquired, transcripts are generated by

replication from a vRNP template, while poly-A tails are produced by reiterative stuttering and copying of the poly-U sequence motif at the conserved 5′ end of the vRNA.

After the primary transcription, viral mRNAs are exported to the cytoplasm and translated into viral proteins by cellular ribosomes; subsequently, the components of vRNPs are imported into the nucleus where progeny vRNP complexes are assembled. The negative-stranded RNA is used for the synthesis of full-length positive-stranded RNA, called complementary RNA (cRNA), which in turn acts as a template for the synthesis of new RNA molecules. The enzyme that catalyzes all these reactions is the viral RdRp that enters the host cell nucleus with the vRNP complex.

At this point, the assembly and the nuclear export can take place: RNA is packaged into vRNP containing two viral proteins, NP and M1. NP coats and protects the sugar phosphate backbone of the RNA, while M1 mediates the interaction of the RNP with the viral NEP/NS2 protein, which in turn interacts with host cell chromosomal maintenance 1 (CRM1) nuclear export protein, allowing the export of the complex from the nucleus. In particular, it seems that NEP simultaneously interacts with M1, the PB1 subunit of the vRNP-associated RdRp and the CRM1 nuclear-export receptor[36]. It is known that the CRM1 nuclear export pathway is essential for vRNP nuclear export; in fact, vRNPs are retained in the nucleus of infected cells in the presence of leptomycin B (LMB), a specific CRM1 inhibitor. Interestingly, LMB treatment leads also to vRNP accumulation at the nuclear periphery, in association with chromatin, suggesting that this localization pattern represents an intermediate step in vRNP nuclear export, preceding vRNP passage through the nuclear pore complex[37-39]. The fact that infected cells microinjected with anti-M1 antibodies exhibit NP confinement to the nucleus[40] and that exogenous M1 expression with impaired “late” gene expression (“late” genes include HA, M1, M2 and NA, and exhibit delayed expression relative to the NP gene)[41] rescued the ability of vRNPs to accumulate in the cytoplasm[42], indicate that also the M1 protein is directly implicated in the regulation of vRNP nuclear export. The influenza NEP protein (or NS2) also plays an important role in vRNP nuclear export; as seen for M1 protein, when anti-NEP antibodies are microinjected into the nucleus of infected cells, NP is retained in the nucleus, suggesting that this process is impaired when NEP protein functions are blocked[43]. Further, influenza viruses lacking NEP expression could not be recovered by reverse genetics, indicating that NEP is essential for the life cycle.

Also human host factors, such as cellular protein kinase activity, could affect vRNP nuclear export. Specifically, it has seen that this process is impaired in infected cells treated with a protein kinase C inhibitor[42], an inhibitor of the Raf/MEK/ERK MAPK signaling cascade[44], a receptor tyrosine kinase inhibitor[45], and a serum- and glucocorticoid-regulated kinase 1 inhibitor[46], implying that phosphorylation of viral and/or cellular factors is required for vRNP export from the nucleus. Also HA seems to have an indirect role in promoting vRNP nuclear export, that can be enhanced by viral HA-mediated activation of the cellular Raf/MEK/ERK MAPK signaling pathway, which occurs when HA is expressed at the plasma membrane[47,48].
In addition, because HA is abundant in virus particles and vRNPs must "meet" HA at plasma membrane sites to form progeny viruses, HA-mediated Raf/MEK/ERK induction could be used as a signal to activate vRNP nuclear export when the budding sites are "ready". It is important to underline that, although specific phosphorylation events and the kinases involved in promoting vRNP nuclear export have not yet been defined, NP, M1 and NEP exist all as phosphoproteins in infected cells[49-53].
Following nuclear export, progeny viral RNPs are transported across the cytoplasm in a Rab11- and microtubule-dependent manner to the budding site near the cell membrane, where assembly of new virions takes place[16]. In particular, shortly after nuclear export, vRNPs accumulate near the microtubule organizing center (MTOC), that is located immediately adjacent to the nucleus, and then they are aligned with microtubule networks. There is strong evidence that microtubule networks are essential for vRNP cytoplasmic transport: cells treated with microtubule depolymerizing agents exhibit altered vRNP distribution and reduced microtubule-like movement. Moreover, live cell imaging studies with fluorescently tagged vRNP components demonstrate vRNP movement along microtubule tracks[54-57]. Both vRNA and vRNPs co-localize extensively with Rab11-positive recycling endosomes in infected cells, suggesting that vRNPs use Rab11 vesicles for the movement through the cytoplasm. A specific role for Rab11 in mediating vRNP cytoplasmic transport is clearly demonstrated because it has seen an impaired vRNP association with Rab11-positive vesicles, a disruption of vRNP accumulation at the plasma membrane and a sharply reduction of infectious progeny virus output in cells with a Rab11 protein knockdown and an exogenous overexpression of a dominant-negative Rab11 mutant protein. Probably, when vRNPs are near the budding site, their extraction from Rab11 vesicle surfaces occurs, and only vRNPs are incorporated into budding virions; this is confirmed by the lack of Rab11 detection in

influenza virus particles[55-60]. Two components of host RNP, that regulate translation of cellular mRNAs, Y box binding protein 1 (YB-1) and double-stranded RNA-binding protein Staufen homolog 1 (STAU1), are associated with influenza vRNPs during late-stage infection. The YB-1 protein seems to be connected with the vRNP nuclear export and the delivery of vRNPs. The connection between YB-1 and the vRNP export process is due to the fact that this protein is localized with vRNA into the nucleus of infected cells and later it is found in the cytoplasm, in complex with α-tubulin, Rab11 and vRNPs, suggesting that YB-1 can undergo nuclear export in complex with vRNPs. It seems also that YB-1 facilitates the delivery of vRNPs to Rab11 endosomes, immediately after leaving the nucleus, even if direct evidence in support of this hypothesis is lacking. The role of STAU1 is less clear, although this factor is thought to promote a late aspect of the influenza virus life cycle, because its knockdown does not impair viral protein expression or vRNP nuclear export[61,62].

Final virus assembly is initiated at the budding site by the entry of the HA, NA and M2 proteins into the endoplasmic reticulum of the host cell; here HAs and NAs are folded and glycosylated. HAs are assembled into a trimer which is exported along with NAs and M2 proteins to the Golgi apparatus, where palmitoylation of cysteine residues on HA and M2 takes place. The budding of the new viral particles is initiated by the accumulation of M1 protein at the inner leaflet of the host cell membrane. As previously said, the Rab11 protein does not appear to be incorporated into a new virion, implying that another mechanism exists for vRNP recruitment at the budding site. Several studies suggest that the M2 protein is required for this process and that it occurs through a direct interaction between M1 and the M2 cytoplasmic tail[63-65]. In the final budding stage, NA hydrolyses the sialic acid conjugates, leading the release of a new virion from the host cell[34].

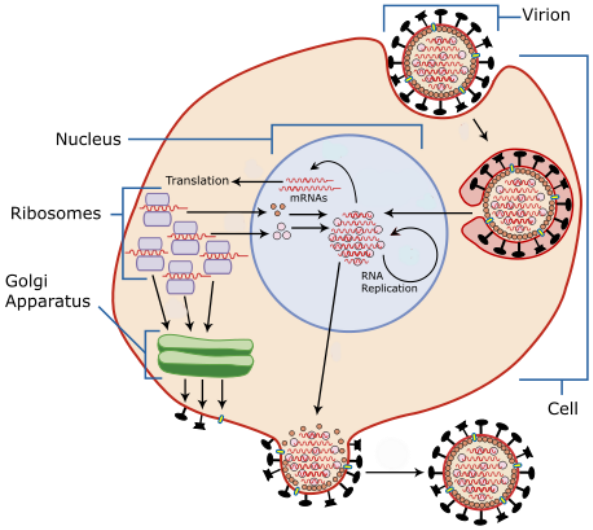

Figure 4. Influenza virus life cycle. Adapted from: Wilson and Gisvold's Textbook of Organic, Medicinal and Pharmaceutical Chemistry, 12th edition.

2.2. Key proteins for viral life

The genome of IAV was mapped during the 1970s[66,67]. Since that time, it was believed that eight viral genome segments encode ten proteins: the polymerase basic proteins 1 (PB1) and 2 (PB2), the polymerase acidic protein (PA), nucleoprotein (NP), hemagglutinin (HA), neuraminidase (NA), matrix proteins 1 (M1) and 2 (M2), and non-structural proteins 1 (NS1) and 2 (NS2). However, in 2001 an eleventh IAV protein, PB1-F2, was discovered. PB1-F2 is translated from a nucleic acid sequence that does not contain a stop codon in a given reading frame, the so called alternative open reading frame (ORF)[68]. Since then, additional viral proteins, PB1-N40[69], PA-X[70], M42[71], NS3[72], PA-N155, PA-N182[73] and PB2-S1[74] have been found and/or re-discovered (**Figure 5.**).

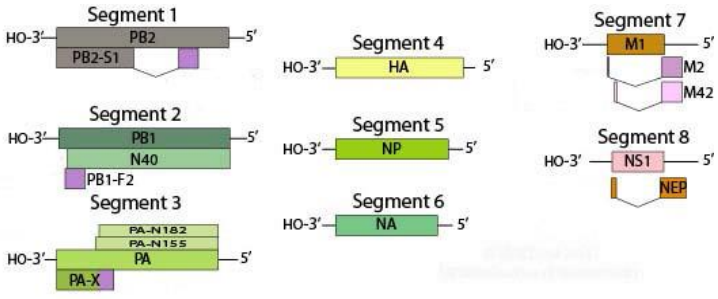

Figure 5. IAV proteins encoded by each segment of the viral genome. Adapted from: https://viralzone.expasy.org/.

2.2.1. Hemagglutinin

Hemagglutinin (HA or H) is a membrane-anchored homotrimer encoded by the fourth negative-stranded RNA segment, essential for virus-cell adsorption and endocytosis[75]. The fourth RNA segment encodes the precursor protein HA0 with 566 residues; HA0 is post-translationally glycosylated and trimerized with chaperons in the endoplasmic reticulum of the infected cell and it undergoes an extra- or intra-cellular cleavage process into HA1 and HA2. Each monomer of HA is composed of a globular head (HA1 domain) of approximately 327 residues organized in antiparallel β-sheets, and a fibrous stalk-like region (HA2 domain) of α-helices of approximately 222 residues. The HA1 and HA2 subunits are linked by a single disulfide bond to form a "mushroom" structure stuck in the viral envelope (**Figure 6.**)[76].

At neutral pH, the trimeric structure of viral HA is stabilized by the electrostatic interactions between positively charged inner surface sites of HA1 and negatively charged sites of HA2. The globular head of HA1, which comes out of the surface of the virus, plays a central role in virus-host interactions: it binds host receptors, is recognized by host antibodies and is responsible for the evasion of host immunity system through mutations and glycosylations at specific epitopes. In the HA1 domain there is the receptor binding site that is characterized by four structural key features: the 190-α helix, the 130-loop, the 220-loop and a hydrogen-bonded network of conserved amino acids at positions 98, 153, 183 and 195, which constitute the base of the site. In the HA2 domain, the first 23 residues, starting from the N-terminal end, form the so called fusion peptide (FP), which is accommodated in a hydrophobic pocket partially formed by the fusion domain of HA1. The sialic acid is bound with chair geometry and with the face of the sugar directed toward the floor of the binding site, while the N-acetyl group is located in a hydrophobic pocket. In all HA subtypes, the binding site and all key structural elements are similar, also in length. It is important to underline that, relatively small changes in length of loops between different viral strains are responsible for changes in the architecture of the site and, subsequently, in the interactions with different conformations associated with the glycosidic linkage type. An example of the connection between HA mutations and receptor preference is represented by the fact that most avian-infecting virus strains carry glutamine in position 226 (Q226), which provides a useful environment for ligands with the α-2,3 bond between sialic acid and galactose; in fact, both oxygens from the carboxyl group on sialic acid and the oxygen from the glycosidic bond can interact with the hydrophilic side chain of glutamine. On the other hand, if in position 226 there is a leucine

(L226) that has a hydrophobic side chain, it promotes ligands with the α-2,6 linkage. Sometimes the Q226 mutation has been found in strains with the human receptor preferring HA. This is probably due to the fact that the hydrophobic effect of the leucine residue can be emulated by residues at 138, 186 and 221, as in the case of some H7 strains[75,77,78].

In a recent study, Ni and colleagues[79] demonstrated that the different length in the 130-loop of HA binding site in pandemic H1 HA *vs* H2/H3 HAs is correlated with virus human adaptation. From this study, the 130-loop appears to be the key determinant to understand the different mutational routes employed by pandemic H1 or H2/H3 HA. In particular, the length of the 130-loop and, more importantly, the sitting position of the sialic acid moiety of the receptor can help first establish if a given HA would likely behave as H1 or H2/H3.

The different antigenic subtypes (1-18) of HA are divided into two groups, based on phylogenetic analysis. The first group includes H1, H2, H5, H6, H8, H9, H11, H12, H13, H16, H17 and H18 subtypes, while the second contains H3, H4, H7, H10, H14 and H15 subtypes. Subtypes 1-16 were identified in avian species, while H17 and H18 were found only in bats[80]. It is important to underline that H17 and H18 should be considered to be only HA-like proteins, because they lack the ability to bind glycans terminated with sialic acid and, furthermore, there is no evidence that the viral genomes identified in bats can be assembled into a real virus or is able to exchange genetic material with IAV from other subtypes[81]. Even in different subtypes, the HA structures are relatively similar; despite these similarities, the rotation of the membrane-distal subdomains relative to the central stem can be different. The variation seems to be related to differences in the structure and positioning of a loop in HA2 that links α-helix A (HA2 residues 38-58) and α-helix B (HA2 residues 75-127). Additionally, the location and nature of ionisable residues near the FP (HA2 residues 1-10), that could be involved in activation of the membrane fusion function of HA at endosomal pH, can also change[78].

The HA protein can also be found in IBV but, as previously said, IBV strains are not classified into subtypes based on properties of the HA and NA proteins. In ICV one external protein called hemagglutinin-esterase-fusion (HEF) combines in a single protein both the roles of HA and NA. It recognizes compounds terminated with *N*-acetyl-9-*O*-acetylneuraminic acid instead of *N*-acetylneuraminic acid like HA of IAV and IBV[82].

To date, there are more than 350 crystal structure of HA of IAV available in the PDB; the majority of them are of good quality and have their HA1 and HA2 subdomains solved with X-

ray diffraction. However, these structures represent only 73 strains, which is only a fraction of all the available HA sequences. In the last years, several new structures of HA have been solved. For example, in 2016 the structure of the drug Arbitol in complex with HAs from the H7N9 and H3N2 viruses was proposed and compared with structures solved with the fusion inhibitor *terz*-butyl-hydroquinone (TBHQ); it is important to underline that in this work, a pocket between the monomers of the HA trimer was described, which can be targeted by other small compounds to stabilize the HA2 in its normal pH conformation. In 2017, the structure of HA from the H15 subtype was solved in complex with the avian receptor analog 30SLN (NeuAca2-3Galb1-4GlcNAc) and in the apo form. The structure of HA from the H10 subtype with a preference toward human-type receptors was proposed and compared with a structure from the wild-type H10; during this study, the role of the 150-loop in modifying preference for HAs belonging to the H7, H10 and H15 subtypes was highlighted[78].

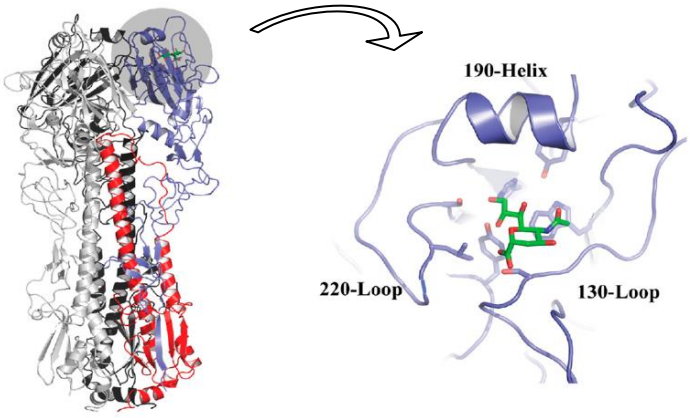

Figure 6. Trimeric HA, with one monomer colored gray, another black, and the third in blue (HA1) and red (HA2). The location of the receptor binding pocket for the monomer is highlighted by the gray circle, and this region is magnified and reoriented in the right panel to depict the location occupied by bound sialic acid, shown in green. Adapted from: *Int J Mol Sci*., 18, 1541 (**2017**).

2.2.2. Neuraminidase

Neuraminidase (NA or N) is a homotetrameric protein encoded by the sixth negative-stranded RNA segment. It is an exosialidase that cleaves the α-ketosidic linkage between the sialic acid and an adjacent sugar residue. Its activity is required at the time of the budding of newly formed viral particles from the surface of the infected cell, to prevent aggregation of viral particles and, in addition, to cleave neuraminic acid residues from the respiratory tract

mucins, facilitating viral movement to the target cell. NA protein is formed by 470 amino acids, with each subunit of the tetramer composed of a stalk domain supporting a head domain (**Figure 7.**)[83].

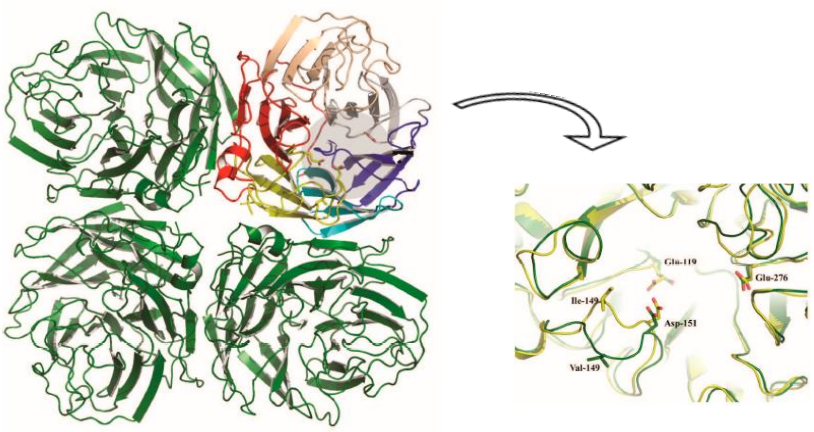

Figure 7. On the left: IAV NA homotetramer with the catalytic site shaded in gray; on the right: superimposition of the catalytic site of the N9 subtype onto the N1 subtype (shown in green). Adapted from: *Int J Mol Sci*., 18, 1541 (**2017**).

Nine subtypes of NA are described for IAV, while only one was revealed for the IBV and ICV. As previously said, for ICV we do not refer to NA but to HEF protein that combines both the roles of HA and NA and promotes the *O*-deacetylation of the *N*-acetyl-9-*O*-acetylneuraminic acid[82]. The nine subtypes of NA found in IAV are divided into two phylogenic groups: the first group consists of NA of N1, N4, N5 and N8 subtypes and the second one consists of N2, N3, N6, N7 and N9 subtypes.

The active site is located within the head domain and it consists of functional amino acids, in particular, Arg118, Asp151, Arg152, Arg224, Glu276, Arg292, Arg371 and Tyr406 and structural amino acids Glu119, Arg156, Trp178, Ser179, Asp (or Asn in N7 and N9) 198, Ile222, Glu227, Glu277, Asp293, and Glu425.

The functional amino acid residues are in direct contact with sialic acid, the product of the enzymatic reaction, and they all form polar contacts with it, excluding Arg224, whose aliphatic part forms a non-polar contact with the glycerol fragment of the *N*-acetylneuraminic acid residue. The structural amino acids provide only a structural framework for the functional residues. Both functional and structural amino acids are constant for all NA subtypes of IAV and IVB. Asparagine residues, especially Asn146, which form the glycosylation site as well as proline and cysteine residues, which provide the required folding

of the polypeptide chain and stabilize the 3D structure of the molecule, are strictly conserved[83]. In addition to the active site, the head domain contains a calcium binding site, which stabilizes the enzyme structure at low pH values. In some strains there is also a secondary sialic acid binding site[84]. The key step in the hydrolysis mechanism of NA is the formation of the oxocarbonium ion at the C2 atom of sialic acid, stabilized by multiple contacts between the intermediate product and the amino acids of the active site. This allows the conformational changes from chair to half-chair, due to strong ionic interactions between the carboxylate of the substrate and the guanidine groups of Arg118, Arg292 and Arg371, leading to glycosidic bond cleavage (**Figure 8.**)[83].

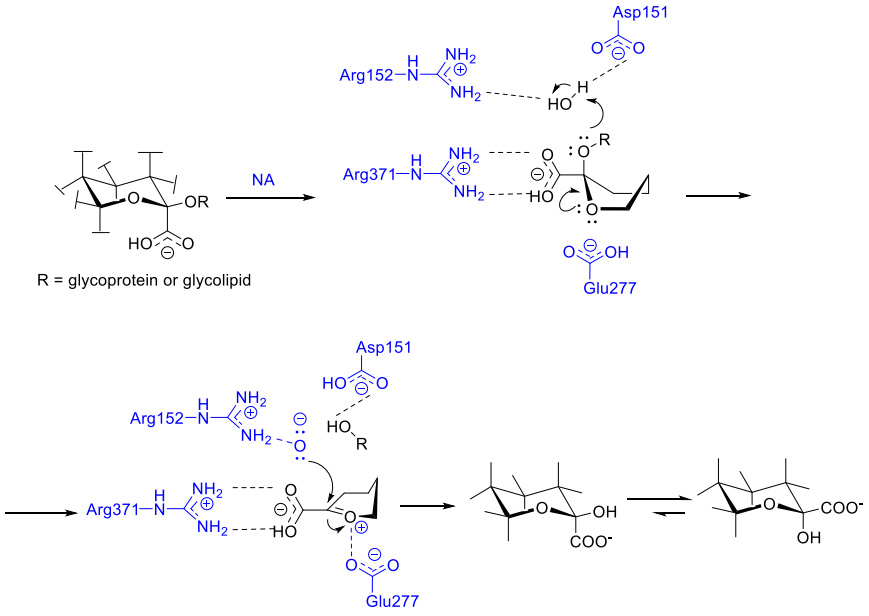

Figure 8. Hydrolysis mechanism of viral NA. Key NA residues are labelled in blue. Adapted from: Patrick, G. L. An Introduction to medicinal chemistry, 5th ed. Oxford University Press. EdiSES s.r.l.

The three dimensional structures of some NA subtypes have been identified. These findings showed that, despite that NA types A and B homology cover only 30%, their 3D structures are virtually identical[85-89].

2.2.3. Matrix proteins 1 and 2

Matrix protein 1 (M1) and matrix protein 2 (M2) are produced by the seventh RNA segment: in particular, M2 is produced by an alternative splicing[90]. M1 protein is a 60-Å long rod that forms a matrix layer underneath the envelope of the virion; it touches the virion membrane

and apparently it is not inserted but associated with it through electrostatic interactions[91]. It consists of two domains, C-terminal and N-terminal, connected by a linker sequence, and differently charged: one side of M1, characterized by the presence of lysine and arginine as amino acids, is positively charged, while the other side has negative charges (**Figure 9.**)[92].

The molecular details of M1 action during the viral replication cycle and its interactions with the membrane are not yet well understood. It has been observed that M1 binds to the inner leaflet plasma membrane at first probably as a dimer and eventually multimerizes, forming large clusters. Multimer growth seems to occur through the interaction between already bound M1 and M1 that are still in solution. This is possible probably because, once bound to the bilayer, M1 undergoes a conformational change or, stably exposes a side that favors interaction with unbound M1 molecules[93]. In a recent study, Bobone and colleagues show that M1 interacts with negatively charged membrane lipids, in particular, with phosphatidylserine[94], while regarding M1 protein involvement in the viral replication cycle, it has been shown that it directly interacts with NP[91,95-99]. Since M1 protein acts as a bridge between cellular membrane lipids and viral genome, and because of its interaction with cytoplasmic tails of HA, NA and M2, it is very important in the viral reproduction cycle. In particular, it induces, with the aid of NS2 (NEP)[100], the export of the newly formed RNP complexes from the nucleus to the cytoplasm[94] and it takes part into the viral assembly at the budding site[101].

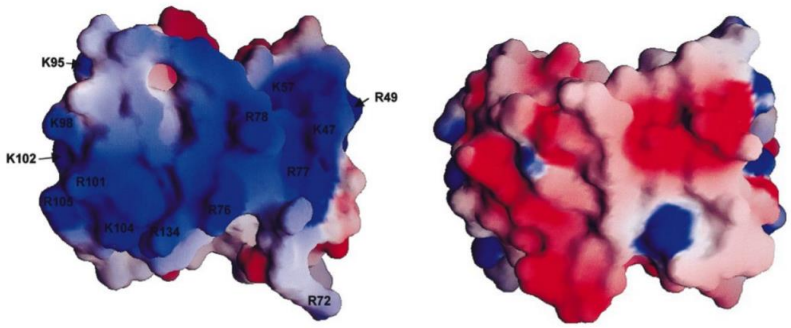

Figure 9. The surface potential of the M1 monomer structure (pH 7). On the right the positively charged residues; on the left the negatively charged surface area (rotation by 180°). Adapted from: *Virology*, 279 (2), 439-446 (**2001**).

M2 protein is a pH-regulated proton channel of IAVs and IBVs. Despite the different structural solutions between M2 channel in IAVs and IBVs the result is similar. Both tetramers form well-defined hydrophilic pores with residues constricting the N and C *termini* of the pore[102]. The M2 proton channel of IAVs is a homotetrameric integral membrane

protein passing through the viral envelope, with each chain containing 96 amino acids. Each chain is formed by a N-terminal extracellular domain, a transmembrane domain (TM domain) and a cytoplasmic tail. The most important part is the TM domain that consists of four parallel left-handed α-helices of 19 amino acids, forming the proton channel pore, which has the N-terminal region packed tightly and the C-terminal region splayed slightly apart from each other. In the TM domain there are five important residues that are Val27, Ala30 and/or Ser31, Gly34, His37 and Trp41 (**Figure 10.**)[103,104]. At the N-terminal end of the TM domain, Val27 side chains form a hydrophobic gate of the channel pore[105]. The pore size increases gradually to reach its maximum value near Gly34 and is occluded again by Trp41 at the C-terminal end of the TM domain that, with its indole side chain, prevents outward proton flux[106-108]. The oxygen atoms in the backbone carbonyl groups of Ala30 and Gly34 and the oxygen atom of Ser31 side chain, acting as hydrogen bond acceptors, facilitate hydration of the channel pore; the water molecules in the channel pore facilitate proton conduction and stabilize the conformations of the pore, facing residues such as Trp41. His37 residue is the pH sensor and the proton filter, allowing conduction of protons but not of other cations[109]. The mechanism of action is dependent on the pH outside the virion: when pH is high, the channel is closed because His37 is not charged, and Trp41 obstructs the pore near its cytoplasmic end, while, when pH is low, His37 is charged and associates with Trp41 *via* interaction between the protonated imidazole and the π-electrons of indole, allowing proton flow[110-115].

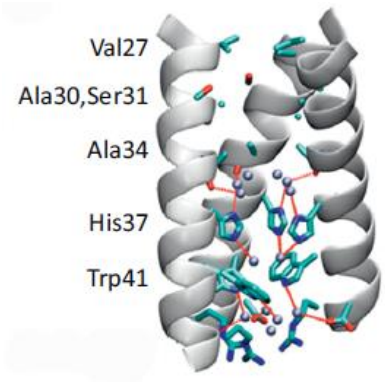

Figure 10. Crystal structure of the M2 proton channel (PDB ID: 3LBW). Only three of the four subunits are shown for clarity. Gly34 was mutated to Ala34 in this structure. The protein backbone is shown in white, whereas the side chains of several key residues and water molecules are shown in the stick and space-filling model, respectively. The carbon, nitrogen, and oxygen atoms of the residues are in cyan, blue, and red, respectively. The oxygen atoms of the water molecules are in light blue. Hydrogen bonds between the water clusters and the protein residues are in red lines. Adapted from: *Trends Pharmacol Sci*., 34, 571-580 (**2013**).

M2 protein is required for uncoating and release of the viral genome into the cytoplasm and for equilibration of the intraluminal pH of the *trans* Golgi network with that of the cytoplasm, thus preventing conformational change of HA[116,117].

A recent study[118] demonstrated that IAV M2 can be ubiquitinated and that an amino acid residue that is present in the cytoplasmic domain, Lys78, plays a central role in this process. The ubiquitination mediates the coordination of efficient packaging of the viral genome into virions and the timing of viral-induced cell death. A M2-K78R mutation (from lysine to arginine at position 78), which produces ubiquitination-deficient M2, causes a severe defect in production of infectious virion. In particular, this mutant progeny has about twice the amount of HA protein, lower levels of viral RNAs, NP and M1 protein. M2-K78R virus is also characterized by a weaker M1-M2 interaction that can explain why many M2-K78R virus particles failed to incorporate internal viral proteins and vRNAs. Moreover, the differences in the biological, physical, and chemical properties of M2 proteins between wild-type and M2-K78R viruses may impact virus-host interactions: in fact, mutant virus triggers autophagy and apoptosis more easily and earlier compared to the wild-type ones.

2.2.4. Non-structural proteins 1 and 2

Non-structural proteins 1 (NS1) and 2 (NS2) are derived from an alternative splicing of the eighth RNA segment; in particular, NS2 is derived from the splicing, while NS1 is produced from the unspliced transcript. NS1 is a multifunctional protein that is not incorporated in the virus, while NS2 is a structural component of the virion, associated with M1 protein[119].

NS1 is a virus virulence factor that, depending on virus strain, is composed of 230-237 amino acids. It has several well-characterized functional domains: the first 73 amino acids form the RNA-binding domain that contains NLS, 10-15 amino acids represent a linker domain, residues 88-202 form the effector domain and 11-33 amino acids form the C-terminal tail[120]. To support efficient viral replication, NS1 interacts with cellular components either in the cytoplasm or in the nucleus. It counteracts different components of the RIG-I/IFN signaling pathway to efficiently inhibit IFN expression, it represses innate antiviral mechanisms of the host cell, acting on type I interferon system through direct interaction with protein kinase R (PKR) and with tripartite motif-containing protein 25 (TRIM25) or through the sequestration of dsRNA[121-125]. NS1 inhibits also nuclear export of cellular mRNA through the interaction with cleavage and polyadenylation specificity factor subunit 4 (CPSF4) and with

polyadenylate-binding nuclear protein 1 (PABPN1)[126], and it seems to hijack the RNA translational machinery in favor of viral protein, for example, by interaction with STAU1[127,128].

NS2 protein is responsible, as previously said, for the export of the newly formed RNP from the nucleus to the cytoplasm, *via* its interaction with CRM1[129]. In addition, because of its interaction with nucleoporins, it probably acts as an adaptor between RNPs and the nuclear pore complex[43], and it seems also to have a role in viral transcription and replication[130]. However, many functions of NS2, in particular, its transit through the cytoplasm and its incorporation into the viral particle, are not fully understood.

There are lots of NS1 and NS2 interactors that have been identified and described in the literature: these interacting host cell proteins are generally expressed in the respiratory epithelium and are potentially involved in many steps of the virus life cycle and some of them can directly control the viral replication[100].

2.2.5. Influenza RNA-dependent RNA polymerase

Influenza RNA-dependent RNA polymerase (RdRp) is a heterotrimeric complex of about 250 kDa that is composed of three different subunits: PA (polymerase acidic protein), referred as P3 in the case of ICV, PB1 and PB2 (polymerase basic proteins 1 and 2). These subunits are encoded by the three largest segments of the viral RNA genome; in particular, segment one encodes for PB2, segment two for PB1 and segment three for PA. RdRp associates with the 3' and 5' ends of each RNA genome segment, forming, together with RNA and NPs, the vRNP complex. Starting from the ss(-)RNA viral genome, RdRp is responsible for the synthesis of the positive-strand messenger (mRNA), used for viral protein production, and for the synthesis of complementary RNA (cRNA), useful to obtain new viral genome (**Figure 11.**)[131,132]. Both the transcription and the replication of vRNA take place in the nucleus of infected cells and therefore, the RdRp has to be transported into the nucleus. Although the NLS is identified in all three RdRp subunits and it is demonstrated that individually expressed PB1, PB2, and PA can enter the nucleus[133-139], different processes have been proposed for the assembly of the RdRp complex. A dimer of PB1-PA could form in the cytoplasm and be transported into the nucleus, where it binds to PB2[140] or a PB2-PB1 dimer could form in the cytoplasm and be transported into the nucleus, where it interacts with PA[141].

The structure of RdRp is highly conserved among A, B and C viral strains[142]. The recent elucidation of the atomic structures of complete influenza A[143] and B[144] polymerase complexes bound to their vRNA promoter sequences and apo-RdRp from influenza C[145], led to an important breakthrough in the understanding of the replication machinery and in the atomic-level mechanistic insight of RdRp. The catalytic site is in PB1; PB2 includes the capped-RNA recognition domain, that is necessary for the generation of the primer for the transcription, while PA is responsible for "cap-snatching", the cleavage of host cell pre-mRNA to utilize its cap for viral generation of the primer for the transcription, and it is also important in the complex assembly[132].

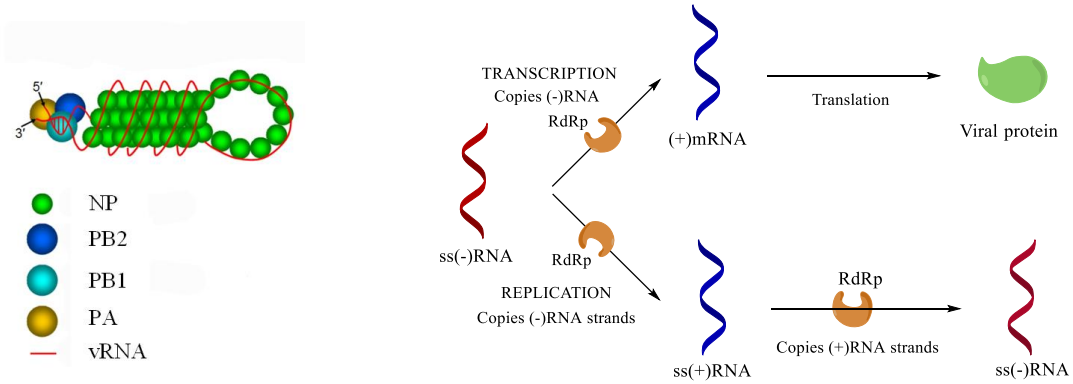

Figure 11. On the left: the structure of viral RNP complex. On the right: the role of RdRp in viral gene expression and regulation pathways. Red lines represent negative-sense RNA; blue lines represent positive-sense RNA. Adapted from: http://cronodon.com/BioTech/Virus_Tech_3.html and http://library.open.oregonstate.edu/microbiology/chapter/the-viruses/.

The IAV RdRp has a U-shaped structure, with approximate height, width and depth of 115 x 100 x 75 Å, respectively, and it is characterized by a complex intertwining of the three subunits. The two protruding arms are formed by the N-terminal domain of PA (PA-N) and PB2 cap-binding domain, which face each other across a solvent channel. The bottom of the U is formed by the large C-terminal domain of PA (PA-C) and one of the sides by the C-terminal part of PB2 (PB2-C). The body of the trimer is formed by PB1, decorated on one side by the N-terminal part of PB2 (PB2-N) and on the other side by the linker (PA-linker) that connects PA-N endonuclease with PA-C. The trimer contains a large, internal, catalytic and RNA-binding cavity, formed by PB1 and PB2-N parts, that is partially open at the top to the solvent channel between the PA-N endonuclease and PB2 cap-binding domains (putative

template/product exit channel). This cavity is accessible *via* two narrow side tunnels, the putative nucleoside triphosphate (NTP) and template entrance channels (**Figure 12.**).

The structure of the RdRp, together with the RNA promoter, can undergo considerable conformational changes to convert the pre-initiation state into the active initiation and elongation states, as revealed by the apo and the crystal structures of the enzyme[144,146].

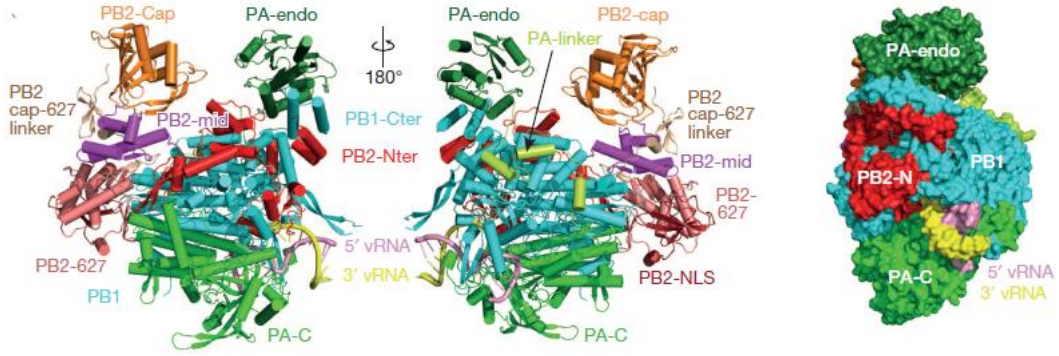

Figure 12. Two views (rotation by 180°) of the overall structure of the bat influenza A polymerase complex with the vRNA promoter. Imagine on the right: Side-view in space-filling representation showing emergence of vRNA duplex at the interface of all three subunits. Adapted from: *Nature*, 355, 516 (**2014**).

2.2.5.1. PB1 subunit

Influenza PB1 protein is the core subunit of the heterotrimeric polymerase complex; it contains in its central region a typical right-handed RdRp fold, comprising fingers, fingertips, palm and thumb domains. There are several characteristic features of PB1: N- and C-terminal extensions that make inter-subunit contacts with PA and PB2, respectively, and an unusually long (55Å) solvent-exposed, flexibly hinged β-ribbon and a β-hairpin insertion in the finger domain (**Figure 13**).

As previously said, the catalytic center responsible for template directed nucleotide addition is located in a PB1 internal cavity and it is formed mainly by four highly conserved motifs[147]: motif I ^{303}TGDN^{306}, motif II ^{403}LSPGMMMGMF^{412}, motif III ^{438}WDGLQSSDDFALI^{450} and motif IV ^{474}GINMSKKKSYI^{484}. Motif I, containing the conserved active site Asp305, promotes catalysis, motif II is methionine-rich and is probably involved in stabilizing the base pair between the incoming NTP and the template, motif III is the key functional domain that is present in other RNA- and DNA-dependent viruses[148], while motif IV contains conserved

Lys 480 and Lys 481 residues that are involved in NTP binding. As in other polymerases, in PB1 there are the NTP tunnel and the putative template entrance channel. The first, with positively charged residues, connects the internal cavity to the outside and seems to electrostatically attract and channel NTPs into the active site; the second has conserved residues from all three subunits and allows the entry of the template[143].

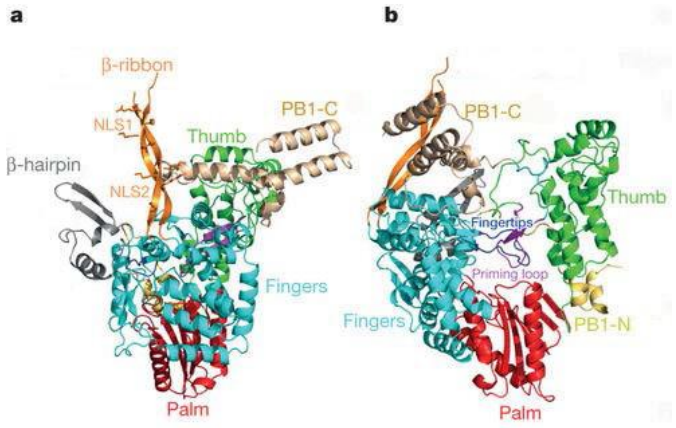

Figure 13. a General structure of PB1 subunit with highlighted the characteristic elements including the PB1-C extension, the β-ribbon and the β-hairpin. **b.** As in **a** but rotated roughly 90°, to show the internal cavity occupied by the putative priming loop and the PB1-N extension. Adapted from: *Nature*, 355, 516 (**2014**).

2.2.5.2. PA subunit

The two domains of PA, the PA-N endonuclease domain[149,150] and the large PA-C domain are on opposite sides, connected by the PA-linker which wraps around the external face of the PB1 fingers and palm domain. The endonuclease domain is solvent-exposed and faces the cap-binding domain. It is anchored to the rest of the polymerase through contacts with PB1-C that interacts with PB2-N, so that all the three subunits are involved in positioning the endonuclease[143]. The crystal structure revealed that PA-N is a member of the PD-(D/E)XK nuclease superfamily. It is composed of seven α-helices and a mixed five-stranded β-sheet, has a negatively charged cavity surrounded by α-helices and β-strands and houses one or two bivalent cations (Mg^{2+} or Mn^{2+}). The active site is characterized by a cluster of three acidic residues (Glu80, Asp108 and Glu119) and a putative catalytic lysine (Lys134) that, together with His41, are all absolutely conserved in influenza viruses (**Figure 14.**)[149,151] In particular, Lys134 is supposed to act as a catalyst of the endonuclease activity; in fact, the mutation of the lysine in position 134 with an alanine (K134A) has been shown to specifically abolish the

enzymatic activity[152]. PA-N cleaves single stranded RNA accordingly to two-metal-ion mechanism[153]. This mechanism implies that the first ion supports formation of attacking nucleophile by withdrawing electrons, while the second facilitates the exit of leaving group through neutralization of its negative charge. Moreover, both ions stabilize the transition state[154-156].

Structural reports are not consistent concerning the type and number of ions in the structures of PA-N. In the crystal structure of the first 197 residues of influenza H5N1 PA-N determined by Yuan[150], the binding metal appears to be a magnesium ion (Mg^{2+}), while in the study of Dias and coworkers[149] and Kowalinski and collaborators[157] there are two Mn^{2+} atoms in the active site. DuBois *et al.*[151] localized two Mn^{2+} ions in both sites coordinated by the same residues as for Kowalinski and co-workers. Pflug and colleagues in their work described in PA-N the presence of two divalent cations[143] while more recent structures of complete influenza virus polymerases showed that the two ions that are coordinated in the PA subunit are Mg^{2+} ions[145,158]. Mg^{2+} is one of the most abundant divalent cations in the living cells (~1 mM)[159] and it is found to be the most frequently used by the nucleic acid enzymes. However, when the Mg-dependent enzyme is activated with other ions, the efficiency and/or substrate specificity might be reduced[160]. Indeed, Mn^{2+}, which commonly replaces Mg^{2+} [161], exhibits less stringent coordination requirements, which lowers the substrate specificity and might rescue the deficient enzymes[162]. Moreover, Mn^{2+} is reported as a better Lewis acid and more efficiently than Mg^{2+} facilitates the formation of the attacking nucleophile[160]. A recent study[163], applying calculations of ion occupancy based on thermodynamic data, suggests Mg^{2+} to be a canonical metal in PA-N processing of RNA *in vivo.*

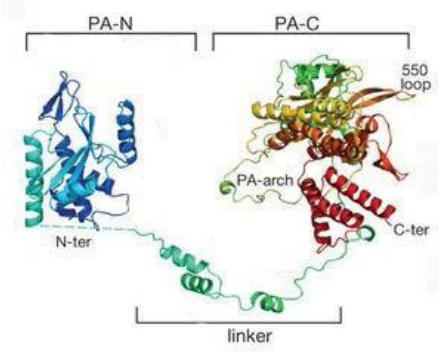

Figure 14. General structure of PA subunit. Adapted from: *Nature*, 355, 516 (**2014**).

2.2.5.3. PB2 subunit

The PB2 subunit is divided into the N-terminal part (PB2-N) and C-terminal portion (PB2-C), each of them formed by several folded sub-domains. PB2-N comprises a series of linked modules that wrap around one edge and face of PB1, interacting mainly with the C-terminal portion of PB1 and the polymerase thumb domain, opposite to where the PA linker binds. PB2-C forms a single, arc-shaped unit divided into sub-domains, which constitutes one arm of the polymerase U-shape. At one end of the arc there is the cap-binding domain, and, at the other end, the PB2 nuclear localization sequence (NLS) domain with, juxtaposed, the 627-domain, the main responsible for virus host-specificity which carry the host-specific PB2 residue 627 (lysine in human, glutamic acid in avian viruses and serine in bats). The central part of the PB2-C arc is composed of two disconnected but interacting sub-domains: the PB2 mid-domain that directly precedes the cap-binding domain, and the cap-627 linker. They seem not to make extensive interfaces with other polymerase subunits. (**Figure 15.**)[143]. The cap-binding domain has a compact, well-ordered α-β fold and it can initiate the "cap-snatching" and direct the capped primer first toward the endonuclease site and then into the polymerase active site for virus transcription[164,165]. As previously said, the 627-NLS-domain is an important determinant for the virulence and host adaptation of influenza viruses; in fact, different studies demonstrated that 627-mutants can greatly affect the virus in several aspects including replication, transcription, temperature sensibility and transmission[166-169].
The loop carrying the host-specific residue 627 is in a solvent-exposed position remote from the PB1 active site[143].

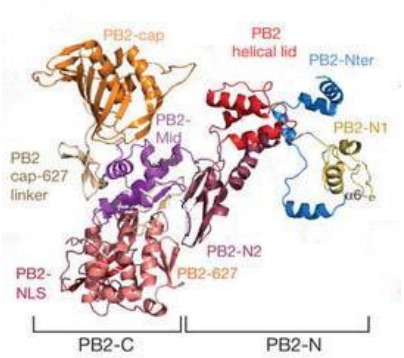

Figure 15. General structure of PB2 subunit. Adapted from: *Nature*, 355, 516 (**2014**).

2.2.6. Other viral proteins

The viral genome, in addition to that mentioned so far, codifies for other more recently discovered proteins, such as PB1-F2, PB1-N40, PA-X, PA-N155, PA-N182, M42, NS3 and PB2-S1, produced by open reading frames (ORFs) or ribosomal frame-shift. All these proteins play regulatory roles in virus replication acting as virulence factors or influencing viral transcription and replication[170].

PB1-F2 is expressed by some viral strains and it originates from the transcription of an alternative ORF on segment two of the IAV genome; it is expressed *via* a different translation initiation process from the fourth AUG codon. PB1-F2 is absent from some animal (particularly swine) influenza virus isolates, it has variable expression in individual infected cells, rapid proteasome-dependent degradation and mitochondrial localization[68,171], although some studies also show additional cytoplasmic or nuclear localization[172,173]. PB1-F2 is a virulence factor, associated with proapoptotic effects[68,174]; in fact, its oligomers assemble in a pH-dependent manner and form amyloid-like structures, inducing cell membrane damage and cytotoxicity in epithelial cells[175,176]. PB1-F2 also interacts with a number of host proteins modulating the IFN response or apoptosis; it interferes with the RIG-I/MAVS signaling pathway and activation of the host immune response[177-179]. Additionally, expression of PB1-F2 down-regulates the host superoxide anion dismutase 1 (SOD1), which increases the levels of reactive oxygen species, causing cell damage[180]. It also seems that PB1-F2 regulates the viral polymerase activity[172,181] and that it is involved in a predisposition for secondary bacterial infections[182].

The PB1-N40 is a 718-amino acid N-terminally truncated protein encoded by leaky ribosome scanning by discarding the first 39 codons from the regular 757-amino acids PB1 on segment two of the viral RNA. It is translated from the fifth AUG codon that is in-frame with the PB1 start codon. PB1-N40 sequence is identical to PB1 except for the 39 missing N-terminal amino acids that normally are responsible for the interaction with PA. Although PB1-N40 does not interact with PA and lacks transcriptase function, it can bind with other viral proteins, such as PB1 and its interaction partners PB2, NP, and PB1-F2. The localization of PB1-N40 is predominantly cytoplasmic, although in virus-infected cells its nuclear uptake is observed. PB1-N40 is able to affect the efficiency in the replication of IAVs, influencing the RdRp activity. Although viruses that lack PB1-N40 show slower replication kinetics, regulatory roles of the protein are not yet completely clear. It is important to underline that the

expression of PB1-N40, PB1-F2 and PB1 are interdependent; in particular, one of the functions of PB1-N40 is clearly associated with the maintenance in the balance between PB1 and PB1-F2 expression[69].

PA-X is a ribosomal frame-shift product of the segment three of the viral RNA; it is a fusion protein incorporating the N-terminal endonuclease domain of PA (191 amino acids) with a short C-terminal domain (61 amino acids) encoded by an overlapping ORF. PA-X modulates the host response and viral virulence, acting as a cellular gene expression repressor. It has been seen that PA-X modulates IAV virulence in a mouse infection model, acting to decrease pathogenicity and that loss of PA-X expression leads to changes in the kinetics of the global host response, notably including increases in inflammatory, apoptotic and T-lymphocyte signaling pathways[70].

PA-N155 and PA-N182 are translated from the eleventh and thirteenth in-frame AUG codons in the PA mRNA, respectively, *via* an alternative translation initiation process and are, therefore, N-terminally truncated forms of PA. The eleventh and thirteenth AUG codons are highly conserved among IAVs, suggesting that PA-N155 and PA-N182 expression is a universal feature. These N-truncated PAs do not show polymerase activity when expressed together with PB1 and PB2. However, these proteins have important functions in the replication cycle of IAV, as demonstrated by the fact that mutant viruses lacking PA-N155 and PA-N182 replicate more slowly in cell culture and have lower pathogenicity in mice than in wild-type viruses[73].

M42 is encoded by the alternative splicing of the seventh RNA segment. It is a M2-related protein with an antigenically distinct ectodomain that can functionally replace M2, despite showing clear differences in intracellular localization, being largely retained in the Golgi compartment. M42 is clearly non-essential for virus replication, as long as sufficient M2 is expressed. It is important to underline that the expression of two distinct ion channel proteins (M2 and M42) is not unique to laboratory-adapted viruses but, most notably, was also a feature of the 1983 North American outbreak of H5N2 highly pathogenic avian influenza virus[71].

NS3 is a product of alternative-splicing due to the NS1 nucleotide substitution of the alanine in position 374 with a glycine (A374G). NS3 is shown to provide replicative gain-of-function: in particular, it seems to be strongly associated with the virus ability to switch from avian to

mammalian hosts, including human, swine and canine populations, suggesting its role in host adaptation and overcoming species barrier[72].

PB2-S1 is encoded by spliced mRNA derived from the PB2 segment (N-terminal 495 amino acids of PB2-S1 are identical to those of PB2). PB2-S1 is localized to mitochondria, inhibits the RIG-I-dependent interferon signaling pathway, and interferes with the RdRp activity by binding to PB1. This viral protein appears to be highly conserved among pre-2009 human pandemic H1N1 virus, but not among human pandemic H1N1 and H3N2 viruses. Moreover, its deficiency has no effect on viral growth kinetics in cultured cells or on virus pathogenicity in mice. These findings suggest that probably PB2-S1 functions as an inhibitory factor for RIG-I-dependent IFN signaling during infection in animals other than mice, or that NS1, which exhibits strong inhibitory effects on innate immune responses, masks the effects of PB2-S1 during infection. However, further analyses are needed[74].

2.3. Antigenic drift and antigenic shift

The two major factors in influenza epidemics and pandemics are genetic drift and genetic shift. Antigenic drift leads to substitution of the amino acids on the surface of the viral transmembrane proteins (HA, NA and M2) that are recognized by existing antibodies.

Some regions of these proteins are more susceptible to change than others and these modifications should be ‘neutral’, as they do not affect the conformation of the proteins, or can cause conformational changes such that the binding of host antibodies is affected. Consequently, infecting viruses can no longer be inhibited effectively by host antibodies, allowing the virus to spread more rapidly among the population. Antigenic drift occurs on average every 2-8 years, in response to selection pressure to evade human immunity. In particular, it occurs in all strains of IAV and IBV, although the observed evolutionary patterns are dependent on the viral strain. It is possible that drift variants co-circulate with multiple co-existing lineages, allowing the re-emergence of old strains or the emergence of new variants that replace the old ones. Antigenic shift is a consequence of a process known as reassortment; it is only seen in IAVs, and results from the replacement of HA (and less frequently NA) subtypes with novel ones; this results in new viruses that have never been present in human circulation or last circulated decades before. Antigenic shift is estimated to

occur approximately three times every 100 years, which is in line with the three antigenic shifts (and resulting pandemics) that occurred during the 20th century (1918, 1957 and 1968).
Once a virus has undergone antigenic shift, it remains susceptible to antigenic drift; in fact, all currently circulating influenza viruses are drift variants of previous pandemic influenza strains. An important process that contributes to major shifts in influenza antigenicity is genetic reassortment, which is due to co-circulation of different IAV and IBV subtypes. It consists in mixing of genetic material between different viral strains and, although genetic reassortment can contribute to antigenic drift, it is primarily responsible for antigenic shift.
In particular, the genetic reassortment between human and avian IAV strains is important because it can produce a new virulent strain that has the potential to result in an influenza pandemic[183-185].

CHAPTER 3. Therapeutic treatments

Influenza is an acute disease that causes inflammation of epithelial cells that are present in the upper and lower respiratory tracts. The virus replicates starting from the time of inoculation and peaking after 48 hours, on average. While mild cases show only less pathological changes in the respiratory tracts, severe cases show clear evidence, such as redness and inflammation with mucous and purulent discharge macroscopically, desquamation and destruction of the pseudo-stratified epithelium of the trachea and bronchi with only the basal layer remained viable but inflamed, microscopically.

The immune reaction to the viral infection and the interferon response are responsible for the viral syndrome that includes high fever, coryza, cough, sore throat, myalgia, headache, runny nose, congested eyes and body aches. The acute symptoms persist for seven to ten days; in healthy persons the disease is self-limited, while high-risk groups who have chronic lung diseases, cardiac disease and pregnancy are more prone to severe complications, such as primary viral pneumonia, secondary bacterial pneumonia, hemorrhagic bronchitis, etc. Severe cases may progress to shortness of breath, tachycardia, hypotension and death[186].

3.1. Vaccination

Vaccination is regarded as the major prophylactic and therapeutic treatment of influenza infections, although the genetic drift in viral genome make it necessary to formulate new vaccines each year and the highly variable nature of the surface glycoproteins HA and NA does not make possible the development of a universal influenza vaccine.

Since their introduction in the 1940s, influenza vaccines have come a long way. Early vaccines were inactivated whole-virus vaccines that were generated in embryonated chicken eggs and inactivated by treatment with formalin. Today the major type, besides the conventional vaccines that consist of purified virus particles inactivated by treatment with formalin or β-propiolactone, are live attenuated influenza virus (LAIV) vaccines. LAIV vaccines are made using virus strains that are cold adapted, temperature sensitive, and attenuated to prevent them from causing illness. They have shown high efficacy in children when compared to inactivated vaccines, because they activate mucosal, systemic humoral,

and cellular immunity, just like natural influenza viruses. However, constantly updated knowledge of the antigenic properties of the new circulating strains is necessary for the timely production of vaccines. Since perfect updates are often unavailable, some strains will not be covered by the vaccines. Apart from the traditional vaccines, other approaches include the development of DNA vaccines against different influenza virus antigens, the research of a possible universal influenza vaccine targeting the HA stalk domain, and the use of influenza-virus-like particles as vaccines[187,188].

3.2. Antiviral agents targeting viral proteins

A part from the use of vaccines, viral infections can be inhibited at several crucial steps, such as entry, assembly and release, by the use of antiviral agents that act as supplementary protective and therapeutic treatments during seasonal influenza epidemics. Antivirals are also capable of reducing the unpredictable impact of a fast-moving pandemic. It is possible to have an antiviral effect both targeting important proteins for the virus life cycle and targeting host proteins that play crucial roles during influenza virus infection. Among antiviral agents targeting functional viral proteins, there are two classes of FDA licensed drugs: neuraminidase inhibitors (NAI) such as oseltamivir (Tamiflu®), zanamivir (Relenza®), peramivir (Rapivab®) and laninamivir (CS-8958), this latest approved only in Japan, and the M2 ion channel inhibitors, which are the adamantane derivatives amantadine (Symmetrel®) and rimantadine (Flumadine®). Very recently (October 2018), FDA approved the cap-dependent endonuclease inhibitor baloxavir marboxil (Xofluza®). However, there are other agents in late stage development or in clinical trials as influenza therapeutics, acting on different key steps of the viral replication; for example, favipiravir, which targets the viral RdRp, is conditionally approved in Japan (**Figure 16.**)[188, 189]. Below, I will mention the main anti-influenza drugs and the most promising molecules, natural and synthetic, recently developed; the molecules are inserted within the different paragraphs according to the target on which they act.

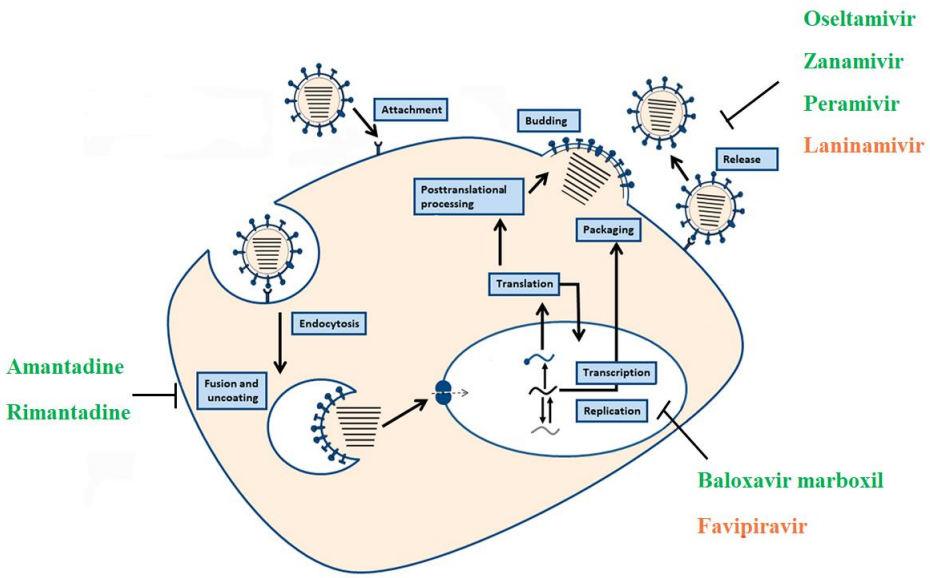

Figure 16. Mode of action of the most important approved influenza virus antivirals. FDA approved drugs are shown in green while those approved in other countries are shown in orange. Adapted from: *ACS Infect Dis*., 3, 691-694 (**2017**).

3.2.1. HA inhibitors

Among HA inhibitors, there are some natural products, as well as synthetic antiviral drugs that have been approved for the influenza treatment or are being tested in clinical trials. In the 1970s, gossypol, **1a**, a natural phenolic aldehyde extracted from cotton plant, was found to be effective against pneumonia caused by influenza virus[190]. Starting from this study, Yang and co-workers synthesized a series of gossypol and gossypol acid derivatives, **1b** and **2** respectively, and tested them *in vitro* for their anti-H5N1 activity. This lead to the discovery of some gossypol-related molecules having a good anti-H5N1 activity, with the HA2 protein as a probable target[191].

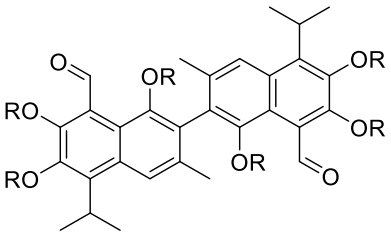

a R = H
b R = CH_3 or $COCH_3$

1

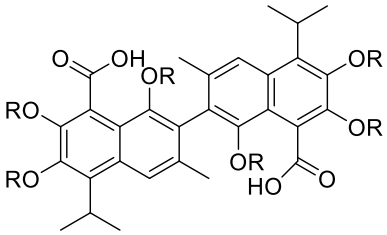

R = CH_3 or $COCH_3$

2

Further studies found that other natural products (or their derivatives) such as rutin **3**[192,193], quercetin **4**[193-195], xylopine **5**[193,196] and theaflavin **6**[197,198] are multitarget antiviral agents, acting especially as HA inhibitors.

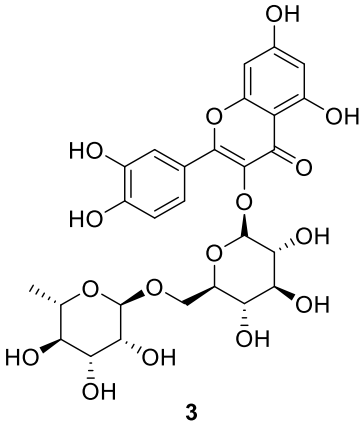

3

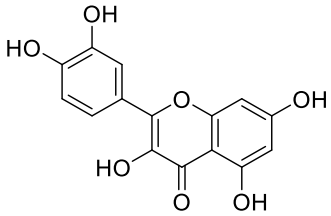

4

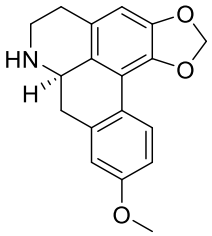

5

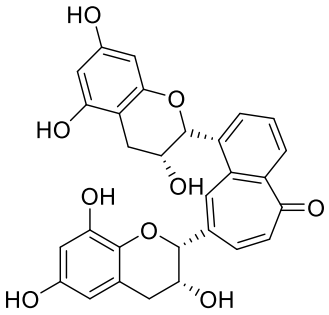

6

In 1996, Luo and colleagues found and characterized a novel inhibitor of influenza virus: BMY-27709, **7**. This compound contains a salicylamide scaffold and has been identified as specific for the IAV. In particular, it has an IC_{50} of 3-8 μM for A/WSN/33 virus and is active against H1 and H2 subtypes, while is inactive against H3. The fact that BMY-27709 is active in the early infection stages, suggests that the target for inhibition is the HA protein. This was confirmed through the use of reassortant viruses and the isolation of a virus resistant to BMY-27709. The isolated resistant virus contained a mutated amino acid in the HA2 subunit (a phenylalanine substituted with a serine in position 110). This single mutation is responsible for the acquisition of resistance to BMY-27709, as demonstrated through reverse genetics: transfectant viruses harboring only the mutation in position 110 were shown to be resistant to

BMY-27709, while the control viruses without this mutation remained sensitive to the inhibitor[199]. Further studies done by the same group indicated that BMY-27709 blocks the HA-mediated fusion process, and it may act either by prematurely promoting the conformational change or through the inhibition of the low pH-induced conformational change of HA; both mechanisms result in the same outcome, the inactivation of the fusion activity of the HA protein[200].

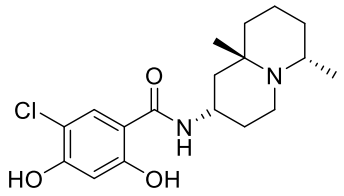

7

Another HA inhibitor that was found in the '90s is stachyflin, **8**. Similarly to BMY-27709, it is active against the H1 and H2 subtypes of IAV. Experiments have suggested that stachyflin blocks the HA-mediated cell fusion process by inhibiting the conformational transition of the HA protein[201].

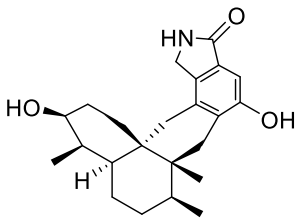

8

Thiazolides are powerful broad-spectrum antiviral drugs. In the case of IAVs, it has been shown that they act at a post-translational level, by selectively blocking the maturation of the viral HA, impairing HA intracellular trafficking and insertion into the host plasma membrane, a key step for correct assembly and exit of the virus from the host cell[202]. Among thiazolides, nitazoxanide, **9**, is active against a great number of RNA and DNA viruses, such as respiratory syncytial virus, coronavirus, rotavirus, norovirus, hepatitis B and C, dengue, yellow fever, japanese encephalitis virus and human immunodeficiency virus in cell culture

assays[203,204]. Belardo and co-workers showed that nitazoxanide inhibits also a broad range of IAV and IBV, with IC_{50} values ranging from 1.0 to 3.2 μM against different viral strains in Madin-Darby canine kidney (MDCK) cell-based CPE (cytopathic effect) assay. They made also combination therapy studies, in order to investigate the effect of nitazoxanide when administered in combination with oseltamivir or zanamivir, using as a model the H1N1 PR8/IAV strain in MDCK cells; the results show that nitazoxanide-neuraminidase inhibitor combination treatments are synergistic[205]. Today nitazoxanide is in clinical trial, under phase III studies[206,207].

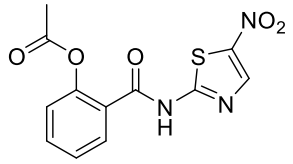

9

Recently, Stachulsky and co-workers developed a series of nitazoxanide derivatives, providing important new lead compounds; some of them show good activity against an H1N1 strain of IAV in MDCK cells, with the most active derivative **10** having an IC_{50} of 0.14 μM[208].

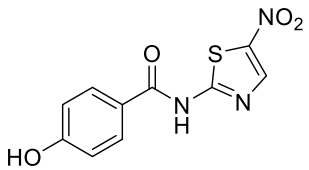

10

CL-385319, **11**, an N-substituted piperidine, was proved to be effective in inhibiting infection of H1-, H2-, and to a lesser extent, H3-type IAVs by interfering with the fusogenic function of the viral HA. In particular, CL-385319 is effective in inhibiting infection of highly pathogenic H5N1 IAV in MDCK cells with an IC_{50} of 27.0 μM and low cytotoxicity. Computer-aided molecular docking analysis suggests that CL-385319 might bind to the cavity of HA2 stem region which is known to undergo significant rearrangement during membrane fusion[209].

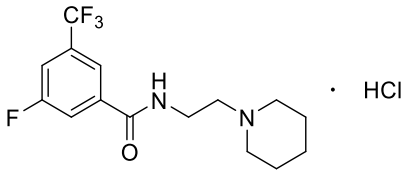

11

Compound **12** is a trivalent glycopeptide mimetic, having a trisubstituted acid derived core which is bound by flexible hexyl chains to a nonapeptide linkers ending with a flexible alkyl chain and the sialic acid epitope. It is an inhibitor of HA (H5) of avian influenza, with a K_i of 15 μM, and binding studies showed that it has an affinity for hemagglutinin H5 (A/Vietnam/1203/2004) increased by a factor of 4,000 compared to the natural ligand α-methyl glycoside of *N*-acetylneuraminic acid[210].

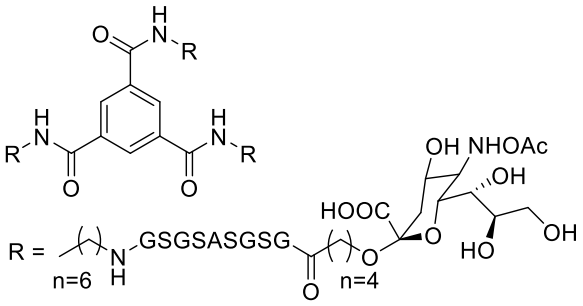

12

One year later, Dang and colleagues found that a series of podocarpic acid derivatives (for example, compound **13**) exhibited potent activities, having EC_{50} values ranging from 140 to 640 nM against MDCK cells infected with an adapted influenza virus (A/PuertoRico/8/34, an oseltamivir- and amantadine-resistant H1N1 strain)[211].

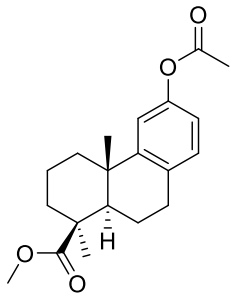

13

Also natural pentacyclic triterpenoids show inhibitory activity against influenza viruses, which are comparable to or even more potent than that of oseltamivir. Mechanistic studies show that these molecules bind tightly HA, disrupting the interaction between HA and the sialic acid receptor and thus the attachment of the virus to the host cell. Among them, compound **14** is effective against the influenza A/HuNan-ZhuHui/1222/2010 H3N2 strain (amantadine- and ribavirin-resistant), A/LiaoNing-ZhenXing/1109/2010 H1N1 strain (oseltamivir-resistant), and even the influenza B/ShenZhen/155/2005, with EC_{50} values of 3.18, 6.58, and 2.80 μM, respectively, in a MDCK cell-based CPE assay[212].

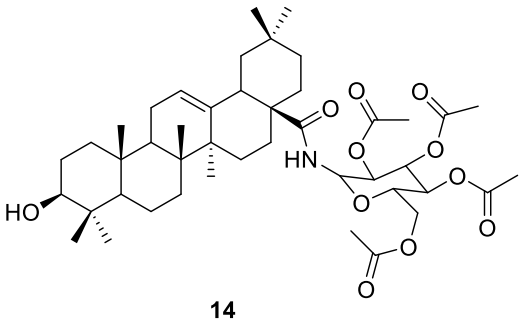

14

In 2015, Chen and colleagues found that the indole alkaloids obtained from the marine fungus *Erotium rubrum* have antiviral activity. In particular, neoechinulin B, **15**, shows a potent inhibition against H1N1 virus in MDCK cells, and is able to inhibit a panel of influenza virus strains including those amantadine- and oseltamivir-resistants. The EC_{50} values of neoechinulin B against A/LiaoNing-ZhenXing/1109/2010 H1N1, A/HuNan ZhuHui/1222/2010 H3N2 and A/WSN/33 H1N1 are 16.89, 22.22 and 27.4 μM, respectively, in MDCK cell-based CPE assay. Mechanisms of action studies indicate that neoechinulin B binds to HA, disrupting its interaction with the sialic acid receptor and the attachment of

viruses to host cells. The high potency and broad-spectrum activities together with low drug resistance make neoechinulin B a new lead for the development of potential inhibitors of influenza viruses[213].

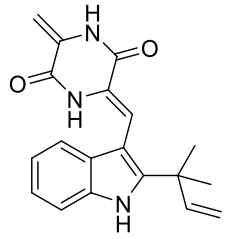

15

Another natural product, aureonitol **16**, a tetrahydrofuran derivative obtained from *fungi*, has demonstrated inhibitory effects in the nanomolar range against both IAV and IBV adsorption. Molecular modeling studies indicate that aureonitol forms hydrogen bonds with highly conserved HA residues. Altogether, these results suggest that the chemical structure of aureonitol should be a promising starting point for future anti-influenza drug design[214].

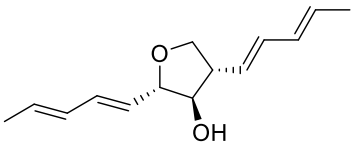

16

Curcumin **17** is a multi-target natural product that can also inhibit the IAV entry acting on HA, with an EC_{50} of approximately 0.47 μM in plaque reduction assay (PRA)[215]. Simulation docking of curcumin with the HA structure revealed that the molecule binds to the region in which there are sialic acid anchoring residues. It seems that the presence of the double bonds in the central seven-carbon chain of curcumin is important for the antiviral activity and interferes with virus entry by interacting with the receptor binding region of viral HA protein[216]. More recently, Liu and collaborators identified curcumin as an inhibitor of RNA binding by NP, highlighting this structure as a potential lead for further drug development in the field of antiviral agents[217].

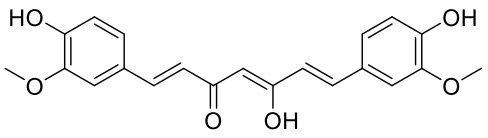

17

Arbidol (known also as umifenovir) **18a** shows efficacy against influenza viruses by targeting the HA fusion machinery. In 2017, Kadam and co-workers determined crystal structures of arbidol in complex with influenza virus HA from H3N2 and H7N9 viruses. It was seen that arbidol binds in a hydrophobic cavity in the HA trimer stem, primarily making hydrophobic interactions with the binding site but also, inducing some conformational rearrangements to form a network of inter- and intra-protomer salt bridges. By functioning as molecular glue, arbidol stabilizes the prefusion conformation of HA inhibiting the large conformational rearrangements associated with membrane fusion in the low pH of the endosome[218]. Wright and co-workers designed and synthesized several molecules to try to improve the antiviral activity of arbidol. They found a new arbidol analogue **18b** with significantly improved binding to HA in comparison to the parent compound; in particular, **18b** has 98-fold and 1150-fold increased affinity against H1 and H3 HAs, respectively[219].

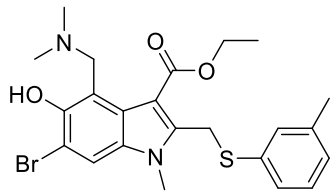

a R = H
b R = OH

18

A number of monoclonal antibodies that target viral HA are recently being investigated as potential influenza therapeutics. All these antibodies bind to the more conserved stalk portion of HA, and thus, they have broad antiviral activity against several IAV subtypes. The compounds in clinical development include MEDI8852 (MedImmune, LLC), MHAA4549A (Genentech, Inc.), VIS-410 (Visterra, Inc.), CT-P27 (Celltrion, Inc.), CR6261 and CR8020 (both Crucell, from 2011 acquired by J&J, Inc.)[220]. Mechanistically, these HA antibodies work by preventing the fusion of the virus with the host cell, and stimulating antibody

dependent cell-mediated cytotoxicity *in vivo*[221,222]. Some antibodies, for example MEDI8852, have been shown to be superior or at least as effective as oseltamivir in preclinical animal studies, depending on the virus subtype[223]. Among engineered human antibody, is worth to mention VIS410, an IgG1 antibody that targets a unique, conserved conformational epitope on the stem of HA protein of IAV[224]. Preclinical studies demonstrated that VIS410 is active against several IAV strains and is able to rapidly reduce viral titers[225]. A more recent phase I clinical trial (NCT02045472) showed that it is generally safe and well tolerated, even at the relatively high dose levels[226]. Today VIS410 is in phase II clinical trial sponsored by Visterra, Inc. (NTC03040141), for evaluating its efficacy and safety of its intravenous administration in addition to oseltamivir in hospitalized adults with influenza A infection. Regarding MHAA4549A, it has shown to be well tolerated in healthy volunteers without IAV infection in two phase I studies[227] and results from an earlier phase II trial (NCT01980966), evaluating its safety and efficacy in an influenza model, show that MHAA4549A is well tolerated and significantly reduces viral loads[228,229]. Two phase II clinical trials (NCT02603952 and NCT02293863) to evaluate the effects of MEDI8852 and MHAA4549A alone or in combination with oseltamivir has been completed, but the results have not yet been published[188,189].

3.2.2. M2 channel blockers

The M2 channel is an important target for antiviral drugs, although mutations surrounding the binding site lead virus to escape drug inhibition. Three major amantadine-resistant M2 mutants have been identified: serine in position 31 to asparagine (S31N), valine in position 27 to alanine (V27A) and leucine in position 26 to phenylalanine (L26F). Among these, S31N is the predominant mutant and is present in more than 95% of currently circulating influenza viruses[230]. M2 inhibitors can be classified in two groups based on their structure. The first group includes the adamantanes, formally named tricyclo[3.3.1.1]decanes, and their analogues; all these compounds have a hydrophilic head and a hydrophobic body, and, due to these features possess the ability to penetrate the bilayer lipid membrane. The second group is composed of non-adamantane derivatives.

The adamantane-based compounds have been approved for a wide spectrum of indications (antivirals, antidiabetics and against Alzheimer's and Parkinson's disease). For example,

memantine **19** was investigated for its antiviral activity, and recently proposed for the treatment of the neuronal death induced by Zika virus infection[231]. Apart from the memantine, the two first major antiviral molecules in the class of the adamantanes are amantadine (Symmetrel®) **20** and rimantadine (Flumadine®) **21**, approved for clinical use in 1966 and in 1993, respectively. They inhibit virus multiplication by interfering with the transmembrane domain of M2 protein of IAVs and with virus assembly. At low concentration (< 1 μg/mL) amantadine and rimantadine inhibit the replication of IAV by blocking the M2 channel, while at higher concentration (> 50 μg/mL), because of their basicity, they buffer the endosomal pH and reduce the acidity of the environment that is essential for the fusion between the viral membrane and the endosome, mediated by HA. It is important to underline that rimantadine is four/ten time more active than amantadine and has less collateral effect, probably because of its extensive biotransformation. Neurotoxic effects (such as confusion, disorientation, anxiety, jitteriness, etc.) caused by amantadine are usually common, especially when the drug is used more than a week. Moreover, today drug resistance has limited adamantane clinical use[34]. Currently, amantadine and rimantadine cannot be recommended as a prophylactic drug for the treatment of influenza both in children and in adults. Nevertheless, if we consider that they are safe drugs and take into account the possibility that the next pandemic virus is susceptible to this class of compounds, as indicated in former pandemics, we can still consider these "old" drugs as a less costly alternative to neuraminidase inhibitors[232].

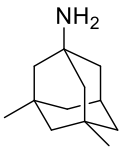

19

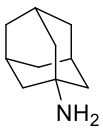

20

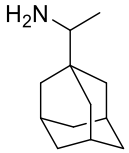

21

Adamantane derivatives **22** e **23** are rimantadine analogs developed by Tataridis and co-workers. In compound **22** the α-methyl group of rimantadine is replaced with a α-(amino methyl) group, while compound **23** resulted by the introduction of a piperidine ring on the 1-aminoethyl pharmacophore group. They are about 2- or 3-fold more potent than amantadine and are equipotent to rimantadine. The presence of two primary and two secondary amino groups, respectively, make the molecules capable of forming favorable hydrogen bonds and Van der Waals interactions with the M2 receptor[233]. Spiropiperidine-adamantanes, such as the

spiro[adamantane-2,2'-piperidine] **24**, are also effective against M2 protein and show activities against amantadine-resistant viruses[234]. Du and co-workers developed a series of adamantane-based inhibitors with the introduction of a supplementary pharmacophore group, synthesizing compounds **25** and **26**. These molecules have a significantly enhanced ability in inhibiting the M2 channel in comparison with amantadine and rimantadine, although the second additional hydrophilic group might cause a decrease in the ability in penetrating the cell membrane[235].

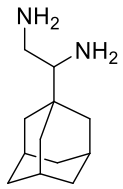

22

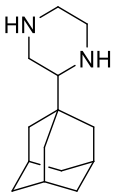

23

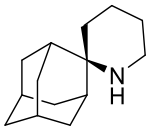

24

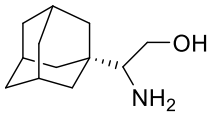

25

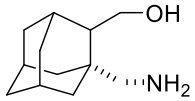

26

Many efforts have been made to discover new small molecular inhibitors of amantadine-resistant mutant forms of IAV M2 channel. Wang and colleagues developed a class of benzyl-substituted amantadine derivatives with activity against both S31N and wild-type M2 viral channel, among which compounds **27** and **28** are the most potent dual inhibitors[230,236,]. Wu and collaborators found other M2 channel blockers that are able to inhibit the wild-type and the S31N mutant comparably with amantadine inhibition of wild-type influenza virus. The most active compound of this series is **29**[237].

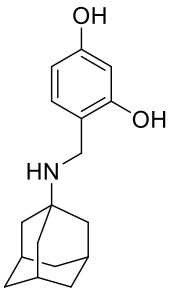

27

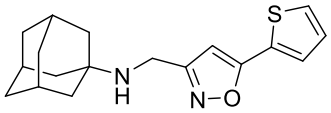

28

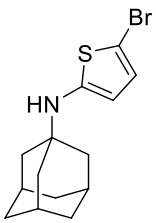

29

Regarding the V27A mutation of the M2 ion channel, Rey-Carrizo and colleagues synthesized and characterized a series of compounds containing the 3-azatetracyclo[5.2.1.1^{5,8}.0^{1,5}]

undecane scaffold, designed as analogs of amantadine; the most active of them, compound **30**, inhibits the A/M2 V27A mutant ion channel in the submicromolar range (IC_{50} = 0.29 μM)[238].

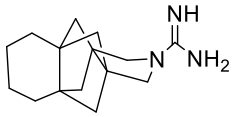

30

Further studies by the same research group on mutants of the M2 channel led to the discovery of amine **31** and guanidine **32** as low micromolar inhibitors of the wild-type channel and the L26F mutant, and submicromolar inhibitors of the V27A variant[239].

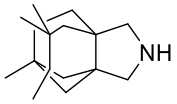

31

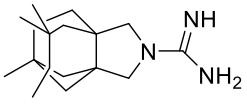

32

Regarding non-adamantane derivatives, polyamines, such as spermine **33** and spermidine **34**, are effective against influenza virus, acting on a specific binding site at the M2 protein. Lin and colleagues showed that the M2 channel inhibition activity of polyamines occurs at lower concentration in conditions in which there is a depletion for Na^+ than in the presence of a physiological Na^+/K^+ gradient, suggesting that influenza M2 protein possesses a binding site for polyamines, distinct from the amantadine binding site, which is normally masked by Na^+. The proposed binding site could be an interesting target for the development of selective antiviral inhibitors[240]. It is important to underline that spermine is one of the component of a polycationic sphingolipid (ceramidecarbamoyl-spermine, CCS) that, in the form of micelles or liposomes with cholesterol (C), is the component of CCS/C-based liposomal vaccine (also known as VaxiSome™)[241,242].

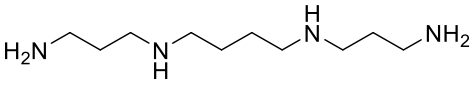

33

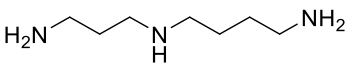

34

Natural products such as pinanamine derivatives also exhibit good anti-influenza activities. In particular, the most promising is compound **35** that is active as inhibitor of A/M2 wild type and A/M2-S31N mutant channels, and in the case of the S31N mutant displays improved inhibition compared to amantadine[243].

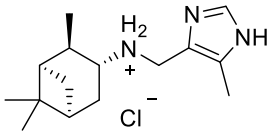

35

TCN032, that is an antibody targeting the IAV M2 protein, is in clinical trial. It has been developed by Theraclone Sciences and specifically binds to the conserved ectodomain of M2, which is exposed on the surface of infected cells; in doing so, it prevents virus budding and thus acts *via* a very different mechanism from the M2 ion channel inhibitors. TCN032 has been evaluated in a phase II study and found to be safe and effective at reducing symptoms and virus shedding, when administered one day post-infection[189,244].

3.2.3. M1 protein inhibitors

Mopyridone **36**, a compound which was identified from a screening of a series of tetrahydro-2(1*H*)-pyrimidinone derivatives by Galabov and colleagues, has a large spectrum anti-influenza activity on different A and B viral strains *in vitro* and *in vivo*. Very importantly, this compound is the first anti-flu agent that has been shown to have M1 protein as a target[245], with a low acute toxicity in mice[246]. Starting from a screening on a library of more than 70,000 commercially available small molecules, Mosier and co-workers found some compounds that act as inhibitors of M1 protein. In particular, the lead compound **37** acts as "wedge", avidly binding to M1-M1 interface and weakening M1-M1 self-association. It was seen that it reduces the thickness of the M1 layer in mature virions and inhibits *in ovo* propagation of multiple IAV strains including H1N1, H3N2 and H5N1. These findings highlight the possibility to develop new promising antiviral agent acting with this innovative mechanism of action[247].

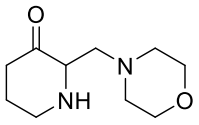

36

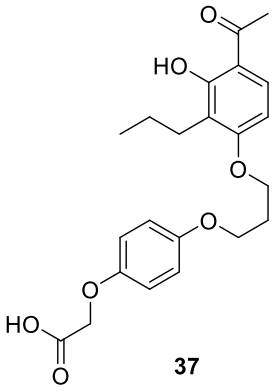

37

More recently, Ai and co-workers proved that some compounds belonging to the Traditional Chinese Medicine, such as *Corydalis Rhizoma*, *Mori Folium*, *Forsythiae Fructus*, *Salvia*, *Lonicerae Japonicae Flos, Menthae Herba*, have efficacy in the treatment of influenza, acting on different targets, including M1 protein[248].

3.2.4. NA inhibitors

Neuraminidase inhibitors (NAIs) act by preventing the release of the new viral particles and, although the emergence of NAI resistance could be a relevant clinical concern, they constitute the only class of antivirals recommended for the control of influenza epidemics and eventual pandemics, being active against all IAV subtypes and the two main IBV lineages. The two major NAI are zanamivir (Relenza®) and oseltamivir (Tamiflu®), that are analogues of the enzymatic transition state. In fact, the study of the crystal structure between the enzyme and the sialic acid, led to the identification of the mechanism of hydrolysis that was the starting point for the development of analogues of the transition state.

In the 1970s Meindl and colleagues synthesized the 2-deoxy-2,3-dehydro-*N*-trifluoroacetylneuraminic acid (FANA)[249] and the 2-deoxy-2,3-dehydro-*N*-acetilneuraminic acid, Neu5Ac2en (DANA)[250] which are analogues of the sialic acid. In the 1990s, Holzer and co-workers modified the structure of DANA, introducing a guanidino group in C4, and obtained zanamivir **38**, that is able to bind NA more efficiently than the previous compounds, by forming a new interaction between amino acids Glu119 and Glu227[251]. In particular, zanamivir is a slow-binding inhibitor with a high affinity for NA. It is effective against influenza A/Singapore/1/57 and B/Victoria/102/85 virus with IC_{50} values of 14 nM and 5 nM,

respectively, in MDCK assays. In 1999, the FDA and EMA approved zanamivir as the first NA inhibitor agent, although for its very low oral bioavailability (2-3%) it must be administered *via* inhalation. Based on the structure of zanamivir and on studies of its three-dimensional conformation[252], Kim and collaborators[253] synthesized oseltamivir **39**, which is an ethyl ester prodrug that requires hydrolysis to be converted to the active form (oseltamivir carboxylate, GS-4071). It shows IC_{50} values in the range 0.3-1.5 nM against representative N3-N9 NAs and it has enhanced oral bioavailability, because of the esterification of the acid function and the bulky lipophilic side chain. In 1999, oseltamivir, as phosphate, was the first NA inhibitor for oral administration approved by FDA and then by EMA, and, by now, it is the most popular NA inhibitor in the clinic. It is important to underline that, although in the past there was a rapid rise in oseltamivir resistance among H1N1 IAVs[254], in the last years this resistance has been observed only sporadically[255].

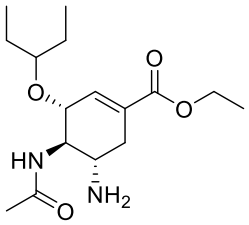

38

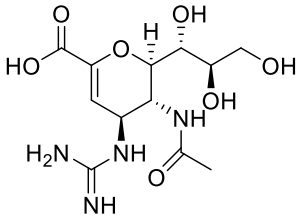

39

Another NAI is peramivir **40** (Rapivab®, BCX 1812); this pentacyclic derivative was developed with the aim of obtaining a compound able to interact, through its side chains, with the lipophilic regions of NA. *In vivo* and *in vitro* studies demonstrated that it has activity against both IAV and IBV[256]. In 2009, peramivir was approved by the FDA for the emergency treatment of hospitalized patients infected by H1N1[257,258]. The emergency use authorization for peramivir expired in June 2010, and on December 2014 the FDA approved its intravenous administration to treat influenza infection in adults[259]. In 2016 the drug was also approved by EMA[260]. The clinical efficacy of peramivir was assessed by randomized controlled trials, in which it was administered by intravenous or intramuscular injection in adults and today further clinical trials are ongoing[188,189,261]. The newest NAI drug is laninamivir **41** (R-125489). It is a long-term NA inhibitor that shows potent NA inhibitory activity against eleven strains of H1N1 viruses, fifteen strains of H3N2 and twenty three strains of IBV with IC_{50} values in the range 1.29-5.97 nM, 7.09-38.80 nM and 10.40-31.40

nM, respectively, in enzymatic assays. Laninamivir octanoate (CS-8958), the prodrug of laninamivir, is approved in Japan since 2010, and appears to be effective for patients with oseltamivir resistance[262-264]. To date, laninamivir octanoate is in phase III clinical trial[265]. Its distinguishing property is a long half-life, and patients can be effectively treated with a single dose[266].

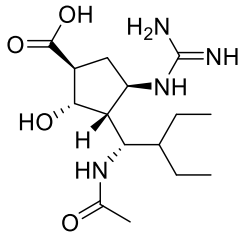

40

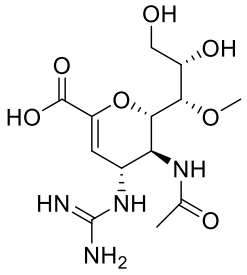

41

The recent progress in researching NA inhibitors has mainly focused on the structure modification/optimization of zanamivir and oseltamivir. Compound **42** (A-315675) is a potent NA inhibitor discovered by Abbott researchers, who demonstrated that the basic group, previously deemed necessary for the interaction with the amino acid residues Glu119, Glu227 and Asp151 in NA, can be replaced by a hydrophobic *cis*-propenyl group[267].

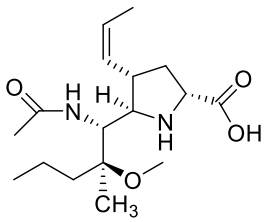

42

Starting from this knowledge, Hanessian and co-workers synthesized a series of analogues of GS-4071, in which the basic amino group is replaced by a hydrophobic vinyl group. Among these molecules, compound **43** is the most active, having a K_i value in the nanomolar range (K_i = 45 nM). Its co-crystal X-ray structure with NA confirmed the binding mode in which the vinyl group projects into the region occupied by the amino group that is present in oseltamivir carboxylate, highlighting the importance of hydrophobic interactions for NA inhibition[268]. It is important to underline that the introduction of a hydrophobic substituent could be

advantageous also in terms of drug pharmacokinetics: in fact, the zwitterionic character of zanamivir and oseltamivir containing a guanidino or amino group limits their oral bioavailability.

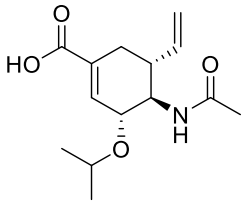

43

A series of triazole substituted carbocycles, synthesized by Mohan and collaborators, is active as NAI. For example, compound **44** has a K_i value of 72 nM against virus-like particles, possessing an IAV N1 activity[269]. The same researchers also discovered a series of N-substituted oseltamivir analogs (general structure **45**). It was seen that derivatives containing relatively small N-guanidine substituents (N-methyl and N-hydroxyl) display enhanced inhibition against NA derived from oseltamivir-resistant and wild-type strains, showing IC_{50} values in the low nanomolar range[270,271]. The spirolactam **46** has an *in vitro* potency that can be comparable to that of compound **45**; it is noteworthy that, although the spiro-fused ring in place of the guanidine group alters the strong hydrogen-bond network, it does not affect the inhibitory activity appreciably. Moreover, this modification could be useful for enhancing the bioavailability[272].

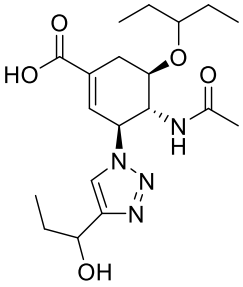

44

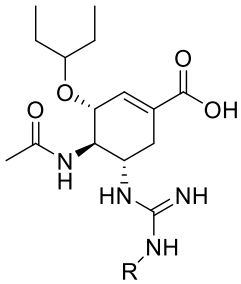

R = small alkyl groups, OH

45

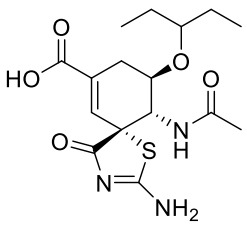

46

In 2012, Cheng and co-workers synthesized a series of oseltamivir analogs: oseltamivir phosphonic acid (tamiphosphor, **47a**), its monoethyl ester (**47b**), guanidine tamiphosphor

(**48a**) and its monoethyl ester (**48b**), as potent NAIs. They inhibit the replication of influenza viruses, including the oseltamivir-resistant H275Y strain, at low nanomolar to picomolar levels. These compounds, when orally administered at 1 mg/kg or higher doses, significantly protect mice from infection with otherwise lethal doses of influenza viruses. These compounds are stable in simulated gastric fluid, liver microsomes and human blood, and are largely free from binding to plasma proteins. Pharmacokinetic properties of these inhibitors have been studied in dogs, rats and mice[273].

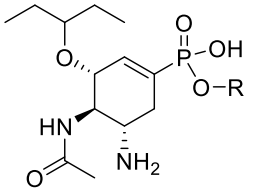

a R = H
b R = CH_2CH_3

47

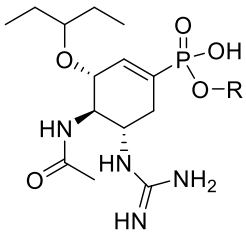

a R = H
b R = CH_2CH_3

48

In 2013, Kim and co-workers designed a series of covalent NA inhibitors (represented by compound **49**) by introducing the strong electronegative fluorine atom in the core-ring of zanamivir and oseltamivir. These compounds form transient covalent intermediates with Tyr406 located in the catalytic domain of NA, thereby gaining potent broad-spectrum inhibitory activity against drug-resistant strains. They show good antiviral activity *in vitro* and high efficacy as enzyme inhibitors. For example, compound **49** has IC_{50} values of 1 and 10 nM against B/Perth/211/01 and A/Fukui/45/01 H3N2, respectively, in PRA. Furthermore, they show good inhibition of NAs from zanamivir- or oseltamivir-resistant influenza virus strains, indicating an altered resistance profile, and they function well in controlling influenza infections in an animal model, at levels comparable to those used for zanamivir[274].

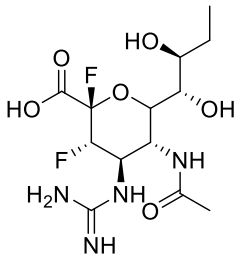

49

Schade and collaborators synthesized other oseltamivir analogs, in particular, oseltamivir amidine **50** and its bifunctional prodrug amidoxime ethyl ester **51**. Compound **50** has a potency comparable to that of oseltamivir against different wild-type IAV strains, but additionally shows efficacy (IC_{50} = 14.5 nM) against oseltamivir-resistant influenza A/Berlin/55/08, H275Y mutant. Docking experiments revealed that the compound is able to make additional interactions in the NA active site, to a similar extent as guanidine-containing NAIs. Amidoxime prodrug **51** exhibits an *in vivo* pharmacokinetic profile that is competitive with oseltamivir, with comparable oral bioavailabilities (31% *versus* 36%). A possible asset of this molecule can be seen in its prolonged plasma half-life (111 minutes *versus* 44 minutes for oseltamivir) that means a retardation effect that could be beneficial for the required dosing regimen. In general, the amidine-based oseltamivir derivatives exhibit excellent *in vitro* properties, have a good pharmacokinetic profile, are stable under various physiologically relevant conditions, do not excessively bind to plasma proteins and are sufficiently bioactivated[275].

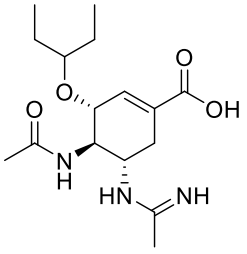

50

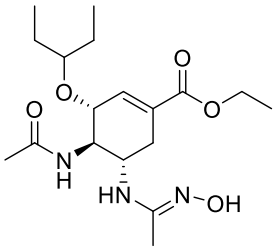

51

Previously, also dimeric (or tethered) zanamivir conjugates were synthesized in order to achieve multivalent binding. Some of these derivatives showed to be highly potent NA inhibitors, with broad-spectrum activity[276-278]. Among dimeric derivatives of zanamivir, the viral NA inhibitor BTA938, containing a fourteen-carbon linker bridging two zanamivir moieties, has high antiviral activity as demonstrated by visual and colorimetric determination

of the inhibition of CPE plus PRA. The EC_{50} values are in the low nanomolar range, with BTA938 exhibiting higher potency than zanamivir, oseltamivir and laninamivir for the majority of viruses tested. Moreover, it was demonstrated that single-dose BTA938 protects mice from pandemic H1N1 virus infection and is equivalent to multiple doses of zanamivir for an oseltamivir-resistant strain (H275Y)[279].

In the field of NAIs having a different structure than that of zanamivir and oseltamivir, we have to remind pyrrolidine and benzoic acid derivatives, dextran sulphate and AV5080. Some pyrrolidine derivatives were found to be effective against IAVs and IBVs acting as NAIs. For example, compound **52** shows an IC_{50} of 0.2 μM against NA A/Tokyo and 8 μM against NA B/Memphis, in the NA inhibition assay[280].

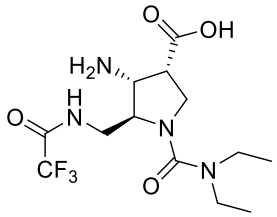

52

With the aim to find novel potent NA inhibitors, benzoic acid derivatives (as example, structures **53** and **54**) have been developed; some of these compounds have antiviral activity with IC_{50} values in the low micromolar range[281-283].

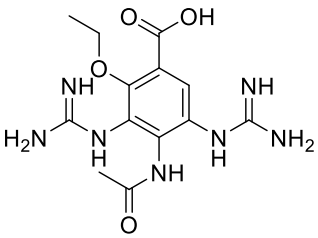

53

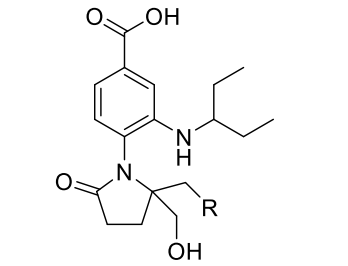

R = OH, NH_2, CH_2OH, CH_2NH_2

54

The negatively charged sulphated polysaccharide dextran sulphate (DS), **55**, was considered an inhibitor of the HA-dependent attachment of the virus to the cell[284,285], while more recently it seems that is mainly involved in the late stage NA-dependent of the viral infection. The

suppression of NA activity and virus release depend on both DS's negative charge and on the characteristics of NA, but it is not yet clear which amino acid(s) of NA are responsible for DS's suppressive effect, and the mechanism by which DS suppresses viral replication[286]. Studies on recombinant viruses having mutation(s) on NA gene show that DS severely suppresses oseltamivir-resistant recombinant virus H274Y in PRA, highlighting the possibility to use it in combination with the currently used NA inhibitors, such as oseltamivir[287].

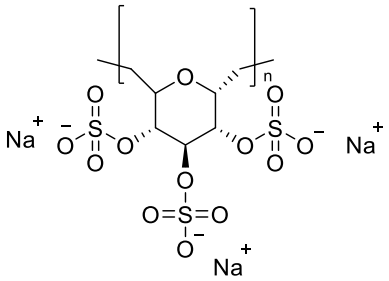

55

AV5080, **56**, has a subnanomolar activity against influenza virus NA *in vitro*, with IC_{50}s of 0.03 nM and 0.07 nM against NA of A/Duck/Minnesota/1525/1981 H5N1 and A/Perth/265/2009 H1N1 in NA enzyme based assays, respectively. It is highly potent also against oseltamivir-resistant strains. Preclinical studies on this molecule are warranted[288].

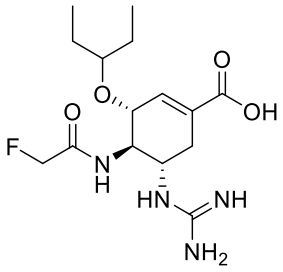

56

Also some natural products and their derivatives have been found to possess anti-influenza activities acting on NA. Ginkgetin-sialic acid conjugates (compound **57**) show potent anti-influenza virus activities *in vivo*, significantly improving the survival rate of mice infected with the A/PR/8/34 (H1N1) strain[289], while the flavanone **58** and the flavonoid **59** show potent NA inhibition (IC_{50} ranges 1.4-20 μM against NA)[290,291]. Nagai and co-workers

showed that isoscutellarein **60** and its derivatives are active in the low micromolar range in cellular assays against influenza A/Guizhou/54/89 H3N2 MDCK cell-based CPE assay and in animal models, acting as NA inhibitors[292,293]. Also compounds extracted from *Ferula assa-foetida* have great potency against IAV (H1N1) (IC_{50} = 0.26-0.86 μg/mL). The most potent molecule is compound **61**[294].

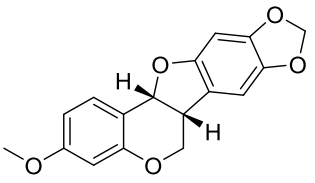

58

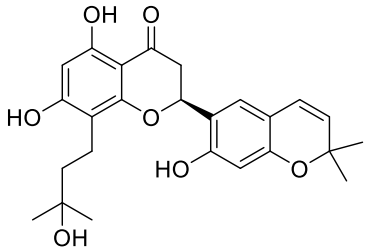

59

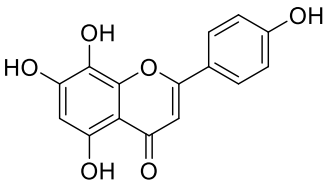

60

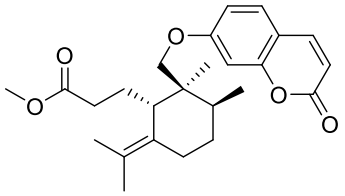

61

In order to develop new anti-influenza virus drugs, several derivatives of resveratrol, a molecule that has an antiviral effect due to is ability to inhibit the protein kinase C (PKC) activity and its dependent pathways[295], have been extracted, isolated or synthesized by Li and co-workers. Using several biological assays and computer aided studies, they demonstrated that the resveratrol related compounds have significant inhibitory effects on influenza H1N1 virus NA. In particular, compound **62** not only exhibits high inhibitory activity on NA, but also possesses anti-influenza virus activity in MDCK cells, which means that its mechanism of action may be through NA inhibition[296].

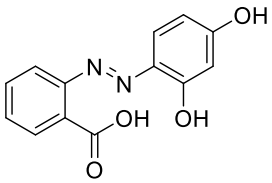

62

3.2.5. NP inhibitors

As previously reported, NP has multiple functions in the virus: among them, it is involved in replication and in the formation of specificity to the host. NPs are the major components of vRNP and within the vRNP complex oligomerize *via* two interaction forces. One comprises an intra-strand interaction through which the tail loop (residues 402-428) is inserted into the neighboring NP tail loop pocket[297], while the other comprises an inter-strand interaction between two NP strands with opposite polarity. The mechanism underlying the interaction between the two NP strands is still not clear; however, it is known that two dimer interfaces, the helix-turn-helix motif (residues 149-167) and the C-terminal region (residues 482-498), of NP are involved in this process[298]. For these reasons, it is an interesting anti-influenza target and some potential inhibitors of NP have been recently discovered. In 2010, Kao and co-workers found a small molecule, nucleozin, **63**, which can trigger the aggregation process of NP, blocking its nuclear accumulation. It inhibits the infection caused by H1N1, H3N2 and H5N1 strains, with EC_{50}s of 0.07 μM, 0.16 μM and 0.33 μM in MDCK cell-based PRA, respectively[299]. In the same year, an anti-influenza screening against a large compound library together with a high-throughput virus yield reduction methodology resulted in the identification of several classes of unique compounds, which appear to act on different targets. One of the identified compound, structure **64**, is an analog of the nucleozin that inhibits influenza RdRp interacting with NP[300]. A year later these findings, Shen and co-workers reported a rational approach to target influenza virus with a new mechanism of disruption of NP-NP interaction. Based on the crystal structures, they predicted that mutations of amino acids in positions 339 (glutamic acid to alanine, E339A) and 416 (arginine to alanine, R416A), and the tail loop deletion (Δ402-428) would perturb NP-NP interactions, and in turn the ability of NP to interact with RdRp productively. Analyses by analytical ultracentrifugation indicated that these three NP-mutants existed as monomers in the free form as opposed to trimers for wild-type NP, and that their ability to bind RNA was significantly perturbed. Moreover, a luciferase-based reporter assay showed that the three mutants were unable to support the RdRp activity. Having demonstrated the importance of the salt bridge between Glu339 and Arg416 for viral survival, the same researchers performed a virtual screening to target this interaction. This study led to identifying some small molecules able to disrupt the formation of NP trimers and inhibit replication of wild-type and nucleozin-resistant virus strains, even though with less activity than nucleozin and its analogs,

previously described. Among these newly identified molecules, the most active is compound **65**, with IC_{50} values of 1.7 µM and 3.2 µM against influenza A/WSN/33 (H1N1) virus and the nucleozin-resistant variant, respectively[301].

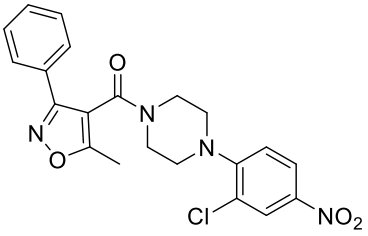

63

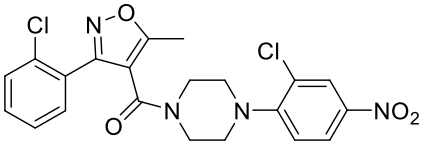

64

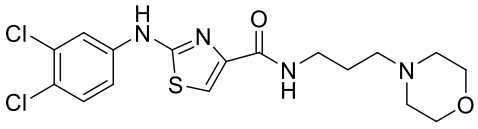

65

Cheng and collaborators replaced the isoxazole ring of nucleozin with a triazole to obtain a series of compounds, among which derivative **66** has IC_{50} values in the low micromolar range for H1N1 and H3N2 viruses and is also effective against amantadine- and oseltamivir-resistant strains[302].

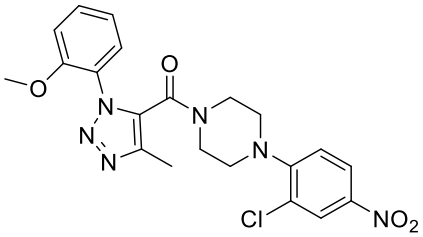

66

In 2016, the crystal structure of NP-nucleozin complex at 3 Å resolution showed the binding sites of nucleozin at NP for the first time. The complex structure reveals how NP and nucleozin interact with each other. The mechanism of action proposed is that nucleozin could link two NP molecules into dimeric subunits, and then further induce the formation of large aggregates[303]. After a screening of a library of 50,000 compounds using cell-based infection assays, the antiviral compound **67** was identified. It shows potent antiviral activity *in vitro*

against many different subtypes of IAV (e.g. IC_{50} value of 0.40 μM against A/California/7/2009 virus (H1N1)) and partially protects mice from a lethal dose of A/WSN/1933 (H1N1) virus, although *in vivo* data show that it is less effective than oseltamivir phosphate. The mechanism of action of **67** is the inhibition of vRNP activity, causing the NP to accumulate in the cell nucleus; *in silico* docking analysis revealed that it bounds to a small pocket in the viral NP[304].

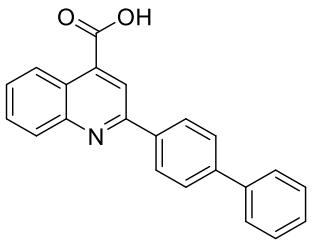

67

Small molecules such as cycloheximide **68**, the eukaryote protein synthesis inhibitor, and naproxen **69**, the known inhibitor of inducible cyclooxygenase type 2 (COX-2), are effective against the functional polymerization of the NP monomers. In particular, naproxen inhibits NP-RNA association required for NP function, and for this reason it is a promising lead compound for the development of novel antivirals against IAVs[305,306]. A licensed antiviral drug named ingavirin **70**, approved in Russia for the treatment of IAV and IBV infections, interacts with NP directly by interrupting the transport of newly synthesized NPs to the nucleus[307].

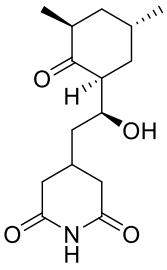

68

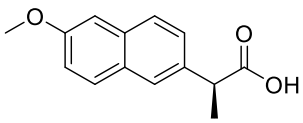

69

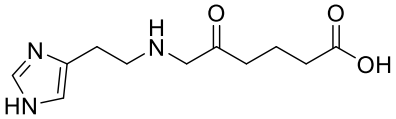

70

3.2.6. NS1 inhibitors

The non-structural protein 1 (NS1) of the influenza virus is a small, multifunctional protein, formed by two domains joined by a flexible linker region, that is encoded by all strains of IAVs and is highly conserved[308-310]. NS1 has different essential roles in viral replication and evasion of the cellular innate immune response. It binds in a non-sequence specific manner to viral RNA protecting it from degradation[311] and it interacts with the tripartite motif-containing protein 25 (TRIM25), preventing the activation of retinoic acid-inducible gene I (RIG-I), thereby suppressing the production of cellular interferon[125,312,313]. It is also able to bind to cleavage and polyadenylation specificity factor (CPSF30), blocking the maturation of the host RNAs, which leads to the reduction of host proteins[308,314-316]. Twu *et al.* found that the binding between NS1 protein of IAVs and CPSF30 is mediated by the second and third zinc fingers (F2F3) of CPSF30; in particular, the viral replication is inhibited when the binding process is blocked by a fragment containing the F2F3 binding motif. This indicates that the CPSF30 binding site in the NS1 protein could be a potential target for antiviral therapies against the IAV[317]. In 2012, Jablonski *et al.* showed that NSC125044, **71**, and a series of derived compounds, such as **72**, are able to display inhibitory activity against NS1 protein in a live cell virus replication assay[318].

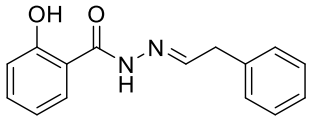

71

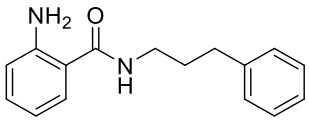

72

3.2.7. RdRp inhibitors

RdRp of influenza virus has been highly conserved among all strains and subtypes during evolution[319]. During the early stages of infection, RdRp synthesizes mRNA using vRNA as a template, while during the advanced stage of infection, it becomes responsible for the catalytic synthesis of cRNA and new vRNA[131]. Playing a critical role during the life cycle of the virus, RdRp has become a promising target for the development of anti-influenza drugs in recent years[132]. Based on the mechanism of the interactions between inhibitor and polymerase, compounds targeting RdRp can be subdivided into four subtypes: PA

endonuclease inhibitors, PB1 inhibitors, PB2 cap-binding (PB2-CBD) inhibitors and RdRp disrupting compounds[19,320].

3.2.7.1. PA endonuclease inhibitors

A promising target in viral RdRp is the conserved residues inside of the catalytic site of N-terminal domain of PA (PA-N). As previously said, PA-N has the catalytic domain for the cleavage of the capped host RNAs. Its core region contains one or two divalent metal ions (Mn^{2+} or Mg^{2+}) and several residues that are conserved among IAVs and IBVs, and are important for the catalysis or metal ion coordination. Moreover, this catalytic center is surrounded by several hydrophobic pockets that are well suited for drug design. Hence, PA inhibitor design is currently focused on chemical scaffolds bearing coplanar oxygens with the right geometry to coordinate the divalent metal ion(s), and also, suitable hydrophobic elements[320]. In the literature, there are several PA inhibitors with inhibitory activity in enzymatic assays on the viral polymerase or isolated PA-N. The first class of PA inhibitors was reported by Merck (Kenilworth, NJ, USA) in the mid-1990s; these molecules have a 4-substituted 2,4-dioxobutanoic scaffold and exhibited IC_{50}s ranging from 0.2 to 29.0 μM. In particular, the most promising compound of this series is the metal chelating inhibitor L-742,001 (structure **73**)[321,322].

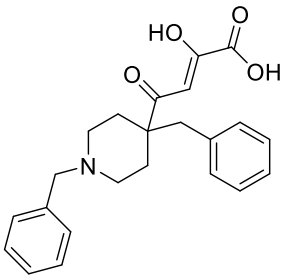

73

Quinoline derivatives bearing a hydroxamic acid moiety were identified as selective inhibitors of RdRp by a high-throughput *in vitro* transcription assay. The hit compound **74** inhibits the capped RNA-dependent transcription of IAV and IBV with a similar potency (IC_{50} of 40 and 50 μM, respectively). SAR of **74** and its analogs indicates that the phenolic hydroxyl group,

the hydroxamic acid moiety and the nitrogen of quinoline are essential for the activity. Interestingly, the incorporation of the hydroxamic acid portion into a cyclic ring system led to two potent inhibitors, **75** and **76**. However, apparent toxicity observed in cell cultures interrupted further evaluation of these compounds as antivirals[323].

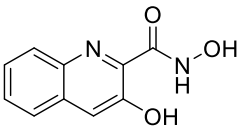

74

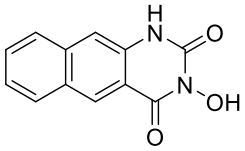

75

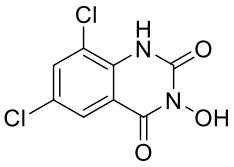

76

The fungal metabolite flutimide, **77**, bearing a 2,6 diketo-piperazine scaffold, has an interesting antiviral activity: it inhibits IAV PR/8/34 RdRp (IC_{50} = 5.5 μM) in a cap-dependent transcription assay and IAV infection of MDCK cells (EC_{50} = 5.9 μM) without apparent toxicity (CC_{50} ≥ 100 μM)[324]. Starting from this interesting activity, several derivatives of flutimide have been designed and synthesized by introducing different aromatic groups at 3 and 5 positions, which led to several more potent inhibitors (general structure **78**), but with overt cytotoxicity to cells at > 10 μM concentrations and unacceptable selectivity index values in cell culture[325,326].

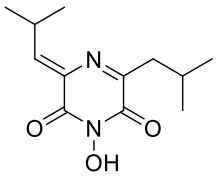

77

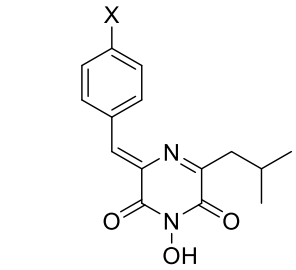

X = halogens, small alkyl groups

78

During studies for the identification of a pharmacophore model useful in the development of more potent PA-N inhibitors, Parkes and co-workers identified a series of potent inhibitors of the endonuclease of both IAV and IBV. Unfortunately, these derivatives show unacceptable activities in MDCK cells, with the exception of compound **79**[327].

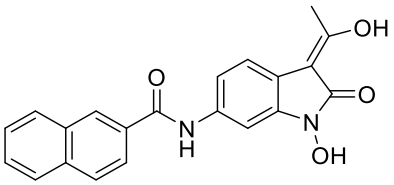

79

The antiviral activity of (-)-epigallocatechin gallate (EGCG) **80** against influenza virus was reported for the first time in 1993. This compound, present in green tea, affects viral infectivity in cell culture and agglutinates influenza viruses, preventing their absorbing to MDCK cells[197]. Moreover, green tea extracts including EGCG exert an inhibitory effect on the acidification of endosomes and lysosomes, resulting in inhibition of influenza virus growth in tissue culture[328]. EGCG and other related polyphenolic compounds are able to inhibit viral NA[329], and the replication of influenza virus, but also, show significant protective effects against oxidative stress through exhibiting antioxidant activity[330]. In 2009, a study demonstrated that green tea cathechins are active as antivirals because they are able to inhibit the PA-N subunit of the RdRp[331].

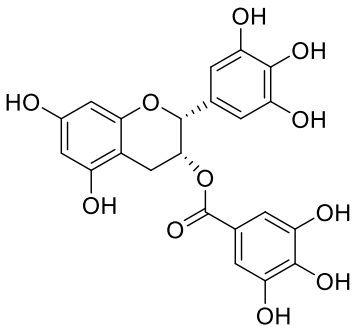

80

Using biological screening on thalidomide analogs, in particular, a PA endonuclease inhibition assay, a PB2 pathogenicity-determinant domain-binding assay, and an anti-IAV assay, Iwai and co-workers found that some phenethylphenylphthalimide analogs (for example, compound **81**) both inhibit PA endonuclease activity and retard the growth of IAV[332].

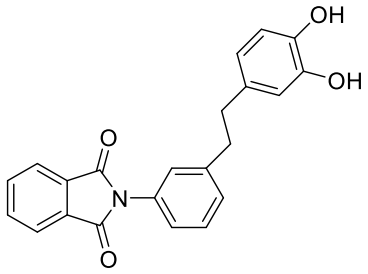

81

The same researchers identified three families of phytochemicals, namely marchantins, plagiochins and perrottetins (represented by marchantin A **82**, plagiochin A **83** and perrottetin F **84**) as inhibitors of influenza endonuclease, by the use of a PA endonuclease inhibition assay and an anti-IAV assay. These compounds have a 3,4-dihydroxyphenethyl group in common, indicating the importance of this moiety for the inhibition of PA endonuclease[333].

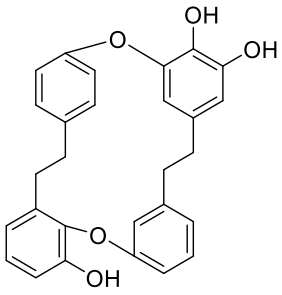

82

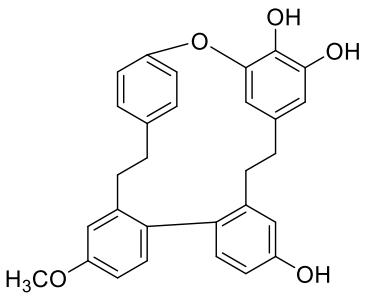

83

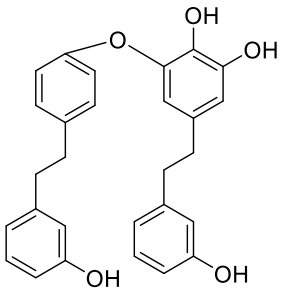

84

In 2013, Shoji and colleagues screened a series of fullerene derivatives using an *in vitro* PA endonuclease inhibition assay, identifying some inhibitors of the endonuclease activity of the PA-N domain or full-length PA protein. *In silico* docking simulation analyses suggest that fullerenes can bind to the active pocket of PA endonuclease. Among them, compound **85** is the most promising, having IC_{50} values of 20 μM and 31 μM against A/PR8/34 (H1N1) and H3N2 Aichi strain, respectively[334].

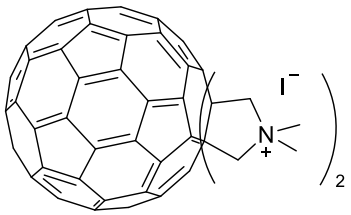

85

In the same year, molecules having the hydroxypyridinone scaffold were synthesized and biologically evaluated, providing useful scaffolds for the development of endonuclease inhibitors that could block the cap snatching associated with IAV replication. Two of the most potent compounds of this series, **86** and **87**, show good IC_{50} values of 11 and 23 nM, respectively, in the enzymatic assay[319,335,336].

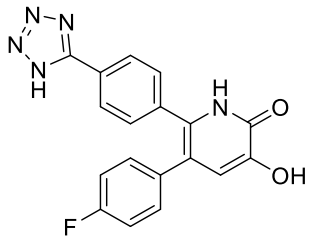

86

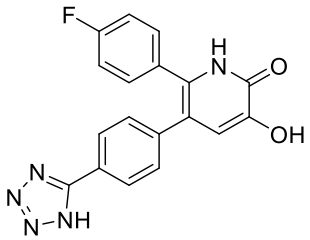

87

Also the hydroxyquinolinone scaffold was found to be promising for the synthesis of new PA inhibitors. This development led to two potent inhibitors **88** and **89**, having both of them IC_{50} values of 0.5 μM with regard to their ability to inhibit the endonuclease activity as measured by a high-throughput fluorescence assay. These compounds, analogously to compounds **86** and **87**, are substituted by a *p*-fluorophenyl group[336]. The same researchers synthesized also a series of substituted hydroxypyrimidinones among which the most active are compounds **90** and **91**, showing good inhibition activity with IC_{50} values of 0.58 μM and 0.15 μM, respectively, in a high-throughput endonuclease assay[337].

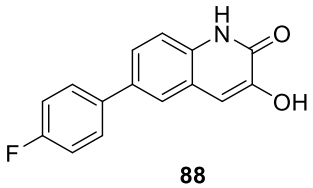

88

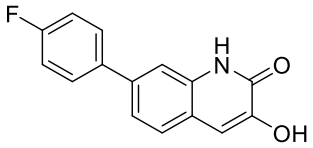

89

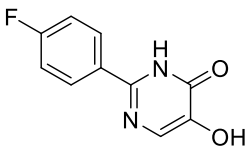

90

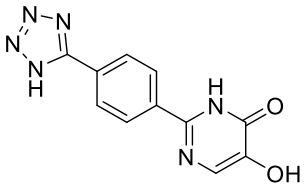

91

In 2014, using an *in silico* screening on a library of 450,000 compounds, Chen and colleagues identified molecules **92** and **93**, bearing four oxygenated functional groups, as potent antiviral agents against PA-N endonuclease (IC_{50}s of 6 µM and 14 µM against H1N1 endonuclease) and active in cell culture without apparent cell toxicity[338].

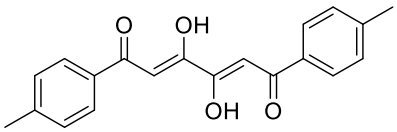

92

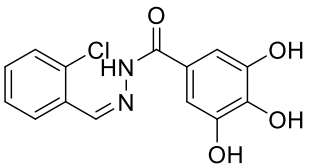

93

With the aim of identifying the essential pharmacophoric motif that could be involved in functional sequestration of the metal ions and consequently in the inhibition of PA subunit, Carcelli and collaborators proposed the 2,3-dihydroxy benzamide scaffold as a versatile platform for designing influenza PA endonuclease inhibitors. Compound **94** is the most active of this series. Its corresponding magnesium complex has an IC_{50} of 18 µM in a PA endonuclease inhibition assay, while the uncomplexed ligand has an IC_{50} of 33 µM, suggesting that the effective inhibitor of the activity of the enzyme is the metal complex and not the free ligand[339]. In 2015, the continuation of this project led to the identification of a series of salicylaldehyde thiosemicarbazone derivatives that seem to be promising PA inhibitors. In particular, thiosemicarbazone **95**, with two hydroxy groups in position 2 and 3

on the phenyl ring, is the most active, having IC_{50} value of 24 μM in an enzymatic assay with recombinant PA-N[340].

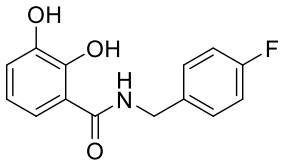

94

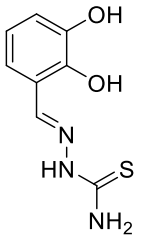

95

The same researchers identified also β-diketo-acid containing molecules as promising lead compounds for the development of new potent inhibitors of the PA catalytic activity. Among others, they synthesized and biologically evaluated some piperidine compounds **96** (analogs of the compound L-242,001) which exhibit IC_{50} values in the low micromolar range[159].

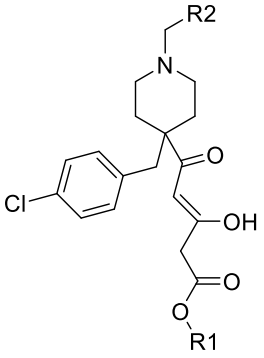

R1 = H, CH_3
R2 = C_6H_{11}, C_6H_5, C_6H_4-*p*F

96

Also trihydroxy-phenyl bearing compounds have provided a useful scaffold for the development of endonuclease inhibitors; for example, compounds **97** and **98** inhibit the PA-N endonuclease activity in a FRET-based endonuclease assay with IC_{50} values of 9.7 and 8.3 μM, respectively, and show inhibition activities in cell culture (EC_{50} = 11.76 and 14.42 μM, respectively) without apparent cytotoxicity (CC_{50} > 200 μM)[341].

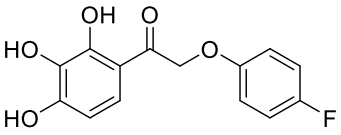

97

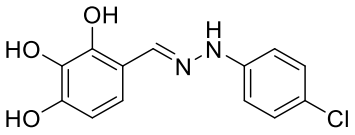

98

Pala and co-workers identified a series of indole carboxamidic compounds with an interesting PA inhibitory activity. Among them, **99** and **100** have IC_{50} values in the low micromolar range in an enzymatic plasmid-based endonuclease assay with influenza virus PA-N. Both molecules also show antiviral activity in cell-based assays and have potency comparable to that of the reference L-742,001 and to the nucleoside analogue inhibitor ribavirin[342].

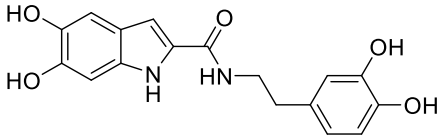

99

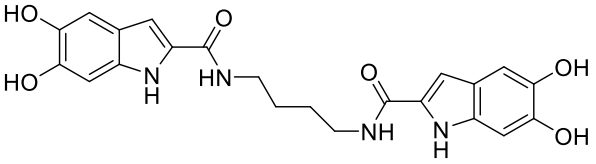

100

Credille and co-workers identified pyromeconic acid and its analogs as efficient PA-N endonuclease inhibitors, by using a fragment-based drug discovery campaign. They synthesized a series of 6-substituted pyromeconic acid derivatives to increase antiviral activity; among them, the most active compound is the tertiary amine **101**, with an IC_{50} of 0.94 μM in a PA endonuclease inhibition assay. Subsequently, they substituted the pyrone ring with a pyridinone one, to tighten the metal binding and increase the ligand basicity. A library of N-substituted pyridinones was synthesized and biologically tested. Compound **102**, containing a tetrazole group at the 4-position of phenyl ring, shows an IC_{50} value of 36 nM. Then, the researchers decided to merge the most potent inhibitors substituted at the 6-position of the pyrone ring with the most potent inhibitors substituted at the 1-position of pyridinone ring. This approach led to compound **103**, which has an IC_{50} value of 14 nM in a PA endonuclease inhibition assay and displays potency against IAV H1N1 in MDCK cells (EC_{50} = 2.1 μM) with low cytotoxicity (CC_{50} = 280 μM)[343].

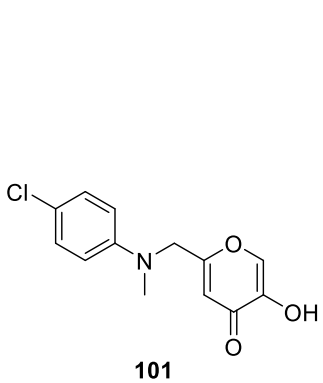

101

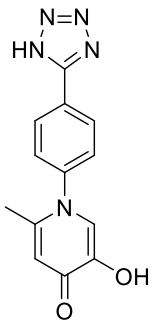

102

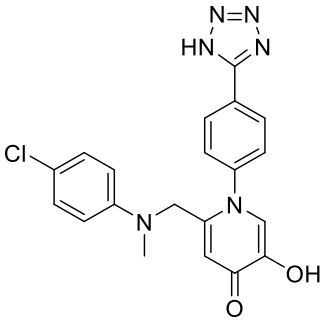

103

ANA-0, **104**, was identified by Yuan and colleagues as a potent endonuclease inhibitor using a screening approach that integrated the fluorescence resonance energy transfer based endonuclease inhibitory assay with the DNA gel-based endonuclease inhibitory assay. ANA-0 inhibits the replication of multiple subtypes of IAV, including H1N1, H3N2, H5N1, H7N7, H7N9 and H9N2, in cell cultures. It has been seen that the combination of zanamivir and ANA-0 has a synergistic anti-influenza effect *in vitro* and its intranasal administration has a good antiviral effect in mice[344].

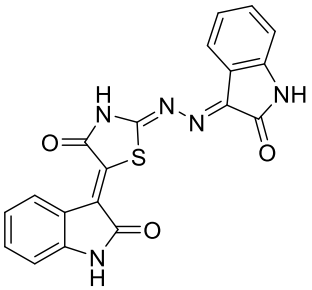

104

While I am writing this thesis, Alios Biopharma, Inc. is testing AL-794 as endonuclease inhibitor in clinical stage evaluation. AL-794 is currently in clinical phase I[345], although recently a study (NCT03411421) to assess the safety, tolerability and pharmacokinetics of repeated dosing regimens of AL-794 in healthy volunteers was closed as the data received did not support the continuation. The structure of this molecule is not disclosed. The prodrug S-033188 (baloxavir marboxil) **105**, that has been developed by Shionogi (Osaka, Japan) in collaboration with F. Hoffmann-La Roche Ltd., has demonstrated safety and acceptable pharmacokinetics in clinical stage evaluation. Moreover, this drug demonstrated efficacy in a wide range of influenza viruses, including oseltamivir-resistant strains (e.g. H7N9, H5N1). A

phase III study (NCT02954354, CAPSTONE-1) showed that patients treated with S-033188 have significantly greater reductions from baseline in both viral titer and RNA content than those treated with oseltamivir or placebo and that S-033188 is generally well tolerated, with overall incidence of treatment-emergent adverse events lower compared with oseltamivir[346]. Very recently (October 2018), the FDA approved baloxavir marboxil (Xofluza™) for the treatment of acute, uncomplicated influenza in people twelve years old or older. Roche announced that Xofluza™ will be further studied in a phase III development programme including pediatric populations, post-exposure prophylaxis and severely ill hospitalized people with influenza, as well as the assessment of its potential in reducing transmission in otherwise healthy people.

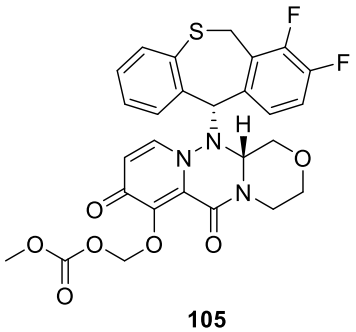

105

3.2.7.2. PB1 inhibitors

The PB1 inhibitors are very promising in anti-influenza drug development because of their low cytotoxicity, high resistance barrier and broad coverage of diverse RNA viruses[19]. Ribavirin **106** and favipiravir **107** (also named T-705 or Avigan) are RdRp inhibitors both containing a purine pseudo base, but have a different mechanism for their antiviral and mutagenic effects on influenza virus. Ribavirin is a guanosine analogue that was approved in 1986 as a broad-spectrum antiviral drug[347-349]. Its anti-influenza effect is based on IMP (inosine monophosphate) dehydrogenase inhibition, which results in fast and profound GTP depletion and an imbalance in the nucleotide pools. In particular, ribavirin causes an increase in both cytosine-to-uracile and guanine-to-adenine transitions and is misincorporated as triphosphate into replicating genomes by the viral RdRp[350]. Favipiravir is a nucleobase mimetic discovered by Toyama Chemical Co., Ltd. It acts as a potent and GTP-competitive inhibitor of the viral polymerase. It is transformed by cellular enzymes into its active form, favipiravir-ribofuranosyl-5'-triphosphate (RTP). This form is recognized by RdRp and

misincorporated into nascent RNA as a purine, which results in chain termination during RNA synthesis. Favipiravir is active against a broad range of influenza viruses, including IAV H1N1, H5N1 and H7N9, inhibits influenza strains resistant to current antiviral drugs, and shows a synergistic effect in combination with oseltamivir[351]. One of the major concerns for favipiravir is its potential teratogenicity, and this is the reason behind the conditional approval of the drug in Japan. Favipiravir pharmacokinetic and efficacy is being tested in several clinical trials (phase II and phase III) in Japan and in USA[352]. In conclusion, in infected cells, viral RNA synthesis is completely inhibited by favipiravir or ribavirin at concentrations > 50 µM, whereas exposure to lower drug concentrations induces formation of non-infectious particles and accumulation of random point mutations in the viral genome. This mutagenic effect is two-fold higher for favipiravir than for ribavirin[350].

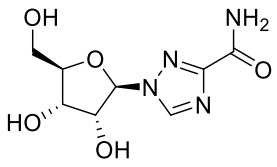

106

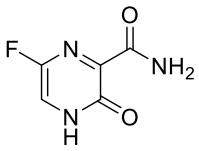

107

Several nucleoside analogues[353], 2′-substituted carba-nucleoside derivatives[354] and deaza-purine nucleoside analogues[355] are reported to have anti-influenza activities against IAV and IBV. For example, as a pyrimidine analogue, 2'-deoxy-2'-fluorocytidine (2'-FdC), **108**, inhibits the polymerase complex of various IAV and IBV strains *in vitro* and *in vivo*, with IC_{50} values ranging from 0.13 µM to 4.60 µM[356]. Although these nucleoside analogues show strong inhibitory activities, the clinical application is limited because their therapeutic window is too narrow[19].

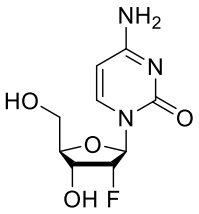

108

Among the PB1 non-nucleoside inhibitors, compound **109** was the first identified influenza inhibitor that was proved to act on the PB1 subunit[300]. Optimization of this compound could

result in the development of new interesting anti-influenza agents. ASN2, **110**, was first reported as an activator of the host innate immune response which can restore the interferon response to influenza-infected cells. However, the PB1 mutant Y499H, showing resistance to ASN2 in a mini-genome assay, suggested that the PB1 subunit should be the direct target. ASN2 shows potent inhibitory activity against IAV and IBV *in vitro* against several viral strains (e.g. H1N1, H3N2 and H5N1) and protects mice infected with influenza A/WSN/33 virus[357].

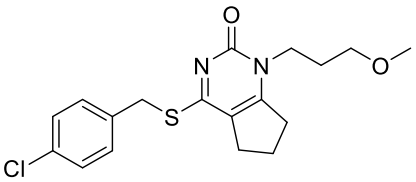

109

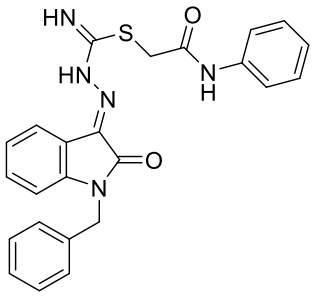

110

3.2.7.3. PB2 Cap-binding inhibitors

The natural ligand of the PB2 domain is the m7GpppN cap (where m7G is 7-methylguanosine, p is a phosphate group and N is the first transcribed nucleotide), so compounds containing a 7-methylguanine group or its analogs could compete with the natural ligand for the PB2 cap-binding domain (PB2-CBD). Pautus and co-workers first identified 7-alkylguanine derivatives as inhibitors of this domain, and further modifications, in order to mimic the negative charges of the triphosphate group of m7GTP with carboxylate groups, led to the synthesis of active compounds, among which compound **111**, that has an IC_{50} of 0.6 µM for H3N2 virus[358].

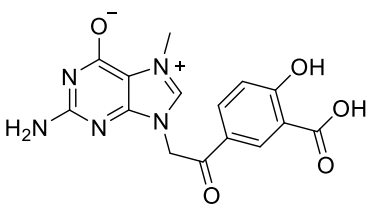

111

Among the PB2 cap-binding inhibitors, there is the azaindole based inhibitor VX-787, **112**, known also as pimodivir or JNJ63623872. It was discovered by Vertex Pharmaceuticals and is being developed by Janssen Pharmaceuticals[359]. VX-787 is a first-in-class, specific, oral polymerase inhibitor which is under phase II development for the treatment of IAV infections[360,361]. It displays potent antiviral activity against a wide range of IAV strains including amantadine- and NAI-resistant strains, with EC_{50}s in the nanomolar range in cellular assays[359,362]. The X-ray structure demonstrates that VX-787 is able to occupy the m7GTP binding pocket in the PB2 cap-binding domain of IAVs[165]. Moreover, more recently, it was found that VX-787 inhibits IAV replication but does not alter cellular antiviral responses[363]. Several VX-787 analogs were synthesized and biologically evaluated, including compound **113** that shows comparable potency and a similar binding mode to VX-787[364].

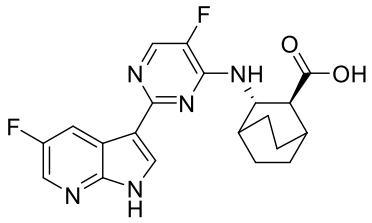

112

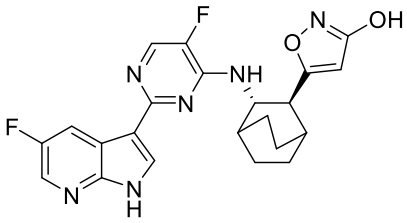

113

Cap-3 and Cap-7 (structures **114** and **115**, respectively), reported by Roch *et al*., are active as PB2 inhibitors; they inhibit the virus replication in cell experiments with EC_{50}s in the low micromolar range[365].

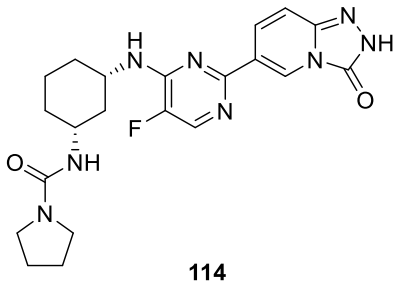

114

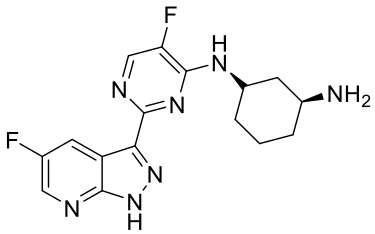

115

Recently, Liu and co-workers identified compound D715-2441, **116**, by screening a library of compounds in a cell-based MTT assay. D715-2441 possesses antiviral activity against multiple subtypes of IAV strains, including H1N1, H5N1, H7N9, H3N2, the clinical isolate

690 (H3), and oseltamivir-resistant strains with the H274Y NA mutation, and suppresses the early steps of the virus replication cycle. Mechanistic studies indicate that D715-2441 inhibits viral polymerase activity, in particular, the PB2 subunit, binding specifically to PB2-cap protein[366].

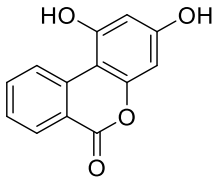

116

3.2.7.4. RdRp disrupting compounds

As reported before, the three subunits of the RdRp bind each other non-covalently in a set of interactions that are essential for the polymerase function. An attractive strategy for developing RdRp inhibitors appears to interrupt the interactions among the three units. Compounds that act with this mechanism of action are called protein-protein interaction inhibitors (PPI inhibitors) because of their interference or inhibition of the protein-protein interaction in the RdRp assembly. Among the interactions between the three different subunits of the RdRp, the PA-PB1 is probably the most interesting one for the development of new inhibitors. In fact, PA and PB1 directly interact to form a stable complex which binds to the vRNA promoter; this interaction has been characterized and is known to occur between the C-terminal region of PA (PA-C) and the N-terminal region of PB1 (PB1-N). Moreover, the interface of PA-PB1 interaction contains several hydrophobic pockets that are important for small-molecule drug design[132,367]. A more detailed description of this interaction and its importance as a target for the development of new promising antiviral drugs will be cited in the project section of this thesis.

In 2007, Ghanem *et al.* identified a 25 amino acid peptide (amino acid sequence ADVNPTLLFLKVPAQNAISTTFPYT) derived from IAV PB1-N, corresponding to the PA-binding domain, that could inhibit RdRp activity by disrupting the PA-PB1 interaction (IC_{50} value of 1.8 nM). This is the first example of small peptides inhibiting the PA-PB1 complex formation[368]. The same research group found smaller peptide inhibitors by generating several truncated fragments of IAV PB1-N. These peptides show good IC_{50} values for IAVs and

IVBs inhibition[369,370]. Anthracene derivative **117** (AL18), an inhibitor of cytomegalovirus DNA polymerase, was also serendipitously identified as a blocker of the connection between RdRp subunits. It shows an interesting activity as disruptor of the interaction between PA and PB1 subunits (IC_{50} = 20.3 μM) both on IAV (A/PR/8/34) with an EC_{50} of 14.5 μM and on IBV (B/Lee/40) having an EC_{50} of 8.3 μM[371]. Other two PA-PB1 PPI inhibitors, benzbromarone, **118**, and diclazuril, **119**, were identified by a Japanese group with an *in silico* screening of a database of about 4,000 drugs[372]. These two compounds are already in clinic for other uses and they can represent a good starting point for further development as well as good alternatives in case of an outbreak of an influenza virus resistant to current drugs.

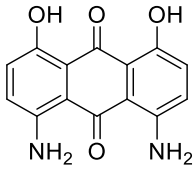

117

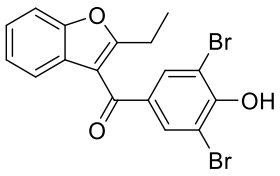

118

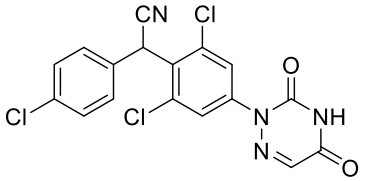

119

More recently, the identification of small molecules and peptides acting as PA-PB1 inhibitors has been mainly based on high-throughput screening (HTS) and structure-based virtual screening (SBVS). Benzofurazan derivatives, a new class of PA-PB1 PPI inhibitors, were identified by HTS using a biochemical ELISA-based screening approach followed by PRA on MDCK cells infected with the virus A/WSN/33 (H1N1). In particular, compound **120** and its analogue **121** show promising antiviral activity against IAV (H1N1), with IC_{50}s in the low micromolar range. Also a series of thioaryl derivatives, for example compound **122**, shows antiviral activity comparable to **120**, as well as improved cytotoxic profile[373]. Additional chemical structure modifications led to the identification of more potent compounds, among which molecule **123** that has an IC_{50} of 1 μM in an *in vitro* inhibition of the PA-PB1 interaction assay (ELISA)[374].

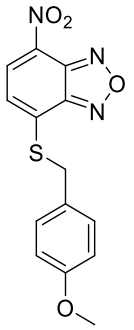

120

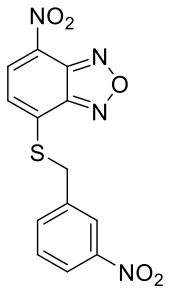

121

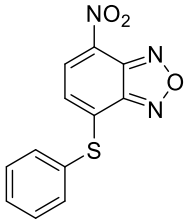

122

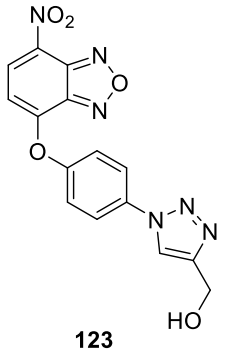

123

Using an *in silico* screening and then testing the selected compounds for their ability to inhibit the interaction between PB1 and PA *in vitro* with an ELISA-based assay and in cells, Muratore *et al.* identified several compounds acting as effective inhibitors of the polymerase PA-PB1 interaction. In particular, the most promising molecules turned out to be compounds **124** and **125**, having IC_{50} values in the low micromolar range and negligible cytotoxicity[375].

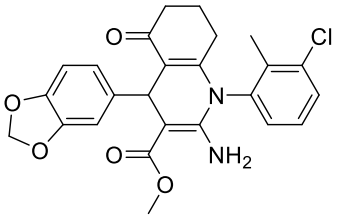

124

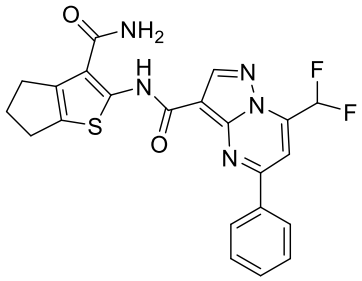

125

During subsequent SAR studies on the chemical structure of compound **125**, the thiophene-3-carboxamide moiety, which emerged as a favourable scaffold in the design of RdRp inhibitors, was preserved. I will describe in more detail molecules **117**, **123**, **124** and **125** in Chapter 4., Paragraph 4.1.

The substitution of the pyrazolo[1,5-*a*]pyrimidine with a triazolo[1,5-*a*]pyrimidine led to compound **126**, which is a three-fold more potent PA-PB1 inhibitor, with an IC_{50} value of 7.5 μM in ELISA PA-PB1 interaction assay[376].

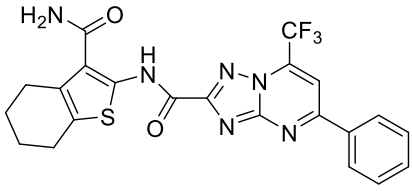

126

Among cycloheptathiophene-3-carboxamide derivatives, compounds **127** and **128** emerged as potent PA-PB1 PPI inhibitors with IC_{50} values of 32 and 35 μM, respectively, in ELISA PA-PB1 interaction assay[377].

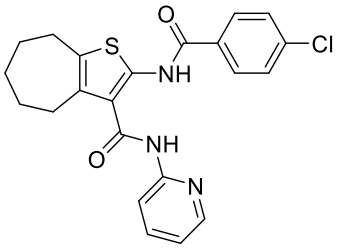

127

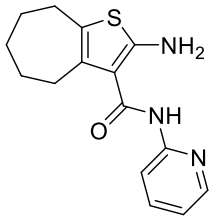

128

In 2015, Massari *et al.* during an optimization study on dihydrotriazolopyrimidine, synthesized some derivatives active as PA-PB1 interaction. Among them, the hybrid molecule **129**, obtained by combining the triazolopyrimidine and the previously explored cycloheptathiophene scaffold, turned out to be a potent PA-PB1 PPI inhibitor with an IC_{50} of 1.1 μM in ELISA PA-PB1 interaction assay[378].

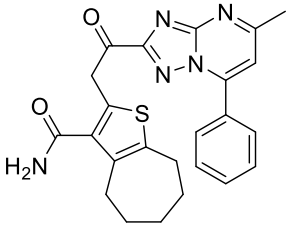

129

In 2016, Yuan and colleagues identified ANA-1, **130**, as a novel compound which could be developed as an anti-influenza drug. It was found to be a strong inhibitor of viral polymerase activity and a potent antiviral agent against infections of multiple subtypes of IAV, including

H1N1, H3N2, H5N1, H7N7, H7N9 and H9N2 subtypes. Molecule **130** shows EC_{50} values ranging between 0.09-1.23 μM in infected MDCK cell cultures[379].

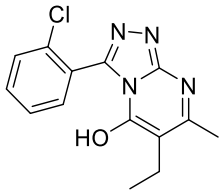

130

Very recently, by screening of an in house library, Shibasaki and co-workers identified MZ7465, **131**, a salcomine derivative, as a potent inhibitor of influenza virus propagation. Treatment with MZ7465 of infected cells decreases both viral protein and RNA synthesis and experimental results suggest that MZ7465 inhibits viral polymerase complex activity. However, the detailed mechanism of its antiviral activity needs to be further investigated[380].

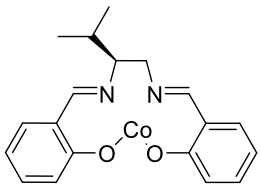

131

3.3. Agents targeting host sites

Another strategy to fight against influenza viruses is to target host sites that are essential for viral replication. Influenza virus exploits a number of cellular signaling pathways during the course of its replication, rendering them potential targets for new therapeutic interventions. It is important to underline that a viral inhibitor that targets host factors, rather than viral mechanisms, may be effective against multiple virus strains and subtypes, and be less likely to elicit viral drug resistance. There are several cellular sites that could be targeted; below I will mention only the main ones with the most promising relative molecules.

3.3.1. V-ATPase inhibitors

Endosomal acidification plays a major role in facilitating the fusion between viral and endosomal membranes, and the vacuolar ATPase (v-ATPase) is a regulating factor on viral replication. The inhibition of v-ATPase activity reduces the influenza viral infection by preventing the pH-dependent membrane fusion between endosomes and virions. Some adamantane drugs tested for the treatment of Parkinson's disease, among which, for example, norakin, **132**, has shown inhibitory activity against IAV and IBV acting as v-ATPase inhibitors[381-383]. The natural compound diphyllin, **133**, seems to be a promising v-ATPase inhibitor for several influenza virus strains. The results of cell-based assays show that it alters cellular susceptibility to influenza viruses through the inhibition of endosomal acidification, thus interfering with downstream virus replication, including that of known drug-resistant strains. Moreover, combinatorial treatment of diphyllin with oseltamivir or amantadine demonstrates enhanced antiviral effects and cell protection *in vitro*[384].

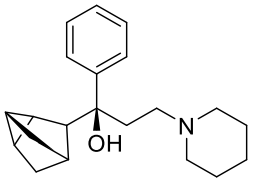

132

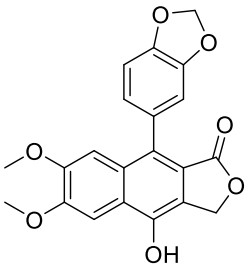

133

3.3.2. Anti-oxidants

Numerous studies have reported that the viral infection is often associated with redox changes characteristic of oxidative stress and emerging evidence has demonstrated that oxidative stress is an important contributor to infectious diseases and, among them, to influenza[385,386]. Indeed, during both *in vivo* and *in vitro* experimental models a shift towards a pro-oxidant state, a decrease in glutathione (GSH) levels, and a general oxidative stress have been observed[387,388]. It was noted that an exogenous administration of molecules able to increase cellular GSH concentration inhibits the replication of several viruses, including the influenza virus, through different mechanisms[389]. Cai *et al*. demonstrated that, when added

extracellularly, GSH has a dose-dependent anti-influenza effect in cultured cells. Moreover, the addition of GSH to the drinking water of influenza infected mice inhibits viral titer in the trachea and lungs[390]. These data strongly suggest that reducing conditions within the host cell could interfere with disulfide bond formation, thus preventing the correct folding and maturation of HA and consequently its transport and insertion into the cell membrane[391]. Moreover, oxidative stress is one of the most important causes of tissue injury, inflammation and apoptosis related to influenza virus infection[392].

A part from GSH, among anti-oxidant compounds, there are tocopherols. They are radical scavengers that deliver an hydrogen atom to quench free radicals, minimizing their damaging effect. Among them, there is α-tocopherol **134** that, alone or in combination, could normalize the lipid peroxidation processes caused by viral infection[393-396].

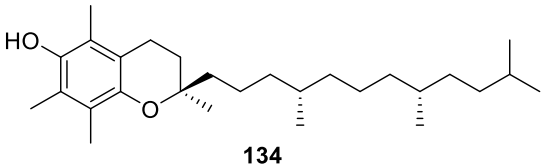

134

There are still other small-molecule antioxidants that work on influenza viruses. For example, the terpenophenol (+)-S-bakuchiol, **135**, that produces an anti-influenza effect through influencing oxidative stress response of host cells[397] or flavonoids biochanin A and baicalein (**136a** and **136b**, respectively) that inhibit highly pathogenic avian H5N1 IAV replication by reducing virus-induced reactive oxygen species (ROS) formation[398].

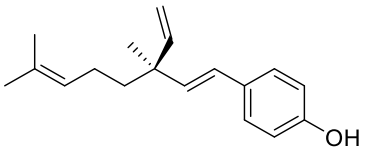

135

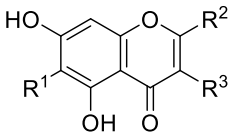

a R^1 = H, R^2 = H, R^3 = C_6H_4-*p*OCH_3
b R^1 = OH, R^2 = C_6H_5, R^3 = H

136

Interestingly, it seems that also NADPH oxidases family is involved in oxidative stress related to viral infection. NADPH oxidases are enzymes whose function is to generate ROS. They are divided in multiple isoforms, which primarily are distinguished by their membrane-spanning

catalytic "NOX" or dual oxidase "DUOX" subunit that it uses to transfer electrons from NADPH to molecular oxygen. In particular, NOX1 and NOX2 oxidases appear to have opposing roles in the regulation of inflammation caused by IAV. NOX 1 oxidase seems to suppress influenza virus-induced lung inflammation and oxidative stress[399], while NOX2 might promote the respiratory symptoms of the IAV infection and impede the clearance of the virus. For this reason, NOX2 could be a promising novel pharmacologic target against IAV infection that will be further investigated[400,401].

3.3.3. Protease inhibitors

Protease inhibitors are a class of influenza virus inhibitors; among them, it is important to mention the sialidase DAS181 (Fludase). It is a recombinant protein designed to remove sialic acid from respiratory epithelium and thereby prevent the attachment of influenza virus or other viruses that use sialic acid as a receptor. The protein, which is delivered *via* inhalation, consists of a heparin binding sequence that anchors the protein on respiratory epithelial cells and a sialidase derived from *Actinomyces viscosus* which cleaves sialic acid linkages from surrounding glycans[402]. Fludase is effective against both IAV and IVB and protects mice when it is administered either as prophylaxis or up to 48 h post-viral infection. Results of phase II trials indicate that the drug is well tolerated and significantly reduces viral load and viral shedding when administered over three days. One of the major concerns for using a protein therapy is the development of antibodies which would prohibit the subsequent use of the drug; neutralizing antibodies to Fludase have been observed, particularly when the drug is given for long periods and so its use must be limited to a once-off treatment[188,189,403,404]. Currently, Fludase is being developed by the USA start-up biopharmaceutical company NexBio Research Pvt. Ltd.[405]. The serine protease inhibitor aprotinin (Trasylol), a monomeric globular polypeptide derived from bovine lung tissue, can be considered as a promising drug against the influenza virus. It was seen that aprotinin inhibits HA cleavage and replication of IAV H1N1 in all host systems, including human tracheo-bronchial epithelium, not inducing any apparent toxic side effects in these hosts. Other serine protease inhibitors, such as camostat, **137**, and leupeptin, **138**, show antiviral activity acting as suppressors of virus HA cleavage. They limit the reproduction of influenza viruses or target a number of host mediators of inflammation, by down regulating their levels in virus-infected hosts[406].

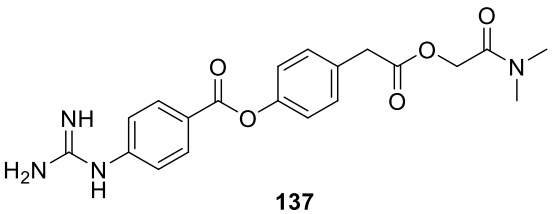

137

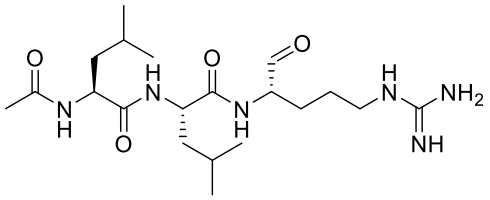

138

However, aprotinin is a protein with unfavorable pharmacokinetics whereas camostat is a covalent binder; both are non-specific protease inhibitors with potential side-effects. To achieve agents with superior potency and safety, other ways were explored. One of these ways was to develop specific inhibitors of the relevant airway proteases, particularly the transmembrane serine protease 2 (TMPRSS2). Among these inhibitors, usually containing either a 4-amidinobenzylamide or a sulfonylated 3-amidinophenylalanylamide, the best inhibitor turned out to be compound **139**, with a K_i value of 0.9 nM. Interestingly, it produced clear inhibition of HA0 cleavage and virus replication in cultured human airway epithelial cells 3 (Calu-3), which endogenously express HA0-activating proteases like TMPRSS2. An entirely different approach to find more potent and safe protease inhibitors that has recently developed aimed at designing exo-site binders or allosteric inhibitors[407].

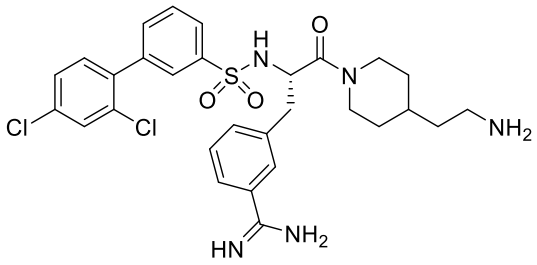

139

VL-01 (ViroLogik GmbH) is an inhibitor of the 20S and 26S proteasome with antiviral properties against influenza virus *in vitro* and *in vivo,* having the ability to reduce influenza virus induced cytokines and chemokines. In particular, it reduces influenza virus replication in human lung adenocarcinoma epithelial cells (A549) as demonstrated with three different influenza virus strains, A/PuertoRico/8/34 (H1N1) (EC_{50} value of 1.7 µM), A/Regensburg/D6/09 (H1N1) (EC_{50} value of 2.4 µM) and A/Mallard/Bavaria/1/2006 (H5N1) (EC_{50} value of 0.8 µM). In *in vivo* experiments in mice VL01-aerosol-treatment results in no

toxic side effects, decreases progeny virus titers in the lung and enhances survival of mice after infection with IAV A/Puerto Rico/8/34 (H1N1) up to 50%. Furthermore, treatment of mice with VL-01 reduces the cytokine release of different types of interleukin, CC-chemokines and tumor necrosis factor α (TNF-α) induced by IAV H5N1[408].

3.3.4. Pathway inhibitors

The intracellular signaling pathways are interesting targets for the development of new anti-influenza strategies. Among the most interesting, there are Raf/MEK/ERK, NF-κB and PI3K/Akt/mTOR pathways and the protein kinase C (PKC) signaling cascade (**Figure 17.**)[409].

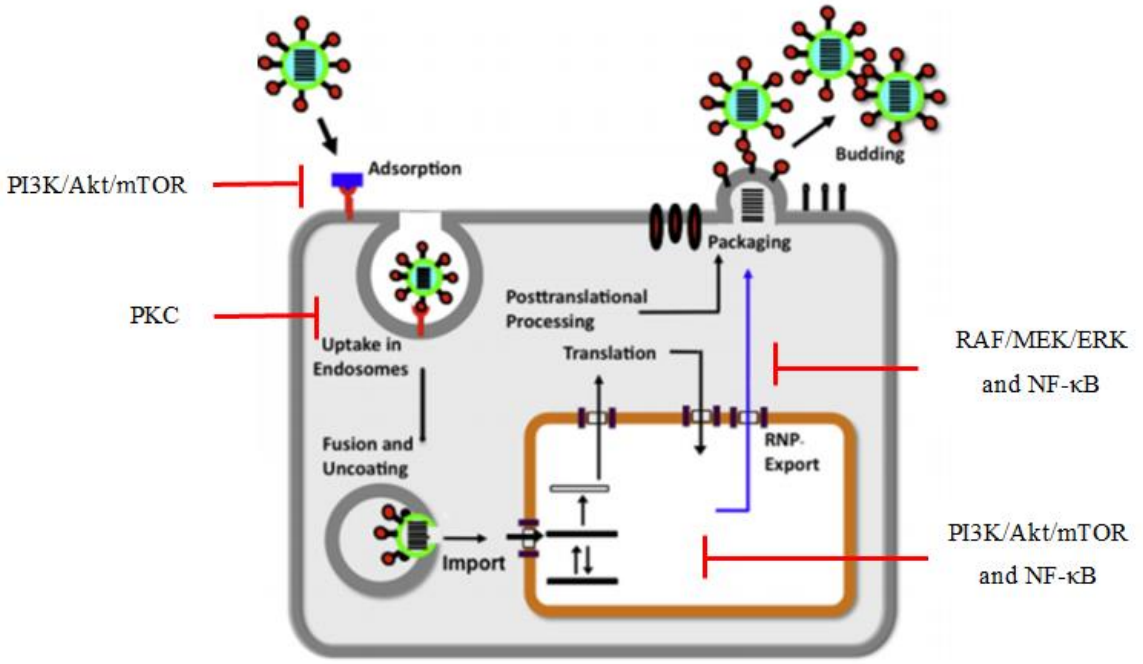

Figure 17. Involvement of cellular Raf/MEK/ERK, NF-κB, PI3K/Akt/mTOR and PKC pathways during the replication of influenza virus. Adapted from: *Antiviral Research.*, 98, 457-468 (**2013**).

The Ras-dependent Raf/MEK/ERK signaling pathway belongs to the family of so-called mitogen-activated protein kinase (MAPK) cascades and it is used by almost all growth factors and cytokines that act through receptor tyrosine kinases, cytokine receptors or G-protein-coupled receptors. This pathway is involved in several cellular responses, such as cell proliferation, survival, differentiation, motility and angiogenesis[410]. Since the activation of the

Raf/MEK/ERK signaling pathway is essential for efficient influenza virus replication and virus titers are enhanced in cells that have this pathway activated, its inhibition might interfere with virus replication. Through the activation of the Raf/MEK/ERK signaling pathway, influenza virus performs the efficient export of RNPs from the nucleus into the cytoplasm, and so the inhibition of this cascade leads to nuclear retention of the viral RNP complexes in late stages of the replication cycle[44,48,411]. PD0325901, PD184352 (CI-1040) and selumetinib (ARRY-142886) are examples of MEK inhibitors[412]. In particular, recently, it was demonstrated that PD184352, **140**, significantly reduces virus titers *in vitro*, holding viral RNP complexes in the cell nucleus, and it is able to reduce virus lung titers *in vivo*. Furthermore, it was proved that PD184352 is effective against a broad range of influenza virus strains[413].

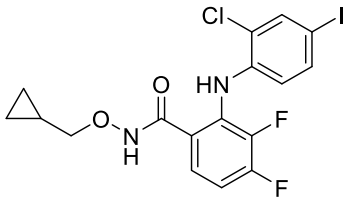

140

Another important influenza virus-induced signaling mediator and potential target for the development of new antiviral drugs is the nuclear factor kappa-light-chain-enhancer of activated B cells (NF-κB). It controls the expression of a variety of genes involved in physiological responses, such as immune and acute phase inflammatory responses, cell adhesion, differentiation, oxidative stress responses, apoptosis and antiviral responses[414]. During virus infection, NF-κB is involved in the activation of caspases, leading to enhanced nuclear export of viral RNPs into the cytoplasm and to the regulation of viral RNA synthesis[415]. In 2007, Leban and co-workers found a new class of NF-kB pathway signaling inhibitors by virtual screening, medicinal chemistry studies and QSAR analysis; among this class, compound **141** possesses activity in the nanomolar range in a cell-based NF-κB reporter gene assay[416]. As an efficient and quite selective inhibitor of the NF-κB-activating kinase (IKK), acetylsalicylic acid (ASA) **142**, aspirin, functions as an antiviral agent against influenza virus. It inhibits the replication of several influenza viruses in MDCK or A549 cells, in a concentration range that is not toxic for host cells, while in animal studies the aerosol

reduces virus titers in the lung and significantly promotes the survival of lethally infected mice. In contrast to the neuraminidase-inhibitor oseltamivir or the M2 ion-channel blocker amantadine, ASA does not lead to the generation of resistant virus variants in multipassaging experiments in cell culture[417]. DL-Lysine acetylsalicylate glycine (BAY 81-8781, LASAG), a water soluble form of acetylsalicylic acid, has antiviral properties against influenza virus. It was demonstrated that BAY 81-8781 is able to control influenza infection of highly pathogenic avian influenza virus strains *in vitro* and, in the mouse infection model, its inhalation resulted in reduced lung virus titers and protection of mice from lethal infection. Moreover, the treatment of mice infected with influenza virus started as late as 48 h after infection is still effective in protecting 50% of the animals from death[418].

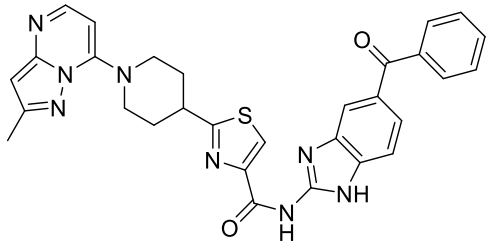

141

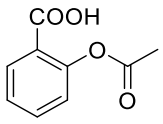

142

SC75741, **143**, is another nanomolar NF-κB inhibitor active against several viral strains in A549 and MDCK cells. It is able to protect mice from lethal influenza virus infection with an activity comparable to that of oseltamivir, at concentrations that do not cause adverse effects[419]. Mode of action studies revealed that it inhibits the caspase mediated nuclear export of RNPs[420]. Since the classical virus-induced activation of the NF-κB pathway requires proteasomal degradation of the inhibitor of NF-κB, it was hypothesized that inhibition of proteasomal inhibitor of NF-κB degradation should impair IAV replication. It was chosen the specific proteasome inhibitor PS-341 **144** (bortezomib; Velcade®) and, as expected, PS-341 treatment of infected A549 cells in a concentration range that was not toxic resulted in a significant reduction of progeny virus titers. However, the proposed suppression of NF-κB-signaling was not observed *in vitro.* Rather, PS-341 treatment resulted in an induction of the inhibitor of NF-κB degradation and activation of NF-κB. This coincides with enhanced expression of antiviral genes, such as interleukin-6 and, most importantly, MxA, which is a strong interferon (IFN)-induced suppressor of influenza virus replication. This suggests that

PS-341 may act as an antiviral agent *via* induction of the type I IFN response instead of inhibition of NF-κB[421].

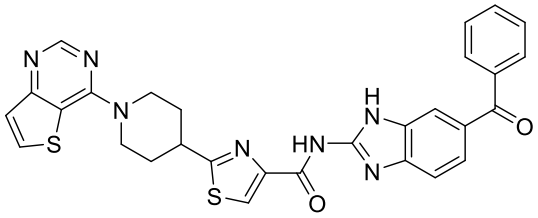

143

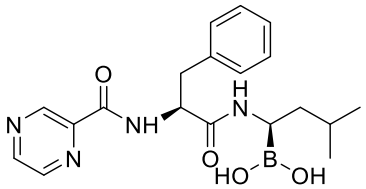

144

Silymarin is a complex mixture of four flavonolignan isomers, namely silybin **145** (the major and most active compound), isosilybin, silydianin and silychristin, which are extracted from milk thistle seeds. Songa and colleagues demonstrated that silymarin possesses strong antiviral activity (about 98%) against influenza A/PR/8/34 virus in MCDK cells at the concentration of 100 μg/mL, and antiviral activity of about 45% at the concentration of 10 μg/mL[422]. Silymarin acts against the elevated autophagy induced by IAV infection, by inhibiting IKK pathways together with oxidative stress, activation of extracellular signal-regulated kinase (ERK)/p38 and mitogen-activated protein kinase (MAPK), as well as expression of autophagic genes. All of these components have been reported to be related to the formation of the Atg12-Atg5/Atg16 heterotrimer, an important regulator of autophagy[423].

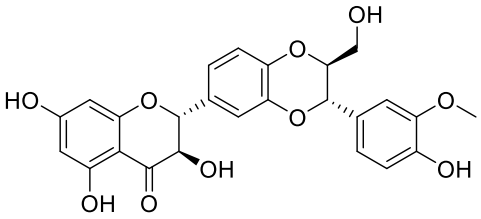

145

Among the hybrid compounds able to inhibit both virus NA and NF-kB signaling pathway, derivatives with a pyridinyl-quinazolinone scaffold are worth mentioning; in particular, compound **146** has the most potent anti-IAV (H1N1) activity *in vitro* with an IC_{50} of 51.6 μM in a H1N1-induced CPE inhibition assay[424].

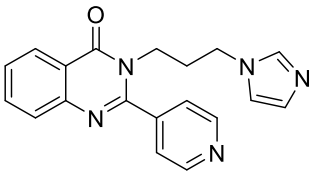

146

The PI3K/AKT/mTOR pathway is another signaling pathway that is activated by influenza virus. It is required for virus uptake and, at a later stage, for localization of RNP complexes[425,426]. Moreover, it supports virus replication by inhibiting premature cellular apoptosis[427]. Among mTOR inhibitors, the macrolide compound everolimus (RAD001), **147**, and sirolimus (also known as rapamycin), **148**, protect from infection of multiple subtypes of the influenza virus *in vitro* and *in vivo*. Although its antiviral activity, they have consistent adverse events associated with a narrow therapeutic window[428-430].

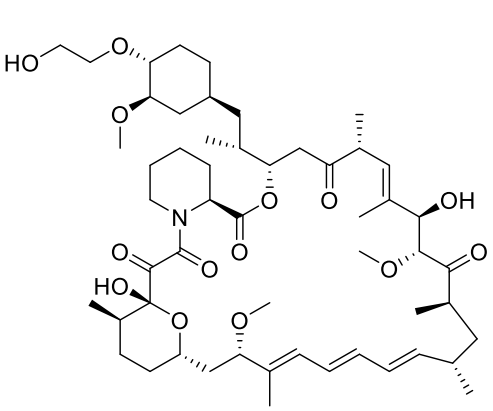

147

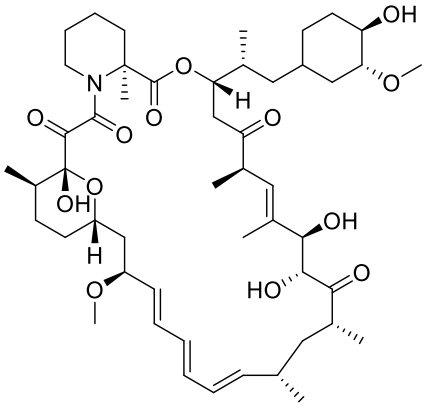

148

The inhibitors targeting PKC, a family of serine/threonine kinases involved in cell signaling, could be promising antiviral agents. The already mentioned resveratrol, **149**, have an antiviral effect related to the inhibition of PKC activity and its dependent pathways[295]. In 2008, through the use of a high-throughput screening of biologically active compounds, Hoffamann and collaborators showed that influenza virus growth can be modulated both positively and negatively by chemical manipulation of Na^+ transport or PKC activity. In fact, it was proved that the treatment with the commercially available PKC inhibitor rottlerin, **150**, at a concentration of 12.5 µM significantly reduces influenza virus replication in A549 cells, while activation of PKC enhances virus production[431].

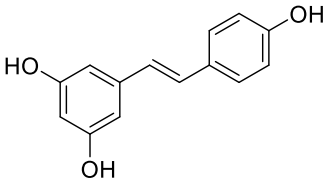

149

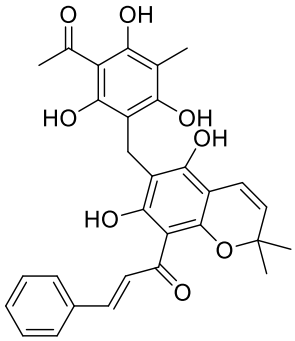

150

More recently, it was found that the kynurenine metabolic pathway is an interesting host site to be targeted for the fight against influenza virus. It might provide potential avenues toward development of anti-influenza strategies *via* immunomodulatory mechanisms, and in general, it should be taken into account for the development of novel antiviral and antibacterial drugs.

The kynurenine pathway is responsible for the degradation of almost all the ingested tryptophan not used for protein synthesis. This pathway constitutes the starting point for the synthesis of nicotinamide adenine dinucleotide (NAD) in mammals, and its dysregulation can lead to alterations in the immune system activation and accumulation of neurotoxic compounds. Kainov *et al.* found that the kynurenine pathway is altered in influenza-infected mice[432] and, more recently, this metabolic pathway received increasing attention and it was confirmed as interesting for the development of anti-influenza agents[433].

Today, most of the signaling inhibitors are licensed or under clinical evaluation as anticancer drugs. One important point in their development as antivirals is to establish if they are suitable from a safety point of view. There are several differences between the use as anticancer drugs and as antivirals; the duration of treatment is an example: cancer therapy usually lasts at least two or three months, while anti-influenza treatment usually only five days. This drastic difference may have an impact on the incidence of adverse events and their severity. Another point that has to be taken into consideration is the drug dosage: the amount of the compound could be reduced when treating influenza, which would presumably reduce the frequency and severity of side effects. One way to reduce the dosage could be to combine a signaling inhibitor with a direct-acting antiviral, such as oseltamivir. For example, studies show that the association between MEK inhibitors and oseltamivir resulted in strong anti-influenza activity *in vitro*, even when the amounts of the single drugs were reduced[409,434].

3.3.5. Phospholipase inhibitors

Phospholipases are enzymes that hydrolyse phospholipids into fatty acids and other lipophilic substances. They are divided into four major classes, termed A, B, C and D, which are distinguished by the type of reaction catalysed. In particular, phospholipase D (PLD), divided in two predominant isoenzymes PLD1 and PLD2, is involved in the formation of phosphatidic acid, an important messenger in cellular signaling and metabolic pathways[435]. In 2014, using novel synthetic compounds and biochemical approaches, the up-regulation of PLD activity during influenza infection was demonstrated, and evidence that PLD inhibition delays virus entry, allowing for a more robust innate antiviral response to be mounted in the infected host cell and leading to a significant reduction in viral titer. Consequently, PLD turned out to be a targetable host restriction factor for influenza viruses that facilitates rapid endosomal trafficking and escape from innate immune detection in the host cell[436]. Moreover, it was demonstrated that the human PLD2 inhibitor ML395, **151**, possesses an interesting antiviral activity against several influenza virus strains[437].

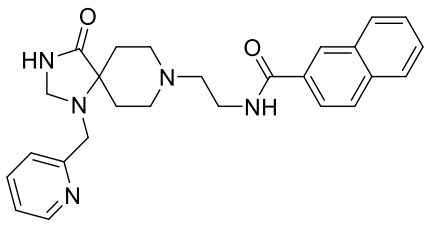

151

3.3.6. vRNPs inhibitors and gene therapy

As the nuclear export of influenza virus vRNPs has been demonstrated to be mediated by host exportin 1 (XPO1)[438,439], the development of inhibitors of XPO1 to interrupt this process and then hinder the replication cycle of the virus could be interesting. Studies performed by Perwitasari and co-workers showed that verdinexor, **152**, a selective inhibitor of XPO1, is able to inhibit the replication process of several IAV and IBV strains *in vitro* and *in vivo* in a selective and potent way[440]. In particular, it was showed that verdinexor reduces influenza virus shedding and pro-inflammatory cytokines expression in bronchoalveolar lavage fluid and reduces inflammatory cell infiltration into the bronchoalveolar space in influenza infected

mice and ferrets. Moreover, verdinexor administration is efficacious when given post-infection in mice[441].

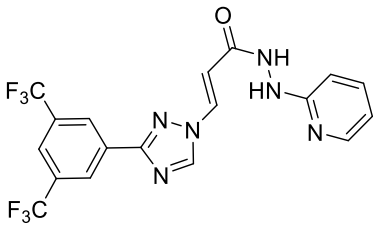

152

Gene therapy consists of modulating (up-regulating or down-regulating) genes and/or their products involved in the response to influenza. MicroRNAs (miRNAs) are small non-coding RNA molecules (about 22 nucleotides) that are able to perform RNA silencing or RNA interference and can regulate the expression of the viral genes in the post-transcriptional phase. Since host miRNAs are able to down-regulate the expression of viral genes, miRNA modulation could be a promising approach in influenza treatment, despite the difficulties of delivering these types of RNA to cells efficiently[442]. Also small interfering RNAs (siRNAs) (about 19-26 nucleotides) are mediators of RNA interference, since they induce sequence-specific degradation of homologous mRNA[443-445]. Long non-coding RNAs (lncRNAs) are able to modulate various biological processes[446]. Ouyang *et al.* found that the negative regulator of antiviral (NRAV), a type of the IncRNA, is able to act as a negative regulator of antiviral response and is down-regulated during influenza infection. In particular, NRAV decreases the transcription of multiple critical interferon-stimulated genes, by remodelling chromatin[447].

3.3.7. Immunomodulatory agents

Inflammatory changes and other immune reactions associated with acute IAV infection may influence the mortality caused by influenza and can be countered by immunomodulatory agents. Among natural molecules, licorice triterpenoid derivatives, in particular, glycyrrhizic acid (or glycyrrhizin), **153**, and glycyrrhetinic acid, **154**, have proved to be effective to interfere with the early phases of influenza virus infection. In particular, these molecules act through the stimulation of interferon-gamma (γ-INF) production by T cells,

immunomodulation, anti-inflammation and reduction of virus uptake by host cells. Moreover, glycyrrhizic acid shows an improvement in survival time of mice after viral infection, suggesting that licorice triterpenoid derivatives may be beneficial for the treatment of inflammatory processes related to viral infection[448-451].

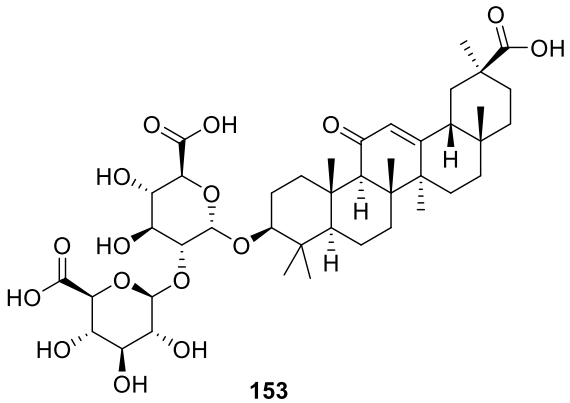

153

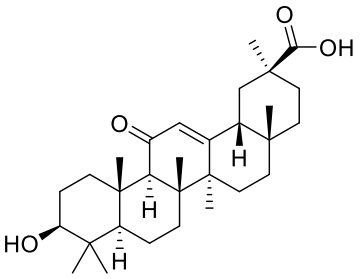

154

Systemic corticosteroids are widely prescribed in patients with influenza in an attempt to halt disease progression and to improve clinical outcomes, based on the findings that marked elevation of pro-inflammatory cytokine levels was associated with a high mortality rate in severe influenza virus infections due to IAVs[452-454].

Except for a small number of studies[455-457], the majority of observational studies[458-462] have shown that, when administered in high dose, corticosteroids may increase the risk of mortality and morbidity, while, to date, the role of low dose systemic corticosteroid requires further evaluation[463]. Statins, among which atorvastatin, **155**, are competitive inhibitors of the enzyme 3-hydroxy-3-methyl-glutaryl-coenzyme A reductase (HMGCR), and commonly prescribed for treatment of hypercholesterolemia. Statins have anti-inflammatory and immunomodulatory effect (e.g. repressing the induction of major histocompatibility complex II (MHC-II) by interferon (IFN)-γ and subsequent T-lymphocyte activation)[464,465] and for this reason could be used for the treatment of influenza[466]. There are currently no published human data based on randomized control trials on the acute use of statins in the management of severe influenza. An on-going study (NCT02056340) is evaluating atorvastatin *vs* placebo, in addition to standard care, for decreasing inflammatory markers in acute influenza.

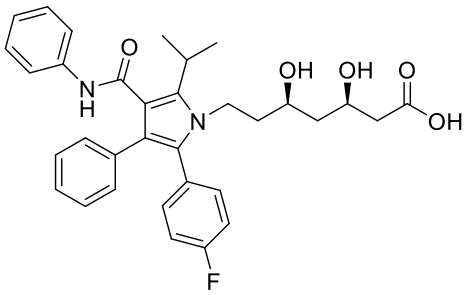

155

Macrolide antibiotics have anti-inflammatory effects in addition to their anti-bacterial properties; *in vitro,* they show to down regulate pro-inflammatory cytokines/chemokines, inhibit signal transduction and adhesion molecules expression, and regulate inflammatory cell functions. Yeganeh and co-workers found that macrolide bafilomycin A1, **156**, has disparate concentration-dependent effects on subcellular organelles and suppresses IAV replication. During this study, it has been seen that bafilomycin A1, at the very low concentration of 0.1 nM, is able to retain the capacity to significantly impair IAV nuclear accumulation as well as IAV replication and release, and it does not exhibit cytotoxic effects or induce apoptotic cell death, based on morphological and fluorescence-activated cell sorting (FACS) analyses[467]. The concanamycins are a family of macrolide antibiotics isolated from *Streptomyces diastatochromogenes.* Guinea and colleagues proved that concanamycin A, **157**, is able to inhibit an early step of influenza virus infection at 5 nM and to completely block it at 10 nM in MDCK cells. The target of concanamycin A seems to be an early event in virus infection, although not related to virus binding to receptors or internalization. In fact, it has been seen that radioactive influenza virus is internalized after binding with the same kinetics and to the same extent in the absence or in the presence of the antibiotic, and the binding takes place both in the absence and presence of the inhibitor[468].

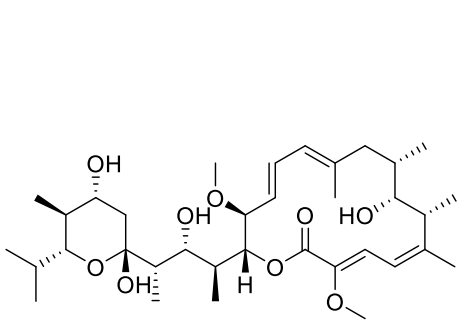

156

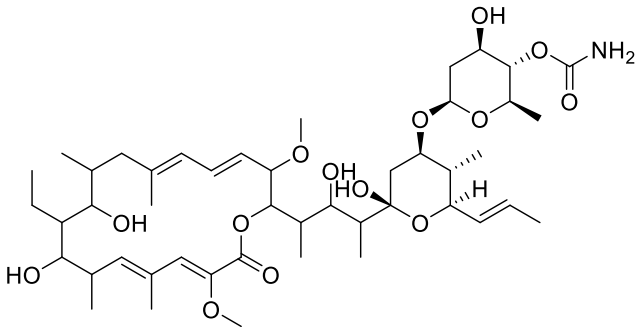

157

Other macrolides that have antiviral activities are erythromycin, clarithromycin, and azithromycin. The triple combination of oseltamivir, clarithromycin, and naproxen for severe influenza was demonstrated to be effective in one randomized control trial, but these findings have to be confirmed. Moreover, it is necessary to perform more studies to assess macrolide efficacy against influenza virus infection[463]. Apart from its clinically useful lipid-lowering activity, the peroxisome proliferator-activated receptor (PPAR) agonists can be useful in the treatment of influenza infection. There is evidence that the PPAR-α-agonist gemfibrozil, **158**, can inhibit production of pro-inflammatory cytokines[469], while several studies based on the mice model showed some anti-inflammatory effects of PPAR-γ-agonists against influenza virus infection, with survival advantage[470-472]. The use of PPAR agonists as anti-inflammatory drugs for treatment of severe influenza in the animal model should be further explored, but clinical utility may be limited by their toxicities.

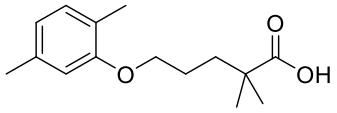

158

Pamidronate, **159**, is a bisphosphonate used for treatment of hypercalcaemia and Paget's disease. It exhibited protective effects against influenza infection caused by IAV H1N1 and H5N1 viruses in both *in vitro* and *in vivo* models, and this effect seems to be partly mediated by IFN-γ[473]. Unfortunately, given the potential side effects (e.g. ocular inflammation, renal failure, electrolyte imbalance etc.), pamidronate-based therapy would not be a high priority candidate for clinical trial on treatment of severe influenza infection.

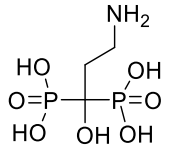

159

Mycophenolic acid, **160a**, or its prodrug mycophenolate mofetil (MMF), **160b**, are widely used as immunomodulatory agents in transplant recipients and other patients with autoimmune diseases[474,475]. PRA showed that **160a** has antiviral activity against multiple

clinical isolates of IAV (H1N1, H3N2, H7N9) and IBV (IC_{50} < 1 μM)[476]. Moreover, it was seen that the protective mechanism of **160b** against A (H5N1) virus infection is due to inhibition of cellular inosine monophosphate dehydrogenase (IMPDH) with a consequent diminution of viral mRNA and protein expression. Furthermore, after treatment with MMF, expression levels of some interferon (e.g. IFN-β) and interleukin (e.g. IL-1β, IL-6) are substantially down regulated in MDCK cells[477]. However, more work is needed to understand the potential role of mycophenolic acid for treatment in severe influenza.

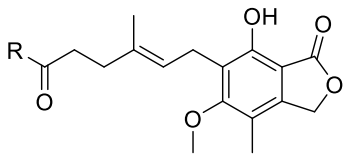

a R = OH
b R = CH_2CH_2-morph

160

Type I interferons (e.g. IFN-α/β) and type III interferons (IFN-λ) are important mediators of the innate immune response against influenza viruses[478]; their expression increases in response to influenza virus infection, resulting in viral restriction and activation of the adaptive immune response[479]. In IFN-α receptor knock-out mice, it was seen that type I IFNs are responsible for direct resolution of viral load and limitation of acute lung injury through suppression of immunopathology caused by IAV *via* IL-10 production[480]. Moreover, it was seen that low-dose IFN-α protected mice against A (H5N1) and A (H1N1) viral infection *in vitro* and in mice[481]. A study has shown that the association of IFN-λ1 with antiviral agents with different mechanisms of action (e.g. oseltamivir) exert a significantly greater synergistic effect against seasonal influenza viruses, highlighting that the use of this type of combination may be a potential therapy for treating infections[482]. Passive immunotherapy in the form of convalescent plasma or immune IVIG may be useful as an adjunct therapy for severe influenza, and definitive studies are on-going. The presumed functional component of both immune plasma and IVIG is the IgG fraction. The efficacy of other agents with potential immunomodulating effects, such as anti-C5a antibodies, human mesenchymal stromal cells (MSC), mesalazine, chloroquine etc. deserves more investigation. However, unfortunately, at the moment there are no immunomodulatory agents that have been conclusively proven to be of benefit in severe influenza[463].

CHAPTER 4. Discussion. Synthesis of hybrid 3-cyano-diphenylpyridine derivatives, pyrimidine and pyridine compounds as inhibitors of influenza virus RdRp PA-PB1 interaction.

4.1. Previous work

As previously said, influenza virus RdRp is essential for viral replication. In particular, the interaction between the C-terminal part of PA (PA-C) and the N-terminal part of PB1 (PB1-N) is an attractive drug target for the discovery of novel anti-influenza agents. The interaction between PA-C and PB1-N is an innovative promising target for several reasons: first of all, it has a high degree of conservation among virus strains, which suggests that its inhibitors may be active against many viral subtypes and less prone to drug-resistance. Moreover, this interaction involves few amino acids and so it could be inhibited by small molecules[483]. The interaction between PA and PB1 subunits was structurally identified by crystallographic studies. He and collaborators used an IAV subtype (A/goose/Guangdong/1/96, H5N1) to clone PA from residues 257-716 and PB1 from residues 2-25[484], while Obayashi and co-workers used a human IAV subtype (A/Puerto Rico/8/1934, H1N1) to clone PA from residues 239-716 and PB1 from 1-81[485]. The structures were determined with a resolution of 2.9 Å (PDB code: 3CM8) and 2.3 Å (PDB code: 2ZNL), respectively. It is worth to mention that, in 2014 Pflug *et al*. published the X-ray structure of IAV H17N10 RdRp (PDB code: 4WSB), that comprises the whole PA in complex with PB1, PB2 and a viral RNA promoter[143]. I have previously described the RdRp structure that comes out from this study. In addition, studies on the crystal structure of PA in the absence of PB1 showed structural changes compared with the same structure when PB1 peptides were present, indicating plasticity of the PA-PB1 binding interface that may be exploited in the development of novel therapeutics[486]. Liu and Yao analyzed and compared the two X-ray structures of PA-C bound to PB1-N (PDB code: 3CM8 and 2ZNL) and found that only some loops of the PA portion far from the PA-PB1 binding site are different from each other and are unable to influence the function of the PA-PB1 binding surface. Starting from one of the two X-ray crystal structure (3CM8), they performed an 8 ns molecular dynamics (MD) simulation with the aim to describe the interaction features of the protein-protein complex. They found that the intramolecular van

der Waals interplays and the non-polar interactions are mainly responsible for the binding of PA-PB1, while polar interactions do not contribute significantly to PA-PB1 interaction. Through the pair interaction analysis and virtual alanine scanning, the authors identified the hot spots for PA and PB1. Residues Trp706, Phe710, Phe411, Asn412, Gln408, Gln670, Leu666, Leu640 and residues 619-623 contribute to PA binding to PB1. For PB1 binding to PA, a basic binding motif that includes residues of Val3, Asn4, Pro5, Leu7, Leu8, Phe9 and Leu10 was identified[487].

As already previously discussed, in the last years the growing interest around this new promising target led to the identification of a number of small molecules able to disrupt PA-PB1 interaction. My research doctorate activity was focused on the synthesis and biological evaluation of novel anti-influenza agents acting as PPI inhibitors, in particular, disrupting the PA-PB1 interaction. My work in this field is the continuation of the project developed in collaboration with the University of Siena and the University of Padua. The research started from the identification of a benzofurazan hit compound **120**, having micromolar potency in the inhibition of viral replication (IC_{50} = 5 μM). In particular, this study was performed by employing an ELISA-based high-throughput screening method using fluorescence polarization, and allowed to quickly screen a library of about 15,000 small molecules for antiviral activity against influenza virus strain A/WSN/33 (H1N1). In order to explore the chemical space around the hit structure, a library of 70 compounds was synthesized. These compounds were found to have a good antiviral activity but, unfortunately, had also too high cytotoxicity[373].

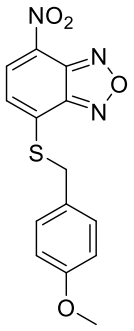

120

Employing a homology model built using the IAV H1N1 sequence and the two PA−PB1 complexes templates 2ZNL and 3CM8, docking studies were performed to better understand

the interactions responsible for the antiviral activity. Results suggested that the residues Trp706, Gln408, and Lys643 are crucial for the binding of the benzofurazan derivatives to the PB1 binding pocket on PA, and therefore could be targeted for the design of novel PA-PB1 interaction inhibitors. In particular, it was seen that Trp706 is involved in a π-stacking interaction with the molecules, Gln408 establishes an H-bond interaction with the oxygen atom of the furazan group and Lys643, with its amino group in the lateral chain, interacts electrostatically with the nitro group of the compounds[374]. As an example, the binding mode of benzofurazan derivative **123** is shown in **Figure 18**.

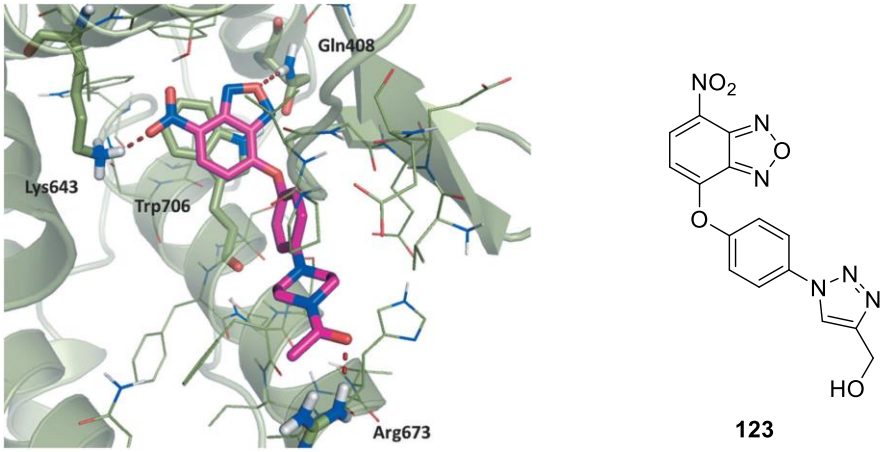

Figure 18. Binding mode of compound **123** to the PB1-binding pocket on PA. Carbon atoms of the compound are colored in pink and the amino acids responsible for the key interactions are highlighted.

It is important to underline that, similar interactions were also found for other identified PA-PB1 inhibitors **117** (AL18) and **124**, previously described. As it is possible to see from **Figure 19.**, the analysis of FLAP docking poses of compounds **117** and **124** showed that they are docked in the same binding region. Seven poses out of ten showed that the aromatic moiety of compound **117** is involved in a π-π stacking with Trp706 and several hydrogen bonds are formed between the molecule and residues Gly408, Lys643 and Asn412. Regarding compound **124**, also the interaction with Ile621 seems to be involved[371,375].

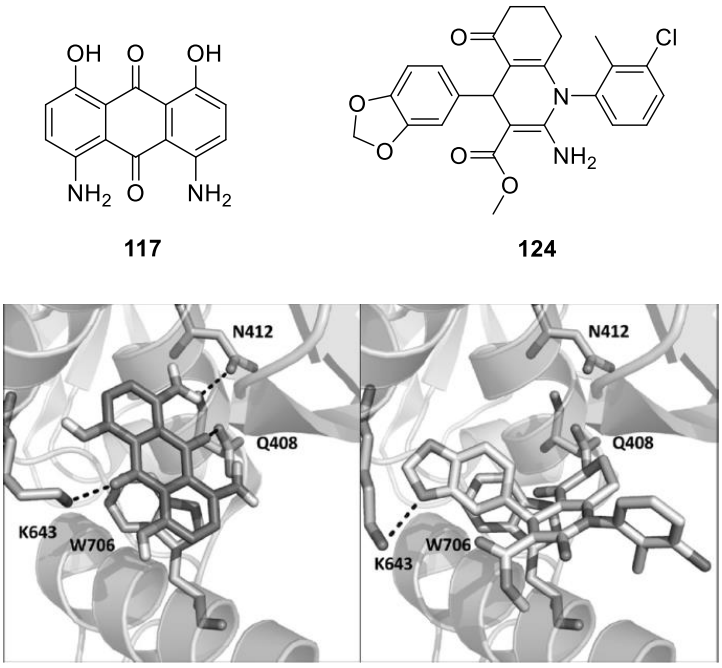

Figure 19. FLAP best pose for **117** (on the left) and compound **124** (on the right) in IAV PA. Flexibility of the Lys643 side chain was considered.

Despite their good antiviral activity, benzofurazan derivatives were found to be unsuitable for further development because of their poor selectivity index. So, on the basis of the information acquired, a computational approach was used to find new scaffolds able to disrupt the PA-PB1 interaction. A molecular dynamic simulation was performed to identify the "hot spots" responsible for the interaction at the protein-protein surface. As a result, in accordance with previous results published by Wunderlich *et al.*[369], amino acids Met1, Val3, Asn4, Pro5, Leu7, Leu8, Phe9 and Leu10 of PB1 were recognized as important for the interaction with residues on PA. Furthermore, several stable hydrogen bonds were identified at the interface, in particular, between amino acids Asn412, Gln408, Trp706, Arg673 and Gln670 of PA-C and Asp2, Val3, Asn4, Leu10 and Pro13 of PB1-N, respectively.

Starting from the information obtained from molecular dynamic experiments, a high-throughput docking approach was used to screen the Asinex database (703,200 molecules) in search of good candidates able to inhibit the PA-PB1 interaction. This screening was performed employing the same docking programs (Glide4, version 5.5 and GOLD[488]) and the same homology model previously described. But, since in 2014, after the publication of the manuscript by Pagano *et al*. regarding benzofurazan derivatives[374], a more detailed X-ray structure of viral RdRp was published[143], a comparison between the PA-C X-ray structure and

that build with the homology model was performed. As a result, it was seen that the two structures had 71.21% identity in sequence alignment and they superposed very well (RMSD 1.09 Å), especially in the PB1-binding site region (RMSD of 0.537 Å), thus validating the reliability of the homology model. Since biological evaluations were performed on the IAV H1N1 strain and the homology model was assessed of good quality, it was used this for the docking simulations. As a result of the high-throughput screening on Asinex database, 115 compounds were selected, according to the overall match between the binding modes proposed by the docking program and the predicted score values. Then, an ELISA protocol[489] was used as a biochemical method to test the virtual screening hits. From this study, compounds possessing a 3-cyano-4,6-diphenylpyridine nucleus were identified as weak inhibitors of the PA-PB1 interaction, being endowed with IC_{50} ranging from 80 to 180 μM. In particular, derivative **161**, having an IC_{50} of 80 μM and an CC_{50} of 150 μM, seemed to be the most promising compound.

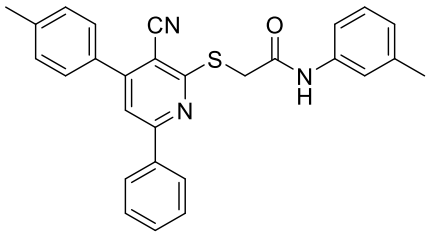

161

To further extend this study, ten derivatives endowed of the same 3-cyano-4,6-diphenylpyridine scaffold, were searched on commercial databases, bought and tested. Among them, molecules **162** and **163** emerged as promising compounds for further development, with IC_{50}s of 30-80 μM in ELISA assay and a low cytotoxicity in preliminary assays (CC_{50} between 100 and 150 μM in MDCK cells)[490].

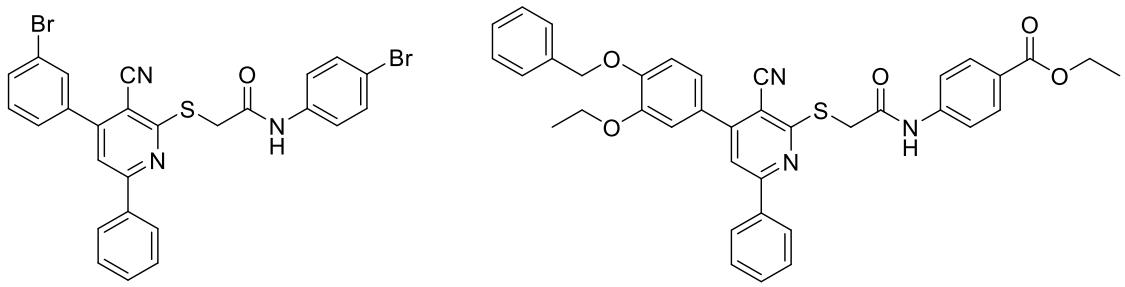

162 **163**

Remarkably, comparing the binding orientation of compound **162** with the pose previously identified for nitrobenzofurazan inhibitor **120**, some common interactions were identified: an hydrogen bond with Gln408, an electrostatic interaction with Lys643 and hydrophobic contacts with Val628 in the region usually occupied by Leu7 of PB1-N (**Figure 20.**).

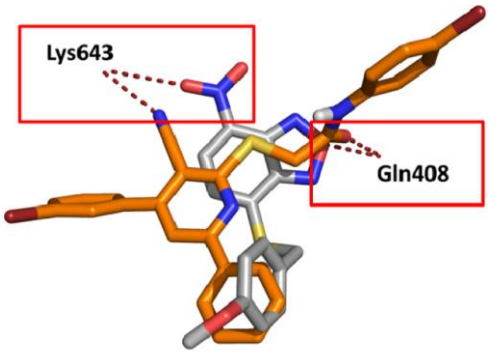

Figure 20. Comparison of the binding orientation of compound **162** (in orange) with the pose of benzofurazan derivative **120** (in grey). The common interactions are highlighted.

For a better understanding of the underlying SAR, starting from the 3-cyano-4,6-diphenylpyridine scaffold, a series of derivatives was synthesized by performing modification or replacement of molecule portions.

From SAR studies it was possible to obtain important information:

- The importance of the sulfur atom in the C2 side chain. When it is removed or substituted with CH_2, O, NH or CH=CH, a decrease of the activity is observed, probably due to different geometry properties of these atoms that do not allow the small molecule to assume a suitable conformation for correct binding. This results in a bad docking pose and explains the inactivity of these molecules.

- The optimal length of the C2 lateral chain seems to be that with only one methylene group.
- The presence of a hydrophilic group at the end of the C2 side chain causes loss of the antiviral activity.
- The two phenyl rings directly attached to the pyridine ring appear to be essential.
- The removal of the cyano moiety does not affect the activity.
- The substitution of the pyridine ring with a pyrimidine one does not affect antiviral activity, but seems to be responsible for a lower ability to dissociate the PA-PB1 complex.

In order to rationalize the SARs, all the synthesized compounds were evaluated by means of docking simulation within the PB1-binding site of PA, in order to produce their putative binding poses. Docking studies were carried out employing the homology model previously described and two widely used programs (Glide, version 6.2 and GOLD[488]). Then, the obtained binding poses of the compounds were compared. Moreover, the PA-compound complexes for one representative derivative for each class of compounds (**168** for cyanopyridine, **169** for pyridine and **170** for pyrimidine) were further investigated by means of MD using Schrödinger Desmond, version 3.7 (**Figure 21.**).

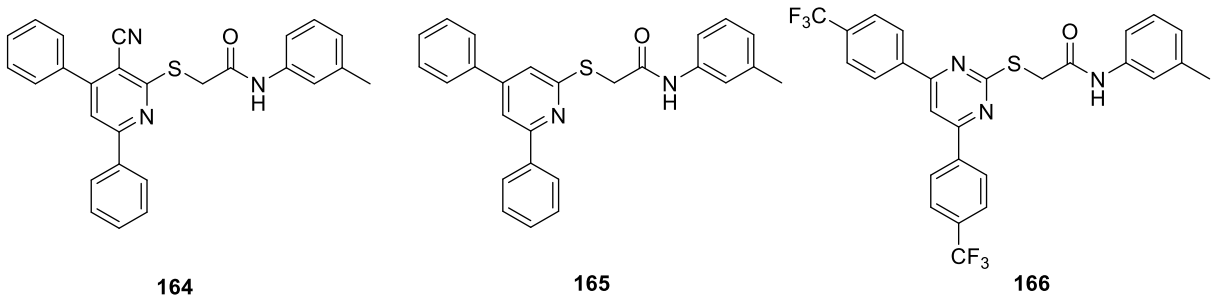

Figure 21. Structures of the molecules representative of the three major classes of compounds analyzed by MD studies: 3-cyanopyridine (**164**), pyridine (**165**) and pyrimidine (**166**).

In particular, after an extensive equilibration, a 14 ns MD simulation was performed for each complex starting from the most representative docking pose and, for a more detailed analysis of the stability of the PA-ligand complexes, the interactions between the protein and the small molecules were investigated on the whole 14 ns simulation time. Occupancy percentages were also calculated (**Table 1.**).

Table 1. Ligand interaction occupancies for **164**, **165**, and **166** in complex with PA.

			Occupancy (%)[c]		
Residue atom[a]	**Ligand atom/group**	**Type of contact[b]**	**Compound 164**	**Compound 165**	**Compound 166**
Val621(O)	NH	bbHB	25.10	98.36	24.97
Gln408(HE)	O	scHB	22.04	97.05	14.68
Lys643(NZ)	CN or S	I	56.35	6.38	25.88
Lys643(HZ)	O	scHB	0.00	0.00	15.78
Lys643	4-phenyl	Pcat	74.54	31.30	3.54
Lys643	N pyrimid.	WB	NA	NA	46.09
Trp706	Pyridine	Hyd	35.41	65.90	50.72
Phe411	3-Me-phenyl	Hyd	16.80	15.63	27.31
Phe 411	3-Me-phenyl	PP	30.29	1.23	33.20
Cys415	3-Me-phenyl	Hyd	5.93	6.72	3.60
Pro620	6-phenyl	Hyd	4.15	0.24	0.00
Val628	6-phenyl	Hyd	3.22	0.79	3.05
Leu666	4-phenyl	Hyd	2.88	2.47	0.79
Phe707	4-phenyl	Hyd	23.69	12.61	30.02
Phe710	4-phenyl	Hyd	46.97	24.16	19.01
Phe710	4-phenyl	PP	25.77	29.66	17.75
His713	4-phenyl	PP	10.04	14.20	0.00

[a] Only for hydrogen bonds and ionic contacts, the interacting atom is reported in brackets using the following abbreviations: O = backbone oxygen; HE = hydrogen of the side chain amide; NZ = nitrogen of the side chain amine; HZ = hydrogen side chain. [b] Type of interaction between the protein and the ligand. Abbreviations used: bbHB = hydrogen bond with residue backbone; scHB = hydrogen bond with residue side chain; I = ionic interaction; Pcat = π-cation interaction; Hyd = hydrophobic interaction; PP = π-π stacking; WB = water bridge.
[c] Percentage of trajectory frames in which the interaction was recorded. NA = not applicable.

From MD simulations it was possible to deduce that hydrogen bonds and ionic interactions are the most stable contacts between PA and the ligand, with occupancy higher than 60%, whereas in general, hydrophobic interactions are weaker. An exception is the hydrophobic interaction with Trp706 which is stable and important, particularly for compound **165** (65.90% occupancy) and for compound **166** (50.72% occupancy). The ionic contact between Lys643 side chain amine group and the compounds is much more important in the complex between the protein and **164**, where the interaction involves the CN group of the small molecule. Differently, weak ionic contacts occur between Lys643 and the sulfur atom of **165** and **166**. Lys643 side chain amine is involved in a π-cation contact with the phenyl moiety in C4 position of the core structure of the ligands which appears to be more stable for compound **164**, and is also involved in a water-bridge contact with one nitrogen of the pyrimidine of compound **166**. It is worth to note that this last type of interaction is not possible for

compounds **164** or **165**. Remarkably, hydrogen bonds between the amide portion of compound **165** and Val621 backbone oxygen and Gln408 side chain amide hydrogen present occupancy values close to 100%, while the same interactions in the other PA-compound complexes are weaker. From the visualization of the trajectories, a change of conformation of compounds **164** and **166** was observed. In particular, in the PA-compound **164** trajectory, the interaction between the CN group and Lys643 occurred during the whole duration of the simulation, while the hydrogen bonds with Val621 and Gln408 broke after approximately 4 ns. A shift of the pyridine core of **164** weakened the interaction of Trp706, placed the phenyl ring in C4 position in a more suitable area for the π-cation contact with Lys643, and enhanced the hydrophobic interactions with the areas II and III, explaining the higher occupancy values for these contacts (Lys643 π-cation contact and Phe707 and Phe710 hydrophobic interactions, in particular). Furthermore, the methyl-substituted phenyl ring lacks the constraints given by the hydrogen bonds involving the amide moiety of the ligands, and is able to give weak T-shaped π-π stacking with Phe411 in the hydrophobic area I. Regarding the PA-compound **166** trajectory, a shift of the central aromatic ring occurred after approximately 3.7 ns, similar to what was observed for the system containing molecule **164**. Also in this case, the change in the binding mode weakened the interaction with Trp706, increased the hydrophobic interactions with the areas II and III and allowed the establishment of a weak T-shaped π-π stacking with Phe411. However, in this simulation Lys643 did not give a π-cation interaction with the phenyl moiety, but it interacted with compound **166** through a direct hydrogen bond (with the carbonyl oxygen) and a water bridge (with the pyrimidine nitrogen), mainly after the compound repositioning. Thus, in the case of **166**, the water molecule has the same role of the CN group (**Figure 22.**)[491].

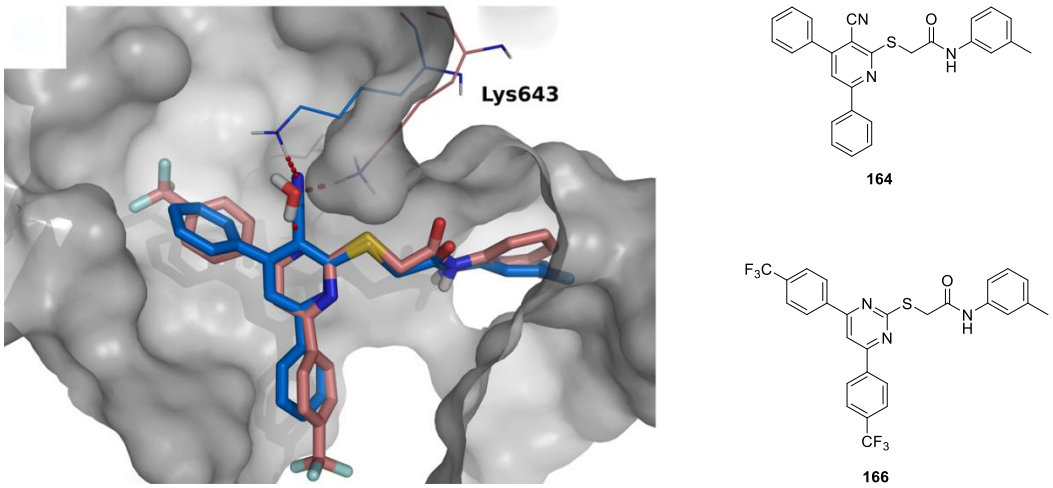

Figure 22. Superposition of the PA-compound **164** and PA-compound **166** complexes extracted after 4 ns of simulation. Carbon atoms of compound **164** are colored in blue; while the ones of compound **166** are in pink. The same color is used for protein carbon atoms. The water molecule is represented in sticks. Hydrogen bonds are indicated in red.

So, to summarize, from docking and MD studies it was seen that:

- The two hydrogen bonds between the amide portion of the ligands and residues Gln408 and Val621 seem to be important for the interaction between PA and the ligands, especially for pyridine derivatives.
- When present in the ligand, a third hydrogen bond occurs between the CN nitrogen of the compound and Lys643 amine side chain.
- The three phenyl rings are accommodated in three hydrophobic areas of PA indicated as I (Val 621, Phe411 and Cys415), II (Pro620, Val628 and His713) and III (Phe658, Leu666, Phe707 and Phe710).
- A hydrophobic interaction involves Trp706 and the pyridine or pyrimidine ring of the ligand.
- In the case of pyrimidine derivatives, a water bridge between the nitrogen group in the ring and Lys643 mimics the interaction that in cyanopyridine derivatives involves the CN group.

My doctorate research has been based upon the foundations described above.

4.2. Synthesis of hybrid 3-cyano-diphenylpyridine derivatives

4.2.1. Background

The overlap of PB1-N in the X-ray crystallography structure of PA[143] with the docking pose of the promising cyanopyridine compound **161** revealed that the cyano-pyridine core fits very well with a central region of PB1-N, but fails in establishing crucial interactions which are instead made with PA by the three terminal amino acids methionine-aspartate-valine (Met1-Asp2-Val3) of PB1-N peptide, highlighting the need to explore the C2 side chain of the cyanopyridine derivatives to find more potent RdRp PPI inhibitors (**Figure 23.**).

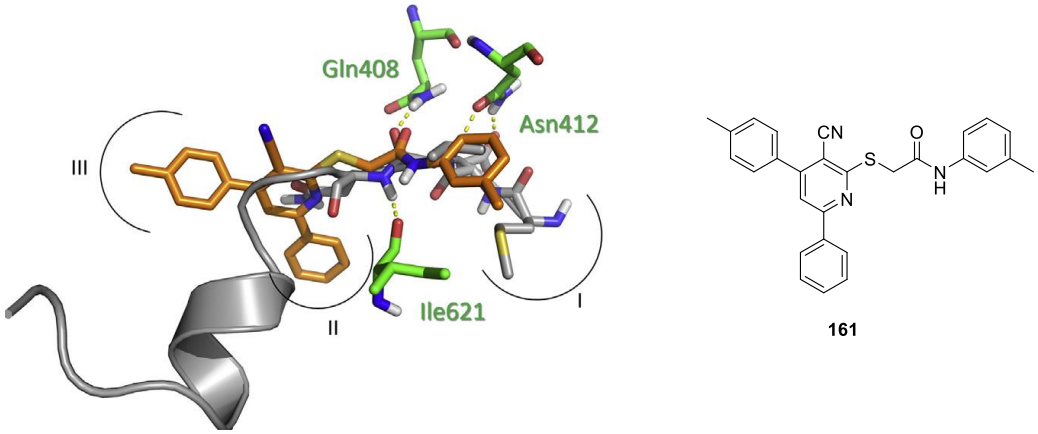

Figure 23. Superimposition of the crystallographic poses of PB1-N and the docking pose of compound **161**. PB1-N is showed as grey cartoon and the last three amino acids (Met1-Asp2-Val3) are represented by sticks. The three amino acids of PA (Gln408, Asn412 and Ile621) that interact with the C2 chain are represented by green sticks and labelled. The three protein regions I, II and III are highlighted.

Starting from this knowledge, I decided to synthesize a library of RdRp PPI inhibitors characterized by a hybrid structure constituted by the promising 3-cyano-4,6-diphenylpyridine core together with an aminoacidic side chain in C2 position[483].

4.2.1.1. Project: synthesis of hybrid 3-cyano-diphenylpyridine derivatives bearing the three final amino acids of PB1 in the C2 side chain

With the aim to enhance the ability of 3-cyano-diphenylpyridine compounds to completely displace PB1 and increase their affinity toward the target protein PA, I decided to synthesize hybrid derivatives combining the cyanopyridine core linked to the last three amino acids of PB1-N (Met-Asp-Val). The rational design was performed choosing the cyano-pyridine ring of compound **161** as the nucleus to which specific amino acids were added on the C2 side chain. Since the majority of the previously described virtual screening hits were characterized by a *p*-methyl group substituent on the C4 phenyl ring, this was maintained.

I synthesized the adducts with valine, valine-aspartate and valine-aspartate-methionine methyl esters (compounds **167a**, **168a** and **169**, respectively). I decided to introduce amino acids as esters because they are more permeable through membranes than the correspondent free acids[492,493]. Moreover, to confirm the hypothesis that the methyl ester derivatives could be hydrolyzed in cell, giving the corresponding free acids, I synthesized mono-amino acid and dipeptide derivatives as free acids **167b** and **168b**, respectively (**Figure 24.**).

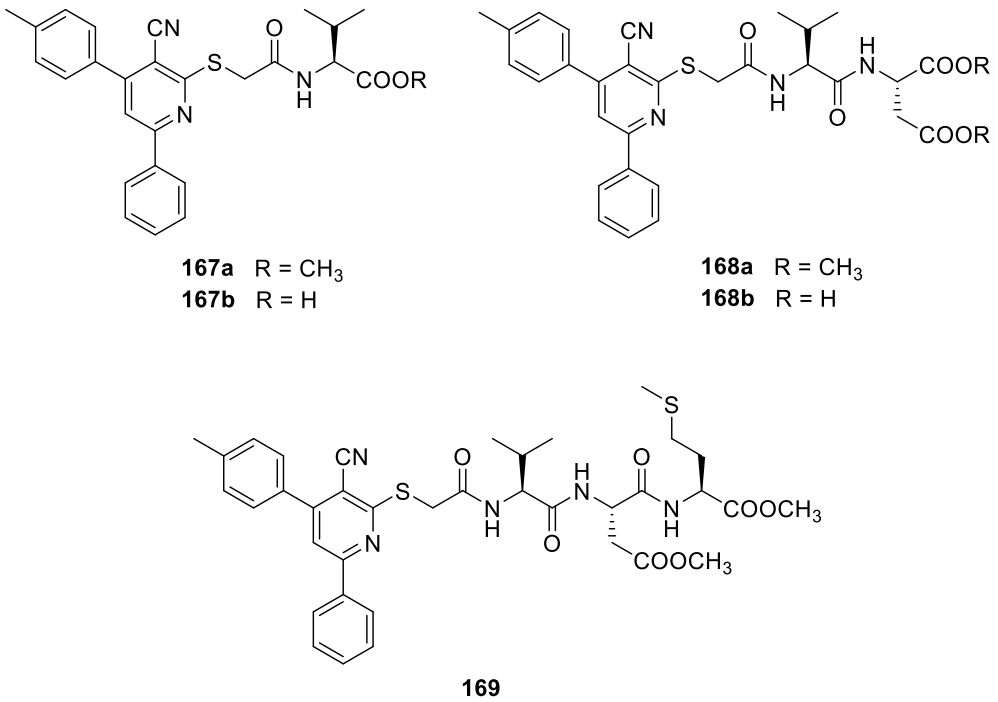

Figure 24. Structures of the synthesized hybrid compounds **167a,b**, **168a,b** and **169**.

4.2.1.1.1. Chemistry

The first part of the synthetic work has been devoted to the set-up of a fast and high yielding procedure for the preparation of the 3-cyano-4,6-diphenylpyridine nucleus. Starting materials were acetophenone and *p*-tolualdehyde which were reacted *via* base catalyzed Claisen-Schmidt-condensation reaction, affording the chalcone derivative **170**[494-496]. This acts as Michael acceptor, and the dihydropyridine derivative **171** was obtained through a Hantzch type cyclization of **170** with cyanothioacetamide using sodium methoxide (MeONa) as a base[497]. Compound **171** was aromatized with 2,3-dichloro-5,6-dicyano-*p*-benzoquinone (DDQ), affording 2-mercapto derivative **172**[498]**.** Then, a nucleophilic substitution with 2-bromoacetic acid was carried out in dimethylformamide (DMF) using potassium hydroxide (KOH) as base, affording the cyanopyridinic core **173** (**Scheme 1.**).

Scheme 1. Synthesis of the key intermediate **173**.

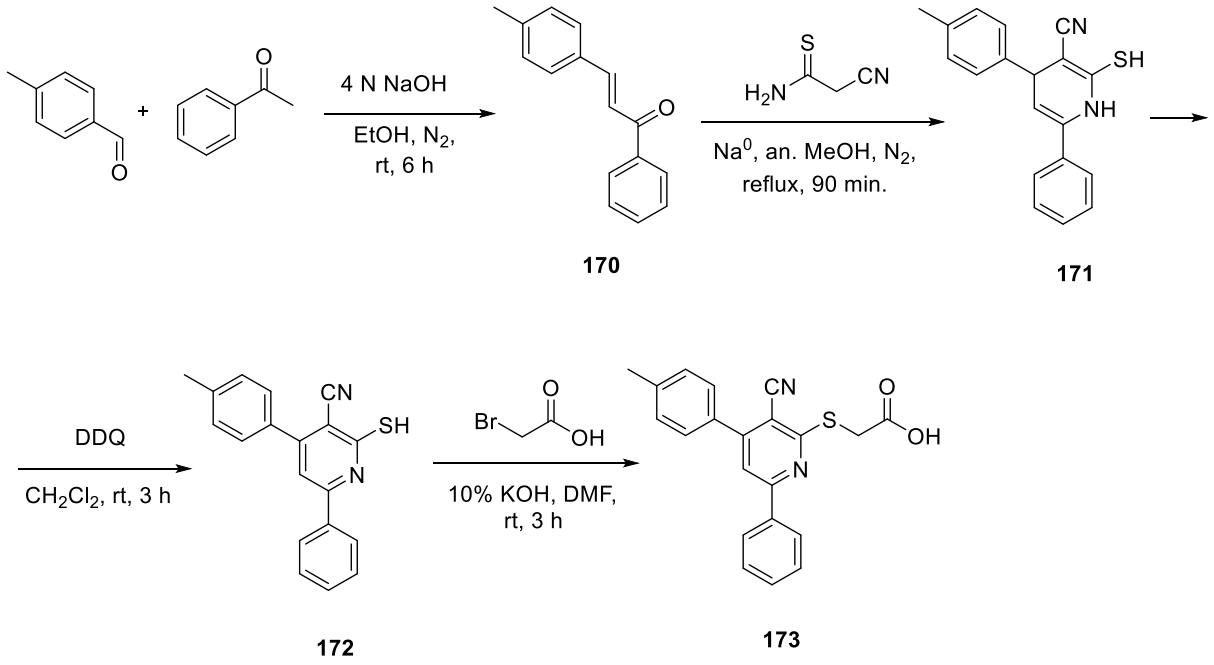

In order to obtain the mono-amino acid derivative **167a**, I performed the coupling reaction between intermediate **173** and L-Val methyl ester, using 1-ethyl-3-(3-dimethylaminopropyl) carbodiimide (EDC) and hydroxybenzotriazole (HOBt) as coupling agents[497] and racemization suppressors[499], and dry *N*,*N*-diisopropylethylamine (DIPEA) in anhydrous DMF.

Methyl ester **167a** was hydrolyzed in mild basic conditions, using 1 N sodium hydroxide (NaOH) solution, to get the free carboxylic derivative **167b** (**Scheme 2.**).

Scheme 2. Synthesis of mono-amino acid adducts **167a,b**.

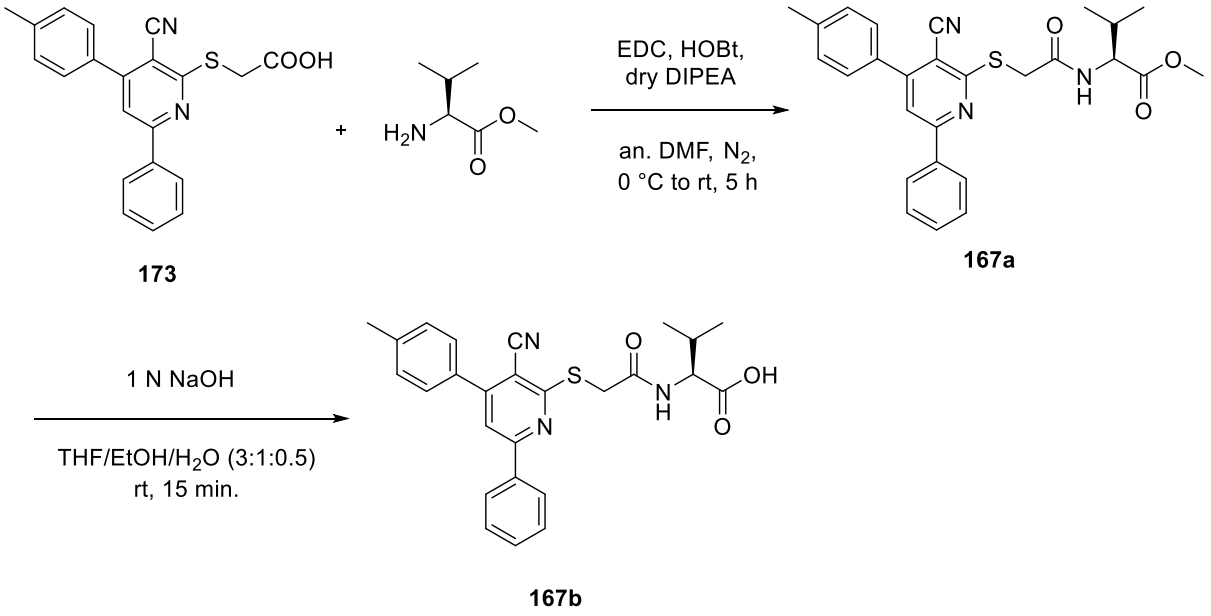

The synthetic route to obtain the diamino acid adduct **168a** is shown in **Scheme 3**. The L-Val-L-Asp dipeptide **168a** was synthesized in solution phase through the previous described amidation procedure, using L-Val amino acid protected with fluorenylmethyloxycarbonyl (Fmoc) group and L-Asp methyl ester. Dipeptide **174** was subjected to the cleavage of the Fmoc protecting group with sodium azide (NaN_3). The free amine **175** was then coupled with acid derivative **173**, furnishing the diamino acid adduct **168a**. Eventually, the ester functions of **168a** were hydrolyzed using the same basic conditions described before, affording the bicarboxylic acid derivative **168b**.

Scheme 3. Synthesis of diamino acid adducts **168a,b**.

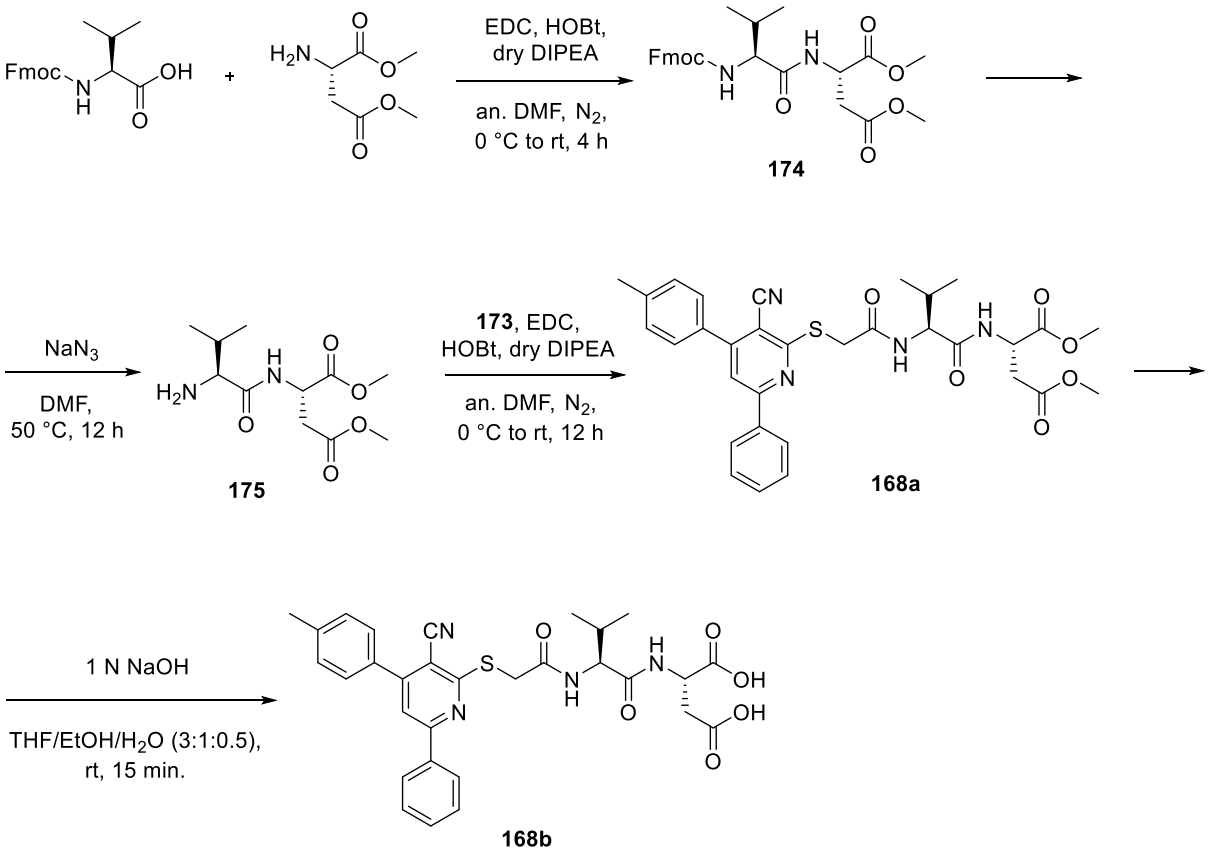

The synthesis of the tri-amino acid adduct **169** required the preparation of the tripeptide Val-Asp-Met, that was performed in solid phase through the Fmoc strategy. MW-SPPS (microwave solid phase peptide synthesis) was conducted by using an automated peptide synthesizer that was charged with a Wang resin bearing the last amino acid of the tripeptide, L-Met, covalently linked. Prior to use, the resin was swallowed for 2 h in DMF. In addition to resin and solvents (DMF and CH_2Cl_2), the instrument was also charged with the other two Fmoc-protected amino acids (Fmoc-L-Asp-(O*t*Bu) and Fmoc-L-Val), the coupling activators HOBt and 2-(1*H*-benzotriazol-1-yl)-1,1,3,3-tetramethyluronium hexafluorophosphate (HBTU), DIPEA and a deprotection solution (20% piperidine in DMF). At the end of the deprotection and coupling cycles, the resin-bounded tripeptide **176** was obtained.

The cleavage of the resin was performed using a solution of trifluoroacetic acid (TFA), water and triisopropylsilane (TIPS) as scavengers for the reactive species produced during the process, and dithiothreithol (DTT) to avoid L-Met oxidation. Under these acid conditions the tertbutyl ester in the L-Asp lateral chain was hydrolyzed, furnishing the resin-free tripeptide

177 that was used directly in the next step. The methyl esterification of dicarboxylic functions of **177**, accomplished by the treatment with a methanolic solution of freshly distilled thionyl chloride ($SOCl_2$), was necessary to avoid side reactions in next steps. The reaction was carried out at room temperature and with controlled equivalents of $SOCl_2$, in order to prevent the acid-catalyzed racemization of the L-Met stereocenter. The obtained tripeptide **178** was then deprotected from the Fmoc group with NaN_3, furnishing the free amine **179**. Intermediate **179** was coupled with carboxylic core **173**, using the amidation procedure previously described (EDC, HOBt and dry DIPEA in anhydrous DMF), affording the final tri-amino acid adduct **169** (**Scheme 4.**).

Scheme 4. Synthesis of tri-amino acid adduct **169**.

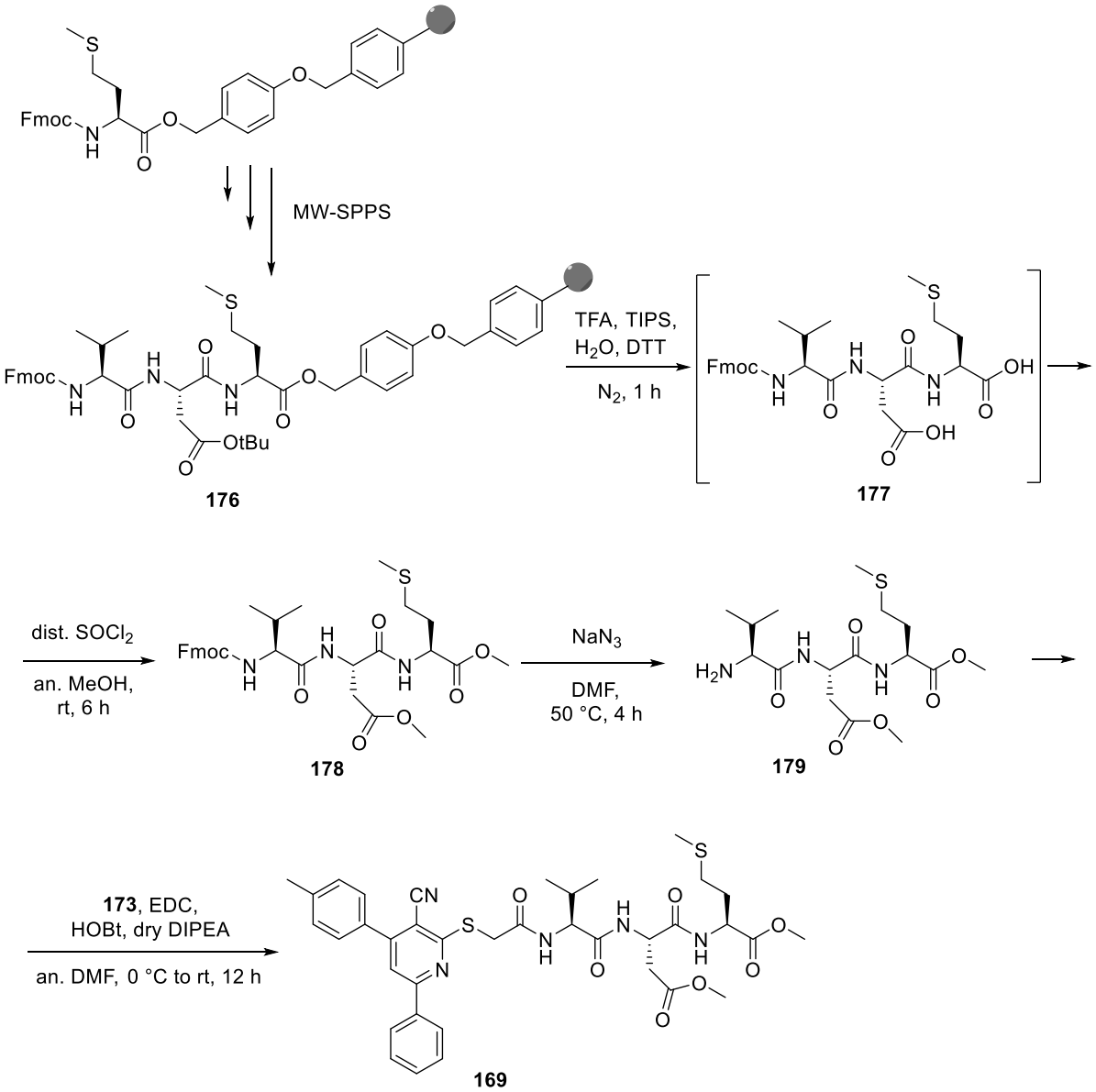

4.2.1.1.2. Biology: *in vitro* evaluation

Amino acid derivatives **167a,b**, **168a,b** and **169** and intermediate **173** were tested as inhibitors of the PA-PB1 interaction. The *in vitro* biological evaluation of these compounds was conducted through enzyme-linked immunosorbent–assays (ELISA) and plaque reduction assays (PRA) in Madin-Darby canine kidney (MDCK) cells infected with IAV (A/PR/8/34 strain). In particular, the ELISA PA-PB1 interaction assay can measure the physical inhibition between the two subunits, providing IC_{50} values. This assay was performed using the $PB1_{(1-}$

$_{15)}$-Tat peptide[370], as a positive control for inhibition. The PRA evaluates the block of the viral replication providing EC_{50} values and includes oseltamivir carboxylic acid (OSV), the active form of oseltamivir (NA inhibitor), and ribavirin (RBV), as positive controls. Cytotoxicity, which is evaluated by measuring CC_{50} values, was assessed both in MDCK cell lines and in human embryonic kidney 293 cells expressing a mutant version of the SV40 large T antigen (HEK 293 T), by MTT assays. Moreover, to confirm the mechanism of action of these molecules, the ability of the most interesting compounds to inhibit IAV RdRp enzymatic activity in a cellular context was assessed by minireplicon assays in transfected HEK 293 T cells, using RBV[500] as a reference drug, since it acts as RNA synthesis inhibitor thanks to its guanosine-like structure (**Table 2.**).

From biological tests, compound **169** turned out to be a weak inhibitor, while more interesting activity profiles have been revealed for compounds **167a** and **168a**. Experimental data show a relevant discordance between the low PA-PB1 interaction inhibition and the good intracellular activity, but minireplicon assays confirm the on-target activity, suggesting a possible enzymatic hydrolysis in the cell. In fact, the biological data of free-acid derivatives **167b** and **168b** seem to confirm that they are the actual responsible for the antiviral activity.

It is worth to mention that the good results of valine adducts **167a,b** are in agreement with experimental data previously reported by Wunderlich *et al.*[369], which revealed Val3 on the PB1 peptide as one of the most important residues for the interaction with PA, exhibiting the lowest binding free energy. This suggests that its displacement could inhibit the RdRp heterodimerization. The intermediate **173** was also tested and it showed an interesting activity profile, even if a low toxic behavior in HEK 293 T cell line was detected.

Table 2. Biological results of the synthesized compounds **167a,b**, **168a,b, 169** and **173**

Compound	CC_{50} (MDCK cells) [μM][c,e]	CC_{50} (HEK 293 T cells) [μM][c,e]	EC_{50} (MDCK cells) [μM][b,e]	IC_{50} (ELISA PA-PB1) [μM][a,e]	EC_{50} (Minireplicon assay) [μM][d,e]
167a	210 ± 8	>250	52 ± 2	167 ± 20	41 ± 16
167b	>250	250	50 ± 7	76 ± 16	77 ± 14
168a	>250	>250	49 ± 8	143 ± 17	59 ± 18
168b	>250	ND	100	77 ± 9	ND
169	>250	ND	>100	68 ± 14	ND
173	>250	218 ± 21	65 ± 11	56 ± 5	43 ± 14
$PB1_{(1-15)}$ - Tat peptide	>250	>250	49.7 ± 5.1	31.7 ± 10.8	15.5 ± 2.6
OSV	>250	>250	0.015 ± 0.006	ND	ND
RBV	>250	>250	12.8 ± 2.1	ND	23.8 ± 4.5

ND: not determined. [a]Activity of the compounds in the ELISA PA-PB1 interaction assay. Values represent the compound concentration (in μM) that reduces the interaction between PA and PB1 by 50% (IC_{50}). [b]Antiviral activity of the compounds in plaque reduction assays against the IAV A/PR/8/34 strain. Values represent the compound concentration (in μM) that inhibits 50% of plaque formation (EC_{50}). [c]Cytotoxicity of the compounds exhibited in MTT assays. Values represent the compound concentration (in μM) that causes a 50% decrease in cell viability (CC_{50}). The CC_{50} were assessed in MDCK and HEK 293 T cells. [d]The EC_{50} values represent the compound concentration that reduces by 50% the activity of IAV RNA polymerase in HEK 293 T cells. [e]All values represent the means ± SD of data derived from at least three independent experiments in duplicate. Reference compounds are $PB1_{(1-15)}$-Tat peptide, oseltamivir carboxylic acid (OSV) and ribavirin (RBV).

4.2.1.1.3. Molecular modeling

Using the GOLD program (GoldScore function)[501], molecular docking studies on the synthesized compounds within the PB1-binding site of PA using the crystallographic structure 4WSB[143] were performed. In particular, studies were carried out to investigate the possible binding mode of molecules **167a,b**, **168a,b**, **169** and intermediate **173** within the PB1 binding site of PA. The 3-cyano-4,6-diphenylpyridine scaffold binds in a hydrophobic cleft of PA, which is known to accommodate the binding partner PB1[144], while the peptide chain occupies a narrow and more solvent-exposed pocket where it establishes a network of H-bond interactions with key PA residues, including Gln408, Asn412, Ile621 and Glu623. Only few compounds are able to contact Lys635 and Glu416. Notably, all compounds show to fit the PB1 site of PA with a binding geometry that is highly comparable with each other (**Figure 25.**).

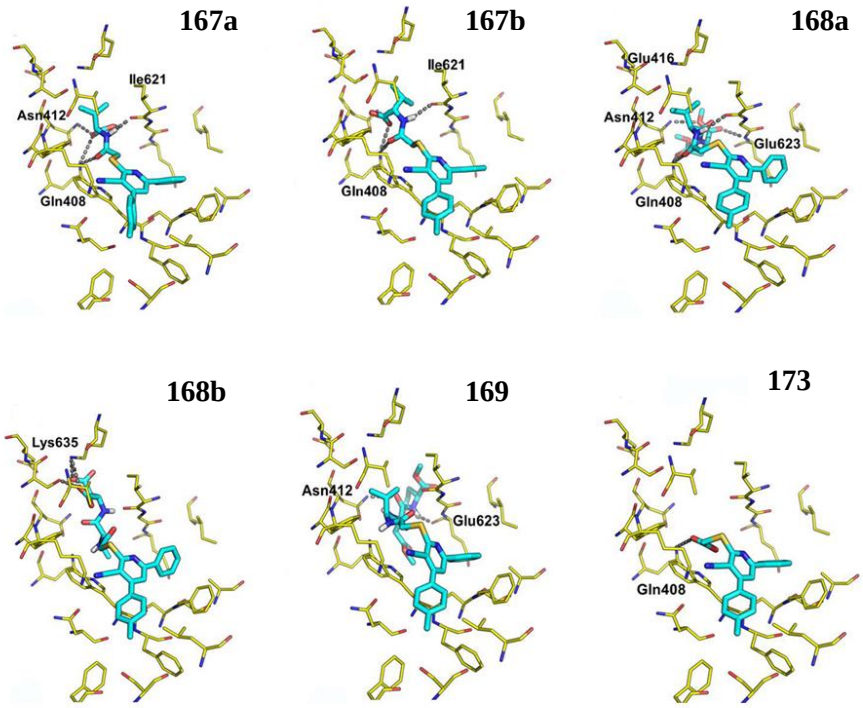

Figure 25. Possible binding mode of the synthesized hybrid derivatives **167a,b**, **168a,b**, **169** and intermediate **173**. The crystallographic structure of PA in complex with PB1 (PDB: 4WSB) is shown as yellow lines. Ligands are shown as cyan sticks. Polar interactions are highlighted by grey dashed lines. Only residues within 4 Å from the ligands are shown; non-polar H atoms are omitted.

Moreover, in order to confirm the initial hypothesis, the superposition of the docking pose of **169** binding mode with the PB1-N fragment was performed. These studies demonstrated that derivative **169** is able to maintain the crucial interactions with PA and show a good overlap of the tripeptide region with PB1-N (**Figure 26.**).

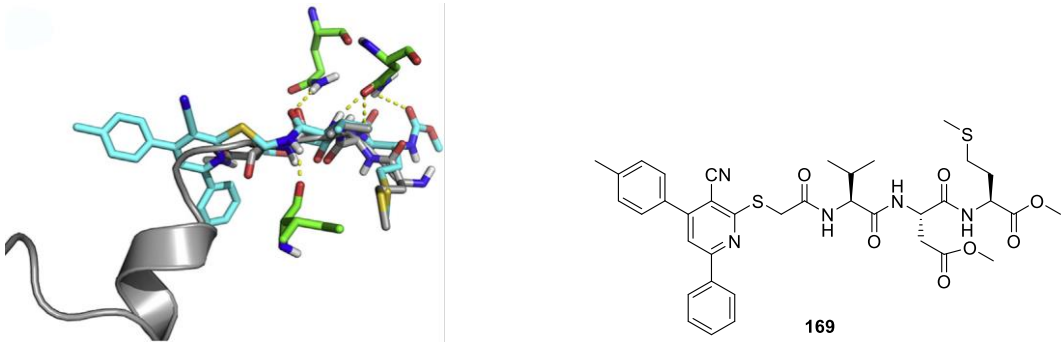

Figure 26. Superposition of docking poses of compound **169** and PB1-N. Ligand is showed as cyan sticks, PA residues are represented by green sticks while PB1-N in grey. Key interactions are highlighted.

4.2.1.1.4. Conclusions

In recent years, the viral polymerase has proved to be an important target for drug design. In particular, the development of small molecules able to interfere with the correct assembly of RdRp complex, through the inhibition of the interaction between PA and PB1, is an attractive goal. Starting from a rational drug design, I synthesized hybrid compounds characterized by a 3-cyano-4,6-diphenylpyridine nucleus and the three last same amino acids of PB1-N (Met-Asp-Val) in the C2 side chain. The biological data results highlighted a major anti-flu activity (EC_{50} in PRA) of **167a** and **168a**, not correlated to the low enzymatic inhibition (IC_{50} in ELISA). To better investigate this discrepancy, minireplicon experiments were performed, confirming the PA-PB1 interaction disruption as the main target of the compounds. Moreover, the hypothesis that these methyl ester derivatives could be hydrolyzed in cells was confirmed by the biological results of the free acid derivatives **167b** and **168b**, which showed a better IC_{50} when compared to that of **167a** and **168a**. In summary, the synthesis of these hybrid compounds allowed to explore the potential antiviral activity of this new class of 3-cyanopyridine derivatives and to acquire information to guide the subsequent syntheses of new hybrid compounds as potential IAV RdRp PPI inhibitors.

4.2.1.2. Project: synthesis of 3-cyano-4,6-diphenylpyridine derivatives bearing different L-amino acids methyl esters in the C2 side chain

Encouraged by the previously described findings, I decided to investigate the effects of the introduction of other amino acids on the interaction between PA and PB1 subunit of RdRp, through the addition of different L-amino acids as methyl esters in the C2 side chain of the 3-cyano-4,6-diphenylpyridine nucleus, synthesizing a small library of derivatives **180a-g** (**Figure 27.**)[483]. L-leucine (L-Leu) (**180a**) and L-isoleucine (L-Ile) (**180b**) have been chosen as good hydrophobic replacement of valine, while other residues have been selected as representatives of all the existing classes of amino acids, to investigate the possible interactions of their different functions. L-histidine (L-His) (**180c**) and L-arginine (L-Arg) (**180d**) bear a positive charge at physiological pH, L-phenylalanine (L-Phe) (**180e**) and L-tyrosine (L-Tyr) (**180f**) are characterized by aromatic lateral chains that can interact with the hydrophobic protein region I. Finally, L-glutamate (L-Glu) (**180g**), if hydrolyzed, bears negative charges that could enhance the affinity of the ligand towards the protein.

Compound	R	Structure of R
180a	L-Leu	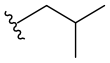
180b	L-Ile	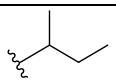
180c	L-His	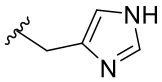
180d	L-Arg	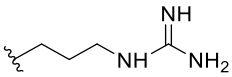
180e	L-Phe	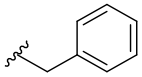
180f	L-Tyr(OH)	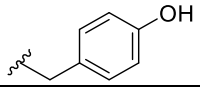
180g	L-Glu(OCH_3)	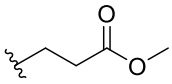

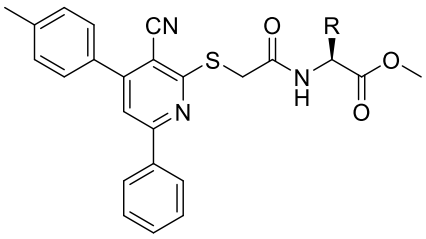

R = L-amino acid methyl ester side chain

180a-g

Figure 27. Synthesized L-mono-amino acid hybrid compounds **180a-g**.

4.2.1.2.1. Chemistry

To synthesize the mono-amino acid adducts **180a-g**, I used the amidation procedure previously described (EDC, HOBt, dry DIPEA in anhydrous DMF) to react together intermediate **173** and the opportune L-amino acid methyl ester (**Scheme 5.**).

Scheme 5. Synthesis of mono-amino acid methyl ester hybrid derivatives **180a-g**.

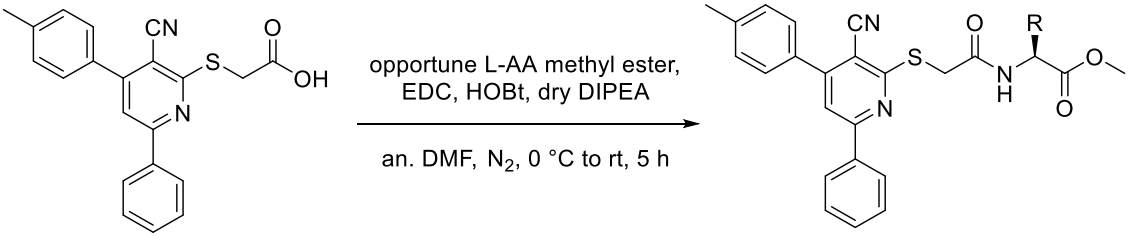

173

R = L-amino acid methyl ester side chain

180a-g

4.2.1.2.2. Biology: *in vitro* evaluation

Derivatives **180a-g** were tested as inhibitors of the PA-PB1 interaction. As for the previously described hybrid molecules, the *in vitro* biological evaluation was conducted through ELISA assay (IC_{50} values) and PRA (EC_{50} values) in MDCK cells infected with IAV (A/PR/8/34 strain), while cytotoxicity was assessed both in MDCK and HEK 293 T cell lines by MTT assays. For the most interesting compounds the ability to inhibit IAV RdRp enzymatic activity in a cellular context was assessed by minireplicon assays in transfected HEK 293 T cells. As before, $PB1_{(1-15)}$-Tat peptide, OSV and RBV were used as positive controls.

The results of the biological tests on the synthesized compounds are promising: apart from **180c**, none of the tested compounds are cytotoxic in MDCK and HEK 293 T cells (CC_{50} > 200 µM), and many of them are endowed with good antiviral activity as disruptor of the PA-PB1 interaction. The most promising derivative is compound **180b** that has a good antiviral activity in infected cells (EC_{50} = 39 ± 2 µM in PRA) and likely acts by inhibiting the PA-PB1 PPI, as suggested by both the ELISA (IC_{50} = 36 ± 3 µM) and the minireplicon assays (EC_{50} = 53 ± 16 µM). It is worth to underline that, although the small difference in the side chain between derivatives **180b** and **180a**, this latest appears to have a low ability to disrupt the PA-PB1 interaction (IC_{50} = 149 ± 15 µM) and to inhibit the activity in infected cells (EC_{50} = 97 ± 9 µM). Regarding the other amino acid derivatives, compounds **180c,d** and **180f** have good activities in the ELISA experiments but, unfortunately, **180c** is cytotoxic (CC_{50} = 152 ± 28 µM in MDCK cells), while **180d** and **180f** does not retain the antiviral activity in cells (EC_{50} > 100 µM). A particular case is the one of the phenylalanine derivative **180e** that seems not to have affinity with PA (IC_{50} > 200 µM), but in infected cells is active, perhaps after the ester hydrolysis or through an off-target mechanism of action. At the end, the glutamate derivative **180g** is found to be inactive (**Table 3.**).

Table 3. Biological results of the synthesized compounds **180a-g**.

Compound	CC_{50} (MDCK cells) [µM][c,e]	CC_{50} (HEK 293 T cells) [µM][c,e]	EC_{50} (MDCK cells) [µM][b,e]	IC_{50} (ELISA PA-PB1) [µM][a,e]	EC_{50} (Minireplicon assay) [µM][d,e]
180a	215 ± 28	ND	97 ± 9	149 ± 15	ND
180b	>250	229 ± 12	39 ± 2	36 ± 3	53 ± 16
180c	152 ± 13	ND	80 ± 6	32 ± 7	ND
180d	>250	ND	>100	48 ± 8	ND
180e	240 ± 18	ND	68 ± 10	>200	ND
180f	>250	ND	>100	18 ± 5	ND
180g	>250	ND	>100	187 ± 14	ND
$PB1_{(1-15)}$-Tat peptide	>250	>250	49.7 ± 5.1	31.7 ± 10.8	15.5 ± 2.6
OSV	>250	>250	0.015 ± 0.006	ND	ND
RBV	>250	>250	12.8 ± 2.1	ND	23.8 ± 4.5

ND: not determined. [a]Activity of the compounds in the ELISA PA-PB1 interaction assay. Values represent the compound concentration (in µM) that reduces the interaction between PA and PB1 by 50% (IC_{50}). [b]Antiviral activity of the compounds in plaque reduction assays against the IAV A/PR/8/34 strain. Values represent the compound concentration (in µM) that inhibits 50% of plaque formation (EC_{50}). [c]Cytotoxicity of the compounds exhibited in MTT assays. Values represent the compound concentration (in µM) that causes a 50% decrease in cell viability (CC_{50}). The CC_{50} were assessed in MDCK and HEK 293 T cells. [d]EC_{50} values represent the compound concentration that reduces by 50% the activity of IAV RNA polymerase in HEK 293 T cells. [e]All values represent the means ± SD of data derived from at least three independent experiments in duplicate. Reference compounds are $PB1_{(1-15)}$-Tat peptide, OSV and RBV.

4.2.1.2.3. Molecular modeling

Similarly to what was done for the previously described hybrid compounds, molecular docking studies on the synthesized compounds **180a-g** within the PB1-binding site of PA, using the crystallographic structure 4WSB, were carried out to investigate their possible binding mode. These studies were performed using the GOLD program (GoldScore function)[501], and confirmed that the 3-cyano-4,6-diphenylpyridine scaffold binds in a PA hydrophobic cleft which is known to accommodate PB1, while the peptide chain occupies a narrow and more solvent-exposed pocket where it establishes a network of H-bond interactions with key PA residues. All synthesized compounds **180a-g** show to fit the PB1 site of PA with a binding geometry that is highly comparable among all the derivatives (**Figure 28.**).

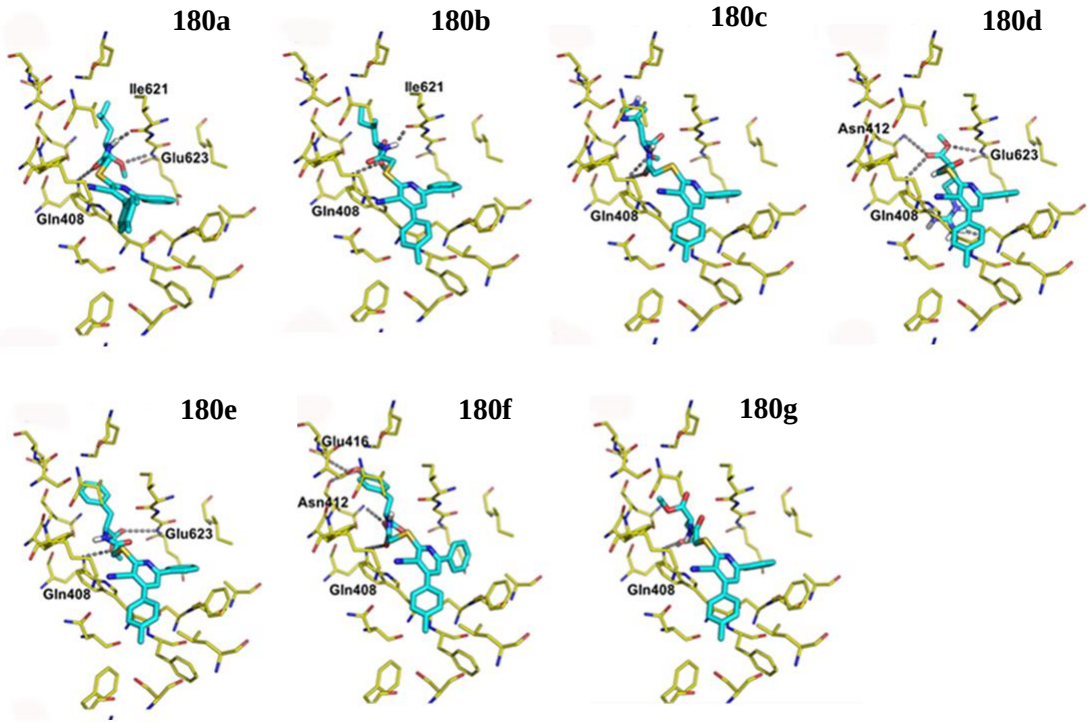

Figure 28. Possible binding mode of the synthesized mono-amino acid derivatives **180a-g.** The crystallographic structure of PA in complex with PB1 (PDB: 4WSB) is shown as yellow lines. Ligands are shown as cyan sticks. Polar interactions are highlighted by grey dashed lines. Only residues within 4 Å from the ligands are shown; non-polar H atoms are omitted.

Therefore, to identify the possible molecular determinants responsible for the strong inhibition in the ELISA assay, MD investigations on the docking-based complexes between PA and compounds **180e** and **180f** were carried out (**Figure 29.**). These two molecules differ each other only for the OH phenol group in **180f** that is missing in **180e**, but were notably different in the ELISA experiment, as **180e** is inactive up to 200 µM concentration**,** while **180f** is a potent PA-PB1 inhibitor. Thus, they represent a suitable model system to challenge MD simulations. In particular, the representative docking complexes of **180e** and **180f** were solvated in a box of water molecules and were energy minimized, heated and equilibrated in density[502,503] before running 250 ns of unrestrained MD simulations. Cluster analysis performed on the whole MD production trajectories coupled with visual inspection, clearly indicate that **180f** is stable in the PB1 binding site, with a conformation that is highly consistent to that identified by molecular docking. The nitrile group of **180f** establishes a H-bond interaction with the side chain of Lys643, the two phenyl rings of the 3-cyano-4,6 diphenylpyridine scaffold are included in a hydrophobic cleft bounded by Pro625, Phe658,

Leu666, Trp706, Phe707, and Phe710. The peptide moiety overlaps with the crystallographic pose of the PB1-N[144] and establishes a network of H-bonds. The amide bond contacts Glu623 and Gln408 (bridged by a water molecule), that, as previously said, are crucial residues for the binding of PA-PB1 inhibitors. The L-Tyr side chain of **180f** is accommodated in a hydrophobic sub-pocket of PA, where it interacts with Asn412 (bridged by a water molecule), Ser415 and Lys635. It is worth mentioning that these three H-bonds are established by the OH phenol group of **180f**, which is missing in **180e**. Different from the docking pose, the peptide moiety of **180e** bends back towards the hydrophobic cleft of PA, thus assuming an unfavorable placement. Moreover, in this conformation, **180e** is unable to establish most of H-bond interactions with PA key residues, with the only exception of a single H-bond to Lys635. So, to conclude, the different binding conformation and interaction network between these two compounds might explain their different behaviors observed in the ELISA PA-PB1 interaction assay.

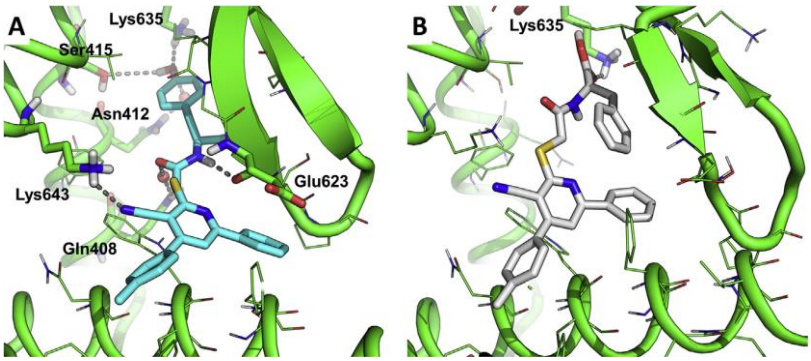

Figure 29. Binding pose of **180f** (panel A) and **180e** (panel B) extrapolated from the most representative cluster of MD frames. The protein is shown as green cartoon, residues within 4 Å from the ligand are shown as lines, residues H-bonded to the ligand are shown as sticks and are labelled. Non-polar H atoms are omitted. Bridged water molecules are shown as red spheres, while the bulky solvent is omitted. **180e** is shown as white sticks, **180f** as cyan sticks. H-bond interactions are highlighted by grey dashed lines.

4.2.1.2.4. Conclusions

The synthesis of the small library of hybrid derivatives **180a-g** was planned to better explore the chemical space around the C2 side chain of the 3-cyano-4,6-diphenylpyridine core and to try to find more potent IAV RdRp PPI inhibitors. Interestingly, the modulation in C2 of the starting chemical structure led to an increase in the on-target activity. In particular, the best results were achieved with the isoleucine derivative **180b**, which exhibited a good biological

profile with no cytotoxic behavior. Moreover, modeling simulations added further insights into the inhibition mechanism of these compounds.

4.2.1.3. Project: synthesis of 3-cyano-4,6-diphenylpyridine hybrid derivatives endowed with an L- or D- amino acid as benzyl or methyl ester in the C2 side chain

With the aim to further explore the mono-aminoacidic peptidomimetic side chain in C2 position of the 3-cyano-4,6-diphenylpyridine core, I synthesized derivatives **181a-e** (**Figure 30.**). I introduced in C2 the same amino acids that were present in the most promising derivatives previously described **181a-g**, exploring the effect of different conformations (D or L) and/or different ester groups (methyl or benzyl ester) of the amino acid.

Compound	R	Structure of R	R^1
181a	L-Val		$CH_2C_6H_5$
181b	D-Val		CH_3
181c	D-Val		$CH_2C_6H_5$
181d	L-Leu	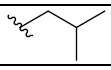	$CH_2C_6H_5$
181e	L-Ile	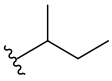	$CH_2C_6H_5$

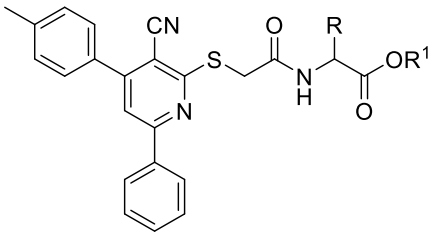

R = D- or L-amino acid side chain
R^1 = CH_3 or $CH_2C_6H_5$

181a-e

Figure 30. Synthesized D or L- mono-amino acid hybrid compounds **181a-e**.

4.2.1.3.1. Chemistry

The synthesis of derivatives **181a-e** was performed using the condensation reaction previously described (EDC, HOBt, dry DIPEA in anhydrous DMF) between intermediate **173** and the methyl or benzyl ester of the opportune D- or L- amino acid (**Scheme 6.**).

Scheme 6. Synthesis of mono-amino acid methyl or benzyl ester hybrid derivatives **181a-e**.

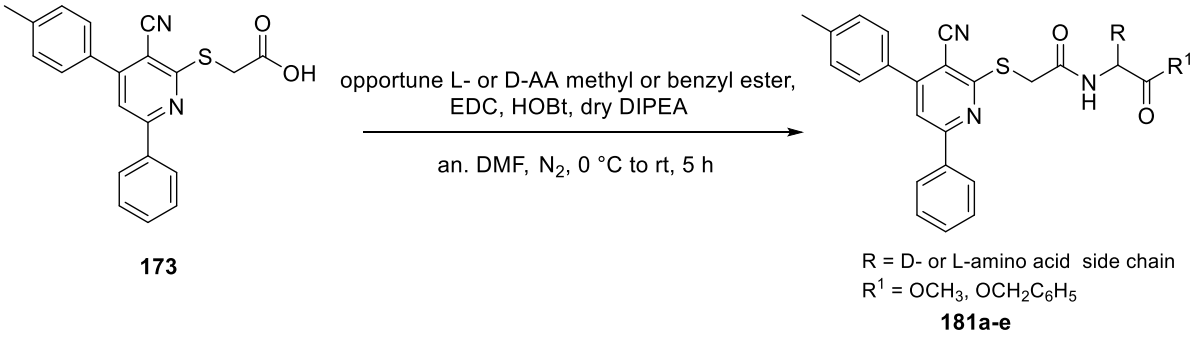

173

R = D- or L-amino acid side chain
R^1 = OCH_3, $OCH_2C_6H_5$

181a-e

4.2.1.3.2. Biology: *in vitro* evaluation

Derivatives **181a-e** were tested as inhibitors of the PA-PB1 interaction through ELISA assay. Their antiviral activity was measured with PRA in MDCK cells infected with IAV virus (A/PR/8/34 strain), while cytotoxicity was assessed in MDCK by MTT assays. $PB1_{(1-15)}$-Tat peptide, OSV and RBV were used as positive controls. In **Table 4.** the biological data are reported. All the synthesized compounds are not cytotoxic but, unfortunately, the majority of them do not have a promising antiviral activity in cell (EC_{50} >100) and also the IC_{50} values are not so good as expected. An exception is the L-Val benzyl ester adduct **181a**, that has a promising antiviral activity in cell (EC_{50} = 69.5 μM) together with a good ability to disrupt the PA-PB1 interaction (IC_{50} = 42 μM).

Table 4. Biological results of the synthesized compounds **181a-e**.

Compound	CC_{50} (MDCK cells) [µM][c,d]	EC_{50} (MDCK cells) [µM][b,d]	IC_{50} (ELISA PA-PB1) [µM][a,d]
181a	>250	69.5	42
181b	>250	>100	153.3 ± 50.3
181c	>250	>100	181.7 ± 14.4
181d	>250	>100	161.7 ± 20.8
181e	>250	>100	98.3 ± 22.5
$PB1_{(1-15)}$-Tat peptide	>250	49.7 ± 5.1	31.7 ± 10.8
OSV	>250	0.015 ± 0.006	ND
RBV	>250	12.8 ± 2.1	ND

[a]Activity of the compounds in the ELISA PA-PB1 interaction assay. Values represent the compound concentration (in µM) that reduces the interaction between PA and PB1 by 50% (IC_{50}). [b]Antiviral activity of the compounds in plaque reduction assays against the IAV A/PR/8/34 strain. Values represent the compound concentration (in µM) that inhibits 50% of plaque formation (EC_{50}). [c]Cytotoxicity of the compounds exhibited in MTT assays. Values represent the compound concentration (in µM) that causes a 50% decrease in cell viability (CC_{50}). The CC_{50} were assessed in MDCK cells. [d]All values represent the means ± SD of data derived from at least three independent experiments in duplicate. Reference compounds are $PB1_{(1-15)}$-Tat peptide, OSV and RBV.

4.2.1.3.3. Conclusions

Despite overall the antiviral activity and the ability as RdRp PPI inhibitors of these compounds were not as good as expected, this small library of mono-amino acid hybrid derivatives **181a-e** allowed to extend SAR evaluations and to add to the previous knowledge important information in the way to find new hybrid antiviral compounds. In fact, from the comparison of the biological results of the three synthesized small library of hybrid compounds is possible to make some important SAR evaluations. For example, in the case of valine derivatives, it is possible to say that **167a** and **181a**, bearing L-Val as amino acid, have better antiviral activity than **181b** and **181c**, bearing D-Val. This is probably due to the fact that the L conformation allows the compound to better enter the cell than the D conformation. Regarding the ability to disrupt the PA-PB1 interaction, the most promising result is that of L-Val benzyl ester adduct **181a**. For L-Leu derivatives, it is possible to say that the methyl and benzyl ester, **180a** and **181d** respectively, have comparable ability to disrupt the PA-PB1 interaction, while in the case of L-Ile derivatives, the benzyl ester **181e** get worse the antiviral activity in cell and inhibition of the PA-PB1 interaction than methyl ester **180b**. However, more studies are needed to go deeper in this class of hybrid compounds and to better

understand for example, why, despite the small difference in the lateral chain, L-Val benzyl ester shows a better ability to disrupt the PA-PB1 interaction than the methyl ester derivative, while for compound having L-Ile as amino acid in the lateral chain is the contrary.

4.3. Synthesis of a library of phenyl pyrimidine derivatives

4.3.1. Background

Since SAR studies seem to show that the cyano group is not essential for the antiviral activity, and considering that it is often related to potential cytotoxicity, it was decided to remove the CN group in C3 position of the pyridine derivatives and to include the nitrogen atom in the ring. For this reason, two representative pyrimidine derivatives **166** and **182** were synthesized and tested (**Figure 31.**). The biological results on these molecules were quite promising: **166** had a good cytotoxicity profile (CC_{50} > 250 µM both in HEK 293T and MDCK cells), but an IC_{50} > 200 µM. On the other hand, **182** had a good antiviral activity as disruptor of PA-PB1 interaction (IC_{50} = 165 ± 18 µM), although the cytotoxicity values were not so good (CC_{50} of 22.3 ± 1.8 µM and 10.1 ± 1.7 µM in HEK 293 T and MDCK cells, respectively)[491].

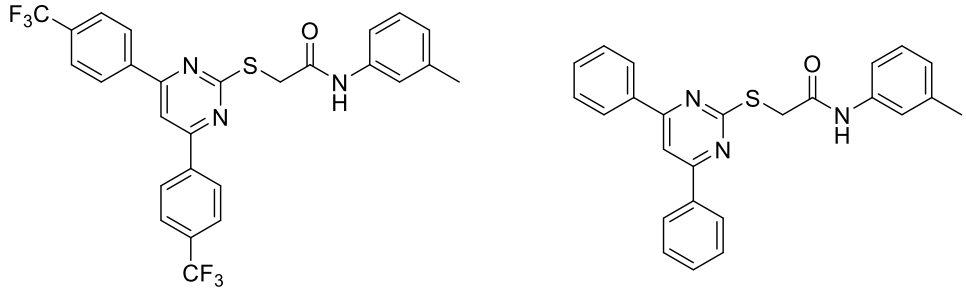

Figure 31. Structure of the two previously synthesized pyrimidine compounds **166** and **182**.

As previously said, another confirmation of the possibility of removing the CN group without affecting the key interactions between the compounds and PA subunit, came from MD simulation. In fact, this study suggested that the lack of the ionic contact between the CN group and Lys643 side chain amine is compensated by the fact that the nitrogen in the pyrimidine core is able to establish a water bridge that mimics the CN group. Interestingly,

this water molecule overlapped very well with the CN nitrogen of the 3-cyanopyridine derivatives, when the structures of PA-compound **164** and PA-compound **166** were extracted after 4 ns of MD simulation and were superposed (see **Figure 22.**)[491].

4.3.2. Project

Starting from these promising results, I decided to synthesize a library of phenyl pyrimidine derivatives **183a-n** (**Figure 32.**). Following a rational design process, I maintained in C2 the 2-mercapto-*N*-(*m*-tolyl)acetamide chain that was present in the promising compound **161**, and I explored the effect of different aromatic substituents in C4 and C6 of the pyrimidine ring. I introduced as substituents the phenyl group unsubstituted or *p*-substituted with halogens (Cl and F) and the 1-naphtyl group, with the aim of extending the hydrophobic interactions of the molecule. Furthermore, I inserted the thiophenolic ring to investigate the effect of a more flexible aromatic substituent on the activity. Finally, in compound **183n** I decided to introduce an aromatic amide to explore possible new interactions with the PA key residues. Moreover, all of these aromatic substituents allowed to explore thoroughly the two hydrophobic areas II and III of the PA subunit.

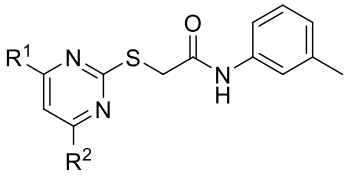

183a-n

a $R^1 = C_6H_5$; R^2 = 1-naph.
b $R^1 = C_6H_4$-4Cl; R^2 = 1-naph.
c $R^1 = C_6H_4$-4F; R^2 = 1-naph.
d $R^1 = C_6H_5$; $R^2 = SC_6H_5$
e $R^1 = C_6H_4$-4Cl; $R^2 = SC_6H_5$
f $R^1 = C_6H_4$-4F; $R^2 = SC_6H_5$
g $R^1 = C_6H_5$; $R^2 = C_6H_4$-4Cl
h $R^1 = C_6H_5$; $R^2 = C_6H_4$-4F
i $R^1 = C_6H_4$-4Cl; $R^2 = C_6H_4$-4F
l $R^1 = C_6H_4$-4Cl; $R^2 = C_6H_4$-4Cl
m $R^1 = C_6H_4$-4F; $R^2 = C_6H_4$-4F
n $R^1 = CONHC_6H_5$; $R^2 = C_6H_5$

Figure 32. Synthesized library of pyrimidine compounds **183a-n**.

4.3.3. Chemistry

Derivatives **183a-i** were synthesized starting from a Suzuki reaction between 2,4,6-trichloropyrimidine and the opportune phenyl boronic acid, in the presence of the catalysts palladium acetate ($Pd(OAc)_2$) and triphenylphosphine (PPh_3) and an aqueous solution of

sodium carbonate (Na_2CO_3) in tetrahydrofuran (THF), to obtain the key intermediates **184a-c**. The reaction was carried out following published Suzuki reaction procedures[504,505] with some modifications, as reported in the experimental section. From derivatives **184a-c** with another Suzuki reaction, using 1-naphthalene boronic acid or the appropriate phenylboronic acid in dimethoxyethane (DME) or THF, I obtained compounds **185a-c** and **185g-i**, respectively. The reaction between intermediates **184a-c** and thiophenol led to molecules **185d-f**. To introduce the thiophenolic moiety, I used two different procedures, NaOH in water and acetone or sodium hydride (NaH) in anhydrous DMF, depending on the starting material. With an aromatic nucleophilic substitution reaction[491] using 2-mercapto-*N*-(*m*-tolyl)acetamide, anhydrous potassium carbonate (K_2CO_3), in anhydrous acetonitrile (MeCN), under nitrogen atmosphere at room temperature for 5 h, I introduced the C2 lateral chain, obtaining the desired final compounds **183a-i** (**Scheme 7.**).

Scheme 7. Synthesis of pyrimidine derivatives **183a-i**.

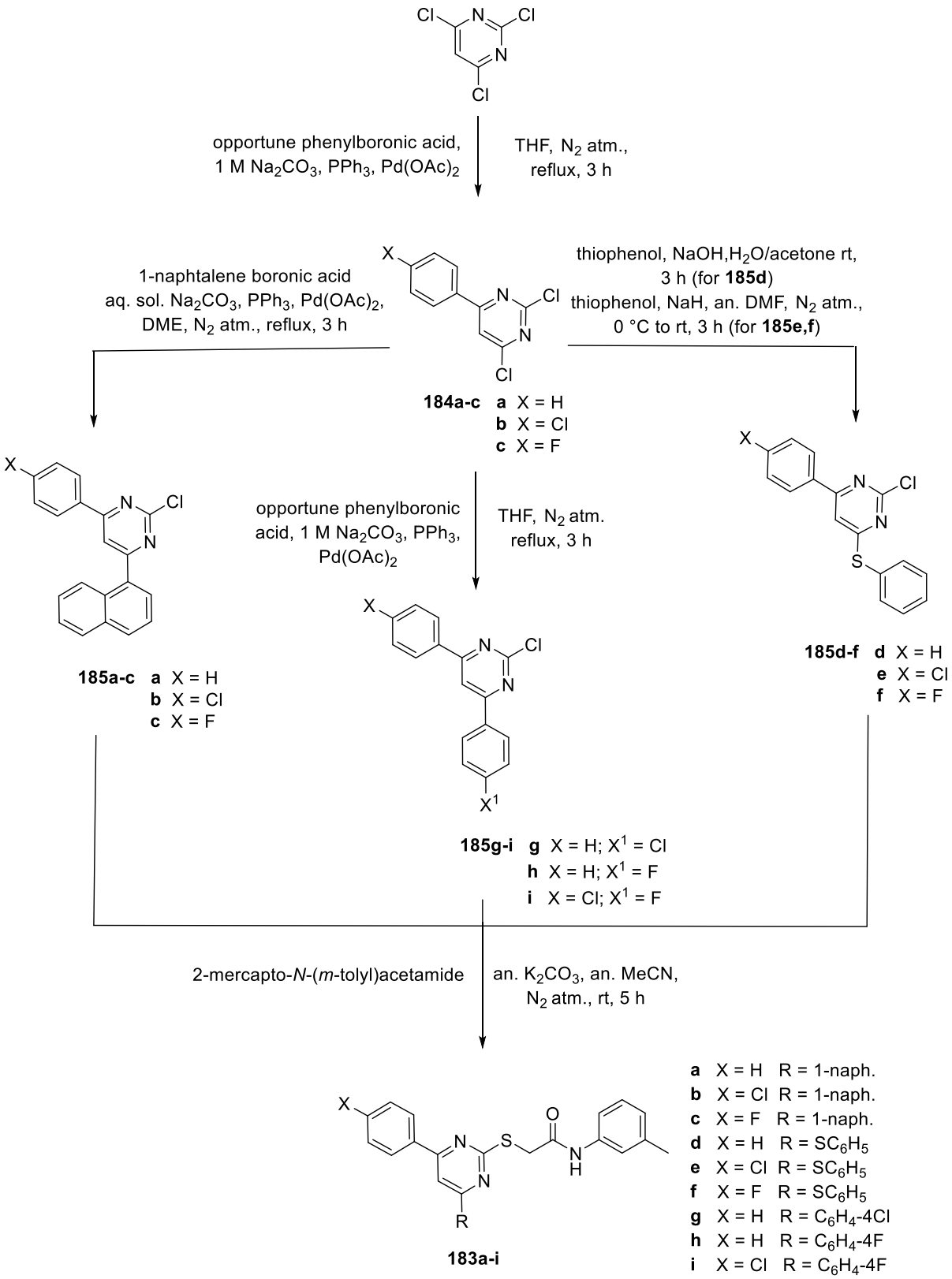

Starting from 2,4,6-trichloropyrimidine, with a Suzuki reaction using two equivalents of the opportune phenylboronic acid[504,505], I obtained intermediates **186a,b**. The following aromatic nucleophilic substitution reaction with 2-mercapto-*N*-(*m*-tolyl)acetamide previously described led to the final compounds **183l**,**m** (**Scheme 8.**).

Scheme 8. Synthesis of pyrimidine derivatives **183l,m**.

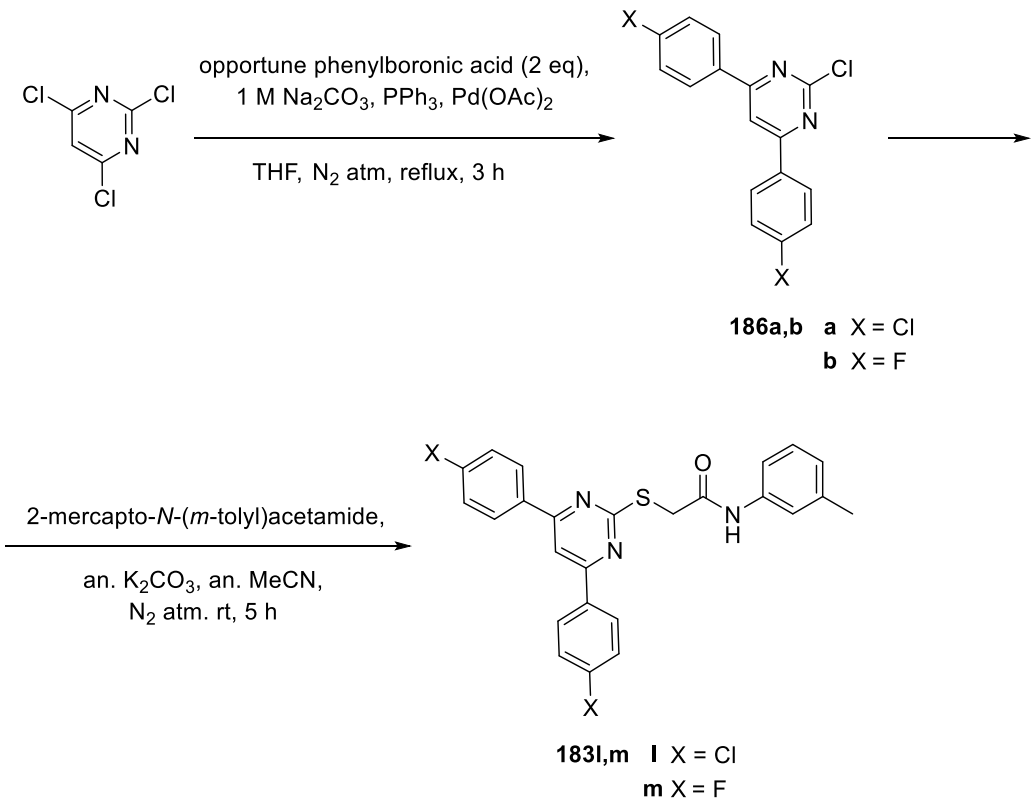

For the synthesis of compound **183n**, I started from a Suzuki reaction between 2,6-dichloro-4-carboxylic acid and phenylboronic acid to get intermediate **187**. The following condensation reaction with aniline in the presence of EDC and HOBt in anhydrous DMF, gave amide **188** and then, the aromatic nucleophilc substitution reaction in the same condition previously described led to the final compound **183n** (**Scheme 9.**).

Scheme 9. Synthesis of pyrimidine derivative **183n**.

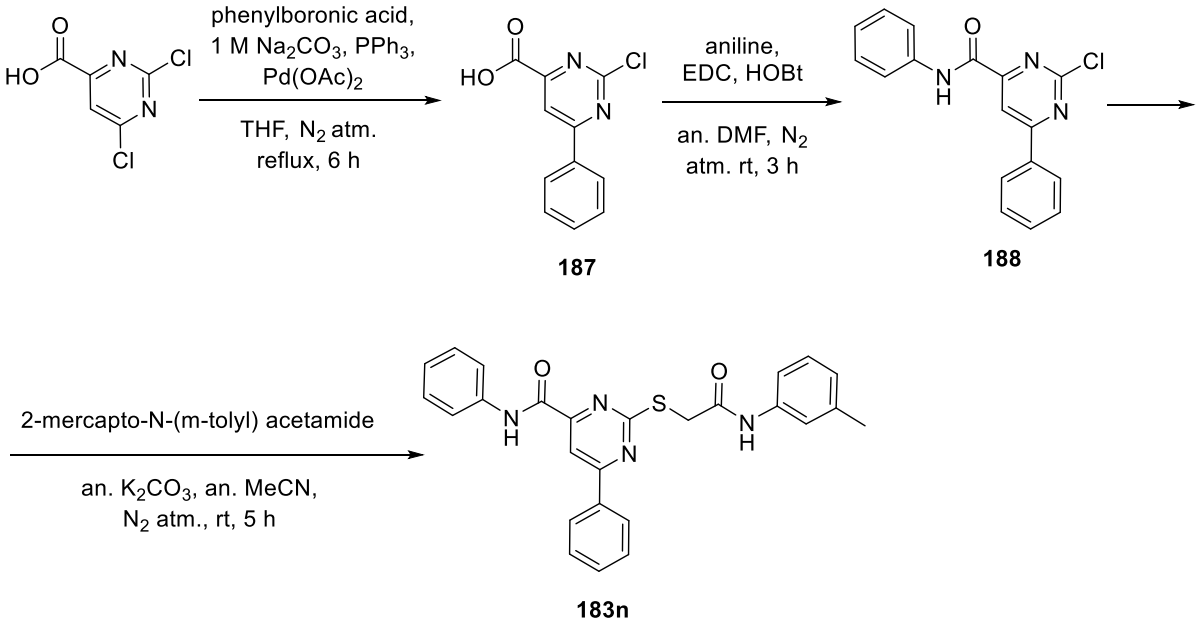

4.3.4. Biology: *in vitro* evaluation

Pyrimidine derivatives **183a-n** were tested as PA-PB1 PPI inhibitors. The *in vitro* biological evaluation of these compounds was conducted through ELISA assay on PA-PB1 complex and PRA in MDCK cells infected with IAV (A/PR/8/34 strain). Cytotoxicity was assessed in MDCK cell line by MTT assays. $PB1_{(1-15)}$-Tat-peptide, OSV and RBV were used as positive controls. In **Table 5.** all the biological data are reported. Derivatives **183a-c**, bearing the 1-naphtyl substituent, are not cytotoxic but are not able to inhibit the interaction between PA and PB1 subunits; their antiviral activity in cell is probably due to an off-target mechanism of action. Compound **183d** shows a good ability to disrupt the PA-PB1 interaction but, unfortunately, its CC_{50} value is too low. Compounds **183e,f** and amide **183n**, unfortunately, have a cytotoxic behavior in MDCK cells and not such a good ability as PPI inhibitors. The most promising derivatives are compounds **183g-i**, endowed with phenyl groups in positions 4 and 6 of the pyrimidine ring. They are not cytotoxic (CC_{50}s > 200 μM), are able to inhibit the interaction between PA and PB1 (IC_{50}s between 86 and 125 μM) and to retain the antiviral activity in cell (EC_{50}s between 2.8 and 45 μM).

Table 5. Biological results of the synthesized pyrimidine derivatives **183a-n**.

Compound	CC_{50} (MDCK cells) [μM][c,d]	EC_{50} (MDCK cells) [μM][b,d]	IC_{50} (ELISA PA-PB1) [μM][a,d]
183a	>250	21.1 ± 8	>200
183b	>250	>100	>200
183c	>250	14.9 ± 1.6	>200
183d	73.3	4.6 ± 0.4	28.8 ± 1.5
183e	16 ± 4	33 ± 4	>200
183f	48 ± 2	16 ± 2	159 ± 29.7
183g	>250	45 ± 2	86 ± 5.3
183h	>250	2.8 ± 0.6	90 ± 30
183i	206 ± 12	30 ± 1	125 ± 37.7
183l	>250	>100	70.8 ± 19.5
183m	>250	62.5 ± 4.3	137.5 ± 35
183n	46.3	13 ± 10.5	125.7 ± 36.7
$PB1_{(1-15)}$-Tat peptide	>250	49.7 ± 5.1	31.7 ± 10.8
OSV	>250	0.015 ± 0.006	ND
RBV	>250	12.8 ± 2.1	ND

[a]Activity of the compounds in the ELISA PA-PB1 interaction assay. Values represent the compound concentration (in μM) that reduces the interaction between PA and PB1 by 50% (IC_{50}). [b]Antiviral activity of the compounds in plaque reduction assays against the IAV A/PR/8/34 strain. Values represent the compound concentration (in μM) that inhibits 50% of plaque formation (EC_{50}). [c]Cytotoxicity of the compounds exhibited in MTT assays. Values represent the compound concentration (in μM) that causes a 50% decrease in cell viability (CC_{50}). The CC_{50} were assessed in MDCK cells. [d]All values represent the means ± SD of data derived from at least three independent experiments in duplicate. Reference compounds are $PB1_{(1-15)}$-Tat peptide, OSV and RBV.

4.3.5. Conclusions

In the field of the research and development of new RdRp PPI inhibitors, starting from previously done SAR studies and from the promising results from MD simulations, I synthesized a library of pyrimidine compounds **183a-n**. I decided to remove the CN group in C3 of the previously synthesized 3-cyanopyridine compounds, to maintain the 2-mercapto-*N*-(*m*-tolyl)acetamide chain in C2 and to explore different aromatic substituents in C4 and C6. Biological data results highlighted a major activity as RdRp PA-PB1 inhibitors for pyrimidine derivatives **183g-i** endowed with small aromatic groups (phenyl groups), that probably can accommodate better in the two hydrophobic areas II and III of the PA subunit than the bulkier naphtyl group or the too flexible thiophenol. This new library of pyrimidine compounds allowed to extend SAR evaluations and to get further insights into this new promising class of

antiviral molecules, exploring the effect of different aromatic substituents in C4 and C6 positions of the pyrimidine core. Moreover, it was possible to find promising IAV RdRp PPI inhibitors which will be a good starting point for further development. In this regard, molecular modeling studies to understand better the biological behavior of this new class of compounds are in progress.

4.4. Synthesis of pyridine derivatives

4.4.1. Background

During the previously described screening work, it was synthesized also one representative pyridine derivative **165**. This molecule showed good biological results, having a promising antiviral activity (EC_{50} = 7.3 µM), a good action as disruptor of the PA-PB1 interaction (IC_{50} = 52.6 µM) and a not cytotoxic behavior (CC_{50} > 250 µM). For these reasons it was decided to get through the mechanism of action, performing the MD simulation on this molecule. As previously said, from this study it was seen that, although the lack of one of the nitrogen atoms and consequently of the interaction with Lys643 of PA subunit seen for the cyanopyridine and pyrimidine scaffold, stronger interactions with critical residues (Val621, Gln408 and Trp706, in particular) seems to be responsible for the good biological profile as PPI inhibitor of compound **165** (**Figure 33.**)[491].

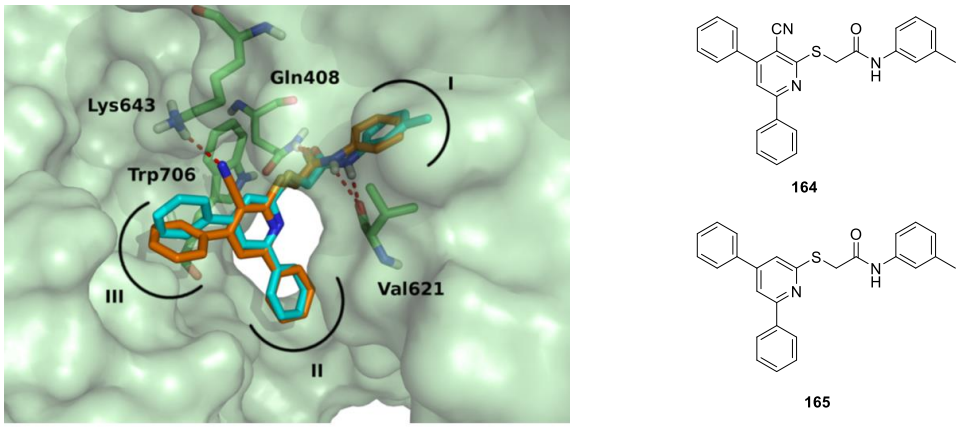

Figure 33. Binding pose of 3-cyanopyridine compound **164** (orange sticks) and pyridine compound **165** (cyan sticks) in PA from docking studies.

4.4.2. Project

With the aim to better explore the behavior of pyridine compounds as RdRp PA-PB1 inhibitors, I decided to try to synthesize some pyridine derivatives **189a-g**, maintaining, as done for the previously described pyrimidine library, the 2-mercapto-*N*-(*m*-tolyl)acetamide chain in C2 and exploring the effect of different substituents in C4 and C6 positions. Unfortunately, the last nucleophilic substitution for the introduction of the lateral acetamidic chain in C2 did not work in all cases, and for this reason I was only able to obtain pyridine derivatives **189a,b** (**Figure 34.**).

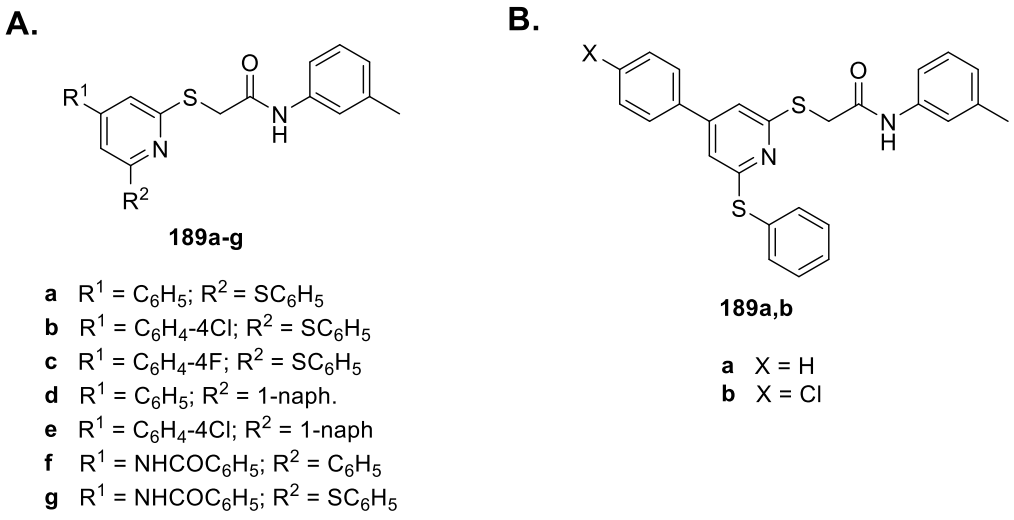

Figure 34. A. Pyridine derivatives planned to be synthesized **189a-g**. **B.** Obtained pyridine compounds **189a,b**.

4.4.3. Chemistry

Derivatives **189a,b** were synthesized starting from a Suzuki reaction between 2,6-dichloro-4-iodopyridine and the opportune phenyl boronic acid, in the presence of the catalysts $Pd(OAc)_2$ and PPh_3 and an aqueous solution of Na_2CO_3 in THF, to obtain the key intermediates **190a-c**. The reaction between **190a-c** and thiophenol, using NaH in anhydrous DMF, led to molecules **191a-c**, while with a Suzuki reaction on intermediates **190a,b** I introduced the 1-naphthalene moiety, obtaining compounds **191d,e**. An Ullman-type reaction of aromatic nucleophilic substitution between intermediates **191a-e** and 2-mercapto-*N*-(*m*-tolyl)acetamide, in the presence of anhydrous K_2CO_3, copper iodide (CuI) and L-proline in anhydrous DME under nitrogen atmosphere at reflux for 30 h[491], gave the desired final compounds **189a,b**.

Unfortunately, this reaction did not work for all the substrates, despite an increase in reaction time or different ratio of reagent equivalents (**Scheme 10.**).

Scheme 10. Synthesis of pyridine compounds **189a,b** and attempts to obtain **189c-e**.

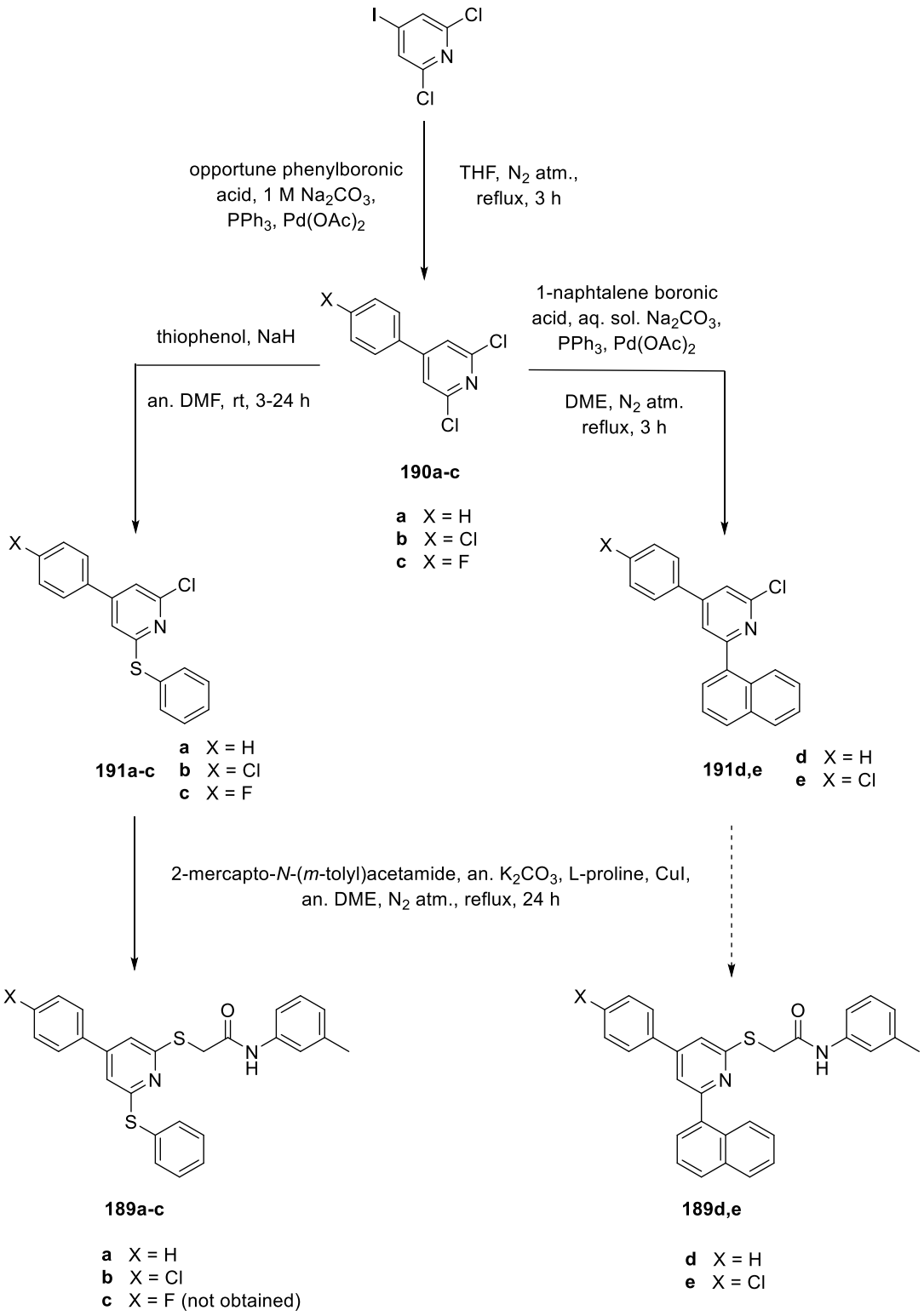

The attempts to obtain final compounds **189f,g** started from 2,6-dichloropyridine-4-carboxylic acid. To prepare intermediate **193a**, I performed the condensation between 2,6-dichloropyridine-4-carboxylic acid and aniline to get amide **192a** followed by the reaction with thiophenol; while to obtain intermediate **193b**, I introduced the phenyl group using a Suzuki reaction followed by the reaction with aniline in the presence of EDC, HOBt in anhydrous DMF. Unfortunately, the last aromatic nucleophilic substitution with 2-mercapto-*N*-(*m*-tolyl)acetamide on intermediates **193a,b** did not work (**Scheme 11.**).

Scheme 11. Attempts to obtain derivatives **189f,g**.

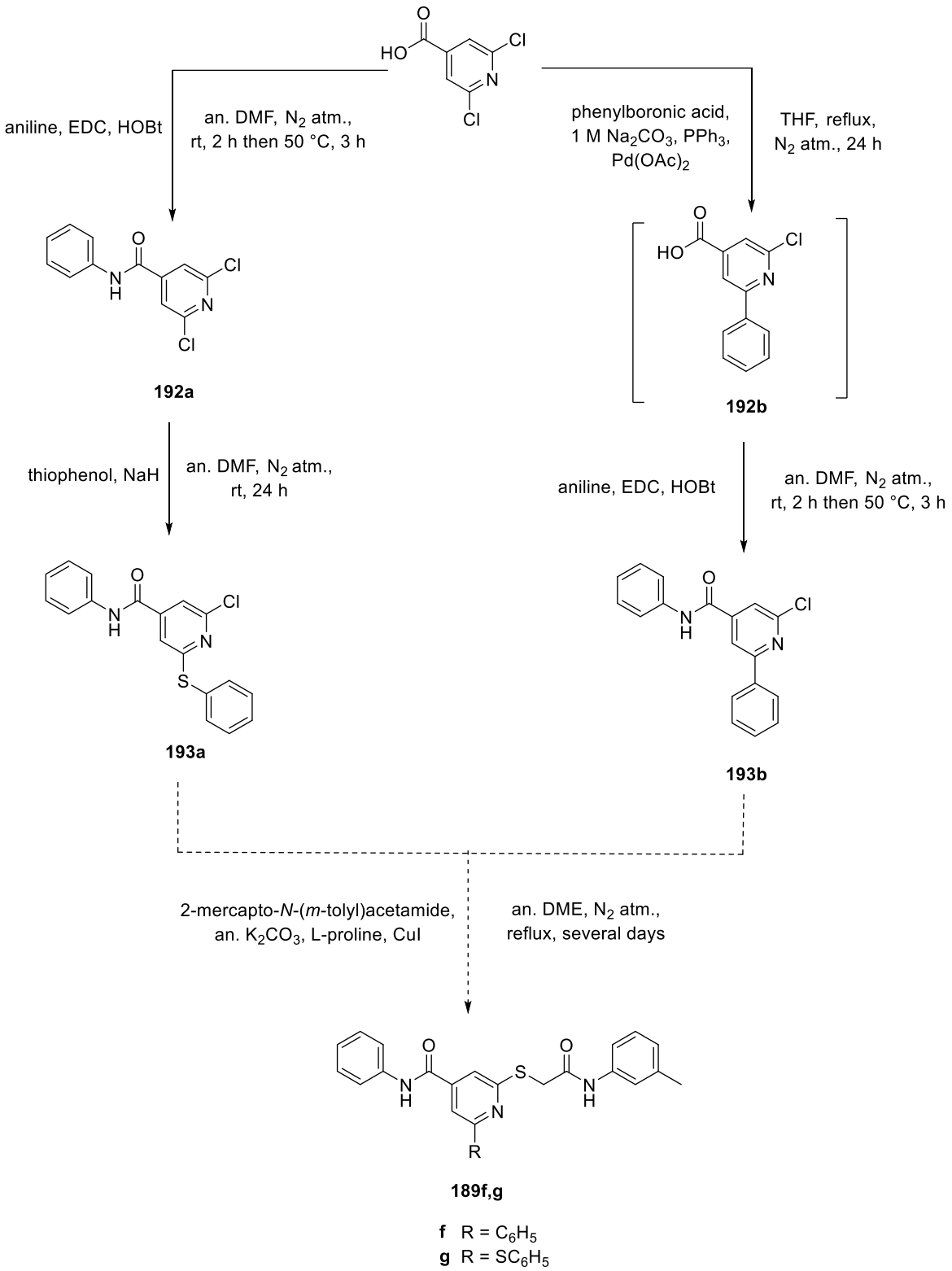

4.4.4. Biology: *in vitro* evaluation

Pyridine derivatives **189a,b** were tested as inhibitors of the PA-PB1 interaction. As for the previously synthesized series, the *in vitro* biological evaluation was conducted through ELISA assay and PRA in MDCK cells infected with IAV (A/PR/8/34 strain), while cytotoxicity was assessed in MDCK cell line by MTT assay. $PB1_{(1-15)}$-Tat-peptide, OSV and RBV were used as positive controls. Pyridine derivatives **189a,b** are not cytotoxic and have a good antiviral activity that, especially in the case of compound **189b**, seems to be strongly related to the ability to disrupt the interaction between PA and PB1 subunits (**Table 6.**).

Table 6. Biological results of the synthesized pyridine derivatives **189a,b**.

Compound	CC_{50} (MDCK cells) [μM][c,d]	EC_{50} (MDCK cells) [μM][b,d]	IC_{50} (ELISA PA-PB1) [μM][a,d]
189a	>250	32.3 ± 3.2	141.3 ± 43.9
189b	>250	62.9 ± 25.2	87 ± 15.7
$PB1_{(1-15)}$-Tat peptide	>250	49.7 ± 5.1	31.7 ± 10.8
OSV	>250	0.015 ± 0.006	ND
RBV	>250	12.8 ± 2.1	ND

[a]Activity of the compounds in the ELISA PA-PB1 interaction assay. Values represent the compound concentration (in μM) that reduces the interaction between PA and PB1 by 50% (IC_{50}). [b]Antiviral activity of the compounds in plaque reduction assays against the IAV A/PR/8/34 strain. Values represent the compound concentration (in μM) that inhibits 50% of plaque formation (EC_{50}). [c]Cytotoxicity of the compounds exhibited in MTT assays. Values represent the compound concentration (in μM) that causes a 50% decrease in cell viability (CC_{50}). The CC_{50} were assessed in MDCK cells. [d]All values represent the means ± SD of data derived from at least three independent experiments in duplicate. Reference compounds are $PB1_{(1-15)}$-Tat peptide, OSV and RBV.

4.4.5. Conclusions

With the aim to find other inhibitors of the interaction between PA and PB1 subunit of the RdRp and to extend SAR evaluations, I decided to try to synthesize some pyridine compounds. I maintained the 2-mercapto-*N*-(*m*-tolyl)acetamide chain in C2, as done for the previously described library of pyrimidine derivatives, exploring the effect of different substituents in C4 and C6 positions of the pyridine core. Despite several attempts, I was able to obtain only molecules **189a,b**. The promising biological results highlight the pyridine scaffold as a promising starting point to develop other potential IAV RdRp PPI inhibitors and

for this reason molecular modeling studies to understand better the biological behavior of this new class of compounds are in progress.

All modeling studies shown up to now have been developed in collaboration with the University of Siena, while biological tests have been performed in collaboration with the University of Padua.

CHAPTER 5. Discussion. Synthesis of substituted pyrazolo[3,4-*b*]pyridines as potent A_1 adenosine antagonists.

5.1. Introduction

Adenosine **194** is an endogenous neuromodulator which mediates its effects by interacting with four G-protein-coupled receptor subtypes named A_1, A_{2A}, A_{2B} and A_3. These receptors are distributed in a wide variety of tissues, including the central nervous system (CNS), cardiovascular system and airways, where they play key roles in the regulation of several biological functions[506,507].

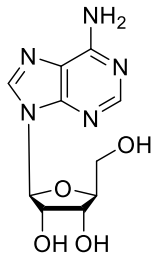

194

The adenosine extracellular baseline physiological level is in the range 20-300 nM[508] and is due to different biological processes: its extracellular production and its intracellular formation and transport. The extracellular production relies on the hydrolysis of adenosine triphosphate or diphosphate (ATP or ADP). This process is controlled by a two-step enzymatic reaction: the first is the conversion of ATP or ADP to adenosine monophosphate (AMP), thanks to the ectonucleoside triphosphate diphosphohydrolase 1 (ENTPD1) enzyme, the second is the hydrolysis of AMP thanks to the ecto-5'-nucleotidase (NT5E) enzyme. The formation of intracellular adenosine raises when the consumption of ATP exceeds its synthesis, leading to an increase of the AMP levels. Then, using different types of transport, such as adenosine transporter[509], vesicles[510] or through endocytosis[511] adenosine can go out of the cell. Normally, the physiological intracellular levels of adenosine are not high, while the increase of these levels is associated with pathologies. Many studies showed that some pathophysiological states are associated with changes of adenosine levels, making the search for adenosine receptor agonist or antagonist an interesting target in medicinal chemistry[512].

Moreover, studies done on knock-out mice for ENTPD1 and NT5E genes and for *Adora* genes, which encode for adenosine receptors, seems to demonstrate that a long-term treatment with adenosine receptors (ARs) antagonists could be tolerated without serious consequences[513-517]. For these reasons, many ARs antagonist have been developed in the last decades, in particular, the A_1 receptor subtype seems to be an interesting target[518]. A_1AR is the more preserved receptor subtype among different species[519] and is widely expressed in many parts of the body. A_1AR activation inhibits the activity of adenylate cyclase, activates potassium channels, blocks calcium transient (T) channels and increases the intracellular levels of calcium and, due to the phospholipase C (PLC) activation, of inositol-1,4,5-triphosphate (IP3). In particular, an excessive stimulation of A_1ARs is related to different pathologies, such as various forms of dementia, including Alzheimer's disease, depression, congestive heart failure, bradyarrhythmias, asystolic arrest, sepsis and cirrhosis of the liver[518,520-523].

Comparison of compounds belonging to different classes of antagonists highlighted that, despite differences in the structure, the adenosine receptor ligands show some common features: in general, the structures are planar, aromatic or π-electron rich and nitrogen-containing heterocycles. The heterocycles are often 6:5 or 6:6 fused bicycles or 6:6:5 fused tricycles, substituted with hydrophobic moieties. Moreover, antagonists lack the ribose moiety, which is essential for agonist activity. Starting from caffeine and theophylline, which are prototypic adenosine receptor antagonists but non selective and of moderate potency[524], several xanthine derivatives have been obtained. For example, compound **195a** (DPCPX) and its analogue derivative **195b**, that has a F18 on the propyl chain in N3, are potent A_1ARs antagonists. Compound **195a** is a highly potent and selective A_1ARs antagonist in a rat model, while for human (h) A_1ARs it is ten-fold less potent with a consequent reduction of selectivity *versus* the other receptor subtypes[525]. Derivative **195b** is active as A_1ARs antagonist both *in vivo* and *in vitro* with K_i values of 0.63, 1.37 and 1.26 nM in mouse, pig and human, respectively. This molecule, bearing a F18 atom, can be used as radio tracer because, as a result of its intravenous injection, it is able to accumulate in different regions of the brain, including the thalamus, the striated body, the cortex and the cerebellum[526].

Xanthine derivatives having a nitroxide group in C3 or C8 can be used as probes for electron paramagnetic resonance (EPR) to study adenosine receptors. Among them, compound **196**

has a K_i value of 5.5 nM for A_1ARs, 1600-fold selectivity *vs* A_{2A}, more than 200-fold *vs* A_{2B}, and 310-fold *vs* A_3 adenosine receptors[527].

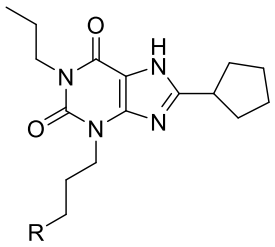

195a R = CH_3
195b R = $CH_2{}^{18}F$

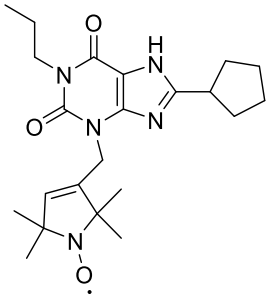

196

Starting from the promising lead compound naxyfilline (BG9719)[528], **197**, norbornyl-substituted lactone xanthine derivatives were developed. Among them, compound **198** shows high A_1 binding affinity and selectivity with a K_i for hA_1ARs of 6 nM and, similarly to BG9719, *in vivo* activity in rat diuresis model. Unfortunately, the poor water solubility of these compounds and the finding of more active molecules led to an interruption of the studies on these derivatives[529].

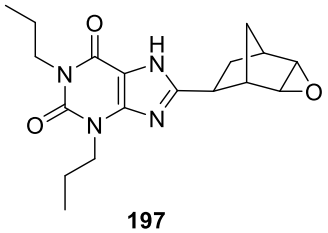

197

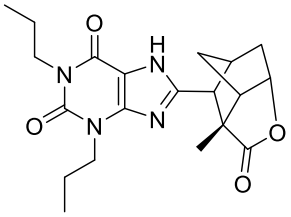

198

Starting from rolofylline (KW-3902) [530,531], **199**, Müller and coworkers synthesized a series of derivatives. Compound **200** has a K_i of 0.12 nM for A_1ARs in rat and 0.7 nM for hA_1AR together with a high selectivity for hA_1 receptors (>>200-fold *versus* the other receptor subtypes). Compound **201**, which was obtained blocking the propyl substituent in C3 position in a cycle, has a K_i value of 13.8 nM for hA_1ARs[532].

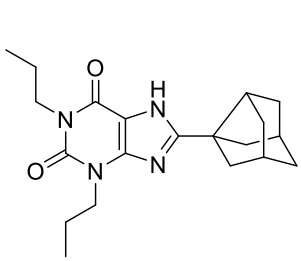

199

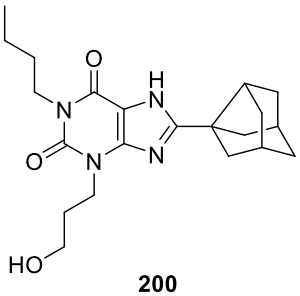

200

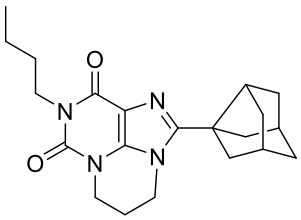

201

With the aim to enhance water solubility, Biogen, Inc. synthesized other xanthine derivatives introducing more polar substituents. One of the obtained compounds is tonapofylline (BG9928), **202**, a selective hA_1ARs antagonist with a K_i of 7.4 nM and a high oral bioavailability in different species[533]. Unfortunately, a phase IIb clinical study showed that BG9928 is not effective for the treatment of acute decompensated heart failure[534].

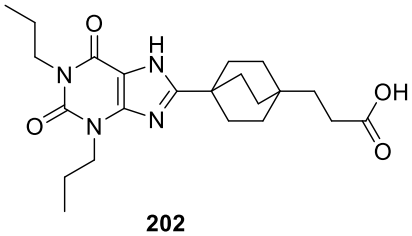

202

Another interesting class of A_1ARs and $A_{2A}ARs$ antagonists were synthesized from the cyclization of the correspondent xanthine derivatives with substituted benzylamines. With the variation of the substituent in N9, the affinity for A_1 receptor subtype was enhanced; for example, compound **203** has a K_i of 89 nM for A_1ARs and only of 88 µM for $A_{2A}ARs$ in membranes of mouse[535].

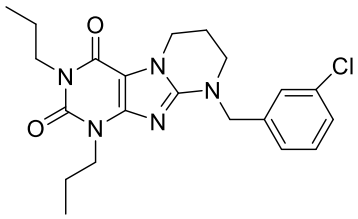

203

On the other hand, many structurally different non-xanthine derivatives have been synthesized and studied as A_1AR antagonists: they are fused polycyclic or monocyclic compounds.

Regarding 6:5-fused heterocyclic compounds, Novellino and co-workers synthesized a series of N-alkyl or N-aryl imidazo-triazine amines among which the most active A_1 antagonist compound turned out to be molecule **204**, having a K_i value of 12 nM for hA_1ARs[536].

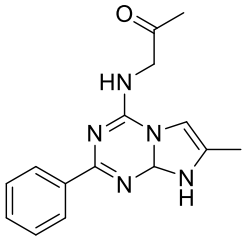

204

Purine derivatives are interesting A_1ARs antagonists; for example, compounds **205a,b** have K_i values of 12 nM and 22 nM, respectively, in bovine cortical membranes. Moreover, derivative **205b** has good water solubility due to the presence of the hydroxypropyl chain in N9[537].

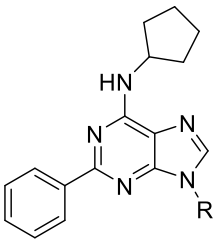

205a R = $CH_2C_6H_5$
205b R = $CH_2CH(OH)CH_3$

Among A_1ARs antagonists, there are also 8-azaadenine derivatives: compound **206** has a K_i value of 26 nM for A_1ARs in bovine cortical membranes, good water solubility (1.2 mg/nL) and a logP of 1.00669[537].

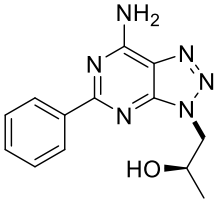

206

In the class of the 2,6,8-trisubstituted purine derivatives, compound **207a** (LUF5962) is a potent and selective A_1AR antagonist (K_i = 0.29 nM for hA_1ARs)[538] and also the 1-deazapurine analog **207b** (LUF5816) shows a similar ability to act as A_1ARs antagonist (K_i = 0.62 nM for hA_1ARs)[539].

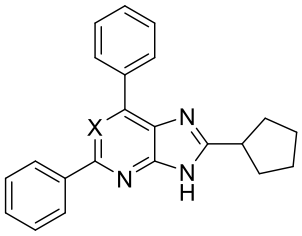

207a X = CH
207b X = N

SLV320, **208**, a 7-deazaadenine derivative synthesized by Solvay Pharmaceuticals (today Abbott), is a potent and selective A_1ARs antagonist, having a K_i value of 1.0 nM for hA_1ARs. This molecule was tested in a phase II clinical trial in patients affected by congestive cardiac failure with renal disfunction[540]. Unfortunately, the studies on this molecule were stopped due to strategic drug development considerations[541].

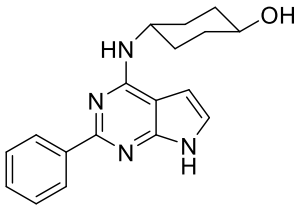

208

Maemoto and colleagues synthesized a library of pyrazolo[1,5-*a*]pyridine derivatives as A_1ARs antagonists. Among them, compound **209** (FR194921) is a potent and selective A_1ARs antagonist, being endowed of a K_i = 2.90 nM and of no affinity for A_{2A} and A_3 adenosine receptors. Moreover, pharmacokinetic studies in rats showed that it can be orally administered and is able to pass the blood-brain barrier (BBB)[542]. [^{11}C]FR194921 derivative, bearing an ^{11}C in the methyl group of the piperidine ring, can be used for cerebral imaging in rats and monkeys as new potential tracer for positron emission tomography (PET)[543].

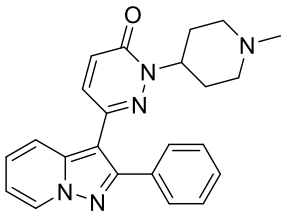

209

Tieno[3,4-*d*]pyridazines, that were found by chance during a study for the identification of new allosteric modulators of adenosine receptors, are potent A_1ARs antagonists. In particular, compound **210** has a K_i value in the low nanomolar range for hA_1ARs[544].

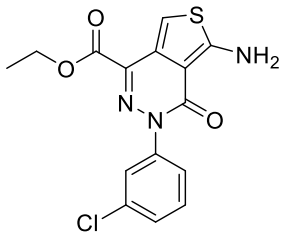

210

Among 6:6-fused heterocycles, it has long been known that amino-substituted pyrido[2,3-*d*]pyrimidindiones bind to A_1ARs and A_2ARs[545]; the most active compound having this structure is molecule **211**, with a K_i value of 25 nM for hA_1ARs.

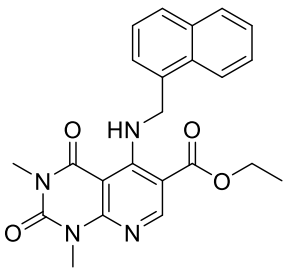

211

Appropriately substituted 1,8-naphthyridine derivatives seems to be promising A_1ARs antagonists. The most interesting is compound **212**, having a K_i value of 0.15 and 300 nM in bovine cortical membranes and human striatal membranes, respectively, associated with a good selectivity for A_1ARs[546,547].

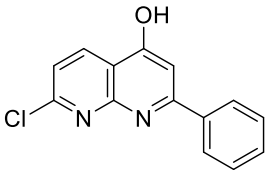

212

Among tricyclic compounds, there are pyrimido[4,5-*b*]indole derivatives. Molecules **213a**,**b** have K_i values for A_1ARs of 36 nM and 21 nM, respectively, in rat cortical membranes[548].

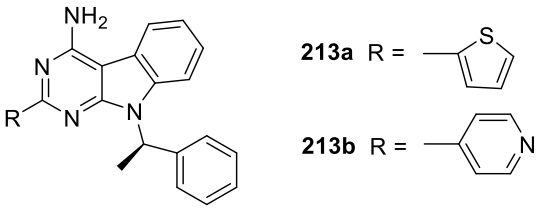

213a R =

213b R =

Other important classes are that of triazine[4,3-*a*]benzimydazolones, such as compound **214** which has a high selectivity and a K_i of 18 nM for bovine (b) A_1ARs[549] and 1,2,4-triazole[4,3-*a*]chinossalyn-1-ones with molecules **215a,b** having K_i values of 0.42 nM and 0.35 nM, respectively, for bA_1ARs[550].

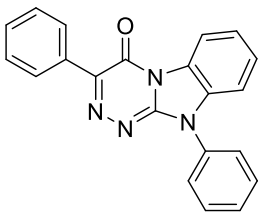

214

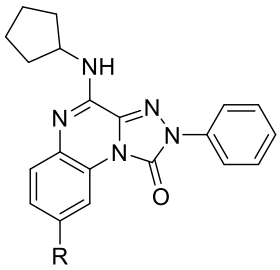

215a R = H

215b R = NO_2

Starting from the structure of BG9928, tricyclic imidazoline derivatives were developed by Vu and co-workers. In particular, imidazoline compound **216** shows the most promising A_1ARs antagonist activity (K_i = 22 nM for hA_1ARs) with good selectivity over the other three adenosine receptor subtypes, a high solubility in water (>100 mg/mL) and a good efficacy in a rat diuresis model[551].

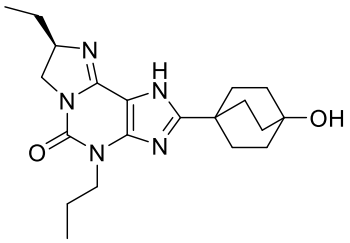

216

Synthesis, biological tests and therapeutic applications of a series of arylidenopyrimidine were patented for their interesting activity both on A_1 and A_{2A} receptors and their possible applications for the treatment of neurodegenerative disorders and other problems related to Parkinson's disease. The most active compound is derivative **217**, with a K_i value of 1.8 and 1.0 nM for A_1ARs and A_{2A}ARs, respectively, in mouse[552-555].

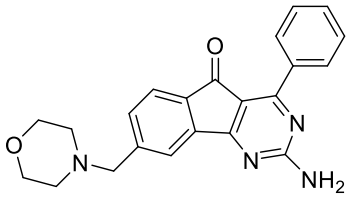

217

Among monocyclic compounds active as A_1ARs antagonists, 1,2,4-thiadiazole-benzamidic compounds LUF5437, **218**, and VUF5472, **219**, have K_i values of 7 and 20 nM, respectively, for A_1ARs in rat cortical membranes[556].

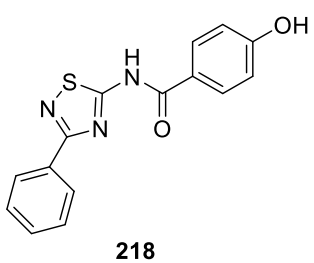

218

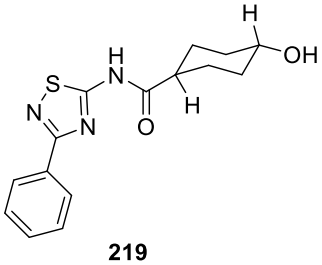

219

Also thiazolic derivatives are potent and selective A_1ARs derivatives: for example, compound **220** has a K_i value of 18 nM for A_1ARs in rat cortical membranes[557]. In 2009, the synthesis and biological tests of these derivatives, in which a cyano group in C5 position was introduced, were patented[558].

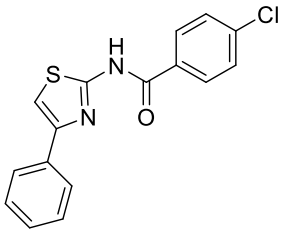

220

2,6-Diphenyl-4-amidopyrimidine and 4,6-diphenyl-2-amidopyrimidine are two important classes of A_1ARs antagonists. LUF5740, **221**, and LUF5735, **222**, are endowed with a K_i of 2.14 and 4 nM, respectively, for hA_1ARs[559].

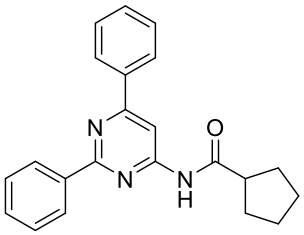

221

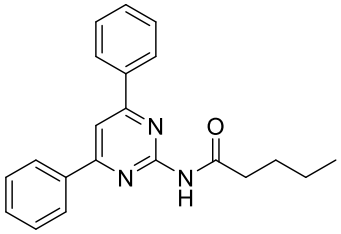

222

The development of new ligands of the adenosine receptors is not easy because it is necessary to take into account some peculiar characteristics of the adenosine signal: the fact that adenosine and its receptors are present ubiquitously and consequently the action on these receptors could be responsible for a wide range of physiological and physiopathological functions and the fact that the signal itself is very complex and so it should be possible to have several side effects.

5.2. Background

In this context, the research group where I worked synthesized a wide library of 4-aminopyrazolo[3,4-*b*]pyridine-5-carboxylic acid esters **223**, introducing various substituents at the N1, C4 and C5 positions of the central scaffold[560-563]. Many of these compounds turned out to be active as A_1AR antagonists both on bovine and human receptors; some of them were also characterized by a good selectivity towards A_1AR. The antagonistic action was demonstrated by monitoring the conversion, catalyzed by adenylate cyclase, of [R_{32}P]-ATP to [R_{32}P]-cAMP. In particular, the ability of the antagonists to block the inhibition of adenylate

cyclase induced by the A_1 adenosinic agonist N6-cyclohexyl-adenosine (CHA) and therefore to determine an increase of [R_{32}P]-cAMP has been assessed.

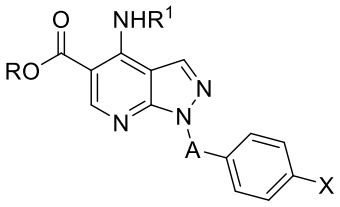

R = alkyl groups
R^1 = aliphatic or aromatic groups
A = $CH_2CH(Cl)$, $CH_2CH(Cl)CH_2O$, CH=CH
X = H, F, Cl, Br

223

The most potent and selective compounds turned out to be those that had in N1 the 2-chloro-2-phenylethyl chain. In particular, compound **223a**, having a phenyl ethylamine chain in C4 and an ethyl ester in C5, showed a K_i of 50 nM when tested on cortical bovine membranes.

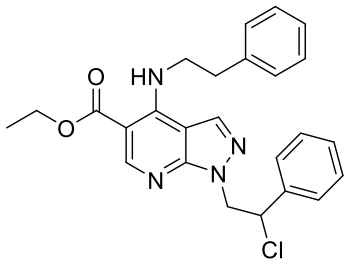

223a

Starting from these promising results, a second generation of A_1ARs antagonists was synthesized, maintaining the 2-chloro-2-phenylethyl chain in N1 and exploring different substituents in C4 and C5. The most active compounds of this series were derivatives **223b** and **223c**, having Ki values of 6 and 7 nM for bA_1ARs, and of 94 and 17 nM for hA_1ARs, respectively.

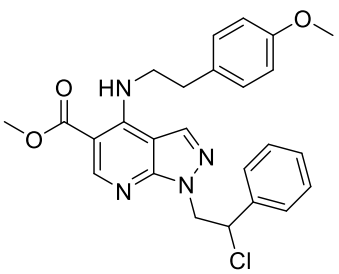

223b

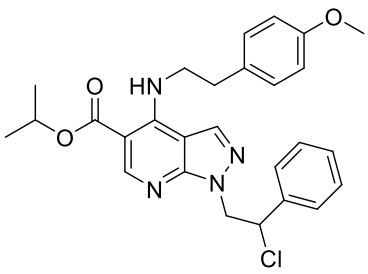

223c

Moreover, the racemic mixture of compound **223b** was separated into the correspondent enantiomers. Enantiomer R turned out to be seven times more active than enantiomer S, with K_i values of 3.5 and 24 nM for bA_1AR and of 31 and 435 nM for hA_1AR, respectively. Thanks to the synthesis of a small library of analogs, it was noticed that the introduction of halogens (F, Cl, Br) in the *para* position on the phenyl group on the N1 lateral chain, determined the maintenance of the affinity for bA_1ARs, while caused a strong diminution of the affinity for hA_1ARs. For example, derivative **223d** showed a K_i value of 8.0 nM for bA_1ARs and only 36% of inhibition for hA_1ARs.

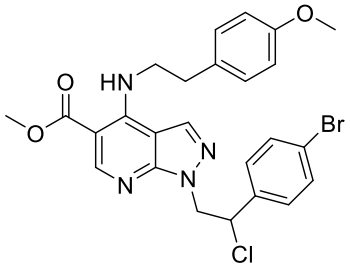

223d

To investigate the binding interaction of these compounds, a model of the bA_1AR was generated using the crystal structure of bovine rhodopsin (1L9H, 2.6 Å resolution)[564] as the template. The bA_1AR model was built applying a homology modeling procedure, which takes into account the flexibility of the receptor, considering a large number of its conformations. In particular, the sequence alignment was studied on several adenosine receptors and was guided by the highly conserved amino acid residues, including asparagine N1.50, the LA-AD (L2.46, A2.47, A2.49, and D2.50) and D/ERY (D/E3.49, R3.50 and Y3.51) motif, the highly conserved tryptophan W4.50, the two prolines P4.59 and P6.50, and the NPXXY motif in the transmembrane domain (TM) 7 (N7.49, P7.50, and Y7.53)[565]. On the basis of this alignment, the bA_1AR model was built, subjected to a Modeller program[566] and then, refined by means of a 2-ns MD simulation. In particular, the binding site of the ligands, defined by taking into account interaction of retinal in the X-ray structures and the major mutagenesis data, was individuated in the region between TM3, TM5, and TM6[567]. The hypothetical binding site was then subjected to a simulated annealing protocol by means of the Modeller program to obtain 500 conformations of the receptor that were then clustered and 42 representative conformations were extracted. Both R and S enantiomers of compound **223b** were docked

into the 42 receptor models using the GOLD software[501]. Docking results were filtered on the basis of the interaction of the two enantiomers with L3.33(88), T3.36(91), Q3.37(92), and H6.52(251), which are the main residues that a mutagenesis study[567] suggested to be important. From this study, it was seen that the pyrazolo-pyridine scaffold of the R-**223b** enantiomer interacted with T3.36(91), the ester chain formed a hydrogen bond with Q3.37(92), the 2-chloro-2-phenylethyl group interacted with H6.52(251) and the *p*-methoxyphenyl substituent was stabilized by the lipophilic interaction with L3.33(88). The S enantiomer showed a disposition very similar to that observed for the R enantiomer with only a slightly different disposition of the 2-chloro-2-phenylethyl side chain. The two ligand-receptor complexes were then subjected to 1.3 ns of MD simulation in a fully hydrated phospholipid bilayer environment. From MD simulation it was possible to see that the pyrazolo-pyridine nucleus of R-**223b** interacted with a lipophilic cleft delimited by F5.43(185), V5.47(189), L6.51(250) and W6.48(247). The hydrogen bond with T3.36(91) was maintained. The ester chain interacted with Q3.37(92) and formed an intramolecular hydrogen bond with the amino group at C4. The terminal methyl substituent of the ester chain was inserted in a cleft limited by L3.33(88), M5.38(180), V5.39(181), N5.42(184) and F5.43 (185). The *p*-methoxyphenyl substituent at C4 showed lipophilic interactions with A3.29(84), L3.33(88), I167, M177, and V5.39(181), and the methoxy group formed a hydrogen bond with N147. Finally, the 2-chloro-2-phenylethyl mainly interacted with V5.47(189), F5.43(185) and H6.52(251). Compound S-**223b** displayed a very similar disposition of the central scaffold. The ester and *p*-methoxyphenyl substituents showed all the above described interactions, whereas the 2-chloro-2-phenylethyl moiety had a different disposition, interacting with L248 and H251, and lacking the lipophilic interactions with V5.47(189) and F5.43(185). The lacking of these latest lipophilic interactions should be the explanation of the fact that enantiomer S turned out to be seven times less active than enantiomer R (**Figure 35.**).

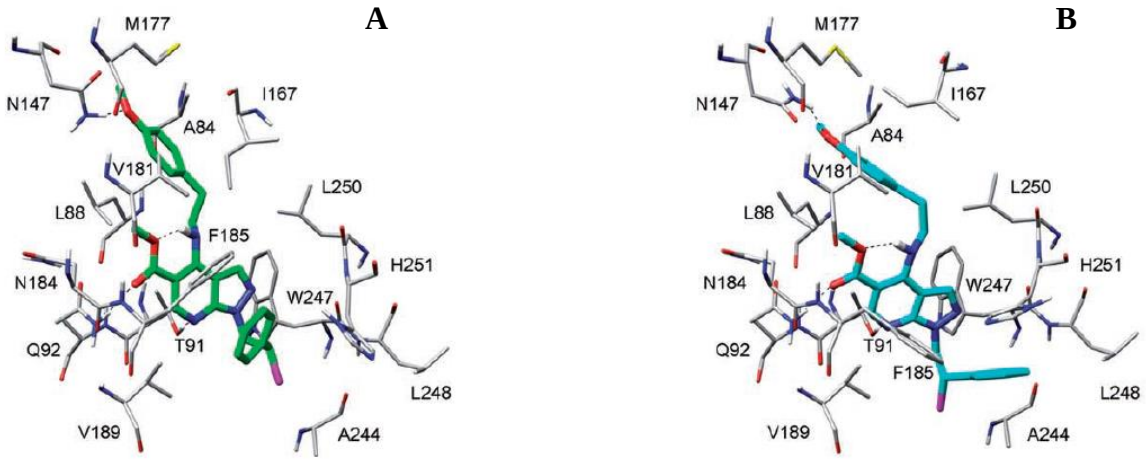

Figure 35. Minimized structures of the average of the last 800 ps of the MD simulation of R-**223b** (**A**) and S-**223b** (**B**). Carbon atoms of enantiomer R are coloured in green, while the ones of enantiomer S are coloured in light blue. Aminoacid residues are represented with grey sticks.

The most promising bA_1AR antagonists were also tested for their affinity toward the hA_1AR. From the analysis of the bovine/human A_1AR affinity profile of new and previously synthesized compounds, the 2-chloro-2-phenylethyl substituent seemed to be allocated in a more flexible or larger cavity in the bA_1AR which also allowed the interaction of *para*-substituted phenyl rings. Similarly, various substituents on the ester chain are tolerated by bovine receptor, while restricted steric characteristics are required for high hA_1AR affinity. Moreover, the difference in affinity toward hA_1AR shown by the two enantiomers is much larger than that shown towards bA_1AR, in agreement with a hypothesized larger cavity for the latter[563]. These observations, combined with computational studies previously carried out by other research groups[547], confirmed the hypothesis that bA_1AR and hA_1AR could be characterized by a different dimension of their binding site. In particular, hA_1AR seem to contain a binding pocket smaller than that of bA_1AR.

5.3. Project

Starting from the results previously described, I decided to synthesize two small libraries of 4-aminopyrazolo[3,4-*b*]pyridine-5-carboxylic acid ester derivatives. These two series of compounds have in C5 of the pyrazolo-pyridine scaffold the ethyl ester chain, while in C6 there are different substituents. Compounds **224a-g** are characterized by a 2-chloropropyl chain in N1, while **225a-g** have the bulkier 2-phenylpropyl chain. Since, as already said,

previous studies indicated that hA_1AR contains a binding pocket smaller than that of bovine receptors, the aim of my work was that of obtaining more potent and selective antagonists for hA_1AR and evaluating their possible different affinity for bovine and human receptors (**Figure 37.**).

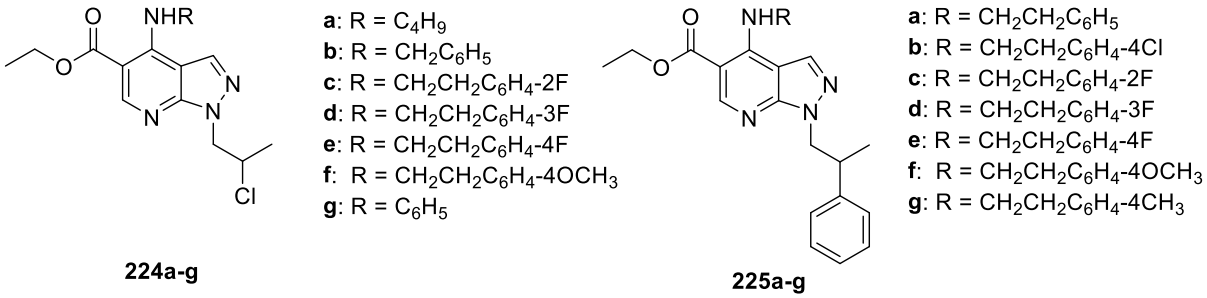

Figure 37. General structure of the synthesized library of 4-aminopyrazolo[3,4-*b*]pyridine-5-carboxylic acid ester derivatives **224a-g** and **225a-g**.

5.4. Chemistry

The synthesis of these two library of compounds was obtained using a synthetic procedure previously published[563,568]. The reaction of hydrazine monohydrate with methyloxirane at reflux for 15 min (Method A) or with 1-bromo-2-phenylpropane in absolute EtOH at reflux for 24 h (Method B), gave 1-hydrazino-propan-2-ole (**226a**) or 1-hydrazino-2-phenypropane (**226b**), respectively. Then, intermediates **226a,b** were treated with ethyl(ethoxymethylene) cyanoacetate in absolute EtOH at reflux, to give the pyrazolo derivatives **227a,b**. The ester group of these intermediates was hydrolyzed using NaOH, giving compounds **228a,b**; then, in order to obtain intermediates **229a,b**, the carboxylic group was eliminated by thermal decarboxylation at 150 °C, without solvents. The successive reaction with diethyl ethoxymethylenemalonate at 120 °C for 2 h gave compounds **230a,b**. The pyrazolo[3,4-*b*]pyridine scaffold was obtained treating intermediates **230a,b** with phosphorous(V) oxychloride ($POCl_3$) at reflux for 18 h, giving compounds **231a,b**. Finally, a reaction of these last molecules with appropriate amines in anhydrous toluene at room temperature for 48 h (Method C) gave the desired compounds **224a-f** and **225a-g**, while the reaction with aniline in absolute EtOH at reflux for 5 h (Method D) allowed to get compound **224g**. (**Scheme 12.**).

Scheme 12. Synthesis of the two small libraries of compounds **224a-g** and **225a-g**.

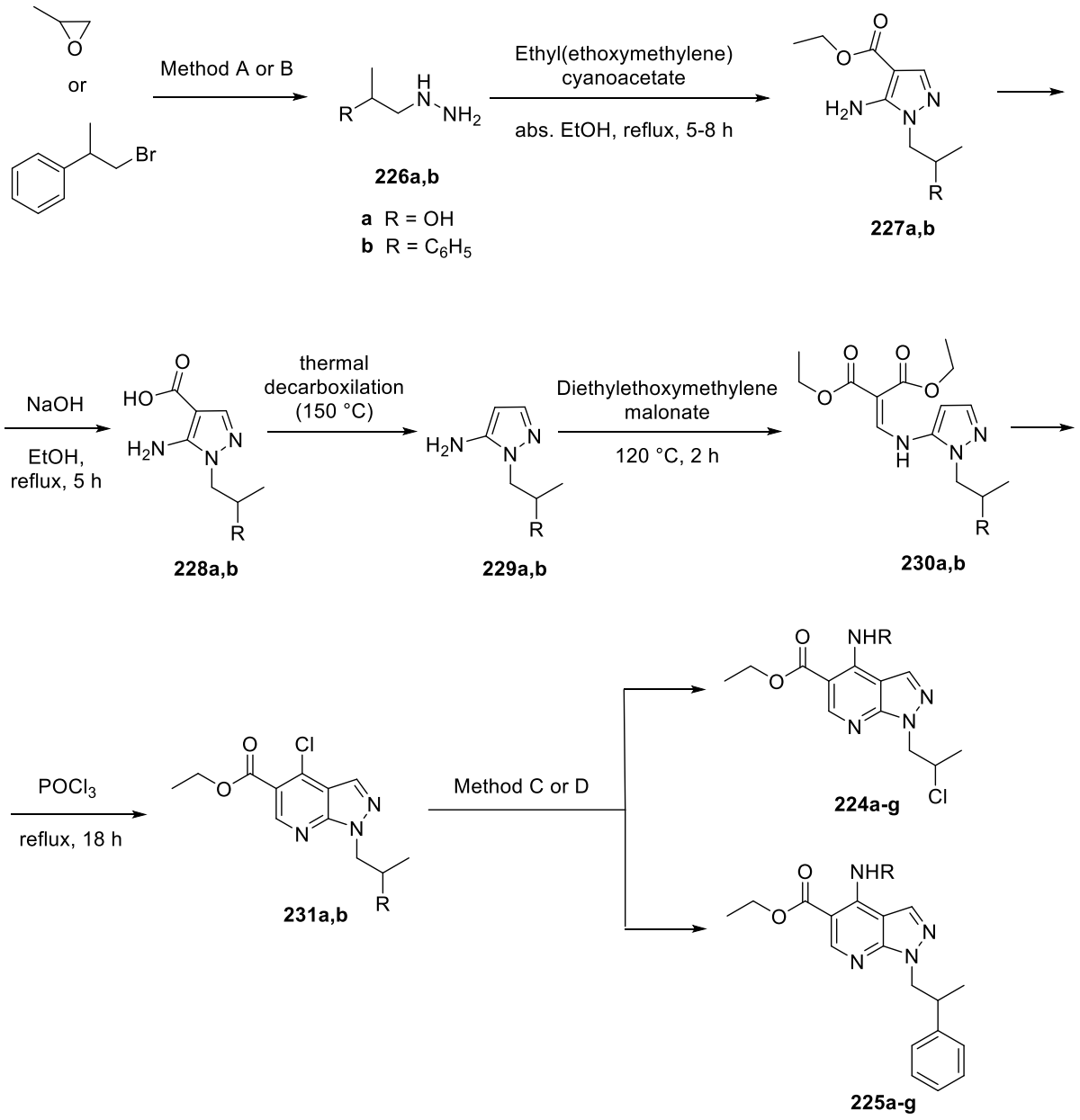

Method A: hydrazine monohydrate, reflux, 15 min. (**226a**). Method B: hydrazine monohydrate, abs. EtOH, reflux, 24 h (**226b**). Method C: appropriate amine, an toluene, rt, 48 h. (**224a-f** and **225a-g**). Method D: aniline, abs. EtOH, reflux, 5 h (**224g**).

5.5. Biology: *in vitro* evaluation

Compounds **224a-g** and **225a-g** were tested for their affinity towards hA_1ARs stably expressed in chinese hamster ovary (CHO) cells and towards bA_1ARs in cortical bovine membranes. In details, the activity was evaluated measuring the capacity of compounds to displace the radio ligand [^{3}H]DPCPX from A_1ARs. Compounds were dissolved in dimethylsulfoxide (DMSO) and diluted in a buffer solution so that the DMSO did not exceed 2% and tested at concentration of 100 and 10 nM; for molecules that showed interesting percentage of binding inhibition at 10 nM, a dose-response plot was built, so obtaining IC_{50} values. Then, these values were transformed in K_i values using Cheng and Prusoff equation[569] (**Table 7.**).

Table 7. Biological results for compounds **224a-g** and **225a-g**.

Compound	R	hA_1AR K_i (nM) or % of inhibition	bA_1AR K_i (nM)
224a	C_4H_9	52.3 ± 8.4	ND[a]
224b	$CH_2C_6H_5$	387.6 ± 35.9	654.2 ± 59
224c	$CH_2CH_2C_6H_4$-2F	764.6 ± 29	ND
224d	$CH_2CH_2C_6H_4$-3F	383.9 ± 37.1	ND
224e	$CH_2CH_2C_6H_4$-4F	851.4 ± 22.9	ND
224f	$CH_2CH_2C_6H_4$-4OCH_3	678.1 ± 71	ND
224g	C_6H_5	57	ND
225a	$CH_2CH_2C_6H_5$	231.9 ± 0.2	5.65 ± 0.62
225b	$CH_2CH_2C_6H_4$-4Cl	61	ND
225c	$CH_2CH_2C_6H_4$-2F	37	3.71 ± 0.36
225d	$CH_2CH_2C_6H_4$-3F	59	27.4 ± 2.63
225e	$CH_2CH_2C_6H_4$-4F	4195 ± 2.15	2.43 ± 0.26
225f	$CH_2CH_2C_6H_4$-4OCH_3	57	2.05 ± 0.07
225g	$CH_2CH_2C_6H_4$-4CH_3	62	ND

[a] ND = not determined

Tests showed that compounds **224a-g**, with the less bulky 2-chloropropyl chain in N1, are endowed with improved activity on hA_1AR. In particular, the most active compound is **224a**, having in C4 a butilammine chain, less bulky and more flexible than other substituents in **224b-g**. On the other hand, compounds **225a-g**, having in N1 a 2-phenylpropyl chain, showed good affinity for bA_1ARs and, as expected, they are less active on hA_1AR. Among this series of derivatives, the most active compound is **225f**, which has a 4-methoxy-phenylethylammine chain in C4, having a K_i value of 2.05 ± 0.07 nM for bA_1ARs. It is worth to mention that the biological results on the synthesized compounds that were tested both on bA_1AR and hA_1AR confirmed the hypothesis of a smaller binding site for hA_1AR. For example, compound **224b** shows more affinity for hA_1AR than for bA_1AR (387.6 *vs* 654 nM) or compound **224e** has a K_i value of 851.4 nM for hA_1ARs while its analog **225e** has a K_i of 4.2 μM for the same receptors, resulting five time less active, despite the fact that is one of the more active of the **225** series.

5.6. Conclusions

Because of A_1AR stimulation plays a central role in a lot of pathologies, the discovery of human A_1 selective antagonists is very significant. With this work it was possible to enrich our library of A_1 antagonists belonging to the class of pyrazolo[3,4-*b*]pyridines, to extend SAR evaluations and, importantly, to confirm that the binding site of the hA_1AR is smaller than that of the bA_1AR. In the complex, the synthesized compounds represent a step forward in the research for active compounds on A_1AR, a field that was not so much explored but that could lead to interesting results in therapy thanks to a modulatory effect on target tissues. Docking studies and biological tests have been developed in collaboration with the University of Pisa.

CHAPTER 6. Discussion. Enantioselective Pd-catalyzed C-H activation reactions and related topics.

6.1. Introduction

During the third year of my PhD, I spent three months at the Department of Organic Chemistry at the University of Basel, within the research group of Prof. Dr. Olivier Baudoin. The research of this group is focused on the development of step-economical transition-metal-catalyzed methods for the functionalization of non-activated C-H bonds, employing catalysis by palladium(0) complexes. Transition-metal catalysis has recently emerged as a powerful tool to functionalize otherwise unreactive C-H bonds. Moreover, using this type of reaction it is possible to create a variety of carbon-carbon and carbon-heteroatom bonds. In this context, several groups have synthesized fused carbocycles and heterocycles by intramolecular Pd(0)-catalyzed reactions, and recently the attention has been directed toward the development of asymmetric versions of these reactions[570]. The literature on this topic is very broad; below I will mention just a few examples. Regarding the C(sp^3)-H activation, interesting examples were reported by the groups of Kündig, Kagan and Cramer. They showed the highly enantioselective synthesis of fused indolines through the activation of methyl or methylene C-H bonds using chiral *N*-heterocyclic carbene (**232**) or phosphine (**233** and **234**) ligands[571-573], while Cramer and co-workers described the enantioselective arylation of cyclopropane C-H bonds using chiral phosphoramidites **235**[574] (**Scheme 13.**).

Scheme 13. Some enantioselective Pd(0)-catalyzed C(sp^3)-H activation reactions and the structures of the ligands **232-235**.

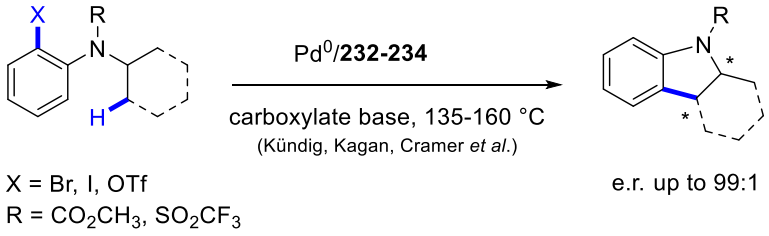

X = Br, I, OTf
R = CO_2CH_3, SO_2CF_3

e.r. up to 99:1

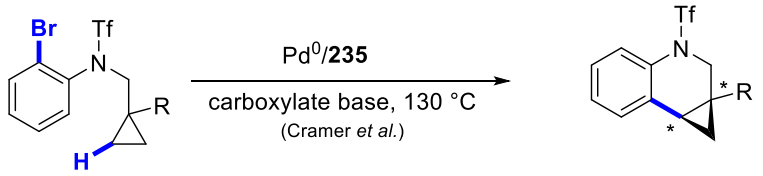

R = CH_3, alkyl chain, aromatic substituent

e.r. up to 97:3

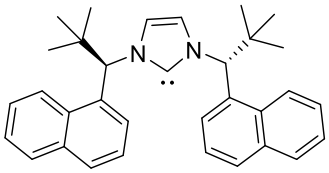

232

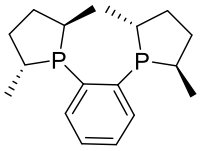

233

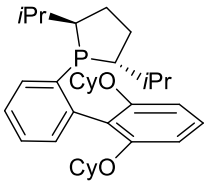

234

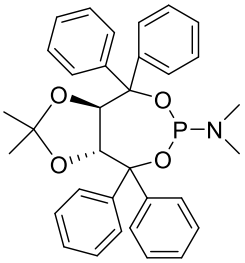

235

In the field of C(sp^3)-H activation, Baudoin and co-workers performed the diastereo and enantioselective synthesis of fused cyclopentanes using a binepine-type ligand **236** (**Scheme 14.**)[575].

Scheme 14. Diastereo and enantioselective synthesis of fused cyclopentanes performed by Baudoin and co-workers.

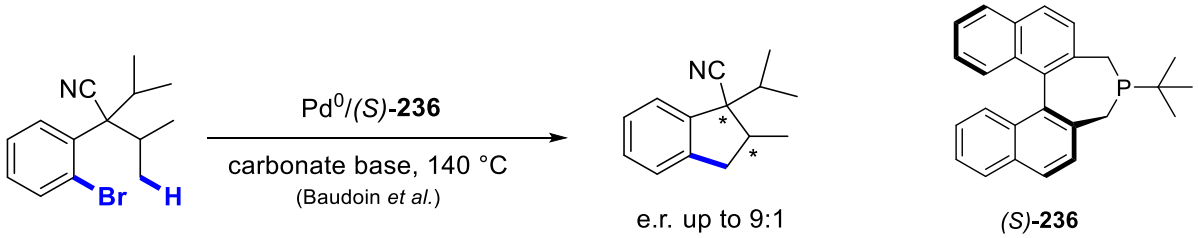

Regarding C(sp^2)-H activation reactions, Cramer and co-workers demonstrated a mild intramolecular direct arylation of vinyl triflates for the synthesis of indanes with quaternary stereocentres. This reaction proceeds with excellent enantioselectivities at room temperature, thanks to the use of tailored taddol-based phosphoramidite ligands (**237**) in combination with highly polar solvents[576]. Other examples of C(sp^2)-H arylation are reactions furnishing P-chiral phosphorous compounds in good yields and stereoselectivities, using taddol-based phosphoramidite ligands (**238** and **239**), described in 2015 by Liu and collaborators and Lin and co-workers[577,578] (**Scheme 15.**).

Scheme 15. Some enantioselective Pd(0)-catalyzed C(sp^2)-H activation reactions and the structures of the ligands **237-239**.

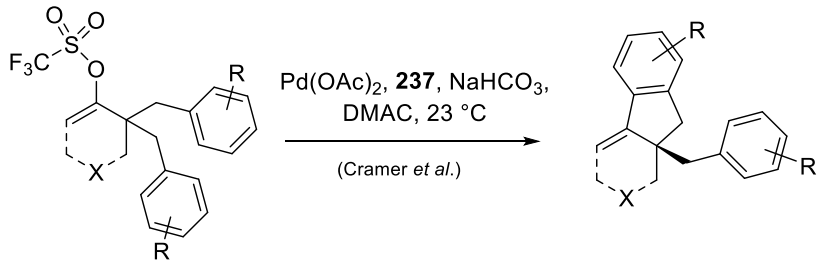

R = H, CH_3, OCH_3, CF_3, halogens
X = CH_2, $CHCH_3$, N-Boc, $NCOOCH_2CH_3$

up to 99% ee

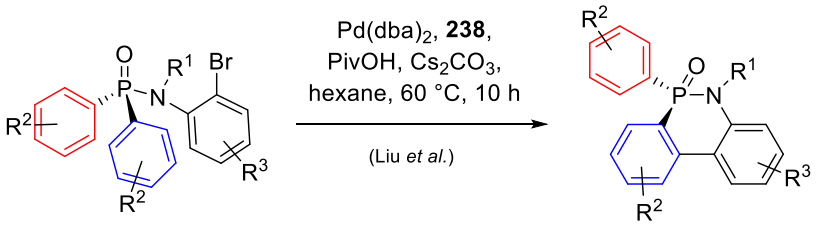

R^1 = CH_3, CH_2CH_3, $CH_2CH_2CH_2CH_3$, $CH_2C_6H_5$
R^2 = H, CH_3, OCH_3, C_6H_5

up to 97% ee

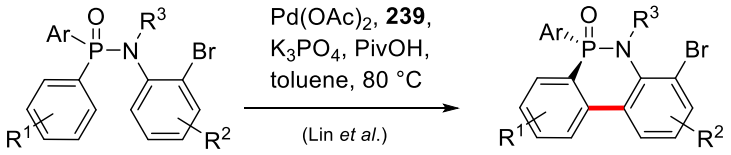

R^1, R^2 = H, CH_3, OCH_3, CF_3, halogens
R^3 = CH_3, $CH_2OC_6H_4p$-OCH_3
Ar = C_6H_5 or variously substituted phenyl groups

up to 93% ee

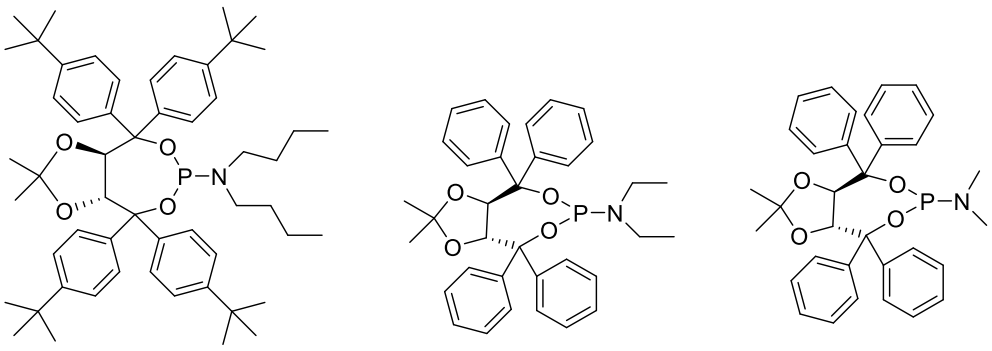

237 **238** **239**

More recently, He and collaborators developed a Pd-catalyzed intramolecular C-H cyclization reaction for the enantioselective construction of indole-based atropoisomers, using a modified taddol-phosphoramidite ligand **240**[579], while Cramer *et al.* showed enantioselective Pd(0)-catalyzed C−H functionalizations of ketene aminal phosphates at room temperature. These reactions provided isoindoline scaffolds with high enantioselectivity, thanks to the use of an electron-rich ligand **241**, obtained by merging a point chiral phospholane module and a bulky atropchiral binaphthyl backbone[580].

Very recently, the same group of researchers developed a Pd(0)-catalyzed C-H functionalization method for the synthesis of chiral 1*H*-isoindoles bearing quaternary stereogenic centres, by using phosphordiamidite ligands **242**. This procedure allowed to obtain perfluoroalkylated-1*H*-isoindoles in high yields and enantioselectivities[581] (**Scheme 16.**).

Scheme 16. Some more recently published enantioselective Pd(0)-catalyzed C(sp^2)-H activation reactions and the structures of the ligands **240**-**242**.

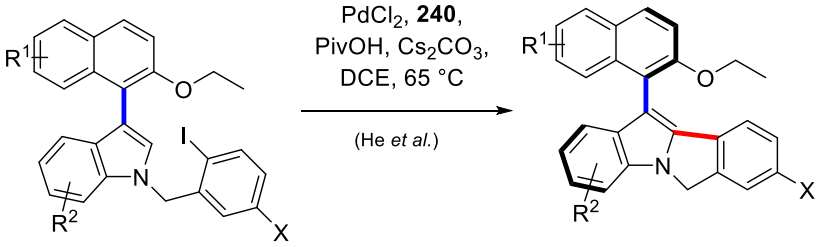

R^1 = H, CH_3, C_6H_5, C_6H_4-pCF_3
R^2 = H, CH_3, alkyl chains, $CH_2C_6H_5$, C_6H_5, NO_2, halogens
X = H, CH_3, Cl, F

up to 92% ee

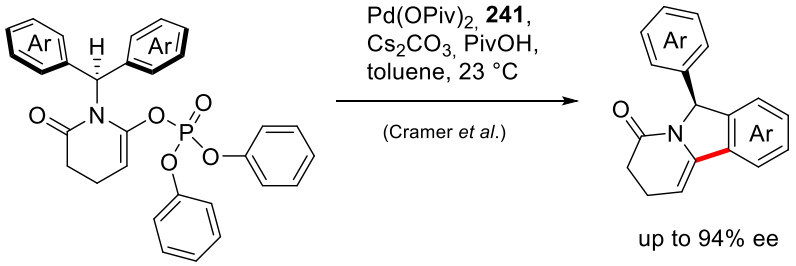

up to 94% ee

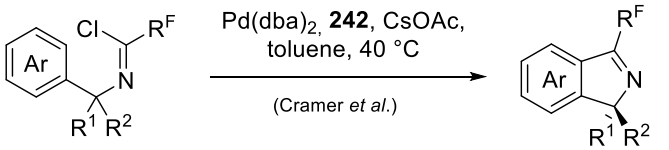

R^1 = CH_3, $CH(CH_3)_2$, cycloalkyl groups
R^2 = C_6H_5, C_4H_3S
R^F = CF_3, CF_2CF_3

up to 97% ee

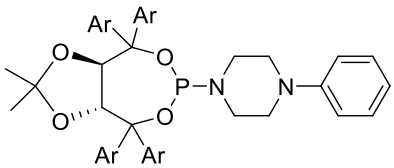

Ar =

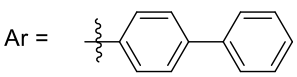

240

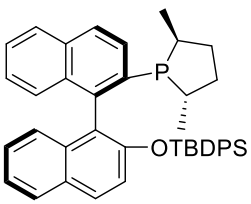

241

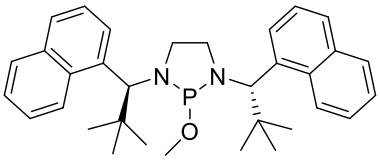

242

Pd(0)-catalyzed C-H activation as well as C-C coupling reactions, proceed through a catalytic cycle that starts from an oxidative addition, continues with the C-H activation and finishes with a reductive elimination by which the product is formed and the Pd(0) species replaced. The enantiodetermining step of this cycle is usually the C-H activation, when the ancillary ligand and the base performing the C-H bond cleavage are all coordinated to the palladium center in the transition state. In particular, a simplified general catalytic cycle for intramolecular C(sp^3)-H arylation from various aryl and heteroaryl chlorides is proposed in **Figure 37.** The oxidative addition of the aryl chloride **A** to Pd^0/trialkylphosphine (PR_3) followed by exchange of the chlorine ligand for carbonate (Y=O^-) or pivalate (Y = *t*Bu) gives rise to Pd(II) complex **C**. From complex **C**, the base-induced concerted demetalation-deprotonation (CMD) mechanism effects the intramolecular C-H bond cleavage to furnish five- or six-membered pallada-cycle **D**, which, by reductive elimination, gives rise to the C-C coupling product **E**[582].

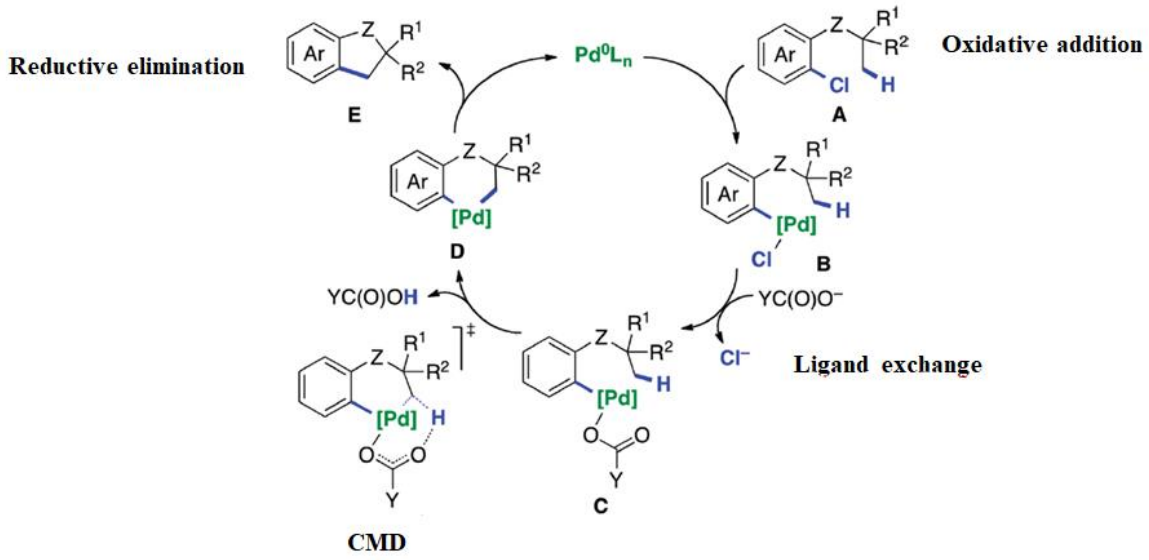

Figure 37. General intramolecular Pd(0)-catalyzed C(sp^3)-H arylation mechanism. [Pd] = Pd-PR_3 complex; Y = *t*Bu or O^-; Z = no atom, CR_2, N-R, O, or C=O. Adapted from: *J. Am. Chem. Soc*., 132 (31), 10706-10716 (**2010**).

Apart from a palladium source, Pd(0)-catalyzed reactions need a ligand and a base to be performed. In particular, their enantioselective version relies on the use of a chiral ancillary ligand and/or a chiral base. Until now, phosphine, phosphoramidite, phosphonite and *N*-heterocyclic carbene have been used as chiral ancillary ligands, while carboxylate and phosphate as chiral bases[570].

6.2. Background

In the context of enantioselective Pd(0)-catalyzed reactions, it would be very interesting to use a bifunctional molecule in which both ancillary ligand and base are present. Such a bifunctional ligand would possess a more organized structure, compared to the corresponding bimolecular system, and might be applicable to several types of asymmetric C-H activation reactions operating by a similar mechanism. Baudoin and co-workers are working on this topic[583]. In particular, they are interested in the development of a bifunctional molecule that can act as ligand and as base at the same time, to use it in enantioselective Pd(0)-catalyzed C-H activation reactions. This compound will be described in details in the following section. The model reaction for the optimization of the catalyst transforms the substrate into a fluoradene derivative. Fluoradenes seem to be key intermediates for the synthesis of buckybowls that can be considered as fragments of fullerenes, having five- and six-membered rings and a curved surface. Buckybowls are interesting compounds for their several possible applications; among them, for example, they can be used in host-guest chemistry or for light-emitters[584,585].

So, to summarize, the work of Baudoin and collaborators has demonstrated that starting from an achiral precursor **243** and using an enantioselective C-H arylation reaction with appropriate conditions, ligand and base, it is possible to obtain fluoradene derivatives **244**. From the obtained fluoradenes, with a second transition-metal catalyzed cyclization, it should be possible to obtain interesting enantioenriched buckybowl systems **245** (**Scheme 17.**).

Scheme 17. General outlook of the synthesis of enantioenriched fluoradene derivatives **244** and their possible application to obtain buckybowl systems **245**.

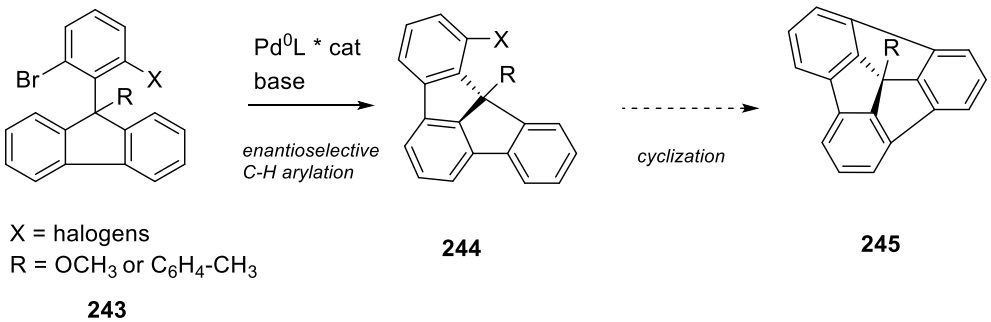

In this context, the work that I have done during my three-months internship within Baudoin's group is related to different aspects linked to C-H activation reactions, and could be divided into three main topics:

- Synthesis of the key intermediate to get the binaphtyl bifunctional ligand
- Enantio and racemic C-H activation reactions
- Attempts to obtain new substrates

6.3. Project: synthesis of the key intermediate to get the binaphtyl bifunctional ligand

As previously said, the enantioselective C-H activation reactions to obtain enantioenriched fluoradene derivatives need, in addition to a palladium source, in particular, tris(dibenzylideneacetone)dipalladium(0)-chloroform adduct ($Pd_2(dba)_3 \cdot CHCl_3$), a chiral ligand **246**. Moreover, the chiral ligand is a phosphine-carboxylate ligand having a binaphthyl scaffold which incorporates both the phosphine and the carboxylic acid moiety. Through optimization studies of the aryl groups on the phosphine it was established that the best enantioselectivity on the catalysis (enantiomeric ratio (e.r.) of 85:15 by chiral HPLC analysis) is achieved when they are substituted with two methyl group in the *meta* positions; other interesting aspects yet to be deeply investigated are the possible effect of different groups on the binaphtyl scaffold (R) (by now, methyl and phenyl substituents have been introduced) and the optimal length of the linker (n) (**Figure 39.**).

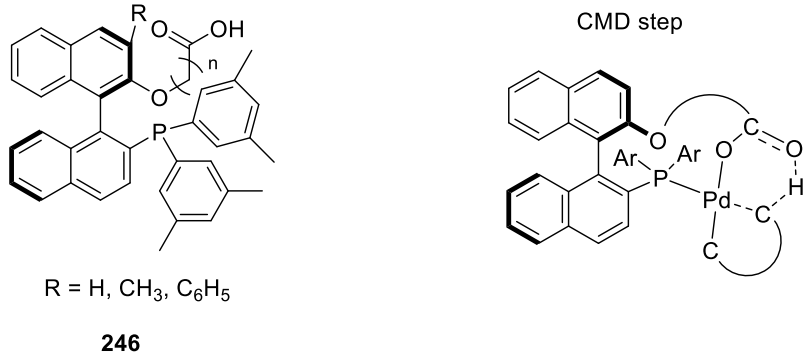

Figure 39. General structure of the phosphine-carboxylate bifunctional ligand **246** and the proposed mechanism of action during CMD step.

6.3.1. Chemistry

Starting from the opportune *in-house* binaphtyl derivative, obtained from the commercially available binol through some methylation and bromination/debromination steps, I synthesized compound **247**, which will be useful as starting material to get the opportune chiral ligand. I stopped my reaction route at intermediate **247** because, before going on, it was necessary to establish the optimal length of the carboxylic lateral chain. I started from a Suzuki reaction on the binaphtyl derivative using phenylboronic acid in the presence of barium hydroxide octahydrate ($Ba(OH)_2 \cdot 8H_2O$) and tetrakis(triphenylphosphine)palladium(0) (($Pd(PPh_3)_4$) in order to introduce the phenyl moiety on the binaphtyl scaffold, obtaining intermediate **248**. The treatment of compound **248** with boron tribromide (BBr_3) followed by the reaction to introduce the triflate group, allowed to obtain first compound **249**, and then intermediate **250**. With a palladium-catalyzed reaction, using $Pd(OAc)_2$, 1,4-bis(diphenylphosphino)butane (Dppb) and DIPEA, I introduced the phosphine moiety and, after the treatment of intermediate **251** with 3 M NaOH, I obtained the desired final compound **247** (**Scheme 18.**). Some of the previously described reactions were carried out following published procedures[586] with some modifications, as reported in the experimental section.

Scheme 18. Synthetic route to obtain compound **247**.

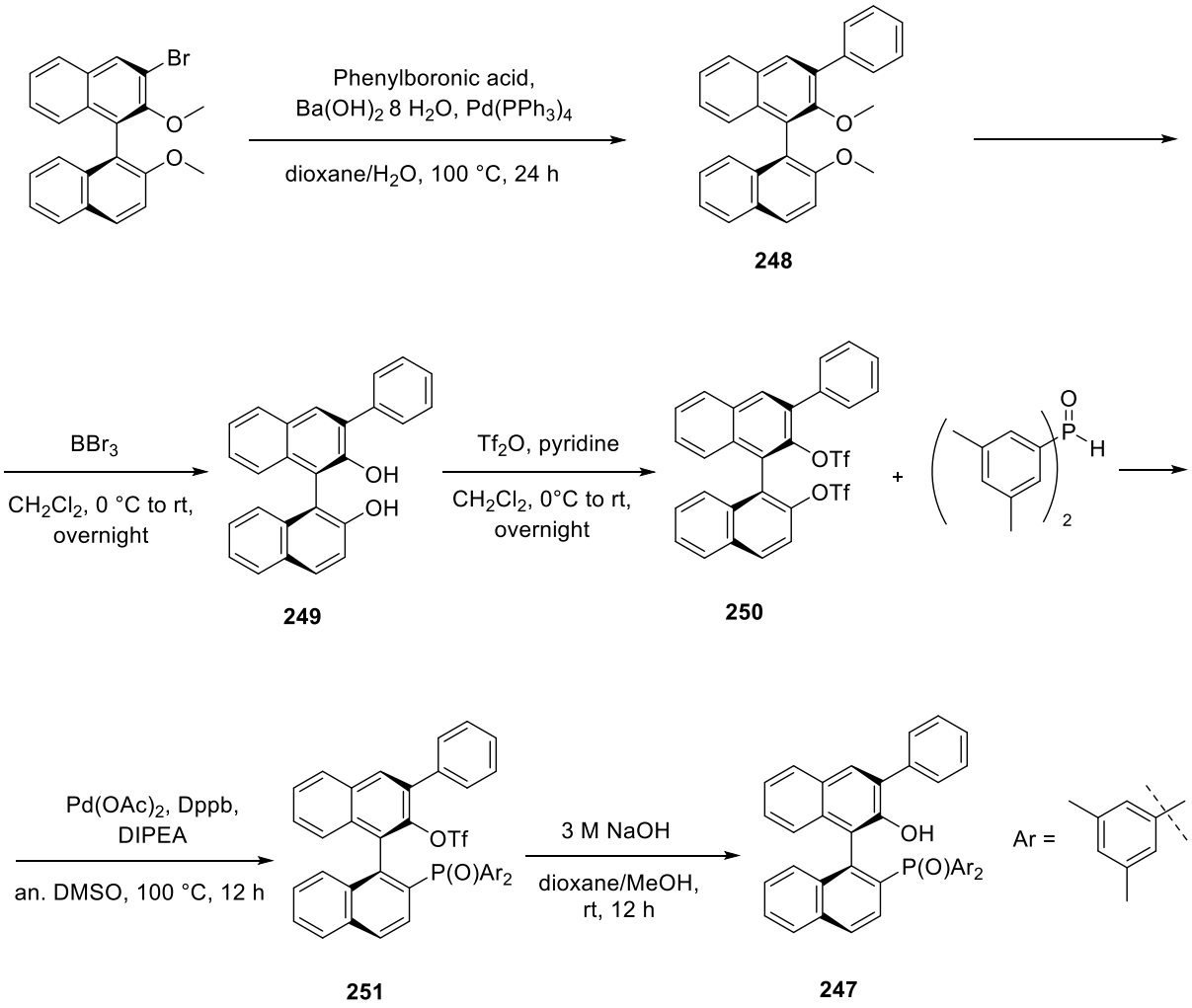

6.4. Project: enantio and racemic C-H activation reactions

Starting from two *in-house* substrates, I performed some C-H activation reactions. I synthesized racemic and enantioenriched derivatives of both compounds **252** and **253** using two different procedures (**Figure 40.**). I obtained derivative **252** in racemic and enantioenriched form (e.r. 77:23 by chiral HPLC analysis), while, unfortunately, compound **253** turned out to be unstable on silica, probably due to the cleavage of the methoxy group (seen from GS-MS) favored by the presence of the oxygen in the ring, and so no further analyses were possible.

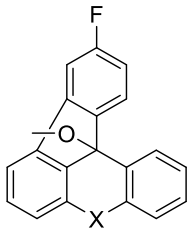

252 X = $C(CH_3)_2$
253 X = O

Figure 40. Xanthone- and anthracenone-based derivatives **252** and **253** obtained employing C-H activation reactions.

6.4.1. Chemistry

For the synthesis of racemic compounds **252a** and **253a**, I used tricyclohexylphosphine tetrafluoroborate ($PCy_3 \cdot HBF_4$) and palladium acetate ($Pd(OAc)_2$) as catalysts, cesium pivalate ($C_5H_9O_2Cs$), Cs_2CO_3 and 4 Å molecular sieves (MS) in anhydrous xylenes at reflux for 16 h. To obtain enantiomeric compounds **252b** and **253b**, I used $Pd_2(dba)_3 \cdot CHCl_3$ adduct, the bifunctional ligand **250a**, Cs_2CO_3 and 4 Å MS in anhydrous and degassed DME at 140 °C for 24 h (**Scheme 19.**). For compound **252b**, e.r. was 77:23, while, unfortunately, compound **253b** turned out to be unstable on silica, and was lost during purification, probably for the cleavage of the methoxy group favored by the presence of the oxygen in the xanthone ring.

Scheme 19. Racemic and enantio C-H activation reactions to obtain compounds **252a,b** and **253a,b**.

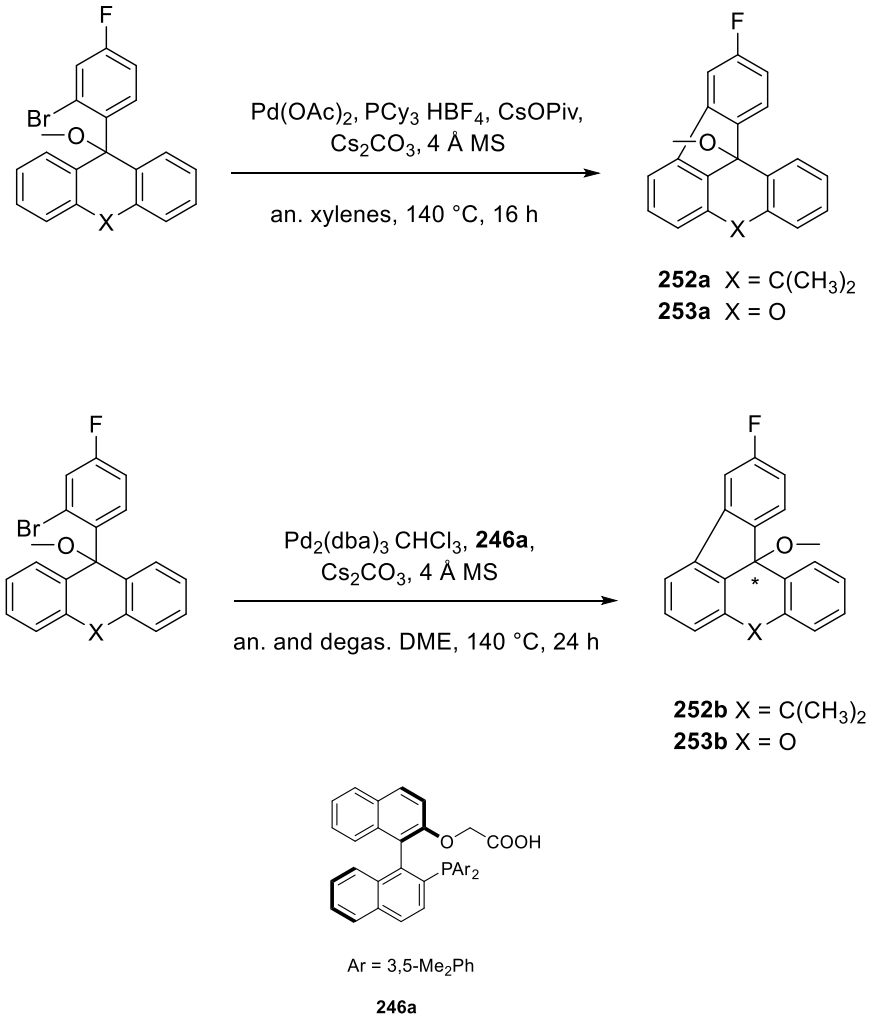

6.5. Project: attempts to synthesize new substrates

Until now, the substrates for the Pd-catalyzed C-H activation reactions have been commercially available tricyclic compounds (**Figure 41.**).

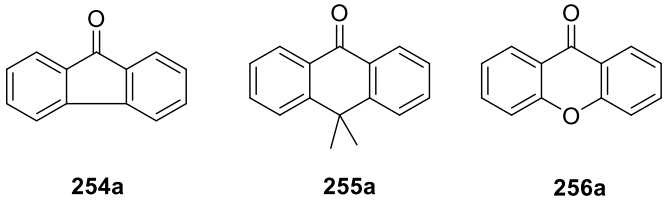

Figure 41. The three main substrates used for C-H activation reaction until now.

To explore better this type of reactivity, it would be interesting to try the enantioselective reactions on benzylic position. It is worth to underline that this time the C-H activation should take place on C(sp^3) and not on C(sp^2) as before. The second part of my research work was devoted to try to develop a high-yield route for the synthesis of new substrates **254b**, **255b** and **256b** (**Figure 42.**).

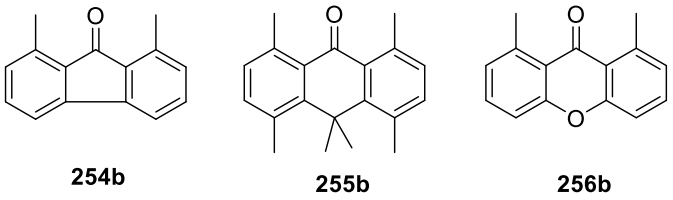

Figure 42. New compounds to be synthesized as substrates for C-H activation reactions

6.5.1. Chemistry

Unfortunately, despite many attempts, I had some problems to get the desired final products (see **Schemes 20-23** below). For the synthesis of compound **254b,** after the first step, I was not able to hydrolyze the stable immine which I obtained; the route for the synthesis of compound **255b** allowed to obtain in high yield an intermediate different from the desired one, while in the case of the synthesis of substrate **256b**, the problematic step was the final cyclization. Since in the literature there is an example of this type of reaction with a substrate having four hydroxyl groups instead of two, I decided to plan another synthetic route to try to obtain substrate **256c** (**Scheme 23.**), which, for the purpose to try C-H activation reactions, is equivalent to substrate **256b**, but unfortunately, also in this case, the final step did not work. In more detail, the attempt to obtain the final compound **254b** started with a Friedel-Crafts reaction between *m*-toluidine and *o*-tolunitrile using boron trichloride (BCl_3) and aluminum chloride ($AlCl_3$) in anhydrous toluene, in order to get the stable immine **257**[587]. At this point, despite many different conditions tried (hydrolysis under different acidic conditions), I did not obtain the desired intermediate; also the attempt to do a Pd-catalyzed hydrogenolysis did not work (**Scheme 20.**).

Scheme 20. Attempt to obtain substrate **254b**.

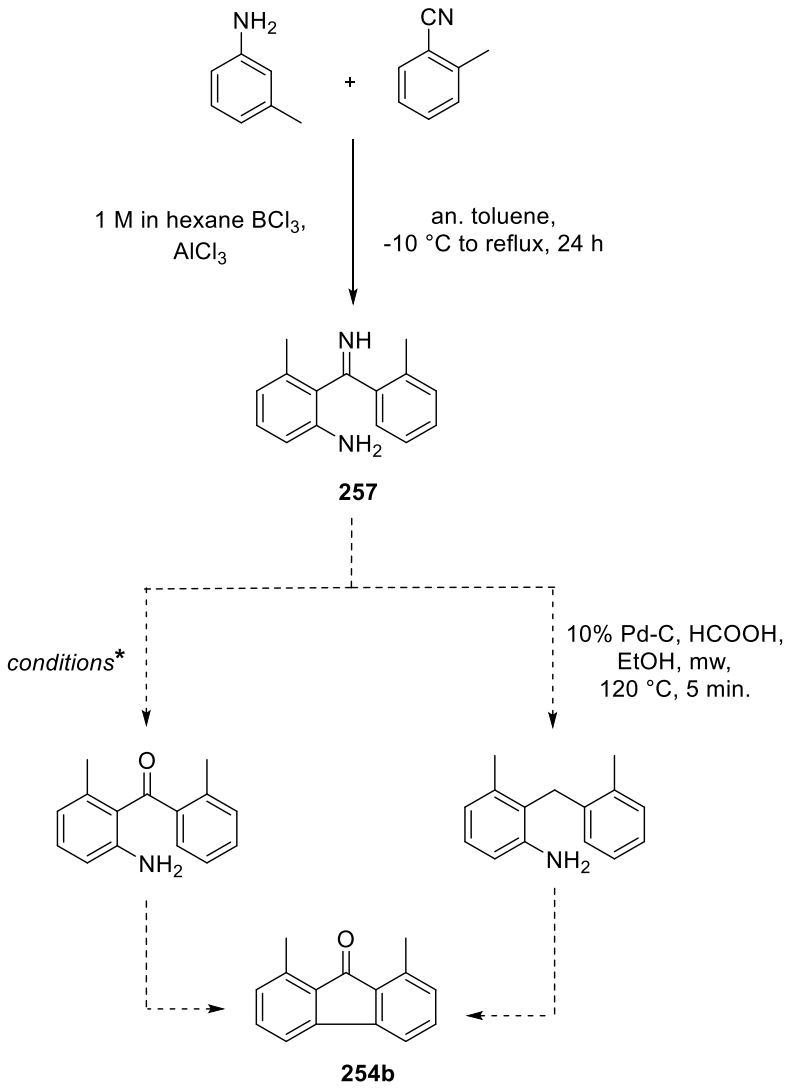

***** *a)* 0.2 N HCl, reflux, 48 h; *b)* 6 N HCl, reflux, 24 h; *c)* 6 N HCl, $CH_3(CH_2)_2OH$, reflux, 24 h; *d)* H_2O, conc. HCl, CH_3COOH, mw, 60-100-140 °C 15 min. *e)* conc. HCl, mw, 100 °C, 15 min; *f)* conc. H_2SO_4, reflux, 24 h.

The attempt to obtain the final compound **255b** started from a Diels-Alder reaction between dimethylfuran and maleic anhydride followed by treatment of the endoxide **258** with concentrated H_2SO_4, to get intermediate **259**[588]. The reaction between compound **259** and the *in-situ* prepared Grignard **260** gave intermediate **261**[589]. The following treatment of compound **261** with zinc in the presence of 10% NaOH allowed to obtain lactone **262**, instead of the desired intermediate[590] (**Scheme 21.**).

Scheme 21. Attempt to obtain substrate **255b**.

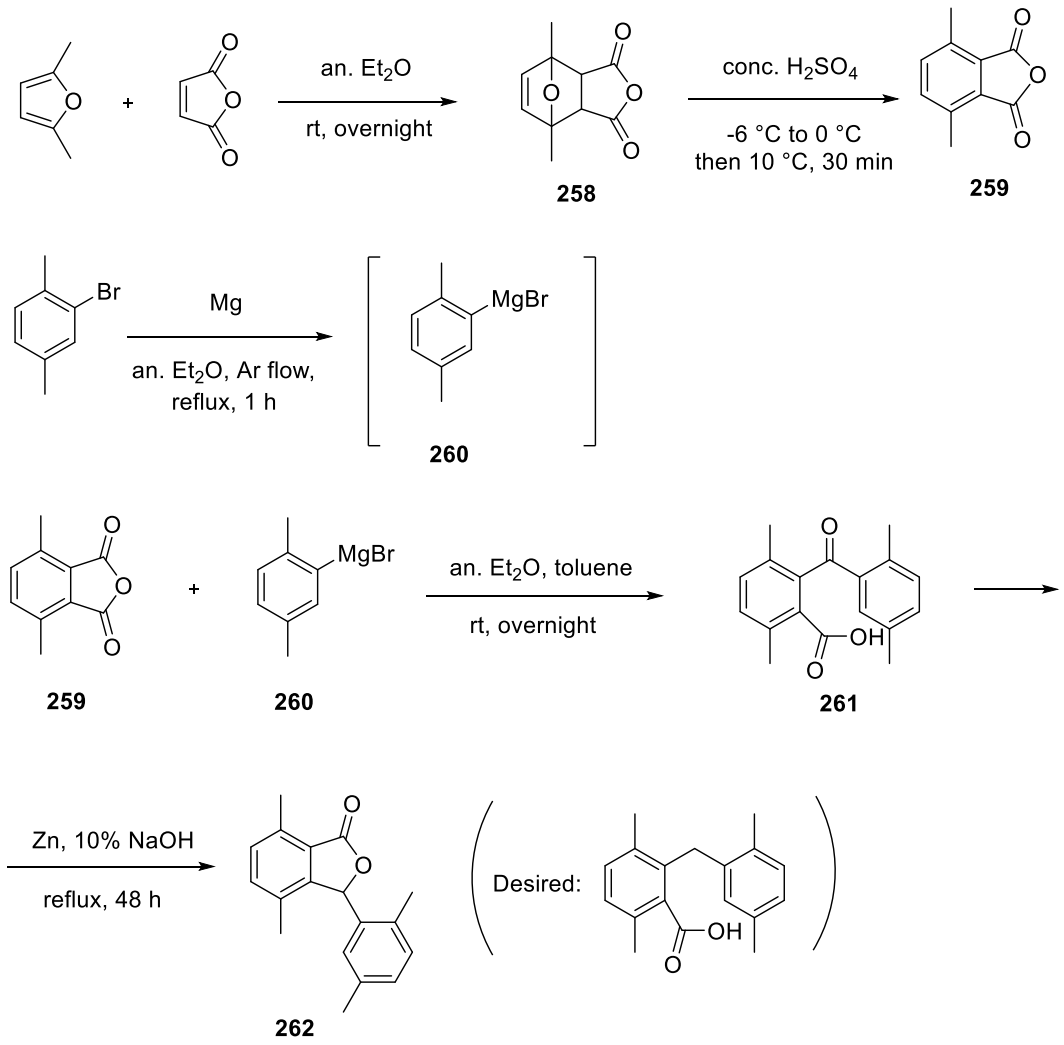

To obtain the desired final compound **256b**, I started from the reaction between 2-amino-6-methylbenzoic acid and sodium nitrite ($NaNO_2$) in the presence of 25% H_2SO_4, leading to intermediate **263**[591]. The benzylation of **263**, using benzyl bromide and tetrabutylammonium bromide[592], allowed to obtain the disubstituted compound **264**, and after the treatment with NaOH and lithium hydroxide (LiOH), I got the desired intermediate **265**. The benzylation on *m*-cresol, performed with benzyl bromide and K_2CO_3 in anhydrous DMF, gave intermediate **266**[593]. With a Friedel-Crafts acylation between **265** and **266**, in the presence of TFA and trifluoroacetic anhydride (TFAA) I obtained compound **267**, and then with a Pd-catalyzed hydrogenation, I got intermediate **268**. At this point, despite different conditions tried, the final reaction to obtain compound **256b** did not work (**Scheme 22.**).

Scheme 22. Attempt to obtain substrate **256b**.

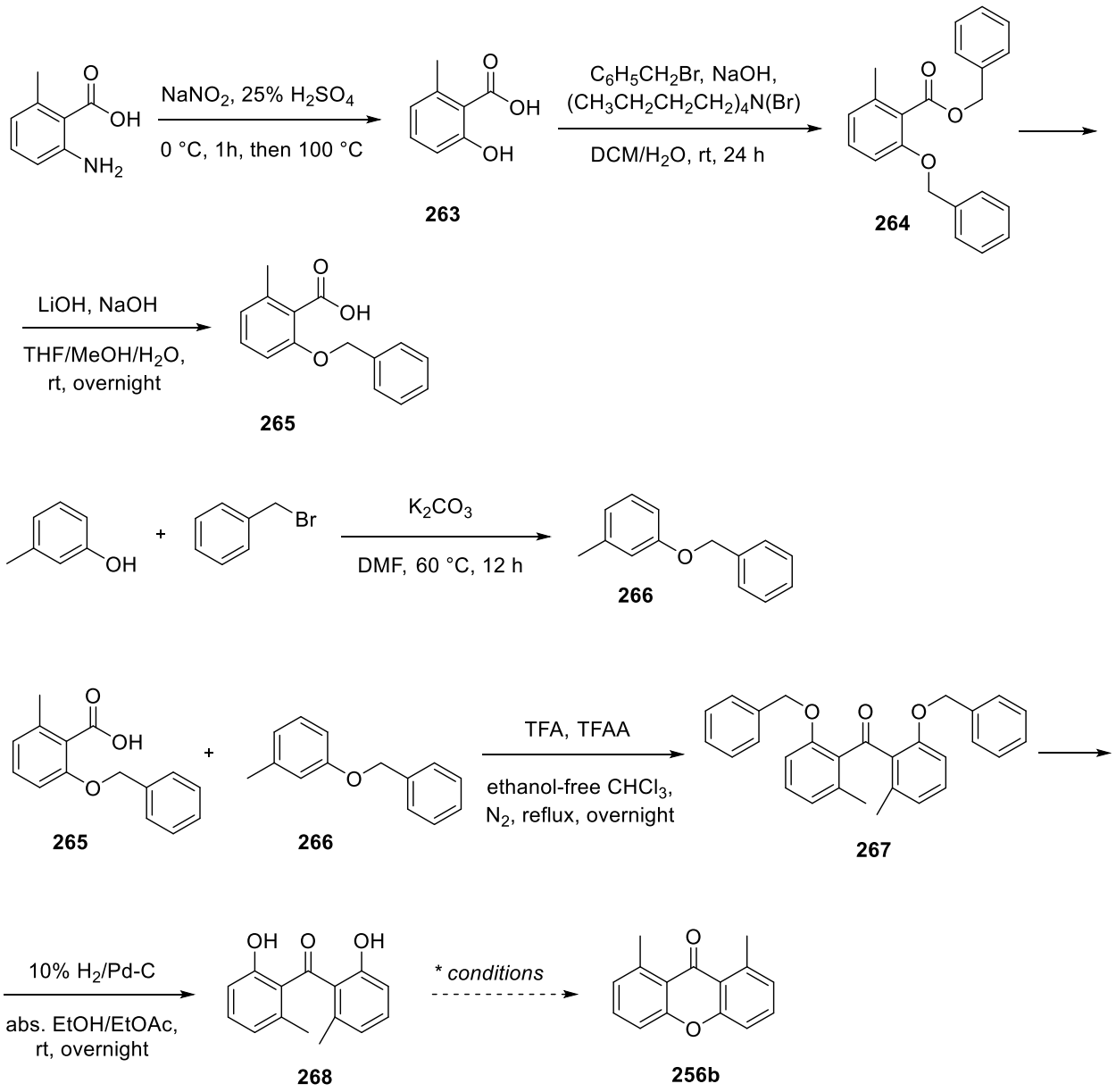

* *a)* AcONa, H_2O, reflux, 26 h; *b)* NaOH, MeOH/H_2O, mw, 100 °C, 30 min.; *c)* DMF/H_2O, 180 °C, 16 h.

As previously said, since in literature there is one example of the final cyclization on a substrate that has more than two hydroxylic groups[594], I decided to try to synthesize compound **256c**. I started from a Vilsmeier reaction on orcinol in order to introduce the aldeidic function and get intermediate **269**. The subsequent benzylation allowed to obtain

compound **270** and after a Pinnick oxidation using sodium chlorite ($NaClO_2$), sodium dihydrogen phosphate (NaH_2PO_4) and 2-methyl-2-butene as a scavenger, I got compound **271** in a quantitative yield. With a direct benzylation on orcinol I obtained intermediate **272**. A Friedel-Crafts acylation between **271** and **272** gave molecule **273**, and then a Pd-catalyzed hydrogenation allowed to obtain compound **274**. But at this point, unfortunately, also in this case, the final reaction did not work (**Scheme 23.**).

Scheme 23. Attempt to obtain substrate **256c**.

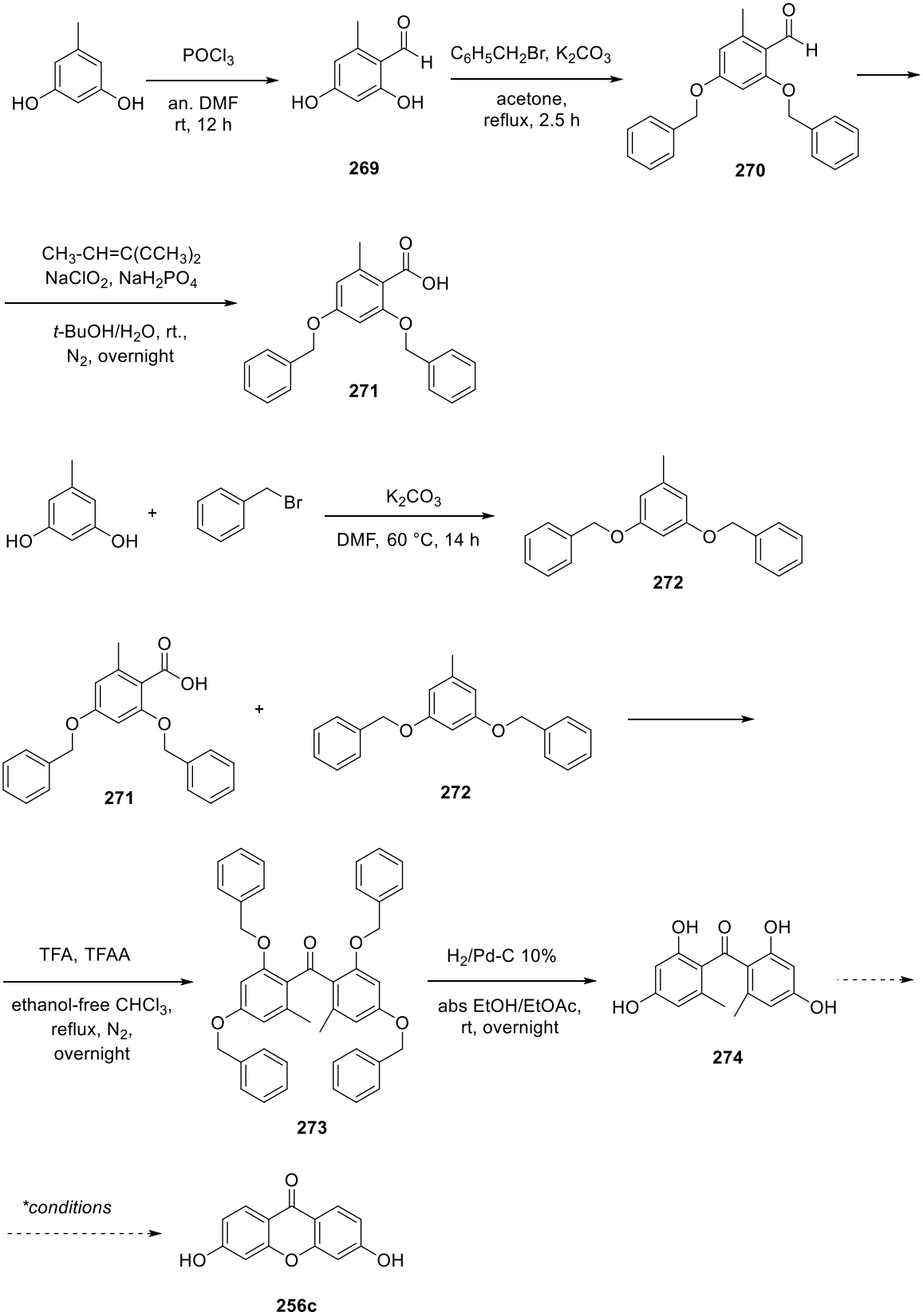

* *a)* AcONa, H_2O, reflux, 26 h; *b)* DMF/H_2O, 180 °C, 16 h.

6.6. Conclusions

During my three months of internship at the Department of Organic Chemistry at the University of Basel, I worked in the Prof. Dr. Baudoin's research group on projects related to Pd(0)-catalyzed reactions. I synthesized a key intermediate to obtain the innovative bifunctional ligand to employ in enantioselective Pd(0)-catalyzed C-H activation reactions. Some of these reactions were performed in order to obtain new compounds both in racemic and enantioenriched form. I also attempted to develop high-yield synthetic routes to get new substrates to employ in these reactions.

CHAPTER 7. Experimental section

Starting materials were purchased from Merck-Sigma Aldrich (Milan, Italy), Alfa Aesar (Lancashire, United Kingdom) and Fluorochem Ltd. (United Kingdom). Melting points (Mp) were determined with a Büchi B-540 apparatus and are uncorrected. ^{1}H-NMR spectra were recorded in a $CDCl_3$, CD_3OD or DMSO-d6 solution using a Bruker Avance DPX400 (400 MHz), Adavance 500 (500MHz) or a Varian Gemini 200 (200 MHz). Chemical shifts are reported as δ (ppm) relative to TMS as the internal standard, coupling constant (*J*) in hertz (Hz) and integration. ^{1}H patterns are described using the following abbreviations: s = singlet, d = doublet, t = triplet, q = quartet, m = multiplet and/or multiplet resonances and br = broad. IR spectra were measured in KBr or $CHCl_3$ with a Perkin-Elmer 398 spectrophotometer. ^{13}C-NMR spectra were recorded at 100 MHz on a Bruker AC200F. Microwave reactions were conducted using a CEM Discover Synthesis Unit (CEM Corp., Matthews, NC). GC-MS analyses were performed with a Shimadzu QP2010SB GCMS apparatus on a Rtx®-5ms-Low-Bleed column lined with a mass (EI) detection system. Mass spectra (MS) data were obtained using an Agilent 1100 LC/MSD VL system (G1946C) with a 0.4 mL/min flow rate using a binary solvent system of 95:5 methanol/water. Mass spectra were acquired in positive mode scanning over the mass range 105-1500 m/z, using a variable fragmentor voltage of 10-70 mV. LC was performed using an LC-20AD liquid chromatograph. HPLC analyses were performed using a Shimadzu Prominence system with SIL-20A auto sample, CTO-20AC column oven, LC-20AD pump system, DGU-20A3 degasser and SPD-M20A Diode Array or UV/VIS detector. The following chiral columns from Daicel Chemical Industries were used: OJ-H (Chiralcel®), IA (Chiralpak®) in 4.6 x 250 mm size. The MW-SPPS was performed using Fmoc strategy on a Liberty™ Microwave Peptide Synthesizer (CEM Corporation, Matthews, NC), an additional module of Discover™ (CEM Corporation, Matthews, NC). TLC (thin layer chromatography) was carried out using Merck TLC plates silica gel 60 F254. UV detection was monitored at 254 nm. Chromatographic purifications were performed on columns packed with silica gel 60 Å (220-440 mesh) or Florisil® (100-200 mesh). Analysis for C, H, N and S were determined using Thermo Scientific Flash 2000 and results were within ± 0.4% of the theoretical value. All target compounds possessed a purity of ≥95% as verified by elemental analyses by comparison with the theoretical values.

Synthesis of (2*E*)-3-(4-Methylphenyl)-1-phenylprop-2-en-1-one 170

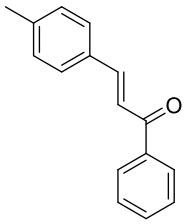

170

To a stirred solution of acetophenone (3.8 mL, 33.00 mmol) in EtOH (50 mL), a solution of *p*-tolualdehyde (3.8 mL, 33.00 mmol) in EtOH (50 mL) and 4 N NaOH (20.6 mL) were added. The mixture was stirred at room temperature for 6 h. The reaction was quenched with 2 N HCl and filtered, then the solvent was partially evaporated under vacuum. The residue was dissolved in AcOEt (30 mL x 3), washed with water (90 mL), dried over Na_2SO_4, filtered and concentrated under reduced pressure. The solid obtained was decanted with EtOH furnishing the pure chalcone as a pale yellow solid.

Yield: 7.26 g, 99%

Mp: 189-190 °C

MW = 222.28

Anal. calcd. for $C_{16}H_{14}O$: C 86.45, H 6.35; found: C 86.47, H 6.45.

^{1}H-NMR (400 MHz, $CDCl_3$): δ (ppm) 2.38 (s, 3H, CH_3), 7.22 (d, *J* = 7.6 Hz, 2H Ar), 7.47-7.59 (m, 6H, 5H Ar + 1H CH=CHCO), 7.79 (d, *J* = 15.6 Hz, 1H, CH=CHCO), 7.97 (d, *J* = 7.6 Hz, 2H Ar).

^{13}C-NMR (100 MHz, $CDCl_3$): δ (ppm) 190.27, 144.74, 140.96, 138.29, 132.60, 132.09, 129.65, 128.52, 128.46, 128.43, 120.94, 21.45.

IR (KBr): cm^{-1} 3022 (CH=CH), 1656 (CO).

Synthesis of 2-mercapto-4-(4-methylphenyl)-6-phenyl-1,4-dihydropyridine-3-carbonitrile 171

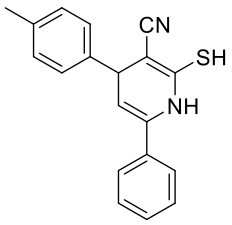

171

To a solution of sodium (0.19 g, 8.10 mmol) in anhydrous MeOH (22 mL) under N_2 atmosphere, chalcone **170** (0.90 g, 4.05 mmol) and cyanothioacetamide (0.41 g, 4.05 mmol) were added. The reaction was stirred at reflux for 90 min. After cooling, the mixture was quenched with 1 N HCl and partially evaporated under vacuum. The residue was diluted in CH_2Cl_2 and then extracted (20 mL x 3), washed with water (60 mL), dried over Na_2SO_4, filtered and concentrated under reduced pressure. The pure yellow solid obtained was used directly in the next step.

Yield: 3.81 g, 94%

Mp: 105-133 °C

MW = 304.41

Anal. calcd. for $C_{19}H_{16}N_2S$: C 74.97, H 5.30, N 9.20, S 10.53; found: C 74.86, H 5.68, N 8.84, S 10.73.

^{1}H-NMR (400 MHz, $CDCl_3$): δ (ppm) 2.04 (s, 1H, SH), 2.35 (s, 3H, CH_3), 5.79 (s, 1H, H-4), 5.92 (d, *J* = 4.8 Hz, 1H, H-5), 7.13-7.46 and 7.55-7.59 (2 m, 9H Ar), 9.11 (br s, 1H, NH).

^{13}C-NMR (100 MHz, $CDCl_3$): δ (ppm) 137.38, 132.95, 129.91, 129.74, 129.21, 128.04, 127.52, 125.34, 116.26, 108.90, 108.64, 49.13, 48.38, 42.15, 21.04.

IR (KBr): cm^{-1} 3203 (NH), 2196 (CN).

Synthesis of 2-mercapto-4-(4-methylphenyl)-6-phenylnicotinonitrile 172

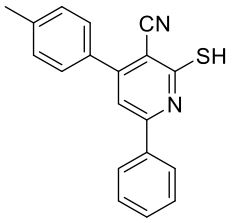

172

To a stirred solution of **171** (0.70 g, 2.23 mmol) in CH_2Cl_2 (15 mL), DDQ (1.01 g, 4.46 mmol) was added. The mixture was stirred at room temperature for 3 h, then filtered and evaporated under reduced pressure. The dark solid obtained was suspended several times in MeOH, water and *n*-hexane and, after decantation, recrystallized from MeOH, obtaining an off-white solid.

Yield: 0.57 g, 84%

Mp: 204-207 °C

MW = 302.39

Anal. calcd. for $C_{19}H_{14}N_2S$: C 75.47, H 4.67, N 9.26, S 10.60; found: C 75.24, H 4.38, N 9.57, S 10.58.

^{1}H-NMR (400 MHz, $CDCl_3$): δ (ppm) 1.56 (s, 1H, SH), 2.46 (s, 3H, CH_3), 7.35-7.40 (m, 5H Ar), 7.53 (d, *J* = 8.0 Hz, 2H Ar), 7.61 (s, 1H, H-5), 7.95 (d, *J* = 7.2 Hz, 2H Ar).

^{13}C-NMR (100 MHz, $CDCl_3$): δ (ppm) 160.57, 158.83, 154.86, 142.72, 140.58, 136.74, 132.85, 130.64, 129.76, 128.82, 128.27, 127.32, 117.35, 115.48, 21.31.

IR (KBr): cm^{-1} 2215 (CN).

Synthesis of {[3-cyano-4-(4-methylphenyl)-6-phenylpyridin-2-yl]thio}acetic acid 173

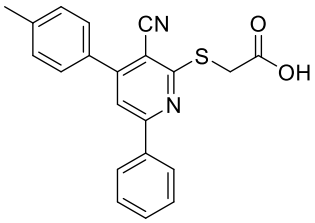

173

To a solution of **172** (0.42 g, 1.38 mmol) in DMF (6 mL), 10% KOH (1.70 mL, 3.04 mmol) and a solution of 2-bromoacetic acid (0.21 g, 1.52 mmol) in DMF (1 mL) were added. The dark red mixture was stirred at room temperature for 3 h. Then, the reaction was treated with 3 N HCl, becoming yellow, and extracted with AcOEt (20 mL x 3). The organic phase was washed with water (60 mL), dried over Na_2SO_4, filtered and concentrated under reduced pressure. The crude solid residue was purified through recrystallization from MeOH, to give compound **173** as yellow crystals.

Yield: 0.73 g, 75%

Mp: 218-220 °C

MW = 360.43

Anal. calcd. for $C_{21}H_{16}N_2O_2S$: C 69.98, H 4.47, N 7.77, S 8.90; found: C 69.73, H 4.78, N 8.13, S 8.51.

^{1}H-NMR (400 MHz, DMSO-d6): δ (ppm) 2.39 (s, 3H, CH_3), 4.16 (s, 2H, CH_2), 7.38 (d, *J* = 8.0 Hz, 2H Ar), 7.50-7.52 (m, 3H Ar), 7.64 (d, *J* = 8.0 Hz, 2H Ar), 7.88 (s, 1H, H-5), 8.23-8.24 (m, 2H Ar).

^{13}C-NMR (100 MHz, DMSO-d6): δ (ppm) 170.29, 162.50, 158.40, 154.56, 140.47, 137.01, 133.11, 131.16, 129.84, 129.25, 128.97, 128.05, 116.44, 116.12, 102.81, 33.37, 21.27.

IR (KBr): cm^{-1} 3200-2400 (OH), 2219 (CN), 1710 (CO).

Synthesis of methyl N-({[3-cyano-4-(4-methylphenyl)-6-phenylpyridin-2-yl]thio}acetyl)-L-valinate (L-valine methyl ester adduct) 167a

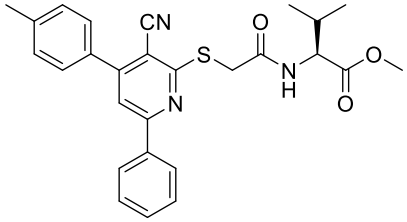

167a

To a stirred solution of **173** (0.10 g, 0.28 mmol) in anhydrous DMF (1 mL) at 0 °C under N_2 atmosphere, a solution of L-Val methyl ester (hydrochloride salt; 0.05 g, 0.30 mmol) in anhydrous DMF (1 mL) was added dropwise. Then, EDC (0.05 g, 0.28 mmol), HOBt (0.04 g, 0.28 mmol) and dry DIPEA (0.06 mL, 0.40 mmol) were added. The mixture was stirred at 0 °C for 30 min. and then at room temperature for 5 h. The reaction was quenched with water and then extracted with AcOEt (20 mL x 3). The organic phase was washed with water (60 mL), dried over Na_2SO_4, filtered and concentrated under reduced pressure. The crude residue was purified through flash chromatography on silica gel, using as eluent *n*-hexane/AcOEt (7:3), to obtain the final product as a white solid.

Yield: 0.03 g, 20%

MW = 473.59

Anal. calcd. for $C_{27}H_{27}N_3O_3S$: C 68.48, H 5.75, N 8.87, S 6.77; found: C 68.37, H 5.59, N 8.77, S 6.64.

^{1}H-NMR (400 MHz, $CDCl_3$): δ (ppm) 0.62 and 0.69 (2 d, J = 6.8 Hz, 3H, CH($\underline{CH_3}$)$_2$), 1.97-2.05 (m, 1H, $\underline{CH}(CH_3)_2$), 2.44 (s, 3H, CH_3), 3.53 (s, 3H, OCH_3), 4.01 (q, J_{AB} = 16.0 Hz, 2H, CH_2S), 4.45-4.51 (m, 1H, $\underline{CH}$NH), 7.17 (d, J = 6.4 Hz, 1H, NH), 7.35 (d, J = 7.6 Hz, 2H Ar), 7.50-7.55 (m, 5H Ar), 7.60 (s, 1H, H-5), 8.03-8.07 (m, 2H Ar).

^{13}C-NMR (100 MHz, $CDCl_3$): δ (ppm) 167.92, 161.62, 158.97, 154.90, 140.65, 136.74, 132.83, 130.74, 129.75, 129.03, 128.22, 127.39, 116.52, 115.36, 103.79, 57.34, 51.84, 33.89, 30.87, 21.29, 18.60, 17.43.

IR (KBr): cm^{-1} 3359 (NH), 2220 (CN), 1749 (CO ester), 1646 (CO amide).

Synthesis of N-({[3-cyano-4-(4-methylphenyl)-6-phenylpyridin-2-yl]thio}acetyl)-L-valine (L-valine free acid adduct) 167b

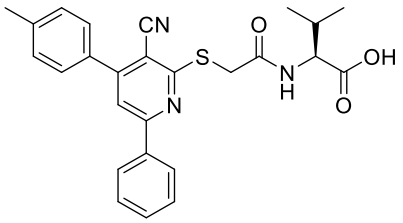

167b

To a stirred solution of **167a** (0.05 g, 0.10 mmol) in a mixture of THF/EtOH/H_2O (3:1:0.5) (4 mL), 1 N NaOH (0.44 mL) was added. The mixture was stirred at room temperature for 15 min. until the solution becomes yellow. The reaction was quenched with 2 N HCl and extracted with AcOEt (10 mL x 3). The organic phase was washed with water (30 mL), dried over Na_2SO_4, filtered and concentrated under reduced pressure. The crude residue was purified through flash chromatography on silica gel, eluting with AcOEt/MeOH/AcOH (9:1:0.5), to give pure **167b**.

Yield: 0.02 g, 40%

MW = 459.56

Anal. calcd. for $C_{26}H_{25}N_3O_3S$: C 67.95, H 5.48, N 9.14, S 6.98; found: C 68.02, H 5.33, N 8.96, S 6.79.

^{1}H-NMR (400 MHz, CD_3OD): δ (ppm) 0.73 and 0.74 (2 d, J = 6.0 Hz, 3H, CH(C$\underline{H_3}$)$_2$), 2.06 (m, 1H, C$\underline{H}$(CH$_3$)$_2$), 2.44 (s, 3H, CH_3), 4.17 (q, J_{AB} = 16.0 Hz, 2H, CH_2S), 4.22-4.26 (m, 1H, C$\underline{H}$NH), 7.38 (d, J = 8.0 Hz, 2H Ar), 7.48-7.52 (m, 3H Ar), 7.58 (d, J = 8.0 Hz, 2H Ar), 7.76 (s, 1H, H-5), 8.19 (d, J = 8.0 Hz, 2H Ar).

^{13}C-NMR (100 MHz, CD_3OD): δ (ppm) 174.15, 171.31, 162.55, 158.39, 154.47, 140.11, 137.09, 133.22, 131.31, 129.74, 129.31, 128.80, 128.15, 116.41, 116.21, 102.78, 31.10, 30.40, 23.40, 21.30, 18.99.

IR (KBr): cm^{-1} 3450-3100 (OH), 3362 (NH), 2221 (CN), 1690 (CO acid), 1646 (CO amide).

Synthesis of dimethyl *N*-[(9*H*-fluoren-9-ylmethoxy)carbonyl]-L-valyl-L-aspartate 174

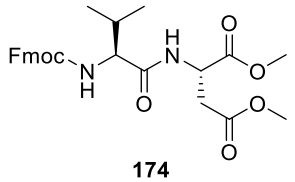

174

It was used the same amidation protocol described before: to a stirring solution of Fmoc-L-valine (0.5 g, 1.47 mmol) in anhydrous DMF (5 mL) under N_2 atmosphere, a solution of L-aspartate dimethyl ester (hydrochloride salt; 0.29 g, 1.47 mmol) in the same solvent (5.3 mL) was added dropwise. Then, EDC (0.28 g, 1.47 mmol), HOBt (0.20 g, 1.47 mmol) and dry DIPEA (0.31 mL, 1.77 mmol) were added. The mixture was stirred at 0 °C for 30 min. and then at room temperature for 4 h. The reaction was quenched with water and extracted with AcOEt (20 mL x 3). The organic phase was washed with water (60 mL), dried over Na_2SO_4, filtered and concentrated under reduced pressure. The crude residue was purified through flash chromatography on silica gel, using *n*-hexane/AcOEt (1:1) as eluent.

Yield: 0.56 g, 79%

MW = 482.53

Anal. calcd. for $C_{26}H_{30}N_2O_7$: C 64.72, H 6.27, N 5.81; found: C 64.51, H 6.25, N 6.09.

^{1}H-NMR (400 MHz, $CDCl_3$): δ (ppm) 0.96 and 0.99 (2 d, *J* = 6.0 Hz, 3H, CH($\underline{CH_3}$)$_2$), 2.13-2.18 (m, 1H, $\underline{CH}(CH_3)_2$), 2.83-3.04 (m, 2H, $\underline{CH_2}CO$), 3.73 and 3.66 (2 s, 3H, OCH_3), 4.10-4.13 (m, 1H, $\underline{CH}NH$), 4.21 (t, *J* = 6.8 Hz, 1H, $\underline{CH}CH_2$), 4.37 (m, 2H, $\underline{CH_2}O$), 4.89-4.93 (m, 1H, CH Fmoc), 5.56 (d, *J* = 8.4 Hz, 1H, NH), 6.92 (d, *J* = 7.6 Hz, 1H, NH), 7.29 and 7.38 (2 t, *J* = 7.2 Hz, 4H Ar), 7.58 (d, *J* = 6.4 Hz, 2H Ar), 7.74 (d, *J* = 8.0 Hz, 2H Ar).

^{13}C-NMR (100 MHz, $CDCl_3$) δ (ppm) 171.08, 170.70, 156.23, 143.71, 141.21, 127.62, 126.99, 125.08, 119.79, 67.10, 60.06, 52.68, 52.04, 48.32, 47.06, 35.80, 31.44, 18.88, 17.62.

IR (KBr): cm^{-1} 3362 (NHCO), 1745 (CO ester), 1649 (CO amide).

Synthesis of dimethyl L-valyl-L-aspartate 175

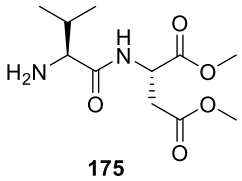

175

To a stirred solution of **174** (0.27 g, 0.56 mmol) in DMF (7 mL), NaN_3 (0.07 g, 1.12 mmol) was added. The mixture was stirred at 50 °C for 12 h. The reaction was quenched with water and extracted with AcOEt (20 mL x 3). The organic phase was washed with water (60 mL), dried over Na_2SO_4, filtered and concentrated under reduced pressure. The crude residue was used in the next step without further purification.

MW = 260.28
LRMS (ESI) m/z = 261.8 $[M+H]^+$.

Synthesis of dimethyl *N*-({[3-cyano-4-(4-methylphenyl)-6-phenylpyridin-2-yl]thio}acetyl)-L-valyl-L-aspartate (diamino acid methyl diester adduct) 168a

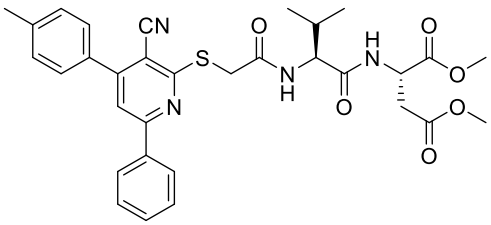

168a

To **175** (0.19 g, 0.31 mmol), anhydrous DMF (3 mL) was added under N_2 atmosphere. Then, a solution of **173** (0.11 g, 0.31 mmol) in the same solvent (3 mL), EDC (0.04 g, 0.31 mmol), HOBt (0.06 g, 0.31 mmol) and dry DIPEA (0.06 mL, 0.37 mmol) were added. The mixture was stirred at 0 °C for 30 min. and then at room temperature for 12 h. The reaction was quenched with water and then extracted with AcOEt (20 mL x 3). The organic phase was washed with water (60 mL), dried over Na_2SO_4, filtered and concentrated under reduced

pressure. The crude residue was purified through flash chromatography on silica gel using AcOEt as eluent.

Yield: (over two steps): 0.04 g, 21%

MW = 602.70

Anal. calcd. for $C_{32}H_{34}N_4O_6S$: C 63.77, H 5.69, N 9.30, S 5.32; found: C 63.81, H 5.75, N 9.09, S 5.64.

^{1}H-NMR (400 MHz, $CDCl_3$): δ (ppm) 0.67 and 0.75 (2 d, J = 6.8 Hz, 3H, CH($\underline{CH_3}$)$_2$), 1.93-1.97 (m, 1H, $\underline{CH}(CH_3)_2$), 2.43 (s, 3H, CH_3), 2.62-2.91 (m, 2H, $\underline{CH_2}CO$), 3.64 and 3.69 (2 s, 3H, OCH_3), 4.00 (q, J_{AB} = 15.6 Hz, 2H, CH_2S), 4.14-4.18 (m, 1H, $\underline{CH}NH$), 4.23-4.27 (m, 1H, $\underline{CH}CH_2$), 4.71-4.75 and 6.77-6.81 (2 m, 1H, NH), 7.27-7.31, 7.46-7.50 and 7.51-7.55 (3 m, 7H Ar), 7.58 (s, 1H, H-5), 8.04 (d, J = 6.0 Hz, 2H Ar).

^{13}C-NMR (100 MHz, $CDCl_3$): δ (ppm) 171.08, 170.70, 156.23, 143.85, 130.73, 129.97, 129.76, 129.04, 128.23, 127.40, 116.58, 115.37, 79.41, 58.60, 52.67, 52.02, 48.15, 35.65, 31.82, 29.59, 29.24, 26.30, 22.58, 21.28, 18.66, 17.54, 14.01.

IR (KBr): cm^{-1} 3361 (NH), 2225 (CN), 1742 (CO ester), 1651 (CO amide).

Synthesis of *N*-({[3-cyano-4-(4-methylphenyl)-6-phenylpyridin-2-yl]thio}acetyl)-L-valyl-L-aspartic acid (diamino acid acid free adduct) 168b

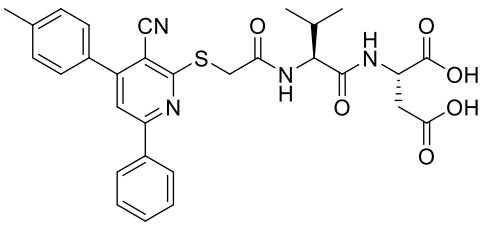

168b

To a stirred solution of **168a** (0.07 g, 0.10 mmol) in a mixture of THF/EtOH/H_2O (3:1:0.5) (4 mL), 1 N NaOH (0.44 mL) was added. The mixture was stirred at room temperature for 15 min. until the solution became yellow. The reaction was quenched with 2 N HCl and extracted with AcOEt (10 mL x 3). The organic phase was washed with water (30 mL), dried over Na_2SO_4, filtered and concentrated under reduced pressure. The crude residue was

purified through flash chromatography on silica gel, eluting with AcOEt/MeOH/AcOH (9:1:0.5) to give pure **168b**.

Yield: 0.04 g, 61%

MW = 574.65

Anal. calcd. for $C_{30}H_{30}N_4O_6S$: C 62.70, H 5.26, N 9.75, S 5.58; found: C 62.80, H 5.35, N 9.89, S 5.62.

^{1}H-NMR (400 MHz, CD_3OD): δ (ppm) 1.01 and 1.02 (2 d, *J* = 7.2 Hz, 3H, CH($\underline{CH_3}$)$_2$), 2.18-2.22 (m, 2H, $\underline{CH_2}$CO), 2.43 (s, 3H, CH_3), 3.14-3.18 (m, 1H, $\underline{CH}$(CH_3)$_2$), 3.83 (q, J_{AB} = 15.6 Hz, 2H, CH_2S), 4.39-4.44 (m, 1H, $\underline{CH}$NH), 4.63-4.67 (m, 1H, $\underline{CH}CH_2$), 7.40-7.54 (2 m, 7H Ar), 7.56 (s, 1H, H-5), 8.04 (d, *J* = 6.8 Hz, 2H Ar).

^{13}C-NMR (100 MHz, CD_3OD): δ (ppm) 173.08, 171.90, 165.58, 160.06, 156.68, 148.15, 145.94, 139.17, 137.92, 129.29, 128.42, 128.23, 127.72, 126.88, 121.38, 118.27, 98.30, 63.48, 58.54, 49.71, 36.71, 30.82, 29.25, 19.87, 18.39, 17.39.

IR (KBr): cm^{-1} 3420-3090 (OH), 3361 (NH), 2225 (CN), 1688 (CO acid), 1640 (CO amide).

Synthesis of the resin-bounded tripeptide 176

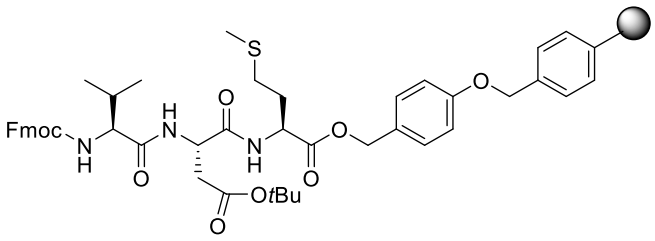

176

Compound **176** has been obtained by MW-SPPS (microwave solid phase peptide synthesis) using an Fmoc strategy on a MW automated CEM Peptide Synthesizer, with Wang resin as the solid support. In detail, the instrument was charged with Fmoc-methionine on Wang resin (0.17 g), previously swallowed in DMF through a fritted buchner funnel under N_2 flux for 2 h. The degree of functionalization was of 0.60 mmol per gram of resin. The instrument was also charged with: Fmoc-Val-OH (2 N, 0.41 g in 6 mL of DMF), Fmoc-Asp(OtBu)-OH (2 N, 0.49 g in 6 mL of DMF), the activating agents HOBt and HBTU (0.27 g and 0.76 g respectively in

4 mL of DMF); DIPEA (2 mL of 34.8% v/v DMF) as base and piperidine (100 mL of 20% v/v DMF) as deprotecting agent; CH_2Cl_2 (2 L); DMF (2 L). Then, the instrument was set and the synthetic procedure lasted for 3 h and 37 min. The coupling was performed in DMF and the peptide chain assembled under computer control of the synthesizer. The synthesis cycles were composed of Fmoc-deprotection and coupling, both under microwave irradiation. Finally, several washing cycles were performed with DMF and CH_2Cl_2. All parameters (t, p, T, Q) have been established automatically by the instrument and were different in every cycle.

Synthesis of *N*-[(9*H*-fluoren-9-ylmethoxy)carbonyl]-L-valyl-L-α-aspartyl-L-methionine (resin-free Fmoc-tripeptide) 177

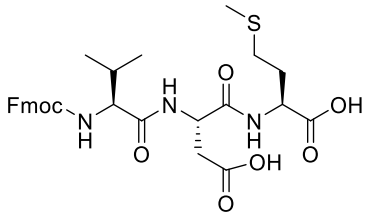

177

Resin-bounded compound **176** was charged in a gooch filter and treated with a cleavage solution of TFA/TIPS/H_2O/DTT (88:2:5:5) (20 mL) under an upward flux of N_2, to quench reactive intermediates under microwave irradiation and to prevent the oxidation of the thioether side chain of methionine. After 1 h the resin was filtered and the filtrate was recovered and evaporated under reduced pressure. The C-terminal end and the carboxylic aspartate side chain of the peptide are obtained as free carboxylic acids. The white solid obtained was washed with *n*-hexane and toluene and used directly in the next step.

MW = 585.67

Synthesis of dimethyl-*N*-[(9*H*-fluoren-9-ylmethoxy)carbonyl]-L-valyl-L-α-aspartyl-L-methioninate (methyl diester Fmoc-tripeptide) 178

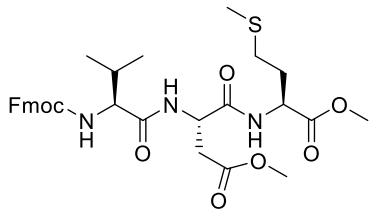

178

To a stirred solution of **177** (0.17 g, 0.29 mmol) in anhydrous MeOH (10 mL), freshly distilled $SOCl_2$ (0.22 mL) was added at 0 °C. The mixture was stirred at 0 °C for 30 min and then at room temperature for 6 h. The solvent was removed under reduced pressure and the crude residue was purified through flash chromatography on silica gel, eluting with AcOEt to give **178**.

Yield: 0.05 g, 28%

MW = 613.72

Anal. calcd. for $C_{31}H_{39}N_3O_8S$: C 60.67, H 6.41, N 6.85, S 5.22; found: C 60.42, H 6.35, N 7.09, S 5.44.

^{1}H-NMR (400 MHz, $CDCl_3$): δ (ppm) 0.95 and 0.98 (2 d, *J* = 6.8 Hz, 3H, $CH(\underline{CH_3})_2$), 1.99-2.04 (m, 1H, $\underline{CH}(CH_3)_2$), 2.16 (s, 3H, SCH_3), 2.51-2.55 (m, 2H, CH_2CO), 2.67-2.72 (m, 2H, CH_2S), 2.83-3.04 (m, 2H, $\underline{CH_2}CH_2$), 3.68 and 3.72 (2 s, 3H, OCH_3), 3.00 (m, 1H, $\underline{CH}NH$), 4.21-4.25 (m, 1H, $\underline{CH}CH_2CH_2$), 4.42-4.46 (m, 2H, CH_2O), 4.60-4.62 (m, 1H, NH), 4.80-4.84 (m, 1H, CH Fmoc), 5.38-5.42 (m, 1H, NH), 7.31 and 7.39 (2 t, *J* = 7.6 Hz, 4H Ar), 7.58 (d, *J* = 7.2 Hz 2H Ar), 7.75 (d, *J* = 7.6 Hz, 2H Ar).

^{13}C-NMR (100 MHz, DMSO-d6): δ (ppm) 172.91, 170.70, 170.31, 156.23, 143.71, 141.21, 127.62, 126.99, 125.08, 119.98, 119.79, 67.10, 65.69, 60.06, 55.11, 52.04, 51.89, 48.32, 47.06, 35.80, 31.44, 31.00, 27.91, 18.88, 17.62, 15.47.

IR (KBr): cm^{-1} 3361 (NH), 1742 (CO ester), 1651 (CO amide).

Synthesis of dimethyl-L-valyl-L-α-aspartyl-L-methioninate (free amine tripeptide) 179

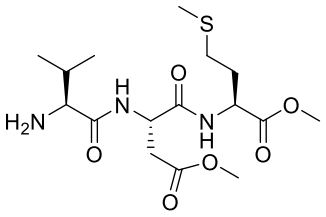

179

It was used the same deprotection protocol employed for **175**. To a stirred solution of **178** (0.05 g, 0.79 mmol) in DMF (10 mL), NaN_3 (0.01 g, 0.20 mmol) was added. The mixture was stirred at 50 °C for 4 h. The reaction was quenched with water and extracted with AcOEt (10 mL x 3). The organic phase was washed with water (30 mL), dried over Na_2SO_4, filtered and concentrated under reduced pressure. The crude residue was purified through flash chromatography on silica gel, eluting with AcOEt/MeOH (9:1).

Yield: 0.19 g, 62%

MW = 391.48

Anal. calcd. for $C_{16}H_{29}N_3O_6S$: C 49.09, H 7.47, N 10.73, S 8.19; found: C 49.24, H 7.38, N 10.89, S 8.44.

^{1}H-NMR (400 MHz, $CDCl_3$): δ (ppm) 0.96 and 0.99 (2 d, *J* = 6.8 Hz, 3H, CH($\underline{CH_3}$)$_2$), 1.95-2.00 (m, 1H, $\underline{CH}(CH_3)_2$), 2.17 (s, 3H, SCH_3), 2.50-2.54 (m, 2H, CH_2CO), 2.65-2-70 (m, 2H, $\underline{CH_2}S$), 2.82-3.03 (m, 2H, $\underline{CH_2}CH_2$), 3.05-3.11 (m, 1H, $\underline{CH}NH$), 3.69 and 3.74 (2 s, 3H, OCH_3), 4.20-4.25 (m, 1H, $\underline{CH}NH$), 4.55-4.61 (m, 1H, $\underline{CH}NH$).

IR (KBr): cm^{-1} 3401 (NH), 3361 (NHCO), 1742 (CO ester), 1651 (CO amide).

Synthesis of dimethyl-*N*-({[3-cyano-4-(4-methylphenyl)-6-phenylpyridin-2-yl]thio}acetyl) -L-valyl-L-α-aspartyl-L-methioninate (tripeptide methyl diester adduct) 169

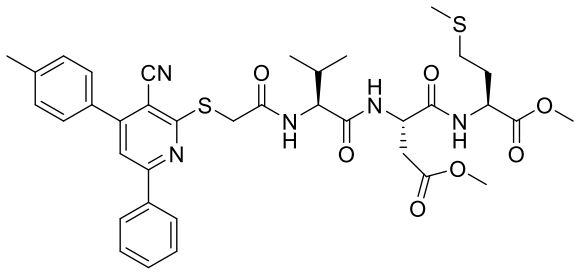

169

To a stirring solution of **179** (0.04 g, 0.10 mmol) in anhydrous DMF (5 mL) under N_2 atmosphere, a solution of **173** (0.02 g, 0.10 mmol) in the same solvent (2.50 mL) was added dropwise. Then, EDC (0.10 g, 0.10 mmol), HOBt (0.10 g, 0.10 mmol) and dry DIPEA (0.05 mL, 0.10 mmol) were added. The mixture was stirred at 0 °C for 30 min. and then at room temperature for 12 h. The reaction was quenched with water and then extracted with AcOEt (10 mL x 3). The organic phase was washed with water (30 mL), dried over Na_2SO_4, filtered and concentrated under reduced pressure. The crude residue was purified through flash chromatography on silica gel, eluting with AcOEt.

Yield: 0.03 g, 41%

MW = 733.90

Anal. calcd. for $C_{37}H_{43}N_5O_7S_2$: C 60.55, H 5.91, N 9.54, S 8.74; found: C 60.41, H 6.15, N 9.59, S 8.84.

^{1}H-NMR (400 MHz, CD_3OD): δ (ppm) 0.76 and 0.81 (2 d, *J* = 6.8 Hz, 3H, $CH(\underline{CH_3})_2$), 1.90-1.95 (m, 1H, $\underline{CH}(CH_3)_2$), 2.00 (s, 3H, SCH_3), 2.20-2.29 (m, 2H, CH_2CO), 2.44 (s, 3H, CH_3), 2.50-2.54 (m, 2H, $\underline{CH_2}CH_2$), 2.82-3.03 (m, 2H, CH_2S), 3.30 (s, 6H, 2 OCH_3), 3.70-3.76 (m, 2H, $COCH_2S$), 4.43-4.48 (m, 1H, $\underline{CH}CH_2CH_2$), 4.52-4.57 (m, 1H, $\underline{CH}CH_2CO$), 4.94-5.00 (m, 1H, $\underline{CH}CH$), 7.38 (d, *J* = 8.0 Hz, 2H Ar), 7.49-7.53 (m, 3H Ar), 7.60 (d, *J* = 8.0 Hz, 2H Ar), 7.77 (s, 1H, H-5), 8.17-8.21 (m, 2H Ar),

^{13}C-NMR (100 MHz, DMSO-d6): δ (ppm) 172.09, 171.65, 156.25, 143.70, 130.69, 129.97, 129.76, 129.04, 128.25, 127.50, 116.45, 115.37, 79.41, 58.60, 55.10, 52.00, 48.15, 35.65, 31.82, 31.09, 29.59, 29.31, 29.24, 26.30, 23.33, 22.49, 21.28, 18.66, 17.54, 15.13, 14.01.

IR (KBr): cm^{-1} 3369 (NH), 2218 (CN), 1749 (CO ester), 1647 (CO amide).

General procedure for the synthesis of monoamino acid adducts 180a-g and 181a-e

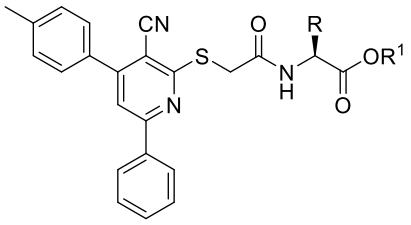

180a-g and **181a-e**

180a R = L-Leu; $R^1 = CH_3$
180b R = L-Ile; $R^1 = CH_3$
180c R = L-His; $R^1 = CH_3$
180d R = L-Arg; $R^1 = CH_3$
180e R = L-Phe; $R^1 = CH_3$
180f R = L-Tyr(OH); $R^1 = CH_3$
180g R = L-Glu(OCH_3); $R^1 = CH_3$

181a R = L-Val; $R^1 = CH_2C_6H_4$
181b R = L-Val; $R^1 = CH_3$
181c R = D-Val; $R^1 = CH_2C_6H_4$
181d R = L-Leu; $R^1 = CH_2C_6H_4$
181e R = L-Ile; $R^1 = CH_2C_6H_4$

It was used the same amidation protocol employed for the synthesis of **167a**. To a stirred solution of **173** (0.10 g, 0.28 mmol) in anhydrous DMF (1 mL) at 0 °C under N_2 atmosphere, a solution of the appropriate L or D-amino acid methyl ester (hydrochloride salt) or benzyl ester (*p*-toluenesulfonate salt) (0.30 mmol) in anhydrous DMF (1 mL) was added dropwise, under N_2 atmosphere. Then, EDC (0.05 g, 0.28 mmol), HOBt (0.04 g, 0.28 mmol) and dry DIPEA (0.06 mL, 0.40 mmol) were added. The mixture was stirred at 0 °C for 30 min. and then at room temperature for 5 h. The reaction was quenched with water and then extracted with AcOEt (20 mL x 3). The organic phase was washed with water (60 mL), dried over Na_2SO_4, filtered and concentrated under reduced pressure. The crude residue was purified through flash chromatography on silica gel, using as eluent *n*-hexane/AcOEt (7:3) (**180a, 180b, 180e**), (6:4) (**180f**), (1:1) (**180g**), AcOEt/MeOH (9:1) (**180c**), CH_2Cl_2/MeOH (9:1) (**180d**) CH_2Cl_2 (**181a-e**), to obtain the final products as white solids.

Methyl N-({[3-cyano-4-(4-methylphenyl)-6-phenylpyridin-2-yl]thio}acetyl)-L-leucinate (L-leucine methyl ester adduct) 180a

Yield: 0.04 g, 31%

Mp: 150-151 °C

MW = 487.61

Anal. calcd. for $C_{28}H_{29}N_3O_3S$: C 68.97, H 5.99, N 8.62, S 6.58; found: C 69.01, H 5.87, N 8.50, S 6.53.

^{1}H-NMR (400 MHz, $CDCl_3$): δ (ppm) 0.27 and 0.31 (2 d, *J* = 6.4 Hz, 3H, CH($\underline{CH_3}$)$_2$), 1.21-1.32 (m, 1H, $\underline{CH}(CH_3)_2$), 1.38-1.43 (m, 2H, CH$\underline{CH_2}$), 2.44 (s, 3H, CH_3), 3.54 (s, 3H, OCH_3),

4.05 (q, J_{AB} = 15.6 Hz, 2H, CH_2S), 4.52-4.58 (m, 1H, CHNH), 7.13 (d, *J* = 8.0 Hz, 1H, NH), 7.34 (d, *J* = 7.6 Hz, 2H Ar), 7.49-7.55 (m, 5H Ar), 7.60 (s, 1H, H-5), 8.06 (d, *J* = 7.6 Hz, 2H Ar).

^{13}C-NMR (100 MHz, $CDCl_3$): δ (ppm) 172.73, 167.71, 161.64, 158.87, 154.90, 140.6, 136.65, 132.82, 130.81, 129.78, 129.07, 128.20, 127.37, 116.43, 103.77, 52.02, 50.81, 41.12, 33.85, 24.53 22.50, 21.50, 21.31.

IR (KBr): cm^{-1} 3362 (NH), 2222 (CN), 1745 (CO ester), 1650 (CO amide).

Methyl N-({[3-cyano-4-(4-methylphenyl)-6-phenylpyridin-2-yl]thio}acetyl)-L-isoleucinate (L-isoleucine methyl ester adduct) 180b

Yield: 0.04 g, 31%

Mp: 163-165 °C

MW = 487.61

Anal. calcd. for $C_{28}H_{29}N_3O_3S$: C 68.97, H 5.99, N 8.62, S 6.58; found: C 68.75, H 5.97, N 8.72, S 6.43.

^{1}H-NMR (400 MHz, $CDCl_3$): δ (ppm) 0.65-0.66 (m, 6H, CH_3CH_2 + CH_3CH), 1.13-1.14 (m, 1H, CH_3CH), 1.63-1.71 (m, 2H, CH_3CH_2), 2.43 (s, 3H, CH_3), 3.52 (s, 3H, OCH_3), 4.06 (q, J_{AB} = 15.6 Hz, 2H, CH_2S), 4.48-4.51 (m, 1H, CHNH), 7.18 (d, *J* = 8.4 Hz, 1H, NH), 7.34 (d, *J* = 7.6 Hz, 2H Ar), 7.48-7.55 (m, 5H Ar), 7.60 (s, 1H, H-5), 8.01-8.06 (m, 2H Ar).

^{13}C-NMR (100 MHz, $CDCl_3$): δ (ppm) 171.66, 167.78, 161.64, 158.96, 154.89, 140.66, 136.73, 132.82, 130.78, 129.76, 129.04, 128.22, 127.40, 116.50, 115.37, 103.37, 56.68, 51.79, 37.51, 33.88, 24.83, 21.30, 15.07, 11.23.

IR (KBr): cm^{-1} 3369 (NH), 2215 (CN), 1732 (CO ester), 1657 (CO amide).

Methyl N-({[3-cyano-4-(4-methylphenyl)-6-phenylpyridin-2-yl]thio}acetyl)-L-histidinate (L-Histidine methyl ester adduct) 180c

Yield: 0.04 g, 30%

Mp: 135-141 °C

MW = 511.59

Anal. calcd. for $C_{28}H_{25}N_5O_3S$: C 65.74, H 4.93, N 13.69, S 6.27; found: C 65.41, H 4.70, N 14.07, S 6.44.

^{1}H-NMR (400 MHz, $CDCl_3$): δ (ppm) 1.13-1.17 (m, 1H, $\underline{CH}CH_2$), 2.44 (s, 3H, CH_3), 2.89 and 3.02 (2 q, *J* = 15.0 Hz, 2H, $\underline{CH_2}CH$), 3.54 (s, 3H, OCH_3), 4.11 (s, 2H, CH_2S), 4.78-4.82 (m, 1H, $\underline{CH}NH$), 6.62 (s, 1H, $N\underline{CH}NH$), 7.34 (d, *J* = 8.0 Hz, 2H Ar), 7.39 (s, 1H, NH), 7.50-7.54 (m, 5H Ar), 7.57 (s, 1H, H-5), 7.94 (d, *J* = 7.2 Hz, 1H, CHN), 8.06-8.08 (m, 2H Ar).
^{13}C-NMR (100 MHz, $CDCl_3$): δ (ppm) 171.42, 167.99, 161.54, 158.70, 154.80, 140.08, 140.04, 136.77, 133.10, 132.96, 130.74, 129.76, 129.02, 128.21, 127.42, 116.33, 115.62, 99.42, 90.97, 52.32, 52.21, 45.20, 29.04, 21.28.
IR (KBr): cm^{-1} 3361 (NH), 2221 (CN), 1741 (CO ester), 1654 (CO amide).

Methyl N^2-({[3-cyano-4-(4-methylphenyl)-6-phenylpyridin-2-yl]thio}acetyl)-L-argininate (L-arginine methyl ester adduct) 180d

Yield: 0.04 g, 27%
Mp: 161-171 °C
MW = 530.64
Anal. calcd. for $C_{28}H_{30}N_6O_3S$: C 63.38, H 5.70, N 15.84, S 6.04; found: C 63.44, H 5.44, N 15.75, S 6.42.
^{1}H-NMR (400 MHz, CD_3OD): δ (ppm) 1.43-1.47 (m, 2H, $CH_2\underline{CH_2}CH_2$), 1.59-1.66 and 1.77-1.86 (2 m, 2H, $\underline{CH_2}CH$), 2.43 (s, 3H, CH_3), 2.98-3.06 (m, 2H, $\underline{CH_2}NH$), 3.59 (s, 3H, OCH_3), 4.22 (q, J_{AB} = 16.0 Hz, 2H, CH_2S), 4.44-4.47 (m, 1H, $\underline{CH}NH$), 7.37 (d, *J* = 8.0 Hz, 2H Ar), 7.50-7.51 (m, 3H Ar), 7.57 (d, *J* = 8.0 Hz, 2H Ar), 7.74 (s, 1H, H-5), 8.18-8.20 (m, 2H Ar).
^{13}C-NMR (100 MHz, CD_3OD): δ (ppm) 171.90, 169.20, 161.91, 158.74, 154.86, 140.40, 136.90, 133.01, 132.02, 130.40, 129.30, 129.25, 128.71, 128.17, 127.49, 126.60, 115.13, 48.16, 47.94, 47.09, 46.87, 40.29, 29.01, 24.59.
IR (KBr): cm^{-1} 3364 (NH), 2225 (CN), 1744 (CO ester), 1653 (CO amide).

Methyl N-({[3-cyano-4-(4-methylphenyl)-6-phenylpyridin-2-yl]thio}acetyl)-L-phenylalaninate (L-phenylalanine methyl ester adduct) 180e

Yield: 0.05 g, 34%
Mp: 167-173 °C
MW = 521.63
Anal. calcd. for $C_{31}H_{27}N_3O_3S$: C 71.38, H 5.22, N 8.06, S 6.15; found: C 71.21, H 5.30, N 8.11, S 5.78.

^{1}H-NMR (400 MHz, DMSO-d6): δ (ppm) 2.40 (s, 3H, CH_3), 2.85 and 2.99 (2 q, *J* = 14.0 Hz, 2H, $\underline{CH_2}CH$), 3.49 (s, 3H, OCH_3), 4.14 (s, 2H, CH_2S), 4.46-4.49 (m, 1H, $\underline{CH}CH_2$), 7.08-7.15 (m, 5H Ar Phe), 7.39 (d, *J* = 7.6 Hz, 2H Ar), 7.50-7.51 (m, 3H Ar), 7.64 (d, *J* = 7.6 Hz, 2H Ar), 7.87 (s, 1H, H-5), 8.25 (m, 2H Ar) 8.65 (d, *J* = 7.6 Hz, 1H, NH).

^{13}C-NMR (100 MHz, DMSO-d6): δ (ppm) 171.37, 167.67, 161.43, 158.77, 154.73, 140.71, 136.60, 135.43, 132.88, 130.80, 129.84, 129.06, 128.71, 128.52, 128.21, 127.35, 126.80, 116.37, 115.32, 103.54, 53.15, 52.12, 37.52, 33.38, 24.04.

IR (KBr): cm^{-1} 3300 (NH), 2217 (CN), 1742 (CO ester), 1655 (CO amide).

Methyl N-({[3-cyano-4-(4-methylphenyl)-6-phenylpyridin-2-yl]thio}acetyl)-L-tyrosinate (L-tyrosine methyl ester adduct) 180f

Yield: 0.03 g, 21%

Mp: 215-217 °C

MW = 537.63

Anal. calcd. for $C_{31}H_{27}N_3O_4S$: C 69.25, H 5.06, N 7.82, S 5.96; found: C 69.61, H 5.32, N 7.99, S 5.83.

^{1}H-NMR (400 MHz, $CDCl_3$): δ (ppm) 2.45 (s, 3H, CH_3), 2.75 and 2.94 (2 q, *J* = 14.0 Hz, 2H, $\underline{CH_2}CH$), 3.57 (s, 3H, OCH_3), 4.00 (q, J_{AB} = 15.6 Hz, 2H, CH_2S), 4.75-4.80 (m, 1H, $\underline{CH}CH_2$), 5.12 (br s, 1H, OH), 6.45 and 6.68 (2 d, *J* = 8.2 Hz, 2H Ar Tyr), 7.10 (d, *J* = 8.0 Hz, 1H, NH), 7.25 (s, 1H, H-5), 7.36 (d, *J* = 7.6 Hz, 2H Ar), 7.49-7.50 (m, 3H Ar), 7.58 (d, *J* = 8.0 Hz, 2H Ar), 8.02-8.04 (m, 2H Ar).

^{13}C-NMR (100 MHz, $CDCl_3$): δ (ppm) 171.47, 167.80, 161.42, 158.90, 154.81, 144.96, 140.69, 136.59, 132.84, 130.94, 129.79, 129.12, 129.02, 128.39, 127.57, 127.15, 116.56, 116.10, 115.40, 103.46, 53.17, 49.84, 36.58, 31.31, 21.29.

IR (KBr): cm^{-1} 3400-3200 (OH), 3306 (NH), 2218 (CN), 1730 (CO ester), 1656 (CO amide).

Dimethyl N-({[3-cyano-4-(4-methylphenyl)-6-phenylpyridin-2-yl]thio}acetyl)-L-glutamate (L-glutammate methyl diester adduct) 180g

Yield: 0.04 g, 27%

Mp: 179-193 °C

MW = 517.60

Anal. calcd. for $C_{28}H_{27}N_3O_5S$: C 64.97, H 5.26, N 8.12, S 6.19; found: C 65.01, H 5.43, N 8.49, S 6.06.

^{1}H-NMR (400 MHz, $CDCl_3$): δ (ppm) δ 1.76-1.80 and 2.03-2.15 (2 m, 4H, CH_2CH_2), 2.44 (s, 3H, CH_3), 3.54 and 3.55 (2 s, 3H, OCH_3), 4.06 (q, J_{AB} = 15.8 Hz, 2H, CH_2S), 4.57-4.58 (m, 1H, CHCH$_2$), 7.25 (s, 1H, NH), 7.35 (d, *J* = 7.6 Hz, 2H Ar), 7.49-7.51 (m, 3H Ar), 7.54 (d, *J* = 7.6 Hz, 2H Ar), 7.61 (s, 1H, H-5), 8.05-8.07 (m, 2H Ar).

^{13}C-NMR (100 MHz, $CDCl_3$): δ (ppm) 171.30, 168.01, 162.70, 161.80, 158.97, 155.00, 140.66, 136.66, 132.85, 130.80, 129.78, 129.11, 128.29, 127.47, 116.61, 115.37, 103.86, 59.91, 59.12, 53.05, 52.20, 41.80, 37.02, 20.50.

IR (KBr): cm^{-1} 3312 (NH), 2215 (CN), 1732 (CO ester), 1653 (CO amide).

Benzyl N-({[3-cyano-4-(4-methylphenyl)-6-phenylpyridin-2-yl]thio}acetyl)-L-valinate (L-valine benzyl ester adduct) 181a

Yield: 0.12 g, 80%

MW = 549.68

Anal. calcd. for $C_{33}H_{31}N_3O_3S$: C 72.11, H 5.68, N 7.64, S 5.83; found: C 72.01, H 5.59, N 7.84, S 5.94.

^{1}H-NMR (400 MHz, $CDCl_3$): δ (ppm) 0.33 and 0.68 (2 d, *J* = 6.8 Hz, 3H, CH(CH$_3$)$_2$), 1.97-2.02 (m, 1H, CH(CH$_3$)$_2$), 2.44 (s, 3H, CH_3), 4.53-4.56 (m, 1H, CHNH), 4.99 (q, J_{AB} = 16.0 Hz, 2H, CH_2S), 5.01 (q, J_{AB} = 12.0 Hz, 2H, CH_2O), 7.21 (d, *J* = 8.0 Hz, 1H, NH) 7.26-7.30 (m, 3H Ar), 7.35 (d, *J* = 8.0 Hz, 2H Ar), 7.49-7.56 (m, 5H Ar), 7.58 (s, 1H, H-5), 8.04-8.06 (m, 2H Ar).

^{13}C-NMR (100 MHz, $CDCl_3$): δ (ppm) 173.25, 171.29, 162.54, 158.27, 154.45, 140.21, 137.00, 136.02, 133.23, 131.32, 129.76, 129.31, 128.88, 128.19, 128.07, 127.43, 116.45, 116.27, 102.78, 66.41, 57.38, 31.10, 30.40, 23.45, 21.30, 18.99.

IR (KBr): cm^{-1} 3290 (NH), 2218 (CN), 1736 (CO ester), 1650 (CO amide).

Methyl N-({[3-cyano-4-(4-methylphenyl)-6-phenylpyridin-2-yl]thio}acetyl)-D-valinate (D-valine methyl ester adduct) 181b

Yield: 0.07 g, 55%

Mp: 159-161 °C

MW = 473.59

Anal. calcd. for $C_{27}H_{27}N_3O_3S$: C 68.48, H 5.75, N 8.87, S 6.77; found: C 68.30, H 5.97, N 8.51, S 6.40.

^{1}H-NMR (400 MHz, $CDCl_3$): δ (ppm) 0.62 and 0.70 (2 d, J = 6.8 Hz, 3H, CH($\underline{CH_3}$)$_2$), 1.94-2.02 (m, 1H, $\underline{CH}(CH_3)_2$), 2.45 (s, 3H, CH_3), 3.53 (s, 3H, OCH_3), 4.09 (q, J_{AB} = 16.0 Hz, 2H, CH_2S), 4.46-4.50 (m, 1H, $\underline{CH}$NH), 7.17 (d, J = 8.4 Hz, 1H, NH), 7.35 (d, J = 7.6 Hz, 2H Ar), 7.50-7.57 (m, 5H Ar), 7.61 (s, 1H, H-5), 8.05-8.07 (m, 2H Ar).

^{13}C-NMR (100 MHz, $CDCl_3$): δ (ppm) 167.93, 161.65, 158.99, 154.91, 140.66, 136.74, 132.84, 130.76, 129.77, 129.04, 128.23, 127.42, 116.54, 115.37, 103.81, 57.36, 51.86, 33.93, 30.91, 21.32, 18.63, 17.45.

IR (KBr): cm^{-1} 3287 (NH), 2215 (CN), 1740 (CO ester), 1659 (CO amide).

Benzyl N-({[3-cyano-4-(4-methylphenyl)-6-phenylpyridin-2-yl]thio}acetyl)-D-valinate (D-valine benzyl ester adduct) 181c

Yield: 0.09 g, 61%

Mp: 133-135 °C

MW = 549.68

Anal. calcd. for $C_{33}H_{31}N_3O_3S$: C 72.11, H 5.68, N 7.64, S 5.83; found: C 72.11, H 5.50, N 7.78, S 5.90.

^{1}H-NMR (400 MHz, $CDCl_3$): δ (ppm) 0.59 and 0.68 (2 d, J = 6.8 Hz, 3H, CH($\underline{CH_3}$)$_2$), 1.97-2.02 (m, 1H, $\underline{CH}(CH_3)_2$), 2.45 (s, 3H, CH_3), 4.08 (q, J_{AB} = 16.0 Hz, 2H, CH_2S), 4.52-4.55 (m, 1H, $\underline{CH}$NH), 4.98 (q, J_{AB} = 12.0 Hz, 2H, CH_2O), 7.21 (d, J = 8.0 Hz, 1H, NH) 7.26-7.30 (m, 3H Ar), 7.35 (d, J = 8.0 Hz, 2H Ar), 7.48-7.55 (m, 5H Ar), 7.58 (s, 1H, H-5), 8.04-8.05 (m, 2H Ar).

^{13}C-NMR (100 MHz, $CDCl_3$): δ (ppm) 171.07, 167.92, 161.62, 158.99, 154.88, 140.65, 136.77, 135.50, 132.84, 130.73, 129.76, 129.04, 128.44, 128.25, 128.06, 127.42, 116.56, 115.37, 103.79, 66.71, 57.36, 33.96, 30.95, 21.32, 18.65, 17.34.

IR (KBr): cm^{-1} 3288 (NH), 2217 (CN), 1735 (CO ester), 1652 (CO amide).

Benzyl N-({[3-cyano-4-(4-methylphenyl)-6-phenylpyridin-2-yl]thio}acetyl)-L-leucinate (L-leucine benzyl ester adduct) 181d

Yield: 0.08 g, 50%

Mp: 151-153 °C

MW = 563.71

Anal. calcd. for $C_{34}H_{33}N_3O_3S$: C 72.44, H 5.90, N 7.45, S 5.69; found: C 72.46, H 6.22, N 7.66, S 6.03.

^{1}H-NMR (400 MHz, $CDCl_3$): δ (ppm) 0.64 and 0.67 (2 d, J = 6.0 Hz, 3H, CH($\underline{CH_3}$)$_2$), 1.23-1.28 (m, 1H, $\underline{CH}(CH_3)_2$), 1.39-1.44 (m, 2H, $CH\underline{CH_2}$), 2.46 (s, 3H, CH_3), 4.05 (q, J_{AB} = 15.6 Hz, 2H, CH_2S), 4.60-4.64 (m, 1H, $\underline{CH}NH$), 5.00 (s, 2H, CH_2O), 7.19-7.37 (m, 8H, 7H Ar + NH), 7.49-7.55 (m, 5H Ar), 7.59 (s, 1H, H-5), 8.06 (m, 2H Ar).

^{13}C-NMR (100 MHz, $CDCl_3$): δ (ppm) 172.13, 167.79, 161.68, 158.91, 154.90, 140.68, 136.68, 132.84, 130.92, 129.90, 129.68, 129.20, 128.98, 128.59, 128.32, 128.10, 127.80, 127.41, 116.54, 116.44, 115.38, 103.80, 66.76, 50.97, 24.54, 22.58, 21.34.

IR (KBr): cm^{-1} 3362 (NH), 2222 (CN), 1745 (CO ester), 1650 (CO amide).

Benzyl N-({[3-cyano-4-(4-methylphenyl)-6-phenylpyridin-2-yl]thio}acetyl)-L-isoleucinate (L-isoleucine benzyl ester adduct) 181e

Yield: 0.05 g, 34%

Mp: 122-126 °C

MW = 563.71

Anal. calcd. for $C_{34}H_{33}N_3O_3S$: C 72.44, H 5.90, N 7.45, S 5.69; found: C 72.48, H 5.94, N 7.78, S 5.58.

^{1}H-NMR (400 MHz, $CDCl_3$): δ (ppm) 0.65-0.69 (m, 6H, $\underline{CH_3}CH_2$ + $\underline{CH_3}CH$), 0.73-0.85 (m, 1H, $CH_3\underline{CH}$), 1.08-1.14 (m, 2H, $CH_3\underline{CH_2}$), 2.45 (s, 3H, CH_3), 4.07 (q, J_{AB} = 15.6 Hz, 2H, CH_2S), 4.55-4.58 (m, 1H, $\underline{CH}NH$), 4.99 (q, J = 12.4 Hz, 2H, CH_2O), 7.21-7.31 (m, 6H, 5H Ar + NH), 7.36 (d, J = 8.0 Hz, 2H Ar), 7.49-7.55 (m, 5H Ar), 7.59 (s, 1H, H-5), 8.04-8.05 (m, 2H Ar).

^{13}C-NMR (100 MHz, $CDCl_3$): δ (ppm) 171.07, 167.85, 161.67, 158.99, 154.89, 140.66, 136.76, 135.24, 132.85, 130.76, 129.76, 129.06, 128.44, 128.26, 128.07, 127.43, 116.55, 115.37, 103.37, 66.68, 56.76, 37.58, 33.94, 24.75, 21.31, 15.11, 11.25.

IR (KBr): cm^{-1} 3369 (NH), 2215 (CN), 1732 (CO ester), 1657 (CO amide).

General procedure for the synthesis of compounds 184a-c

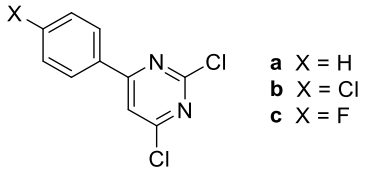

184a-c

To a solution of 2,4,6-trichloropyrimidine (1.00 g, 5.45 mmol) in THF (9 mL), the opportune phenylboronic acid (4.52 mmol), $Pd(OAc)_2$ (24.47 mg, 0.11 mmol), PPh_3 (57.70 mg, 0.22 mmol) and 1 M Na_2CO_3 (9 mL) were added. The resulting mixture was stirred at reflux under nitrogen atmosphere for 3 h. Then, the solvent was removed under vacuum and the reaction extracted with CH_2Cl_2 (3 x 30 mL). The organic phase was washed with water (90 mL), dried over Na_2SO_4, filtered and concentrated under reduced pressure. The crude product was purified by column chromatography using PE (bp 40-60 °C)/AcOEt (95:5) as eluent, to afford the pure products as white solids.

2,4-Dichloro-6-phenylpyrimidine 184a

Yield: 0.92 g, 90%

Mp: 73-74 °C

MW = 225.07

Anal. calcd. for $C_{10}H_6Cl_2N_2$: C 53.36, H 2.69, N 12.45; found C 53.65, H 2.58, N 12.37.

^{1}H-NMR (200 MHz, $CDCl_3$): δ (ppm) 7.55-7.61 (m, 3H Ar), 7.71 (s, 1H pyr), 8.07-8.13 (m, 2H Ar).

2,4-Dichloro-6-(4-chlorophenyl)pyrimidine 184b

Yield: 0.97 g, 83%

Mp: 128-132 °C

MW = 259.52

Anal. calcd. for $C_{10}H_5Cl_3N_2$: C 46.28, H 1.94, N 10.79; found C 46.47, H 2.14, N 10.51.

^{1}H-NMR (200 MHz, $CDCl_3$): δ (ppm) 7.53 (d, *J* = 8.0 Hz, 2H Ar), 7.68 (s, 1H pyr), 8.06 (d, *J* = 8.0 Hz, 2H Ar).

2,4-Dichloro-6-(4-fluorophenyl)pyrimidine 184c

Yield: 35%

Mp: 134-135 °C

MW = 243.06

Anal. calcd. for $C_{10}H_5Cl_2FN_2$: C 49.41, H 2.07, N 11.53; found C 49.59, H 1.96, N 11.13.

^{1}H-NMR (200 MHz, $CDCl_3$): δ (ppm) 7.20-7.29 (m, 2H Ar), 7.67 (s, 1H pyr), 8.10-8.17 (m, 2H Ar).

General procedure for the synthesis of compounds 185a-c

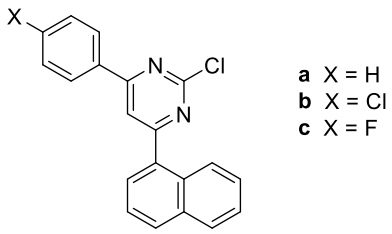

185a-c

To a solution of the opportune intermediate **184a-c** (2.00 mmol) in DME (10 mL), naphthalene boronic acid (0.38 g, 2.20 mmol), $Pd(OAc)_2$ (22.45 mg, 0.10 mmol), PPh_3 (52.36 mg, 0.20 mmol) and Na_2CO_3 (0.66 g, 6.20 mmol) dissolved in the minimum amount of water, were added. The resulting mixture was stirred at reflux under nitrogen atmosphere for 3 h. Then, solvent was removed under vacuum and the reaction extracted with CH_2Cl_2 (3 x 30 mL). The organic phase was washed with water (90 mL), dried over Na_2SO_4, filtered and concentrated under reduced pressure. The crude product was purified by column chromatography using PE (bp 40-60 °C)/Et_2O (8:2) (**185a**), CH_2Cl_2 (**185b**), *n*-hexane/AcOEt (9:1) (**185c**) as eluent, to afford the pure products as white solids.

2-Chloro-4-(1-naphthyl)-6-phenylpyrimidine 185a

Yield: 0.27 g, 43%

Mp: 99-101 °C

MW = 316.78

Anal. calcd. for $C_{20}H_{13}ClN_2$: C 75.83, H 4.14, N 8.84; found C 75.93, H 4.21, N 8.69.

^{1}H-NMR (200 MHz, $CDCl_3$): δ (ppm) 7.58-7.65 (m, 6H, 3H Ar + 3H naph), 7.75 (s, 1H pyr), 7.96-7.98 and 8.00-8.20 (2 m, 6H, 4H naph + 2H Ar).

2-Chloro-4-(4-chlorophenyl)-6-(1-naphthyl)pyrimidine 185b

Yield: 0.25 g, 36%

Mp: 122-123 °C

MW = 351.23

Anal. calcd. for $C_{20}H_{12}Cl_2N_2$: C 68.39, H 3.44, N 7.98; found C 68.30, H 3.31, N 8.33.

^{1}H-NMR (200 MHz, $CDCl_3$): δ (ppm) 7.52-7.63 (m, 5H, 2H Ar + 3H naph), 7.94 (s, 1H pyr), 7.96-8.17 (m, 6H, 4H naph + 2H Ar).

2-Chloro-4-(4-fluorophenyl)-6-(1-naphthyl)pyrimidine 185c

Yield: 0.49 g, 73%

Mp: 123-124 °C

MW = 334.77

Anal. calcd. for $C_{20}H_{12}ClFN_2$: C 71.75, H 3.61, N 8.37; found C 71.63, H 3.46, N 8.30.

^{1}H-NMR (200 MHz, $CDCl_3$) : δ (ppm) 7.21-7.25, 7.58-7.66 and 7.75-7.79 (3 m, 7H, 2H Ar + 5H naph) 7.92 (s, 1H pyr), 7.93-8.06 and 8.18-8.25 (2 m, 4H, 2H Ar + 2H naph).

Synthesis of 2-chloro-4-phenyl-6-(phenylthio)pyrimidine 185d

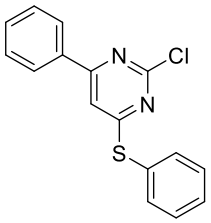

185d

To a solution of NaOH (0.43 g, 1.07 mmol) in water (7 mL) and acetone (7 mL), thiophenol (0.14 mL, 1.33 mmol) was added; the mixture was stirred at room temperature for 1 h. Then, **184a** (0.30 g, 1.33 mmol) was added. The mixture was stirred at room temperature and after 2 h NaOH pellets (0.43 g, 1.07 mmol) was added. The reaction was stirred at room temperature

for an additional 1 h. Then, acetone was removed under vacuum and the reaction extracted with AcOEt (3 x 20 mL). The organic phase was washed with water (60 mL), dried over Na_2SO_4, filtered and concentrated under reduced pressure. The crude was purified by column chromatography using PE (bp 40-60 °C)/CH_2Cl_2 (6:4) as eluent, obtaining **185d** as a white solid.

Yield: 0.28 g, 71%
Mp: 87-88 °C
MW = 298.79
Anal. calcd. for $C_{16}H_{11}ClN_2S$: C 64.32, H 3.71, N 9.38, S 10.73; found C 64.44, H 3.80, N 9.68, S 10.53.
^{1}H-NMR (200 MHz, $CDCl_3$): δ (ppm) 7.01 (s, 1H pyr), 7.44-7.71 and 7.82-7.86 (2 m, 10H Ar).

General procedure for the synthesis of compounds 185e,f

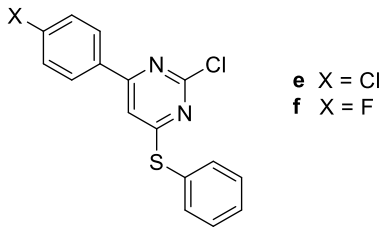

185e,f

To a suspension of NaH (60% dispersion in mineral oil, 0.16 g, 4.00 mmol) in anhydrous DMF (9 mL) at 0 °C, thiophenol (0.10 mL, 1.00 mmol) was added. The mixture was stirred at 0 °C under nitrogen atmosphere for 1 h, then a solution of the opportune derivative **184b**,**c** (1.00 mmol) in anhydrous DMF (2 mL) was added. The reaction was stirred at room temperature under nitrogen atmosphere for 3 h. Then, water was added dropwise, cooling in ice bath, and the reaction extracted with CH_2Cl_2 (3 x 30 mL). The organic phase was washed with water (90 mL), dried over Na_2SO_4, filtered and concentrated under reduced pressure. The crude product was purified by column chromatography using *n*-hexane/AcOEt (95:5) to afford the pure products as white solids.

2-Chloro-4-(4-chlorophenyl)-6-(phenylthio)pyrimidine 185e

Yield: 0.16 g, 47%

Mp: 101-105 °C

MW = 333.24

Anal. calcd. for $C_{16}H_{10}Cl_2N_2S$: C 57.67, H 3.02, N 8.41, S 9.62; found C 57.55, H 3.31, N 8.76, S 9.92.

^{1}H-NMR (200 MHz, $CDCl_3$): δ (ppm) 6.86 (s, 1H pyr), 7.33-7.48 and 7.57-7.69 (2 m, 9H Ar).

2-Chloro-4-(4-fluorophenyl-6-(phenylthio)pyrimidine 185f

Yield: 0.22 g, 71%

Mp: 98-99 °C

MW = 316.78

Anal. calcd. for $C_{16}H_{10}ClFN_2S$: C 60.66, H 3.18, N 8.84, S 10.12; found C 60.52, H 3.30, N 8.51, S 10.50.

^{1}H-NMR (200 MHz, $CDCl_3$): δ (ppm) 6.85 (s, 1H pyr), 7.41-7.43, 7.57-7.62 and 7.65-7.75 (3 m, 9H Ar).

General procedure for the synthesis of compounds 185g-i

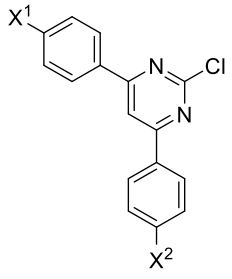

185g-i

g X^1 = H; X^2 = Cl
h X^1 = H; X^2 = Cl
i X^1 = Cl; X^2 = F

It was used the same procedure employed to obtain intermediate **185a-c**. To a solution of intermediates **184a,b** (1.00 g, 5.45 mmol) in THF (9 mL), the opportune phenylboronic acid (5.45 mmol), $Pd(OAc)_2$ (24.47 mg, 0.11 mmol), PPh_3 (42.88 mg, 0.16 mmol) and 1 M Na_2CO_3 (9 mL) were added. The resulting mixture was stirred at reflux under nitrogen atmosphere for 3 h. Then, the solvent was removed under vacuum and the reaction extracted with CH_2Cl_2 (3

x 30 mL). The organic phase was washed with water (90 mL), dried over Na_2SO_4, filtered and concentrated under reduced pressure. The crude product was purified by column chromatography using PE (bp 40-60 °C)/AcOEt (95:5) (**185g**), *n*-hexane/AcOEt (95:5) (**185h**) or (98:2) (**185i**) as eluent, to afford the pure products as white solids.

2-Chloro-4-(4-chlorophenyl)-6-phenylpyrimidine 185g

Yield: 0.74 g, 45%

Mp: 137-140 °C

MW = 301.17

Anal. calcd. for $C_{16}H_{10}Cl_2N_2$: C 63.81, H 3.35, N 9.30; found C 63.65, H 3.37, N 9.31.

^{1}H-NMR (200 MHz, $CDCl_3$): δ (ppm) 7.57-7.60 (m, 5H Ar), 8.02 (s, 1H pyr), 8.15-8.19 (m, 4H Ar).

2-Chloro-4-(4-fluorophenyl)-6-phenylpyrimidine 185h

Yield: 0.98 g, 63%

Mp: 121-124 °C

MW = 284.72

Anal. calcd. for $C_{16}H_{10}ClFN_2$: C 67.50, H 3.54, N 9.84; found C 67.44, H 3.84, N 9.89.

^{1}H-NMR (200 MHz, $CDCl_3$): δ (ppm) 7.24-7.30 and 7.56-7.60 (2 m, 5H Ar), 8.00 (s, 1H pyr), 8.15-8.21 (m, 4H Ar).

2-Chloro-4-(4-chlorophenyl)-6-(4-fluorophenyl)pyrimidine 185i

Yield: 0.42 g, 24%

Mp: 147-149 °C

MW = 319.16

Anal. calcd. for $C_{16}H_9Cl_2FN_2$: C 60.21, H 2.84, N 8.78; found C 60.09, H 2.78, N 8.98.

^{1}H-NMR (200 MHz, $CDCl_3$): δ (ppm) 7.26-7.30 and 7.52-7.57 (2 m, 4H Ar), 7.97 (s, 1H pyr), 8.11-8.21 (m, 4H Ar).

General procedure for the synthesis of compounds 186a,b

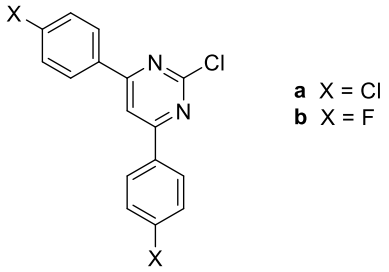

186a,b

To a solution of 2,4,6-trichloropyrimidine (1.00 g, 5.45 mmol) in THF (9 mL), an excess of the opportune phenylboronic acid (10.90 mmol), $Pd(OAc)_2$ (24.47 mg, 0.11 mmol,), PPh_3 (42.88 mg, 0.16 mmol) and 1 M Na_2CO_3 (9 mL) were added. The resulting mixture was stirred at reflux under nitrogen atmosphere for 3 h. Then, solvent was removed under vacuum and the reaction extracted with CH_2Cl_2 (3 x 40 mL). The organic phase was washed with water (100 mL), dried over Na_2SO_4, filtered and concentrated under reduced pressure. The crude was purified by column chromatography using PE (bp 40-60 °C)/CH_2Cl_2 (6:4) (**186a**) or (1:1) (**186b**) as eluent, obtaining the final products as white solids.

2-Chloro-4,6-bis(4-chlorophenyl)pyrimidine 186a

Yield: 1.12 g, 61%

Mp: 133-138 °C

MW = 335.62

Anal. calcd. for $C_{16}H_9Cl_3N_2$: C 57.26, H 2.70, N 8.35; found C 57.19, H 2.64, N 8.20.

^{1}H-NMR (200 MHz, $CDCl_3$): δ (ppm) 7.52-7.56 (m, 4H Ar), 7.99 (s, 1H pyr), 8.04-8.15 (m, 4H Ar).

2-Chloro-4,6-bis(4-fluorophenyl)pyrimidine 186b

Yield: 0.78 g, 47%

Mp: 153-154 °C

MW = 302.71

Anal. calcd. for $C_{16}H_9ClF_2N_2$: C 63.48, H 3.00, N 9.25; found C 63.47, H 3.28, N 9.44.

^{1}H-NMR (200 MHz, $CDCl_3$): δ (ppm) 7.21-7.28 (m, 4H Ar), 7.95 (s, 1H, pyr), 8.15-8.22 (m, 4H Ar).

Synthesis of 2-chloro-6-phenylpyrimidine-4-carboxylic acid 187

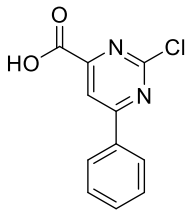

187

To a solution of 2,6-dichloropyrimidine-4-carboxylic acid (0.50 g, 2.59 mmol) in THF (5 mL), phenylboronic acid (0.26 g, 2.15 mmol), $Pd(OAc)_2$ (11.63 mg, 0.05 mmol), PPh_3 (20.38 mg, 0.08 mmol) and 1 M Na_2CO_3 (4.50 mL) were added. The resulting mixture was stirred at reflux under nitrogen atmosphere for 6 h. Then, the solvent was removed under vacuum, 1 N HCl was added and the reaction extracted with CH_2Cl_2 (3 x 30 mL). The organic phase was washed with water (90 mL), dried over Na_2SO_4, filtered and concentrated under reduced pressure. The crude residue was used in the next reaction without any further purification.

MW = 234.64
LRMS (ESI) m/z = 235.8 $[M+H]^+$.

Synthesis of 2-chloro-*N*,6-diphenylpyrimidine-4-carboxamide 188

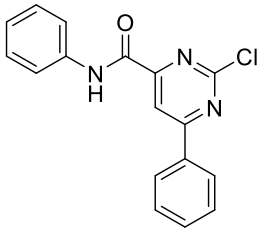

188

To a solution of intermediate **187** (0.61 g, 2.60 mmol) in anhydrous DMF (8 mL), aniline (0.28 mL, 3.13 mmol), EDC (0.60 g, 3.13 mmol) and HOBt (0.35 g, 2.60 mmol) were added. The mixture was stirred under nitrogen atmosphere at room temperature for 3 h. Then, the reaction was quenched with water and extracted with AcOEt (3 x 30 mL). The organic phase was washed with saturated $NaHCO_3$ solution (2 x 30 mL) and with saturated NaCl solution (2 x 30 mL), dried over Na_2SO_4, filtered and concentrated under reduced pressure. The crude product was purified by column chromatography using *n*-hexane/AcOEt (7:3) as eluent, to obtain the desired compound as an off-white solid.

Yield: 0.09 g, 20%

Mp: 182-183 °C

MW = 309.75

Anal. calcd. for $C_{17}H_{12}ClN_3O$: C 65.92, H 3.90, N 13.57; found C 66.04, H 3.98, N 13.49.

^{1}H-NMR (200 MHz, $CDCl_3$): δ (ppm) 7.24-7.27, 7.42-7.62, 7.81-7.84 and 8.23-8.28 (4 m, 10H, Ar), 8.60 (s, 1H pyr), 9.70 (br s, 1H, NH).

IR (KBr): cm^{-1} 3364 (NH), 1692 (CO), 1531 (NH).

General procedure for the synthesis of compounds 183a-n

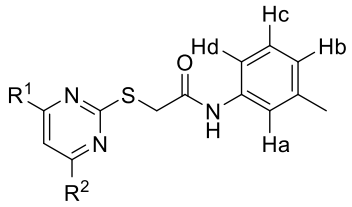

183a-n

a $R^1 = C_6H_5$; R^2 = 1-naph.
b $R^1 = C_6H_4$-4Cl; R^2 = 1-naph.
c $R^1 = C_6H_4$-4F; R^2 = 1-naph.
d $R^1 = C_6H_5$; $R^2 = SC_6H_5$
e $R^1 = C_6H_4$-4Cl; $R^2 = SC_6H_5$
f $R^1 = C_6H_4$-4F; $R^2 = SC_6H_5$
g $R^1 = C_6H_5$; $R^2 = C_6H_4$-4Cl
h $R^1 = C_6H_5$; $R^2 = C_6H_4$-4F
i $R^1 = C_6H_4$-4Cl; $R^2 = C_6H_4$-4F
l $R^1 = C_6H_4$-4Cl; $R^2 = C_6H_4$-4Cl
m $R^1 = C_6H_4$-4F; $R^2 = C_6H_4$-4F
n $R^1 = CONHC_6H_5$; $R^2 = C_6H_5$

To a suspension of the appropriate intermediate **185a-i**, **186a,b** or **188** (1.00 mmol) in anhydrous MeCN at 0 °C, 2-mercapto-*N*-(*m*-tolyl)acetamide (0.20 g, 1.10 mmol) and anhydrous K_2CO_3 (0.21 g, 1.50 mmol) were added. The reaction was stirred at room temperature under nitrogen atmosphere for 5 h. Then, the solvent was removed under vacuum and the reaction extracted with CH_2Cl_2 (3 x 30 mL). The organic phase was washed with water (90 mL), dried over Na_2SO_4, filtered and concentrated under reduced pressure. The crude product was purified by column chromatography using CH_2Cl_2 as eluent, to obtain the final products as white solids.

N-(3-Methylphenyl)-2-{[4-(1-naphthyl)-6-phenylpyrimidin-2-yl]thio}acetamide 183a

Yield: 0.09 g, 20%

Mp: 147-148 °C

MW = 461.58

Anal. calcd. for $C_{29}H_{23}N_3OS$: C 75.46, H 5.02, N 9.10, S 6.95; found C 75.23, H 5.29, N 8.81, S 6.60.

^{1}H-NMR (400 MHz, $CDCl_3$): δ (ppm) 2.04 (s, 3H, CH_3), 4.01 (s, 2H, CH_2), 6.58 (s, 1H, Ha), 6.73-6.75 (m, 1H, Hb), 6.94-7.01 (m, 2H, Hc + Hd), 7.52-7.64 and 7.75-7.78 (2 m, 8H, 3H Ar + 4H naph + H-5), 7.97 and 8.04 (2 d, *J* = 8.0 Hz, 1H naph), 8.15-8.20 (m, 3H, 2H Ar + 1H naph), 9.32 (br s, 1H, NH).

^{13}C-NMR (100 MHz, $CDCl_3$): δ (ppm) 203.06, 192.71, 183.39, 167.57, 167.22, 165.07, 157.51, 151.29, 138.42, 133.91, 130.77, 129.16, 128.72, 128.50, 127.45, 127.35, 126.49, 125.24, 124.65, 124.54, 119.74, 116.33, 113.79, 78.82, 68.74, 35.86, 21.07.

IR (KBr): cm^{-1} 3239-2915 (NH), 1663 (CO).

2-{[4-(4-Chlorophenyl)-6-(1-naphthyl)pyrimidin-2-yl]thio}-N-(3-methylphenyl)acetamide 183b

Yield: 0.10 g, 20%

Mp: 103-107 °C

MW = 496.02

Anal. calcd. for $C_{29}H_{22}ClN_3OS$: C 70.22, H 4.47, N 8.47, S 6.46; found 70.45, H 4.73, N 8.15, S 6.80.

^{1}H-NMR (400 MHz, $CDCl_3$): δ (ppm) 2.06 (s, 3H, CH_3), 4.00 (s, 2H, CH_2), 6.60 (s, 1H, Ha), 6.75-6.76 (m, 1H, Hb), 6.96-6.99 (m, 2H, Hc + Hd), 7.51-7.65 and 7.75-7.78 (2 m, 7H, 2H Ar + 4H naph + H-5), 7.98 (d, *J* = 8.0 Hz, 1H naph), 8.04-8.06 and 8.10-8.12 (2 m, 3H, 2H Ar + 1H naph), 8.19 (d, *J* = 7.6 Hz, 1H naph), 9.25 (br s, 1H, NH).

^{13}C-NMR (100 MHz, $CDCl_3$): δ (ppm) 203.01, 192.71, 183.39, 167.72, 167.02, 163.05, 138.49, 138.00, 137.67, 134.27, 133.94, 130.89, 130.35, 129.41, 128.74, 128.55, 127.99, 127.43, 126.56, 125.25, 124.66, 124.57, 119.75, 116.36, 113.46, 35.89, 21.07.

IR (KBr): cm^{-1} 3221-2918 (NH), 1666 (CO).

2-{[4-(4-Fluorophenyl)-6-(1-naphthyl)pyrimidin-2-yl]thio}-N-(3-methylphenyl)acetamide 183c

Yield: 0.26 g, 55%

Mp: 145-147 °C

MW = 479.57

Anal. calcd. for $C_{29}H_{22}FN_3OS$: C 72.63, H 4.62, N 8.76, S 6.69; found C 72.49, H 4.36, N 8.42, S 6.93.

^{1}H-NMR (400 MHz, $CDCl_3$): δ (ppm) 2.05 (s, 3H, CH_3), 3.99 (s, 2H, CH_2), 6.61 (s, 1H, Ha), 6.75-6.79 (m, 1H, Hb), 6.95-6.99 (m, 2H, Hc + Hd), 7.20-7.26, 7.52-7.64 and 7.73-7.76 (3 m, 7H, 2H Ar + 4H naph + H-5), 7.97 and 8.04 (2 d, *J* = 8.0 Hz, 1H naph), 8.14-8.16 (m, 3H, 2H Ar + 1H naph), 9.27 (br s, 1H, NH).

^{13}C-NMR (100 MHz, $CDCl_3$): δ (ppm) 198.01, 189.39, 167.75, 167.05, 163.05, 138.49, 137.65, 133.93, 131.91, 130.91, 130.33, 129.73, 129.65, 128.79, 128.54, 128.02, 127.43, 126.56, 125.25, 124.69, 124.55, 119.80, 116.39, 116.16, 113.38, 35.86, 21.07.

IR (KBr): cm^{-1} 3241-2916 (NH), 1665 (CO).

N-(3-Methylphenyl)-2-{[4-phenyl-6-(phenylthio)pyrimidin-2-yl]thio}acetamide 183d

Yield: 0.12 g, 27%

Mp: 127-128 °C

MW = 443.58

Anal. calcd. for $C_{25}H_{21}N_3OS_2$: C 67.69, H 4.77, N 9.47, S 14.46; found C 67.75, H 4.77, N 9.47, S 14.10.

^{1}H-NMR (400 MHz, $CDCl_3$): δ (ppm) 2.34 (s, 3H, CH_3), 3.70 (s, 2H, CH_2), 6.91 (d, *J* = 7.6 Hz, 1H, Hb), 7.21-7.27 (m, 3H, Ha + Hc + Hd), 7.31-7.50 (m, 6H Ar), 7.51 (s, 1H, H-5), 7.68 (d, *J* = 7.2 Hz, 2H Ar), 7.92 (d, *J* = 7.6 Hz, 2H Ar), 8.61 (br s, 1H, NH).

^{13}C-NMR (100 MHz, $CDCl_3$): δ (ppm) 203.06, 171.98, 171.09, 169.19, 166.77, 138.66, 137.64, 135.20, 131.42, 129.59, 129.21, 128.84, 128.60, 127.25, 125.33, 124.95, 120.55, 117.00, 110.02, 33.44, 21.39.

IR (KBr): cm^{-1} 3244-2912 (NH), 1662 (CO).

2-{[4-(4-Chlorophenyl)-6-(phenylthio)pyrimidin-2-yl]thio}-N-(3-methylphenyl)acetamide 183e

Yield: 0.10 g, 20%

Mp: 150-154 °C

MW = 478.03

Anal. calcd. for $C_{25}H_{20}ClN_3OS_2$: C 62.81, H 4.22, N 8.79, S 13.42; found C 62.51, H 4.38, N 9.19, S 13.46.

^{1}H-NMR (400 MHz, $CDCl_3$): δ (ppm) 2.34 (s, 3H, CH_3), 3.70 (s, 2H, CH_2), 6.91 (d, *J* = 7.2 Hz, 1H, Hb), 7.17-7.21 and 7.25-7.31 (2 m, 4H, Ha + Hd + Hc + H-5), 7.37-7.46 (m, 5H Ar), 7.67 (d, *J* = 7.2 Hz, 2H Ar), 7.85 (d, *J* = 8.4 Hz, 2H Ar), 8.61 (br s, 1H, NH).

^{13}C-NMR (100 MHz, $CDCl_3$): δ (ppm) 202.01, 172.18, 169.48, 166.67, 138.50, 137.76, 137.60, 135.51, 133.68, 129.68, 129.25, 129.14, 128.63, 128.50, 125.01, 120.55, 116.99, 116.10, 109.76, 33.47, 21.40.

IR (KBr): cm^{-1} 3240-2926 (NH), 1667 (CO).

2-{[4-(4-Fluorophenyl)-6-(phenylthio)pyrimidin-2-yl]thio}-N-(3-methylphenyl)acetamide 183f

Yield: 0.09 g, 20%

Mp: 146-147 °C

MW = 461.57

Anal. calcd. for $C_{25}H_{20}FN_3OS_2$: C 65.05, H 4.37, N 9.10, S 13.89; found C 65.03, H 4.31, N 9.28, S 13.89.

^{1}H-NMR (400 MHz, $CDCl_3$) : δ (ppm) 2.34 (s, 3H, CH_3), 3.70 (s, 2H, CH_2), 6.91 (d, *J* = 7.2 Hz, 1H, Hb), 7.10-7.13 and 7.17-7.21 (2 m, 3H, Ha + Hd + Hc), 7.25-7.27 (m, 2H Ar), 7.31 (s, 1H, H-5), 7.37-7.46 (m, 3H Ar), 7.67 (d, *J* = 7.2 Hz, 2H Ar), 7.90-7.93 (m, 2H Ar), 8.53 (br s, 1H, NH).

^{13}C-NMR (100 MHz, $CDCl_3$): δ (ppm) 201.95, 172.10, 169.30, 166.73, 161.49, 138.67, 137.62, 135.50, 129.65, 129.44, 129.36, 129.25, 128.63, 124.98, 120.55, 116.99, 116.07, 115.86, 109.61, 33.47, 21.41.

IR (KBr): cm^{-1} 3235-2915 (NH), 1659 (CO).

2-{[4-(4-Chlorophenyl)-6-phenylpyrimidin-2-yl]thio}-N-(3-methylphenyl)acetamide 183g

Yield: 0.09 g, 20%

Mp: 204-206 °C

MW = 445.96

Anal. calcd. for $C_{25}H_{20}ClN_3OS_2$: C 67.33, H 4.52, N 9.42, S 7.19; found C 67.25, H 4.54, N 9.10, S 7.40.

^{1}H-NMR (400 MHz, $CDCl_3$): δ (ppm) 2.19 (s, 3H, CH_3), 4.09 (s, 2H, CH_2), 6.81 (d, *J* = 7.6 Hz, 1H, Hb), 6.91 (s, 1H, Ha), 7.03-7.14 (m, 2H, Hc + Hd), 7.51-7.57 (m, 5H Ar), 7.82 (s, 1H, H-5), 8.09-8.15 (m, 4H Ar), 9.14 (br s, 1H, NH).

^{13}C-NMR (100 MHz, $CDCl_3$): δ (ppm) 201.50, 170.99, 167.05, 164.28, 138.60, 137.68, 136.04, 134.51, 131.58, 129.36, 129.19, 129.05, 128.66, 127.37, 124.82, 120.10, 116.55, 116.10, 108.76, 35.89, 21.24.

IR (KBr): cm^{-1} 3239-2914 (NH), 1663 (CO).

2-{[4-(4-Fluorophenyl)-6-phenylpyrimidin-2-yl]thio}-N-(3-methylphenyl)acetamide 183h

Yield: 0.09 g, 20%

Mp: 186-190 °C

MW = 429.51

Anal. calcd. for $C_{25}H_{20}FN_3OS$: C 69.91, H 4.69, N 9.78, S 7.47; found C 69.75, H 4.82, N 10.05, S 7.41.

^{1}H-NMR (400 MHz, $CDCl_3$): 2.16 (s, 3H, CH_3), 4.05 (s, 2H, CH_2), 6.81 (d, *J* = 7.2 Hz, 1H, Hb), 6.92 (s, 1H, Ha), 7.03-7.13 (m, 2H, Hc + Hd), 7.21-7.26 and 7.56-7.59 (2 m, 5H Ar), 7.82 (s, 1H, H-5), 8.14-8.17 (m, 4H Ar), 9.17 (br s, 1H, NH).

^{13}C-NMR (100 MHz, $CDCl_3$): δ (ppm) 202.95, 170.05, 167.13, 165.51, 137.70, 136.09, 131.55, 129.62, 129.52, 129.20, 128.64, 127.39, 124.82, 120.13, 116.58, 116.34, 116.12, 114.48, 108.70, 35.97, 21.23.

IR (KBr): cm^{-1} 3235-2917 (NH), 1662 (CO).

2-{[4-(4-Chlorophenyl)-6-(4-fluorophenyl)pyrimidin-2-yl]thio}-N-(3-methylphenyl) acetamide 183i

Yield: 0.11 g, 23%

Mp: 213-217 °C

MW = 463.95

Anal. calcd. for $C_{25}H_{19}ClFN_3OS$: C 64.72, H 4.13, N 9.06, S 6.91; found C 64.88, H 4.49, N 9.46, S 7.24.

^{1}H-NMR (400 MHz, $CDCl_3$): 2.19 (s, 3H, CH_3), 4.04 (s, 2H, CH_2), 6.83 (d, *J* = 7.2 Hz, 1H, Hb), 6.98 (s, 1H, Ha), 7.06-7.16 (m, 2H, Hc + Hd), 7.23-7.26 and 7.51-7.52 (2 m, 4H Ar), 7.77 (s, 1H, H-5), 8.08-8.16 (m, 4H Ar), 8.98 (br s, 1H, NH).

^{13}C-NMR (100 MHz, $CDCl_3$): δ (ppm) 201.05, 170.93, 166.88, 164.48, 138.69, 137.87, 137.60, 134.48, 132.13, 129.60, 129.52, 129.41, 128.66, 124.95, 120.17, 116.61, 116.39, 116.17, 108.37, 35.98, 21.26.

IR (KBr): cm^{-1} 3241-2914 (NH), 1665 (CO).

2-{[4,6-Bis(4-chlorophenyl)pyrimidin-2-yl]thio}-N-(3-methylphenyl)acetamide 183l

Yield: 0.10 g, 20%

Mp: 225-227 °C

MW = 480.41

Anal. calcd. for $C_{25}H_{19}Cl_2N_3OS$: C 62.50, H 3.99, N 8.75, S 6.67; found C 62.43, H 4.25, N 8.83, S 6.60.

^{1}H-NMR (400 MHz, $CDCl_3$): δ (ppm) 2.19 (s, 3H, CH_3), 4.03 (s, 2H, CH_2), 6.83 (d, *J* = 8.0 Hz, 1H, Hb), 6.96 (s, 1H, Ha), 7.08 and 7.15 (2 t, *J* = 8.0 Hz, 2H, Hc + Hd), 7.52 (d, *J* = 8.4 Hz, 4H Ar), 7.78 (s, 1H, H-5), 8.09 (d, *J* = 8.4 Hz, 4H Ar), 8.96 (br s, 1H, NH).

^{13}C-NMR (100 MHz, $CDCl_3$): δ (ppm) 203.05, 167.10, 164.41, 163.50, 137.94, 134.41, 129.41, 128.71, 128.63, 124.96, 120.12, 116.56, 112.15, 108.39, 35.81, 21.23.

IR (KBr): cm^{-1} 3238-2912 (NH), 1661 (CO).

2-{[4,6-Bis(4-fluorophenyl)pyrimidin-2-yl]thio}-N-(3-methylphenyl)acetamide 183m

Yield: 0.10 g, 23%

Mp: 210-211 °C

MW = 447.50

Anal. calcd. for $C_{25}H_{19}F_2N_3OS$: C 67.10, H 4.28, N 9.39, S 7.17; found C 67.42, H 4.11, N 9.34, S 6.80.

^{1}H-NMR (400 MHz, $CDCl_3$): δ (ppm) 2.18 (s, 3H, CH_3), 4.04 (s, 2H, CH_2), 6.82 (d, *J* = 7.2 Hz, 1H, Hb), 6.99 (s, 1H, Ha), 7.07 (t, *J* = 7.8 Hz, 1H, Hc), 7.13 (d, *J* = 8.0 Hz, 1H, Hd), 7.21-7.26 (m, 4H Ar), 7.76 (s, 1H, H-5), 8.14-8.17 (m, 4H Ar) 9.03 (br s, 1H, NH).

^{13}C-NMR (100 MHz, $CDCl_3$): δ (ppm) 203.06, 166.92, 164.36, 163.66, 137.63, 129.55, 129.46, 128.69, 124.92, 120.12, 116.55, 116.37, 116.15, 108.20, 35.78, 21.23.

IR (KBr): cm^{-1} 3541-2963 (NH), 1659 (CO).

2-({2-[(3-Methylphenyl)amino]-2-oxoethyl}thio)-N,6-diphenylpyrimidine-4-carboxamide 183n

Yield: 0.28 g, 62%

Mp: 181-182 °C

MW = 454.54

Anal. calcd. for $C_{26}H_{22}N_4O_2S$: C 68.70, H 4.88, N 12.33, S 7.05; found C 68.40, H 5.18, N 12.14, S 6.70.

^{1}H-NMR (400 MHz, DMSO-d6): δ (ppm) 2.19 (s, 3H, CH_3), 4.21 (s, 2H, CH_2), 6.83 (d, *J* = 7.6 Hz, 1H, Hb), 7.13-7.19 (m, 3H, Ha + Hc + Hd), 7.36-7.43 and 7.46-7.50 (2 m, 5H Ar),

7.57 (t, *J* = 7.2 Hz, 1H Ar), 7.88 (d, *J* = 8.0 Hz, 2H Ar), 8.24-8.26 (m, 3H, 2H Ar + H-5), 10.29 and 10.52 (2 br s, 1H, 2 NH).

^{13}C-NMR (100 MHz, DMSO-d6): δ (ppm) 167.24, 166.23, 160.10, 158.50, 141.10, 139.21, 138.33, 138.17, 135.48, 132.39, 129.52, 129.20, 128.98, 127.99, 125.01, 124.55, 120.93, 120.20, 116.83, 109.95, 36.43, 21.48.

IR (KBr): cm^{-1} 3339-2911 (NH), 1695 and 1656 (2 CO).

General procedure for the synthesis of compounds 190a-c

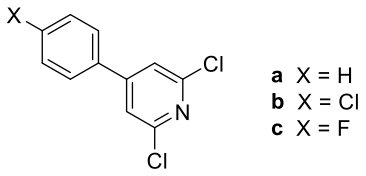

190a-c

To a solution of 2,6-dichloro-4-iodopyridine (0.50 g, 1.83 mmol) in THF (6 mL), the opportune phenylboronic acid (2.01 mmol), $Pd(OAc)_2$ (8.20 mg, 0.04 mmol), PPh_3 (14.36 mg, 0.05 mmol) and 1 M Na_2CO_3 (4.50 mL) were added. The resulting mixture was stirred at reflux under nitrogen atmosphere for 3 h. Then, solvent was removed under vacuum and the reaction extracted with CH_2Cl_2 (3 x 30 mL). The organic phase was washed with water, dried over Na_2SO_4, filtered and concentrated under reduced pressure. The crude was purified by column chromatography using PE (bp 40-60 °C)/AcOEt (95:5) as eluent, to afford the pure products as white solids.

2,6-Dichloro-4-phenylpyridine 190a

Yield: 0.30 g, 73%

Mp: 54-55 °C

MW = 224.09

Anal. calcd. for $C_{11}H_7Cl_2N$: C 58.96, H 3.15, N 6.25; found C 58.88, H 3.12, N 5.96.

^{1}H-NMR (200 MHz, $CDCl_3$): δ (ppm) 7.49 (s, 2H pyr), 7.50-7.54 and 7.60-7.63 (2 m, 5H Ar).

2,6-Dichloro-4-(4-chlorophenyl)pyridine 190b

Yield: 0.35 g, 74%

Mp: 151-152 °C

MW = 258.53

Anal. calcd. for $C_{11}H_6Cl_3N$: C 51.10, H 2.34, N 5.42; found C 51.14, H 2.25, N 5.07.

^{1}H-NMR (200 MHz, $CDCl_3$): δ (ppm) 7.47 (s, 2H pyr), 7.54-7.55 (m, 4H Ar).

2,6-dichloro-4-(4-fluorophenyl)pyridine 190c

Yield: 0.23 g, 53%

Mp: 164-166 °C

MW = 242.08

Anal. calcd. for $C_{11}H_6Cl_2FN$: C 54.58, H 2.50, N 5.79; found C 54.33, H 2.53, N 5.55.

^{1}H-NMR (200 MHz, $CDCl_3$): δ (ppm) 7.19-7.27 (m, 2H Ar), 7.46 (s, 2H pyr), 7.58-7.65 (m, 2H Ar).

General procedure for the synthesis of compounds 191a-c

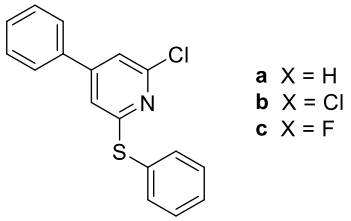

191a-c

To a suspension of NaH (60% dispersion in mineral oil, 0.16 g, 4.00 mmol) in anhydrous DMF (9 mL) at 0 °C, thiophenol (0.10 mL, 1.00 mmol) was added. The mixture was stirred at 0 °C under nitrogen atmosphere for 1 h. Then, a solution of the opportune derivative **190a-c** (1.00 mmol) in anhydrous DMF (2 mL) was added and the reaction was stirred at room temperature under nitrogen for 3 h (**191a,b**) or 24 h (**191c**). Water was added dropwise, cooling in ice bath, and the reaction extracted with CH_2Cl_2 (3 x 30 mL). The organic phase was washed with water, dried over Na_2SO_4, filtered and concentrated under reduced pressure.

The crude product was purified by column chromatography using *n*-hexane/AcOEt (95:5) (**191a,b**), or (9:1) (**191c**) as eluent, to afford the pure products as white solids.

2-Chloro-4-phenyl-6-(phenylthio)pyridine 191a

Yield: 0.28 g, 95%

Mp: 57-58 °C

MW = 297.80

Anal. calcd. for $C_{17}H_{12}ClNS$: C 68.56, H 4.06, N 4.70, S 10.77; found C 68.41, H 3.90, N 5.00, S 11.11.

^{1}H-NMR (200 MHz, $CDCl_3$): δ (ppm) 6.94 and 7.25 (2 s, 1H pyr), 7.44-7.51 and 7.63-7.70 (2 m, 10H Ar).

2-Chloro-4-(4-chlorophenyl)-6-(phenylthio)pyridine 191b

Yield: 0.27 g, 82%

Mp: 82-86 °C

MW = 332.25

Anal. calcd. for $C_{17}H_{11}Cl_2NS$: C 61.45, H 3.34, N 4.22, S 9.65; found C 61.40, H 3.54, N 4.45, S 9.82.

^{1}H-NMR (200 MHz, $CDCl_3$): δ (ppm) 6.88 and 7.21 (2 s, 1H pyr), 7.37-7.52 and 7.65-7.68 (2 m, 9H Ar).

2-Chloro-4-(4-fluorophenyl)-6-(phenylthio)pyridine 191c

Yield: 0.32 g, quantitative

Mp: 47-50 °C

MW = 315.79

Anal. calcd. for $C_{17}H_{11}ClFNS$: C 64.66, H 3.51, N 4.44, S 10.15; found C 64.65, H 3.41, N 4.76, S 10.29.

^{1}H-NMR (200 MHz, $CDCl_3$): δ (ppm) 6.88 and 7.10 (2 s, 1H pyr), 7.14-7.22, 7.38-7.52 and 7.66-7.67 (3 m, 9H Ar).

General procedure for the synthesis of compounds 191d,e

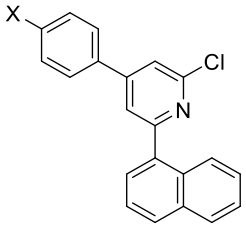

197d X = H
197e X = Cl

191d,e

To a solution of the opportune intermediate **190a,b** (2.00 mmol) in DME (10 mL), naphthalene boronic acid (0.28 g, 1.60 mmol), $Pd(OAc)_2$ (22.45 mg, 0.10 mmol), PPh_3 (52.36 mg, 0.20 mmol) and Na_2CO_3 (0.66 g, 6.20 mmol) dissolved in the minimum amount of water, were added. The resulting mixture was stirred at reflux under nitrogen atmosphere for 3 h. Then, solvent was removed under vacuum and the reaction extracted with CH_2Cl_2 (3 x 30 mL). The organic phase was washed with water, dried over Na_2SO_4, filtered and concentrated under reduced pressure. The product was purified by column chromatography using PE (bp 40-60 °C)/CH_2Cl_2 (1:1) (**191d**) or *n*-hexane/AcOEt (95:5) (**191e**), to afford the pure products as white solids.

2-Chloro-6-(1-naphthyl)-4-phenylpyridine 191d

Yield: 0.21 g, 33%

Mp: 128-130 °C

MW = 315.80

Anal. calcd. for $C_{21}H_{14}ClN$ C 79.87, H 4.47, N 4.44, found C 79.69, H 4.41, N 4.71.

^{1}H-NMR (200 MHz, $CDCl_3$): δ (ppm) 7.52-7.77 (m, 11H, 5H Ar + 4H naph + 2H pyr), 7.96-8.01 and 8.15-8.22 (2 m, 3H naph).

2-Chloro-4-(4-chlorophenyl)-6-(1-naphthyl)pyridine 191e

Yield: 0.14 g, 20%

Mp: 112-113 °C

MW = 350.24

Anal. calcd. for $C_{21}H_{13}Cl_2N$: C 72.01, H 3.74, N 4.00; found C 71.89, H 3.67, N 4.25.

^{1}H-NMR (200 MHz, $CDCl_3$): δ (ppm) 7.50-7.73 (m, 10H, 4H Ar + 4H naph + 2H pyr), 7.94-8.00 and 8.13-8.17 (2 m, 3H naph).

General procedure for the synthesis of compounds 192a and 193b

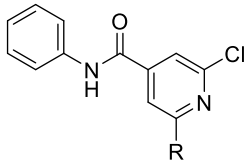

192a R = Cl
193b R = C_6H_5

To a solution of 2,6-dichloroisonicotinic acid (0.50 g, 2.60 mmol) or intermediate **192b** (2.60 mmol) in anhydrous DMF (8 mL), aniline (0.28 mL, 3.13 mmol), EDC (0.60 g, 3.13 mmol) and HOBt (0.35 g, 2.60 mmol) were added. The mixture was stirred under nitrogen atmosphere at room temperature for 2 h and then at 50 °C for 3 h. Then, the reaction was quenched with water and extracted with AcOEt (3 x 30 mL). The organic phase was washed with saturated $NaHCO_3$ solution (2 x 30 mL) and with saturated NaCl solution (2 x 30 mL), dried over Na_2SO_4, filtered and concentrated under reduced pressure. The crude product was purified by column chromatography using *n*-hexane/AcOEt (8:2) (**192a**) or CH_2Cl_2 (**193b**) as eluent, to afford the pure products as off-white solids.

2,6-dichloro-N-phenylisonicotinamide 192a

Yield: 0.54 g, 78%

Mp: 180-181 °C

MW = 267.11

Anal. calcd. for $C_{12}H_8Cl_2N_2O$: C 53.96, H 3.02, N 10.49; found C 53.78, H 3.00, N 10.50.

^{1}H-NMR (200 MHz, $CDCl_3$): δ (ppm) 7.21-7.29 (m, 1H Ar), 7.37 (t, *J* = 7.7 Hz, 2H Ar), 7.61 (d, *J* = 8.0 Hz, 2H Ar), 7.69 (s, 2H, H-3 + H-5), 8.01 (br s, 1H, NH).

IR (KBr): cm^{-1} 3281 (NH), 1650 (CO).

2-chloro-N,6-diphenylisonicotinamide 193b

Yield: 0.09 g, 20%

Mp: 160-161 °C

MW = 308.76

Anal. calcd. for $C_{18}H_{13}ClN_2O$: C 70.02, H 4.24, N 9.07; found C 70.04, H 4.02, N 8.86.

^{1}H-NMR (200 MHz, $CDCl_3$): δ (ppm) 7.24-7.29 and 7.39-7.52 (2 m, 6H, 5H Ar + H-3), 7.61 (s, 1H, H-5), 7.67 (d, *J* = 8.0 Hz, 2H Ar), 8.03-8.07 (m, 3H Ar).

IR (KBr): cm^{-1} 3288 (NH), 1654 (CO).

Synthesis of 2-chloro-6-phenylisonicotinic acid 192b

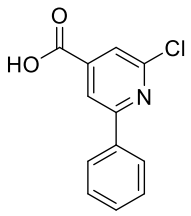

192b

To a solution of 2,6-dichloropyrimidine-4-carboxylic acid (0.50 g, 2.59 mmol) in THF (5 mL), phenylboronic acid (0.26 g, 2.15 mmol), $Pd(OAc)_2$ (11.63 mg, 0.05 mmol), PPh_3 (20.38 mg, 0.08 mmol) and 1 M Na_2CO_3 (4.50 mL) were added. The resulting mixture was stirred at reflux under nitrogen atmosphere for 24 h. Then, the solvent was removed under vacuum, 1 N HCl was added and the reaction extracted with CH_2Cl_2 (3 x 30 mL). The organic phase was washed with water (90 mL), dried over Na_2SO_4, filtered and concentrated under reduced pressure. Compound **192b** were used in the next reaction without any further purification.

MW = 233.65

Synthesis of 2-chloro-N-phenyl-6-(phenylthio)isonicotinamide 193a

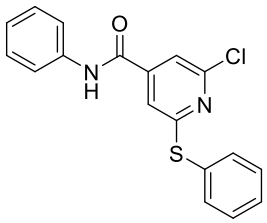

193a

To a suspension of NaH (60% dispersion in mineral oil, 0.16 g, 4.00 mmol) in anhydrous DMF (9 mL) at 0 °C, thiophenol (0.10 mL, 1.00 mmol) was added. The mixture was stirred at 0 °C under nitrogen atmosphere for 1 h, then a solution of **192a** (0.27 g, 1.00 mmol) in anhydrous DMF (2 mL) was added. The reaction was stirred at room temperature under nitrogen atmosphere for 24 h. Then, water was added dropwise, cooling in ice bath, and the reaction extracted with CH_2Cl_2 (3 x 30 mL). The organic phase was washed with water (90 mL), dried over Na_2SO_4, filtered and concentrated under reduced pressure. The crude product was purified by column chromatography using *n*-hexane/CH_2Cl_2/AcOEt (5:4:1), to afford the pure product as a white solid.

Yield: 0.57 g, 89%

Mp: 158-159 °C

MW = 340.83

Anal. calcd. for $C_{18}H_{13}ClN_2OS$: C 63.43, H 3.84, N 8.22, S 9.41; found C 63.53, H 3.95, N 8.05, S 9.15.

^{1}H-NMR (200 MHz, $CDCl_3$): δ (ppm) 7.10 (s, 1H, H-3), 7.17-7.25 and 7.35-7.63 (2 m, 11H, 10H Ar + H-5), 7.83 (br s, 1H, NH).

IR (KBr): cm^{-1} 3329 (NH), 1682 (CO).

General procedure for the synthesis of compounds 189a,b

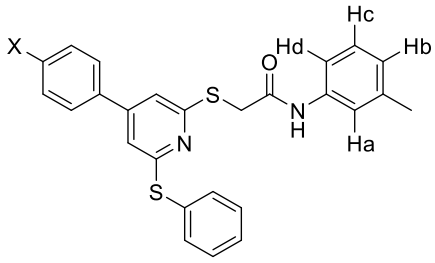

189a,b

A round-bottom flask was charged with the appropriate intermediate **191a,b** (1.00 mmol), anhydrous K_2CO_3 (0.28 g, 2.00 mmol), CuI (19.05 mg, 0.10 mmol) and L-proline (34.54 mg, 0.30 mmol). The flask was evacuated and filled with nitrogen. 2-mercapto-*N*-(*m*-tolyl)acetamide (0.20 g, 1.10 mmol) dissolved in anhydrous DME (5 mL) was introduced *via* syringe and the mixture was stirred at reflux under nitrogen atmosphere for 24 h. Then, the reaction was extracted with CH_2Cl_2 (3 x 30 mL), the organic phase was washed with saturated NaCl solution, dried over Na_2SO_4, filtered and concentrated under reduced pressure. The crude was purified by column chromatography, using CH_2Cl_2 as eluent, obtaining the final products as off-white solids.

N-(3-methylphenyl)-2-{[4-phenyl-6-(phenylthio)pyridin-2-yl]thio}acetamide 189a

Yield: 0.09 g, 20%

Mp: 122-123 °C

MW = 442.60

Anal. calcd. for $C_{26}H_{22}N_2OS_2$: C 70.56, H 5.01, N 6.33, S 14.49; found C 70.52, H 5.31, N 6.07, S 14.84.

^{1}H-NMR (400 MHz, $CDCl_3$): δ (ppm) 2.33 (s, 3H, CH_3), 3.76 (s, 2H, CH_2), 6.89 (d, *J* = 7.2 Hz, 1H, Hb), 7.00 (s, 1H, Ha), 7.17-7.21 (m, 2H, Hc + Hd), 7.39-7.45 and 7.62-7.63 (2 m, 12H, 10H Ar + 2H pyr), 9.34 (br s, 1H, NH).

^{13}C-NMR (100 MHz, $CDCl_3$): δ (ppm) 168.05, 167.50, 161.14, 150.29, 146.18, 138.59, 138.16, 136.98, 135.00, 129.87, 129.74, 129.60, 129.10, 128.58, 126.94, 124.65, 120.45, 116.88, 116.68, 116.31, 34.58, 21.41.

IR (KBr): cm^{-1} 3237-2913 (NH), 1666 (CO).

2-{[4-(4-chlorophenyl)-6-(phenylthio)pyridin-2-yl]thio}-N-(3-methylphenyl)acetamide 189b

Yield: 0.10 g, 20%

Mp: 93-95 °C

MW = 477.04

Anal. calcd. for $C_{26}H_{21}ClN_2OS_2$ C 65.46, H 4.44, N 5.87, S 13.44, found C 65.13, H 4.64, N 6.20, S 13.58.

^{1}H-NMR (400 MHz, $CDCl_3$): δ (ppm) 2.34 (s, 3H, CH_3), 3.74 (s, 2H, CH_2), 6.90 (d, *J* = 7.2 Hz, 1H, Hb), 7.01 (s, 1H, Ha), 7.16-7.20 (m, 2H, Hc + Hd), 7.37-7.44 and 7.61-7.62 (2 m, 11H, 9H Ar + 2H pyr), 9.34 (br s, 1H, NH).

^{13}C-NMR (100 MHz, $CDCl_3$): δ (ppm) 181.05, 168.15, 161.30, 151.80, 146.20, 138.62, 136.90, 135.02, 129.80, 129.55, 129.34, 128.59, 128.27, 128.16, 126.90, 124.90, 120.43, 120.21, 116.80, 116.68, 29.59, 19.50.

IR (KBr): cm^{-1} 3237-2911 (NH), 1664 (CO).

Synthesis of 1-hydrazinopropan-2-ol 226a

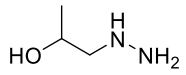

226a

To monohydrate hydrazine (12.50 g, 248.75 mmol) at 70 °C, 2-methyloxirane (2.75 g, 47.50 mmol) was added dropwise. The reaction was stirred under reflux for 15 minutes and then the excess of hydrazine was removed under reduced pressure. The obtained residue was purified by bulb to bulb distillation with an oil pump, obtaining a colourless liquid which crystallized slowly. Compound **226a** was used in the next reaction without any further characterization.

Yield: 72%
MW = 90.12

Synthesis of (2-phenylpropyl)hydrazine 226b

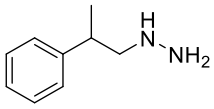

226b

A solution of 1-bromo-2-phenylpropane (1.99 g, 10.00 mmol) and hydrazine monohydrate (4.00 g, 80.00 mmol) in absolute EtOH (20 mL) was refluxed for 24 h. The solvent was evaporated under reduced pressure and the crude was treated with anhydrous K_2CO_3, then extracted with $CHCl_3$ (3 x 20 mL). The organic solution was dried over Na_2SO_4, filtered and concentrated under reduced pressure. The crude was purified by bulb to bulb distillation to obtain the pure product**,** as pale yellow oil. Compound **226b** was used in the next reaction without any further characterization.

Yield: 0.95 g, 63%
MW = 150.22

General procedure for the synthesis of compounds 227a,b

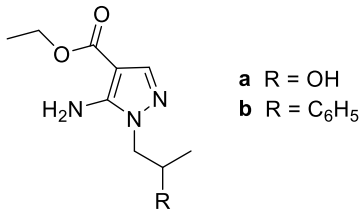

227a,b

The appropriate hydrazine derivative **226a,b** (5.00 mmol) was added to a solution of ethyl(ethoxymethylene)cyanoacetate (0.68 g, 5.00 mmol) in absolute EtOH (5 mL) and the mixture was refluxed for 8 h (**227a**) or for 5 h (**227b**). The solution was washed with water (10 mL), dried over Na_2SO_4 and concentrated under reduced pressure. The crude was purified by column chromatography using silica gel and CH_2Cl_2/MeOH (8:2) as eluent (**227a**) or Florisil® and Et_2O as eluent (**227b**), to afford the pure products.

Ethyl 5-amino-1-(2-hydroxypropyl)-1H-pyrazole-4-carboxylate 227a

Yield: 0.65 g, 61%

Mp: 66-68 °C

MW = 213.23

Anal. calcd. for $C_9H_{15}N_3O_3$: C 50.69, H 7.09, N 19.71; found C 50.79, H 7.06, N 19.88.

^{1}H-NMR (200 MHz, $CDCl_3$): δ 1.26 (d, *J* = 6.4 Hz, 3H, $\underline{CH_3}CH$), 1.35 (t, *J* = 7.0 Hz, 3H, $\underline{CH_3}CH_2$), 3.13 (br s, 1H, OH), 3.78-4.42 (m, 5H, CH_2O + CH_2N + $\underline{CH}CH_3$), 5.44 (br s, 2H, NH_2), 7.61 (s, 1H, H-3).

IR (KBr): cm^{-1} 3426, 3390, 3313 (NH_2 + OH), 1697 (CO).

Ethyl 5-amino-1-(2-phenylpropyl)-1H-pyrazole-4-carboxylate 227b

Yield: 0.82 g, 60%

Mp: 85-86 °C

MW = 273.33

Anal. calcd for $C_{15}H_{19}N_3O_2$: C 65.91, H 7.01, N 15.37; found C 65.90, H 6.99, N 15.25.

^{1}H-NMR (200 MHz, $CDCl_3$): δ 1.06-1.20 (m, 6H, 2 CH_3), 3.24-3.26 (m, 1H, CH), 3.78-3.83 and 3.85-3.90 (2 m, 2H, CH_2N), 4.10 (q, *J* = 7.0 Hz, 2H, CH_2O), 4.79 (br s, 2H, NH_2), 7.00-7.16 (m, 5H Ar), 7.55 (s, 1H, H-3).
IR (KBr): cm^{-1} 3400-3200 (NH_2), 1681 (CO).

General procedure for the synthesis of compounds 228a,b

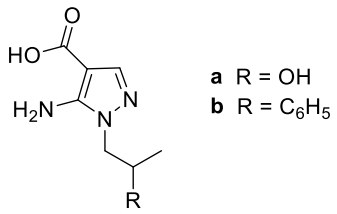

228a,b

To a solution of the opportune intermediate **227a,b** (7.00 mmol) in EtOH (10 mL), 3.5 M NaOH (8 mL) was added and the reaction was stirred at reflux for 5 h. The solvent was removed under reduced pressure and the mixture was acidified with 6 N HCl, cooling with an ice-bath, obtaining a white solid. The solid was washed with water, filtered and recrystallized from absolute EtOH to obtain **228a,b** as white solids.

5-Amino-1-(2-hydroxypropyl)-1H-pyrazole-4-carboxylic acid 228a

Yield: 0.99 g, 76%
Mp: 142-143 °C
MW = 185.18
Anal. calcd for $C_7H_{11}N_3O_3$: C 45.40, H 5.99, N 22.69, found C 45.04, H 6.31, N 23.06.
^{1}H-NMR (200 MHz, DMSO-d6): δ (ppm) 1.09 (d, *J* = 5.8 Hz, 3H, $\underline{CH_3}CH$), 3.99-4.06 (m, 3H, CH_2N + $\underline{CH}CH_3$), 5.71 (br s, 1H, OH), 7.91 (s, 1H, H-3).
IR (KBr): cm^{-1} 3400-2510 (OH), 3390-3307 (NH_2), 1658 (CO).

5-Amino-1-(2-phenylpropyl)-1H-pyrazole-4-carboxylic acid 228b

Yield: 1.32 g, 77%
Mp: 149-150 °C

MW = 245.28

Anal. calcd for $C_{13}H_{15}N_3O_2$: C 63.66, H 6.16, N 17.13; found C 63.14, H 6.65, N 17.10.

^{1}H-NMR (200 MHz, DMSO-d6): δ (ppm) 1.41-1.43 (m, 3H, CH_3), 3.34-3.40 (m, 1H, CH), 3.87-3.92 e 4.08-4.28 (2 m, 2H, CH_2N), 4.75 (br s, 2H, NH_2), 5.32 (br s, 1H, OH), 7.05-7.70 (m, 5H Ar), 8.23 (s, 1H, H-3).

IR (KBr): cm^{-1} 3450-3100 (NH_2), 1628 (CO).

Synthesis of 1-(5-amino-1*H*-pyrazol-1-yl)propan-2-ol 229a

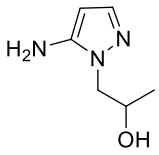

229a

Intermediate **228a** (5.00 mmol) was heated at 150 °C until the effervescence disappeared. Then, the reaction was cooled and Et_2O (20 mL) was added. The precipitate was filtered and the crude obtained was used in the next reaction without any further purification.

Yield: 0.38 g, 54%

MW = 141.17

Synthesis of 1-(2-phenylpropyl)-1*H*-pyrazol-5-amine 229b

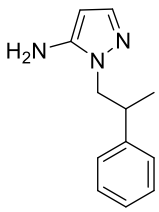

229b

Intermediate **228b** (5.00 mmol) was heated at 150 °C until the effervescence disappeared. Then, after cooling, $CHCl_3$ (15 mL) was added to the reaction, the mixture was washed with a

saturated $NaHCO_3$ solution (15 mL), dried over Na_2SO_4, filtered and concentrated under reduced pressure The crude brown oil obtained was used in the next reaction without any further purification.

Yield: 0.81 g, 80%
MW = 201.27

General procedure for the synthesis of compounds 230a,b

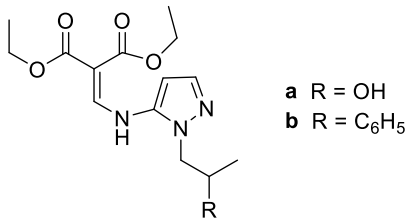

230a,b

A mixture of the opportune intermediate **229a,b** (5.00 mmol) and diethyletoxymethylene malonate (1.08 g, 5.00 mmol) was stirred at 120 °C for 2 h. After cooling, Et_2O was added (20 mL) and a solid precipitated. It was filtered obtaining **230a** as a pure white solid, while pure **230b** was obtained after recrystallization with absolute EtOH.

Diethyl ({[1-(2-hydroxypropyl)-1H-pyrazol-5-yl]amino}methylene)malonate 230a

Yield: 1.53 g, 98%
Mp: 111-113 °C
MW = 311.33
Anal. calcd for $C_{14}H_{21}N_3O_5$: C 54.01, H 6.80, N 13.50; found C 54.28, H 6.93, N 13.13.
^{1}H-NMR (200 MHz, DMSO-d6): δ (ppm) 1.29 (d, *J* = 6.0 Hz, 3H, $\underline{CH_3}CH$), 1.42 (t, *J* = 6.0 Hz, 6H, $2CH_3$), 4.00-4.37 (m, 7H, $2CH_2O + CH_2N + \underline{CH}CH_3$), 6.14 (d, *J* = 4.04 Hz, 1H, H-3), 7.51 (d, *J* = 4.04 Hz, 1H, H-4), 8.13 (d, *J* = 11.8 Hz, 1H, CHC), 11.18 (br s, 1H, OH).
IR (KBr): cm^{-1} 3448 (NH), 1689 (C=C), 1662, 1601 (2 CO).

Diethyl ({[1-(2-phenylpropyl)-1H-pyrazol-5-yl]amino}methylene)malonate 230b

Yield: 1.63 g, 88%

Mp: 88-89 °C

MW = 371.43

Anal. calcd for $C_{20}H_{25}N_3O_4$: C 64.67, H 6.78, N 11.31; found C 64.33, H 7.19, N 11.29.

^{1}H-NMR (200 MHz, DMSO-d6): δ (ppm) 1.32-1.42 (m, 9H, 3 CH_3), 3.43-3.52 (m, 1H, $\underline{CH}CH_3$), 4.11-4.13, 4.19-4.27 and 4.29-4.38 (3 m, 2H, CH_2), 5.93 (d, *J* = 4.04 Hz, 1H, H-4), 7.11-7.26 (m, 5H Ar), 7.28 (d, *J* = 4.04 Hz, 1H, H-3), 7.83 (d, *J* = 12.0 Hz, 1H, $\underline{CH}$NH), 10.67 (br s, 1H, NH).

IR (KBr): cm^{-1} 3222 (NH), 1720 (CO), 1606 (CH=CH).

General procedure for the synthesis of compounds 231a,b

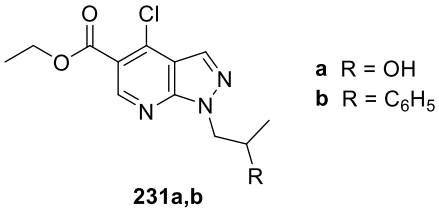

231a,b

A solution of the opportune intermediate **230a,b** (5.00 mmol) with $POCl_3$ (6.00 g, 39.50 mmol) was stirred at reflux for 18 h. After cooling, the mixture was quenched with ice-water (20 mL) and extracted with CH_2Cl_2 (20 mL x 3). The organic phase washed with water (60 mL), dried over Na_2SO_4, filtered and concentrated under reduced pressure. The crude product was purified by column chromatography, using Florisil® and CH_2Cl_2 as eluent, to obtain the desired compounds as yellow oils.

Ethyl 4-chloro-1-(2-hydroxypropyl)-1H-pyrazolo[3,4-b]pyridine-5-carboxylate 231a

Yield: 0.76 g, 54%

MW = 283.71

Anal. calcd for $C_{12}H_{14}ClN_3O_3$: C 50.80, H 4.97, N 14.81; found C 50.91, H 4.99, N 14.85.

^{1}H-NMR (200 MHz, $CDCl_3$): δ (ppm) 1.46 (t, *J* = 7.0 Hz, 3H, $\underline{CH_3}CH_2$), 1.58 (d, *J* = 6.1 Hz, 3H, $\underline{CH_3}CH$), 4.47-4.69 (m, 5H, CH_2O + CH_2N + $\underline{CH}CH_3$), 8.25 (s, 1H, H-3), 9.07 (s, 1H, H-6).

IR ($CHCl_3$): cm^{-1} 1724 (CO).

Ethyl 4-chloro-1-(2-phenylpropyl)-1H-pyrazolo[3,4-b]pyridine-5-carboxylate 231b

Yield: 1.10 g, 64%

MW = 343.81

Anal. calcd for $C_{18}H_{18}ClN_3O_2$: C 62.88, H 5.28, N 12.22; found C 62.53, H 4.99, N 12.31.

^{1}H-NMR (200 MHz, $CDCl_3$): δ (ppm) 1.25-1.29 (m, 3H, $\underline{CH_3}CH$), 1.41 (t, *J* = 7.2 Hz, 3H, $\underline{CH_3}CH_2$), 3.47-3.52 (m, 1H, $\underline{CH}CH_3$), 4.32 (q, *J* = 7.2 Hz, 2H, CH_2O), 4.48-4.58 (m, 2H, CH_2N), 7.00-7.50 (m, 5H Ar), 8.03 (s, 1H, H-3), 8.80 (s, 1H, H-6).

IR ($CHCl_3$): cm^{-1} 1723 (CO).

General procedure for the synthesis of compounds 224a-f and 225a-g

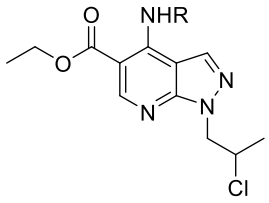

a: R = C_4H_9
b: R = $CH_2C_6H_5$
c: R = $CH_2CH_2C_6H_4$-2F
d: R = $CH_2CH_2C_6H_4$-3F
e: R = $CH_2CH_2C_6H_4$-4F
f: R = $CH_2CH_2C_6H_4$-4OCH_3

224a-f

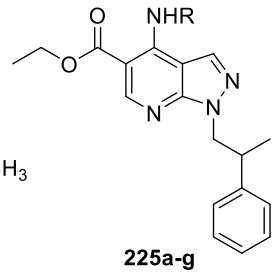

a: R = $CH_2CH_2C_6H_5$
b: R = $CH_2CH_2C_6H_4$-4Cl
c: R = $CH_2CH_2C_6H_4$-2F
d: R = $CH_2CH_2C_6H_4$-3F
e: R = $CH_2CH_2C_6H_4$-4F
f: R = $CH_2CH_2C_6H_4$-4OCH_3
g: R = $CH_2CH_2C_6H_4$-4CH_3

225a-g

To a solution of the opportune intermediate **231a,b** (1.00 mmol) in anhydrous toluene (10 mL) the appropriate amine (4.00 mmol) was added and the mixture was stirred at room temperature for 48 h. The organic phase was washed with water (30 mL), dried over Na_2SO_4, filtered and concentrated under reduced pressure. The crude oils were purified with column chromatography using Florisil® and Et_2O as eluent, obtaining compounds **224a-f** and **225a-g** as white solids.

Ethyl 4-(butylamino)-1-(2-chloropropyl)-1H-pyrazolo[3,4-b]pyridine-5-carboxylate 224a

Yield: 0.21 g, 61%

Mp: 69-70 °C

MW = 338.83

Anal. calcd for $C_{16}H_{23}ClN_4O_2$: C 56.72, H 6.84, N 16.54; found C 56.71, H 7.01, N 16.57.

^{1}H-NMR (200 MHz, DMSO-d6): δ (ppm) 1.10 (t, *J* = 7.4 Hz, 3H, CH_3 but.) 1.44 (t, *J* = 7.0 Hz, 3H, $\underline{CH_3}CH_2$), 1.40-1.70 (m, 7H, 2 CH_2 but. + $\underline{CH_3}CH$), 3.66-3.69 (m, 2H, $\underline{CH_2}NH$), 4.40-4.72 (m, 5H, CH_2O + CH_2N + $\underline{CH}CH_3$), 8.24 (s, 1H, H-3), 9.03 (s, 1H, H-6).
IR (KBr): cm^{-1} 3278 (NH), 1674 (CO).

Ethyl 4-(benzylamino)-1-(2-chloropropyl)-1H-pyrazolo[3,4-b]pyridine-5-carboxylate 224b

Yield: 0.22 g, 59%
Mp: 130-131 °C
MW = 372.84
Anal. calcd for $C_{19}H_{21}ClN_4O_2$: C 56.72, H 6.84, N 16.54; found C 56.71, H 7.01, N 16.57.
^{1}H-NMR (200 MHz, DMSO-d6): δ (ppm) 1.45 (t, *J* = 7.0 Hz, 3H, $\underline{CH_3}CH_2$), 1.58 (d, *J* = 6.1 Hz, 3H, $\underline{CH_3}CH$), 4.40-4.52 and 4.60-4.72 (2 m, 7H, CH_2O + CH_2N + $\underline{CH_2}NH$ + $\underline{CH}CH_3$), 7.25-7.43 (m, 5H Ar), 8.25 (s, 1H, H-3), 9.07 (s, 1H, H-6).
IR (KBr): cm^{-1} 3274 (NH), 1678 (CO).

Ethyl 1-(2-chloropropyl)-4-{[2-(2-fluorophenyl)ethyl]amino}-1H-pyrazolo[3,4-b]pyridine-5-carboxylate 224c

Yield: 0.23 g, 58%
Mp: 92-93 °C
MW = 404.87
Anal. calcd for $C_{20}H_{22}ClFN_4O_2$: C 59.33, H 5.48, N 13.84; found C 59.60, H 5.75, N 13.64.
^{1}H-NMR (200 MHz, DMSO-d6): δ (ppm) 1.40 (t, *J* = 7.0 Hz, 3H, $\underline{CH_3}CH_2$), 1.60 (d, *J* = 6.0 Hz, 3H, $\underline{CH_3}CH$), 3.15 (t, *J* = 7.0 Hz, 2H, CH_2Ar), 3.92 (q, *J* = 7.0 Hz, 2H, $\underline{CH_2}NH$), 4.43-4.55 and 4.63-4.82 (2 m, 5H, CH_2O + CH_2N + $\underline{CH}CH_3$), 7.12-7.60 (m, 4H Ar), 8.12 (s, 1H, H-3), 8.88 (s, 1H, H-6).
IR (KBr): cm^{-1} 3272 (NH), 1667 (CO).

Ethyl 1-(2-chloropropyl)-4-{[2-(3-fluorophenyl)ethyl]amino}-1H-pyrazolo[3,4-b]pyridine-5-carboxylate 224d

Yield: 0.17 g, 43%
Mp: 97-99 °C
MW = 404.87
Anal. calcd for $C_{20}H_{22}ClFN_4O_2$: C 59.33, H 5.48, N 13.84; found C 59.60, H 5.75, N 13.64.

^{1}H-NMR (200 MHz, DMSO-d6): δ (ppm) 1.41 (t, *J* = 7.0 Hz, 3H, $\underline{CH_3}CH_2$), 1.60 (d, *J* = 6.0 Hz, 3H, $\underline{CH_3}CH$), 3.11 (t, *J* = 7.0 Hz, 2H, CH_2Ar), 3.93 (q, *J* = 7.0 Hz, 2H, CH_2NH), 4.40-4.55 and 4.64-4.80 (2 m, 5H, CH_2O + CH_2N + $\underline{CH}CH_3$), 7.15-7.58 (m, 4H Ar), 8.08 (s, 1H, H-3), 8.88 (s, 1H, H-6), 9.35 (br s, 1H, NH).
IR (KBr): cm^{-1} 3273 (NH), 1669 (CO).

Ethyl 1-(2-chloropropyl)-4-{[2-(4-fluorophenyl)ethyl]amino}-1H-pyrazolo[3,4-b]pyridine-5-carboxylate 224e

Yield: 0.21 g, 51%
Mp: 84-85 °C
MW = 404.87
Anal. calcd for $C_{20}H_{22}ClFN_4O_2$: C 59.33, H 5.48, N 13.84; found C 59.60, H 5.75, N 13.64.
^{1}H-NMR (200 MHz, DMSO-d6): δ (ppm) 1.41 (t, *J* = 7.0 Hz, 3H, $\underline{CH_3}CH_2$), 1.61 (d, *J* = 6.0 Hz, 3H, $\underline{CH_3}CH$), 3.12 (t, *J* = 7.0 Hz, 2H, CH_2Ar), 3.92 (q, *J* = 7.0 Hz, 2H, CH_2NH), 4.38-4.54 and 4.65-4.78 (2 m, 5H, CH_2O + CH_2N + $\underline{CH}CH_3$), 7.13-7.48 (m, 4H Ar), 8.08 (s, 1H, H-3), 8.89 (s, 1H, H-6), 9.31 (br s, 1H, NH).
IR (KBr): cm^{-1} 3284 (NH), 1667 (CO).

Ethyl 1-(2-chloropropyl)-4-{[2-(4-methoxyphenyl)ethyl]amino}-1H-pyrazolo[3,4-b]pyridine-5-carboxylate 224f

Yield: 0.23 g, 54%
Mp: 52-53 °C
MW = 416.90
Anal. calcd for $C_{21}H_{25}ClN_4O_3$: C 60.50, H 6.04, N 13.44; found C 60.48, H 6.34, N 13.54.
^{1}H-NMR (200 MHz, DMSO-d6): δ (ppm) 1.40 (t, *J* = 7.0 Hz, 3H, $\underline{CH_3}CH_2$), 1.61 (d, *J* = 6.0 Hz, 3H, $\underline{CH_3}CH$), 3.06 (t, *J* = 7.0 Hz, 2H, CH_2Ar), 3.83 (s, 3H, OCH_3), 3.88 (q, *J* = 7.0 Hz, 2H, CH_2NH), 4.37-4.54 and 4.62-4.74 (2 m, 5H, CH_2O + CH_2N + $\underline{CH}CH_3$), 7.13-7.45 (m, 4H Ar), 8.08 (s, 1H, H-3), 8.89 (s, 1H, H-6), 9.28 (br s, 1H, NH).
IR (KBr): cm^{-1} 3281 (NH), 1668 (CO).

Ethyl 4-[(2-phenylethyl)amino]-1-(2-phenylpropyl)-1H-pyrazolo[3,4-b]pyridine-5-carboxylate 225a

Yield: 0.28 g, 66%

Mp: 109-110 °C

MW = 428.53

Anal. calcd for $C_{26}H_{28}N_4O_2$: C 72.87, H 6.57, N 13.07; found C 72.64, H 6.76, N 12.70.

^{1}H-NMR (200 MHz, $CDCl_3$): δ (ppm) 1.23-1.28 (m, 3H, $\underline{CH_3}CH$), 1.42 (t, *J* = 7.2 Hz, 3H, $\underline{CH_3}CH_2$), 3.08 (t, *J* = 6.8 Hz, 2H, CH_2Ar), 3.57-3.75 (m, 1H, $\underline{CH}CH_3$), 3.95 (q, *J* = 6.8 Hz, 2H, $\underline{CH_2}NH$), 4.37 (q, *J* = 7.2 Hz, 2H, CH_2O), 4.51-4.65 (m, 2H, CH_2N), 7.00-7.30 (m, 10H Ar), 8.03 (s, 1H, H-3), 8.85 (s, 1H, H-6), 9.25 (br s, 1H, NH).

IR (KBr): cm^{-1} 3280 (NH), 1673 (CO).

Ethyl 4-{[2-(4-chlorophenyl)ethyl]amino}-1-(2-phenylpropyl)-1H-pyrazolo[3,4-b]pyridine-5-carboxylate 225b

Yield: 0.28 g, 60%

Mp: 96-97 °C

MW = 462.97

Anal. calcd for $C_{26}H_{27}ClN_4O_2$: C 67.45, H 5.88, N 12.10; found C 67.47, H 6.09, N 12.08.

^{1}H-NMR (200 MHz, $CDCl_3$): δ 1.20-1.27 (m, 3H, $\underline{CH_3}CH$), 1.38 (t, *J* = 7.2 Hz, 3H, $\underline{CH_3}CH_2$), 3.07 (t, *J* = 6.8 Hz, 2H, CH_2Ar), 3.58-3.61 (m, 1H, $\underline{CH}CH_3$), 3.90 (q, *J* = 6.8 Hz, 2H, $\underline{CH_2}NH$), 4.33 (q, *J* = 7.2 Hz, 2H, CH_2O), 4.54-4.60 (m, 2H, CH_2N), 7.15-7.33 (m, 9H Ar), 8.02 (s, 1H, H-3), 8.84 (s, 1H, H-6), 9.26 (br s, 1H, NH).

IR (KBr): cm^{-1} 3279 (NH), 1661 (CO).

Ethyl 4-{[2-(2-fluorophenyl)ethyl]amino}-1-(2-phenylpropyl)-1H-pyrazolo[3,4-b]pyridine-5-carboxylate 225c

Yield: 0.31 g, 69%

Mp: 86-87 °C

MW = 446.52

Anal. calcd for $C_{26}H_{27}FN_4O_2$: C 69.94, H 6.09, N 12.55; found C 70.23, H 6.38, N 12.22.

^{1}H-NMR (200 MHz, $CDCl_3$): δ (ppm) 1.21-1.30 (m, 3H, $\underline{CH_3}CH$), 1.34 (t, *J* = 7.2 Hz, 3H, $\underline{CH_3}CH_2$), 3.04 (t, *J* = 6.8 Hz, 2H, CH_2Ar), 3.55-3.63 (m, 1H, $\underline{CH}CH_3$), 3.85 (q, *J* = 6.8 Hz, 2H, $\underline{CH_2}NH$), 4.32 (q, *J* = 7.2 Hz, 2H, CH_2O), 4.49-4.55 (m, 2H, CH_2N), 7.08-7.29 (m, 9H Ar), 8.05 (s, 1H, H-3), 8.82 (s, 1H, H-6), 9.24 (br s, 1H, NH).
IR (KBr): cm^{-1} 3283 (NH), 1662 (CO).

Ethyl 4-{[2-(3-fluorophenyl)ethyl]amino}-1-(2-phenylpropyl)-1H-pyrazolo[3,4-b]pyridine-5-carboxylate 225d

Yield: 0.32 g, 71%
Mp: 85-86 °C
MW = 446.52
Anal. calcd for $C_{26}H_{27}FN_4O_2$: C 69.94, H 6.09, N 12.55; found C 69.92, H 5.93, N 12.34.
^{1}H-NMR (200 MHz, $CDCl_3$): δ (ppm) 1.20-1.24 (m, 3H, $\underline{CH_3}CH$), 1.33 (t, *J* = 7.2 Hz, 3H, $\underline{CH_3}CH_2$), 3.01 (t, *J* = 6.8 Hz, 2H, CH_2Ar), 3.50-3.59 (m, 1H, $\underline{CH}CH_3$), 3.88 (q, *J* = 6.8 Hz, 2H, $\underline{CH_2}NH$), 4.30 (q, *J* = 7.2 Hz, 2H, CH_2O), 4.50-4.57 (m, 2H, CH_2N), 7.11-7.35 (m, 9H Ar), 8.00 (s, 1H, H-3), 8.77 (s, 1H, H-6), 9.19 (br s, 1H, NH).
IR (KBr): cm^{-1} 3296 (NH), 1674 (CO).

Ethyl 4-{[2-(4-fluorophenyl)ethyl]amino}-1-(2-phenylpropyl)-1H-pyrazolo[3,4-b]pyridine-5-carboxylate 225e

Yield: 0.34 g, 77%
Mp: 93-94 °C
MW = 446.52
Anal. calcd for $C_{26}H_{27}FN_4O_2$: C 69.94, H 6.09, N 12.55; found C 69.78, H 6.33, N 12.19.
^{1}H-NMR (200 MHz, $CDCl_3$): δ (ppm) 1.22-1.28 (m, 3H, $\underline{CH_3}CH$), 1.39 (t, *J* = 7.2 Hz, 3H, $\underline{CH_3}CH_2$), 3.09 (t, *J* = 6.8 Hz, 2H, CH_2Ar), 3.59-3.63 (m, 1H, $\underline{CH}CH_3$), 3.91 (q, *J* = 6.8 Hz, 2H, $\underline{CH_2}NH$), 4.34 (q, *J* = 7.2 Hz, 2H, CH_2O), 4.53-4.60 (m, 2H, CH_2N), 7.10-7.32 (m, 9H Ar), 8.03 (s, 1H, H-3), 8.80 (s, 1H, H-6), 9.23 (br s, 1H, NH).
IR (KBr): cm^{-1} 3282 (NH), 1660 (CO).

Ethyl 4-{[2-(4-methoxyphenyl)ethyl]amino}-1-(2-phenylpropyl)-1H-pyrazolo[3,4-b]pyridine-5-carboxylate 225f

Yield: 0.26 g, 56%

Mp: 99-100 °C

MW = 458.55

Anal. calcd for $C_{27}H_{30}N_4O_3$: C 70.72, H 6.59, N 12.22; found C 71.06, H 6.41, N 11.88.

^{1}H-NMR (200 MHz, $CDCl_3$): δ 1.22-1.27 (m, 3H, $\underline{CH_3}CH$), 1.41 (t, *J* = 7.2 Hz, 3H, $\underline{CH_3}CH_2$), 3.07 (t, *J* = 6.8 Hz, 2H, CH_2Ar), 3.55-3.71 (m, 1H, $\underline{CH}CH_3$), 3.90-4.00 (m, 5H, OCH_3 + $\underline{CH_2}NH$), 4.35 (q, *J* = 7.2 Hz, 2H, CH_2O), 4.50-4.63 (m, 2H, CH_2N), 6.83-7.44 (m, 9H Ar), 8.07 (s, 1H, H-3), 8.86 (s, 1H, H-6), 9.25 (br s, 1H, NH).

IR (KBr): cm^{-1} 3285 (NH), 1661 (CO).

Ethyl 4-{[2-(4-methylphenyl)ethyl]amino}-1-(2-phenylpropyl)-1H-pyrazolo[3,4-b]pyridine-5-carboxylate 225g

Yield: 0.24 g, 55%

Mp: 120-121 °C

MW = 442.55

Anal. calcd for $C_{27}H_{30}N_4O_2$: C 73.28, H 6.83, N 12.66; found C 73.64, H 7.19, N 12.96.

^{1}H-NMR (200 MHz, $CDCl_3$): δ 1.21-1.27 (m, 3H, $\underline{CH_3}CH$), 1.38 (t, *J* = 7.2 Hz, 3H, $\underline{CH_3}CH_2$), 2.35 (s, 3H, CH_3Ar), 3.06 (t, *J* = 6.8 Hz, 2H, CH_2Ar), 3.55-3.60 (m, 1H, $\underline{CH}CH_3$), 3.89 (q, *J* = 6.8 Hz, 2H, $\underline{CH_2}NH$), 4.34 (q, *J* = 7.2 Hz, 2H, CH_2O), 4.52-4.57 (m, 2H, CH_2N), 7.15-7.28 (m, 9H Ar), 8.04 (s, 1H, H-3), 8.84 (s, 1H, H-6), 9.24 (br s, 1H, NH).

IR (KBr): cm^{-1} 3284 (NH), 1663 (CO).

Synthesis of ethyl 4-anilino-1-(2-chloropropyl)-1*H*-pyrazolo[3,4-*b*]pyridine-5-carboxylate 224g

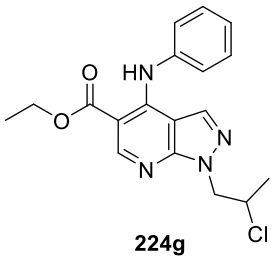

224g

To a solution of intermediate **231a** (0.37 g, 1.22 mmol) in absolute EtOH (5 mL) aniline (0.23 g, 2.44 mmol) was added and the reaction was stirred at reflux for 5 h. The solvent was removed under vacuum, water (40 mL) was added and the mixture was extracted with CH_2Cl_2 (40 mL x 3). The organic phase was washed with water (80 mL), dried over Na_2SO_4, filtered and concentrated under reduced pressure. The obtained solid was filtered using Et_2O to get the final desired compound **224g** as a white solid.

Yield: 0.20 g, 46%

Mp: 126-128 °C

MW = 358.82

Anal. calcd for $C_{18}H_{19}ClN_4O_2$: C 60.25, H 5.34, N 15.61; found C 60.16, H 5.70, N 15.24.

^{1}H-NMR (200 MHz, DMSO-d6): 1.44 (t, *J* = 7.0 Hz, 3H, $\underline{CH_3}CH_2$), 1.60 (d, *J* = 6.0 Hz, 3H, $\underline{CH_3}CH$), 4.41 (q, *J* = 7.2 Hz, 2H, CH_2O), 4.62-4.94 (m, 3H, CH_2N + $\underline{CH}CH_3$), 6.67 (s, 1H, H-3), 7.25-7.45 (m, 5H Ar), 8.96 (s, 1H, H-6), 9.57 (br s, 1H, NH).

IR (KBr): cm^{-1} 3261 (NH), 1664 (CO).

Synthesis of 2,2'-dimethoxy-3-phenyl-1,1'-binaphthalene 248

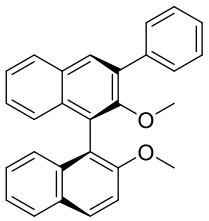

248

A schlenk tube was charged with the opportune *in-house* naphtyl intermediate (1.00 g, 2.54 mmol), phenylboronic acid (0.47 g, 3.82 mmol) and $Ba(OH)_2$ octahydrate (1.30 g, 7.63 mmol). In the glovebox, $Pd(PPh_3)_4$ (300 mg, 0.25 mmol) was added. The tube was sealed with a rubber septum and taken out of the glovebox. The tube was placed under argon and dioxane (5 mL) and water (1.25 mL) were added sequentially *via* syringe. The septum was replaced by a glass lid and the reaction mixture stirred at 100 °C for 24 h. Then, the reaction was cooled to room temperature and filtered over celite. Dioxane was removed under vacuum and the residue was extracted with CH_2Cl_2 (30 mL x 3). The combined organic phase was washed with saturated NaCl solution (90 mL), dried over Na_2SO_4, filtered and concentrated under reduced pressure. The crude product was purified by column chromatography using PE (bp 40-60 °C)/CH_2Cl_2 (7:3) as eluent, to obtain compound **248** as a white solid.

Yield: 0.42 g, 42%

MW = 390.47

$C_{28}H_{22}O_2$

^{1}H-NMR (500 MHz, $CDCl_3$): δ (ppm) 3.10 and 3.80 (2 s, 3H, CH_3), 7.13-7.15, 7.20-7.39 and 7.43-7.47 (3 m, 10H naph), 7.75 (d, *J* = 5.0 Hz, 2H Ar), 7.80-7.90 and 7.95-7.99 (2 m, 4H, 3H Ar + 1H naph).

Synthesis of 3-phenyl-1,1'-binaphthalene-2,2'-diol 249

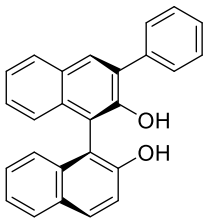

249

To a solution of compound **248** (0.50 g, 1.28 mmol) in CH_2Cl_2 (40 mL) at 0 °C under argon atmosphere, BBr_3 (0.30 mL, 3.08 mmol) was added dropwise. The reaction was allowed to warm up and was stirred at room temperature overnight. The mixture was cooled down to 0 °C and was quenched with water (75 mL). The organic phase was washed with water and saturated NaCl solution (40 mL), dried over Na_2SO_4, filtered and concentrated under reduced pressure. The crude product was purified by column chromatography using PE (bp 40-60 °C)/AcOEt as eluent with a gradient elution (9:1 → 8:2), obtaining the desired compound as a white solid.

Yield: 0.42 g, 90%

MW = 362.42

$C_{26}H_{18}O_2$

^{1}H-NMR (500 MHz, $CDCl_3$): δ (ppm) 5.07 and 5.29 (2 br s, 2H, 2 OH), 7.10-7.12, 7.17-7.38 and 7.45-7.47 (3 m, 10H naph), 7.70 (d, *J* = 5.0 Hz, 2H Ar), 7.82-7.90 (m, 3H Ar), 7.97 (s, 1H naph).

Synthesis of 3'-phenyl-2'-{[(trifluoromethyl)sulfonyl]oxy}-1,1'-binaphthalen-2-yl trifluoromethanesulfonate 250

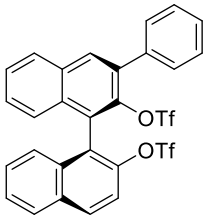

250

To a solution of compound **249** (0.5 g, 1.38 mmol) and pyridine (0.45 mL, 5.52 mmol) in CH_2Cl_2 (10 mL) at 0 °C under argon atmosphere, triflic anhydride (0.70 mL, 4.14 mmol) was added dropwise. The reaction was allowed to warm up and was stirred at room temperature overnight. The mixture was cooled down to 0 °C, quenched with 1 M HCl (10 mL) and diluted with CH_2Cl_2 (20 mL). The organic phase was washed with 1 M HCl (10 mL x 2) and saturated NaCl solution (10 mL), dried over Na_2SO_4, filtered and concentrated under reduced pressure. The crude was purified by column chromatography using PE (bp 40-60 °C)/AcOEt (9:1) as eluent, to obtain compound **250** as a white solid.

Yield: 0.66 g, 76%

MW = 626.54

$C_{28}H_{16}F_6O_6S_2$

^{1}H-NMR (500 MHz, $CDCl_3$): δ (ppm) 7.21-7.23, 7.34-7.57 and 7.62-7.63 (3 m, 12H, 9H naph + 3H Ar), 7.98 (d, *J* = 5.0 Hz, 2H Ar), 8.09 (s, 1H naph), 8.12-8.14 (m, 1H naph).

^{19}F-NMR (500 MHz, $CDCl_3$): -74.74 and -74.51 (2 s, 3F, CF_3).

Synthesis of 2'-[bis(3,5-dimethylphenyl)phosphoryl]-3-phenyl-1,1'-binaphthalen-2-yl trifluoromethanesulfonate 251

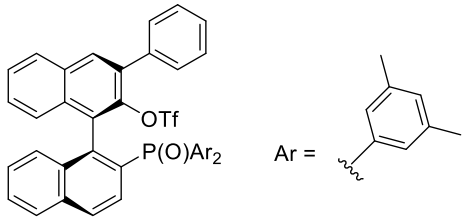

251

A schlenk tube was charged with compound **250** (0.50 g, 0.80 mmol) and the phosphine oxide (0.44 g, 1.60 mmol). In the glovebox, $Pd(OAc)_2$ (17.94 mg, 0.08 mmol) and Dppb (33.97 mg, 0.08 mmol) were added. The tube was sealed with a rubber septum and taken out of the glovebox. Anhydrous DMSO (4 mL) and DIPEA (0.55 mL, 3.20 mmol) were added sequentially *via* syringe. The rubber septum was replaced by a glass stopper and the reaction mixture was stirred at 100 °C for 12 h. After cooling down at room temperature, anhydrous DMSO was partially removed under vacuum. The residue was diluted in AcOEt (30 mL) and washed with a mixture water/saturated NaCl solution (1:1) (10 mL x 3). The organic phase was dried over Na_2SO_4, filtered and concentrated under reduced pressure. The crude product was purified by column chromatography using PE (bp 40-60 °C)/AcOEt as eluent, with a gradient elution (7:3 → 6:4), to obtain the desired compound as a white solid.

Yield: 0.53 g, 90%

MW = 734.76

$C_{43}H_{34}F_3O_4PS$

^{1}H-NMR (500 MHz, $CDCl_3$): δ (ppm) 2.04 and 2.29 (2 s, 3H, CH_3), 6.74 (s, 1H Ar), 6.90-6.95, 7.12-7.17, 7.26-7.49, 7.55-7.57, 7.66-7.72 and 7.78-7.80 (6 m, 18H, 10H Ar + 8H naph) 7.89 (s, 1H naph), 7.94-7.95 and 8.01-8.03 (2 m, 2H naph).

^{19}F-NMR (500 MHz, $CDCl_3$): -74.64 (s, 3F, CF_3).

^{31}P-NMR (500 MHz, $CDCl_3$): 27.31 (s, 1P, PO).

Synthesis of 2'-[bis(3,5-dimethylphenyl)phosphoryl]-3-phenyl-1,1'-binaphthalen-2-ol 247

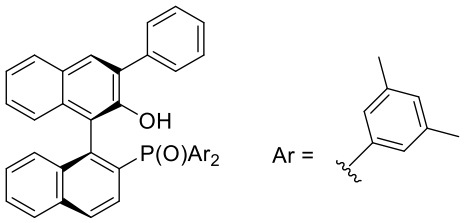

247

Compound **251** (0.50 g, 0.68 mmol), 3 M NaOH solution (1.40 mL, 4.08 mmol), dioxane (2.80 mL) and MeOH (1.40 mL) were added to a flask and the mixture was stirred at room temperature for 12 h. Then, the reaction was acidified by the addition of a few drops of concentrated HCl and extracted with AcOEt (30 mL x 3). The organic phase was dried over Na_2SO_4, filtered and concentrated under reduced pressure. The crude was purified by column chromatography using PE (bp 40-60 °C)/AcOEt (8:2) as eluent, to get compound **247** as a white solid.

Yield: 0.29 g, 70%

MW = 602.70

$C_{42}H_{35}O_2P$

^{1}H-NMR (500 MHz, $CDCl_3$): δ (ppm) 1.88 and 2.37 (2 s, 3H, CH_3), 6.35-6.40, 6.81-6.84 and 6.94-6.98 (3 m, 5H Ar), 7.09-7.13, 7.21-7.23, 7.34-7.38 and 7.43-7.59 (4 m, 12H, 6H Ar + 6H naph), 7.70 (s, 1H naph), 7.81-7.84 and 7.89-7.93 (2 m, 4H naph), 8.85 (br s, 1H, OH).

Procedures for the synthesis of racemic and enantioenriched compounds 252 and 253

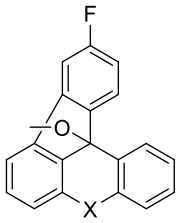

252 X = $C(CH_3)_2$
253 X = O

General procedure for the synthesis of racemic compounds 252a and 253a

An oven-dried pyrex tube was charged with the opportune *in-house* substrate (1.00 mmol). In the glovebox, Cs_2CO_3 (0.49 g, 1.50 mmol), $PCy{\cdot}HBF_4$ (36.80 mg, 0.10 mmol), CsOPiv (0.07 g, 0.30 mmol), $Pd(OAc)_2$ (11.25 mg, 0.05 mmol) and molecular sieves (1.50 mmol) were added. The flask was sealed and taken out of the glovebox. Anhydrous xylenes (10 mL) was added, the rubber septum was replaced by a glass stopper and the reaction was stirred at 140 °C for 16 h. The mixture was allowed to cool to room temperature, diluted with AcOEt (20 mL) and filtrated through a pad of celite. The filtrate was concentrated under reduced pressure and purified by column chromatography, using PE (bp 40-60 °C)/AcOEt (98:2) as eluent.

General procedure for the synthesis of enantioenriched compounds 252b and 253b

An oven-dried J-Young tube was charged with the opportune *in-house* substrate (1.00 mmol). In the glovebox, Cs_2CO_3 (0.49 g, 1.50 mmol), chiral bifunctional ligand (56.90 mg, 0.10 mmol), $Pd(dba)_3{\cdot}CHCl_3$ (26.00 mg, 2.50 mmol%) and molecular sieves (2.00 mmol) were added. The tube was sealed, taken out of the glovebox, and anhydrous and degassed DME (10 mL) was added under argon flux. The reaction mixture was degassed by three freeze-pump-thaw cycles and heated at 140 °C for 24 h. Then, the reaction was cooled to room temperature, diluted with AcOEt (20 mL) and filtrated through a pad of celite. The crude was purified with a column chromatography, using PE (bp 40-60 °C)/AcOEt (98:2) as eluent (**253b**).

3-fluoro-12b-methoxy-8,8-dimethyl-8,12b-dihydrobenzo[a]aceanthrylene 252a (racemic) and 253b (enantioenriched)

Yield: 0.29 g, 88% (racemic); 0.17 g, 50% (enantioenriched)

MW = 330.39

$C_{23}H_{19}FO$

^{1}H-NMR (500 MHz, $CDCl_3$): δ (ppm) 1.82 and 1.87 (2 s, 3H, CH_3), 2.71 (s, 3H, OCH_3), 7.14 (ddd, *J* = 8.0 Hz, *J* = 1.2 Hz, *J* = 0.6 Hz, 1H Ar), 7.29 (ddd, *J* = 7.6 Hz, *J* = 7.6 Hz, *J* = 1.3 Hz, 1H Ar), 7.34-7.43 and 7.48-7.51 (m, 5H Ar), 7.69 (dd, *J* = 8.0 Hz, *J* = 0.6 Hz, 1H Ar), 7.93-7.97 (m, 2H Ar)

GS-MS: 299 (330-OCH_3), 284 (299-CH_3).

252b e.r.77:23 (chiral HPLC)

10-fluoro-12b-methoxy-12bH-indeno[1,2,3-kl]xanthene 253a (racemic) and 253b (enantioenriched)

MW = 304.31

$C_{20}H_{13}FO_2$

GS-MS (on the crude): 273 (304-OCH_3).

Synthesis of 2-[imino(2-methylphenyl)methyl]-3-methylaniline 257

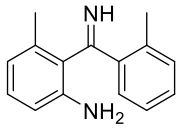

257

To a cold (-10 °C) solution of *m*-toluidine (3.00 g, 28.00 mmol) in anhydrous toluene (35 mL), BCl_3 (1 M in heptane, 5.32 mL, 33.60 mmol) was slowly added. After the addition was complete, the cooling bath was removed and the mixture was stirred at room temperature for 1 h. Then, a solution of *o*-tolunitrile (3.65 mL, 30.80 mmol) in anhydrous toluene and $AlCl_3$ (4.11 g, 30.80 mmol) were added. The mixture was stirred at reflux under N_2 atmosphere for 24 h. The reaction was cooled and quenched by the addition of 18 N H_2SO_4 (60 mL), with vigorous stirring. The organic layer was separated and washed with additional 18 N H_2SO_4 (60 mL). The acid extracts were combined and back-washed once with Et_2O (120 mL). The acid layer was cooled to 5 °C before the pH was adjusted to ~ 10 by treatment with 20% NaOH solution. The aqueous layer was extracted with Et_2O (150 mL) and the organic phase was washed with water (150 mL x 3), filtered and concentrated under reduced pressure. The crude was purified with column chromatography using CH_2Cl_2/MeOH (98:2) as eluent, to obtain immine **257** as a brownish solid.

Yield: 2.51 g, 40%

MW = 224.30

$C_{15}H_{16}N_2$

^{1}H-NMR (400 MHz, $CDCl_3$): δ (ppm) 2.32 and 2.49 (2 s, 3H, CH_3), 6.82-6.85, 7.19-7.30 and 7.43-7.44 (3 m, 7H Ar).

Synthesis of 4,7-dimethyl-3a,4,7,7a-tetrahydro-4,7-epoxy-2-benzofuran-1,3-dione 258

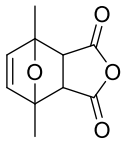

258

To a stirred suspension of maleic anhydride (1.00 g, 10.20 mmol) in anhydrous Et_2O (1.00 mL) at room temperature, dimethylfurane (1.09 mL, 10.20 mmol) was added and the mixture was stirred overnight. The resulting crystals were filtered and washed with anhydrous Et_2O. The mother liquid was concentrated and the second crop of crystals were combined with those obtained previously, getting endoxide **258** as a brown solid.

Yield: 0.83 g, 42%

MW = 194.18

$C_{10}H_{10}O_4$

^{1}H-NMR (400 MHz, $CDCl_3$): δ (ppm) 1.77 (s, 6H, 2 CH_3), 3.16 (s, 2H, 2 CH), 6.35 (s, 2H, CH=CH).

Synthesis of 4,7-dimethyl-2-benzofuran-1,3-dione 259

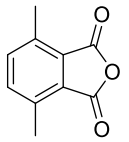

259

Endoxide **258** (4.00 g, 20.00 mmol) was added in small portions to concentrated H_2SO_4 (40 mL) cooled at -6 °C. The mixture was stirred vigorously, not allowing the temperature to rise above 0 °C. After all the endoxide was added and the mixture became orange in colour, it was poured slowly into crushed ice. The resulting white crystals were collected and washed with ice-water. The crystals were then dissolved in a solution 25 M NaOH, and AcOH (5 mL) was added to the solution. The solution was filtered to remove the insoluble materials and acidified with 36% HCl (3 mL). The resulting precipitate was collected and washed with water until the washing was neutral, to obtain compound **259** as a white solid.

Yield: 1.45 g, 41%

MW = 176.17

$C_{10}H_8O_3$

^{1}H-NMR (400 MHz, $CDCl_3$): δ (ppm) 2.67 (s, 6H, 2 CH_3), 7.50 (s, 2H Ar).

Synthesis of (2,5-dimethylphenyl)magnesium bromide 260

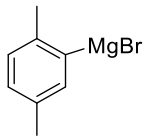

260

In a two-necks flask filled with Mg powder (0.39 g, 16.00 mmol) and placed under argon flow, anhydrous Et_2O (15 mL) was added. Then, bromo-2,5-dimethylbenzene (2.24 mL, 16.00 mmol) was added dropwise and the reaction was stirred at reflux for 1 h. The obtained Grignard **260** was not isolated but used immediately in the next reaction.

MW = 209.37

Synthesis of 2-(2,5-dimethylbenzoyl)-3,6-dimethylbenzoic acid 261

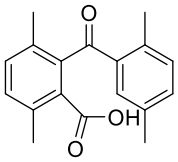

261

To an ice-cold Et_2O solution of Grignard **260** (3.40 g, 16.24 mmol), the solution of compound **259** (2.38 g, 13.53 mmol) in toluene (33 mL) was added dropwise. The mixture was stirred at room temperature overnight. Then, the reaction was quenched with a saturated NH_4Cl solution (40 mL) and extracted with AcOEt (40 mL x 3). The organic phase was dried over Na_2SO_4, filtered and concentrated under reduced pressure. The crude product was purified

with column chromatography, using PE (bp 40-60 °C)/AcOEt as eluent, with a gradient elution (7:3 → 6:4), to obtain compound **261** as a white solid.

Yield: 2.33 g, 61%

MW = 282.33

$C_{18}H_{18}O_3$

^{1}H-NMR (400 MHz, $CDCl_3$): δ (ppm) 2.07, 2.10, 2.31 and 2.62 (4 s, 3H, CH_3), 7.03, 7.08, 7.24, 7.29 (4 d, *J* = 8.0 Hz, 1H Ar), 7.42 (s, 1H Ar).

Synthesis of 3-(2,5-dimethylphenyl)-4,7-dimethyl-2-benzofuran-1(3*H*)-one 262

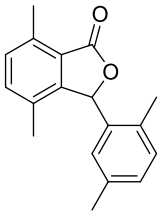

262

To a well-stirred solution of compound **261** (2.00 g, 7.08 mmol) in 10% NaOH (220 mL) heated at reflux, zinc dust (7.52 g, 115.00 mmol) was added over a period of 48 h. The mixture was refluxed for an additional 48 h and then filtered. The filter cake was washed with 10% NaOH and with boiling water. The treatment of the filter cake with boiling ethanol, followed by concentration under reduced pressure gave compound **262** as white needles, and also the acidification of the filtrates with concentrated HCl and the extraction with toluene gave compound **262**, instead of the desired one.

Yield: 1.57 g, 83%

MW = 266.33

$C_{18}H_{18}O_2$

^{1}H-NMR (400 MHz, $CDCl_3$): δ (ppm) 1.96, 2.18, 2.45 and 2.72 (4 s, 3H, CH_3), 6.50 (s, 1H, CH), 6.52 (s, 1H Ar), 7.05, 7.12, 7.24 and 7.30 (4 d, *J* = 8.0 Hz, 1H Ar).

Synthesis of 2-hydroxy-6-methylbenzoic acid 263

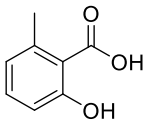

263

A solution of 2-amino-6-methylbenzoic acid (5.00 g, 6.62 mmol) and 25% H_2SO_4 (50 mL) was stirred until the amino acid dissolved. Then, the reaction was cooled to 0 °C and a solution of $NaNO_2$ (3.00 g, 8.70 mmol) in 50 mL of water was added dropwise. After stirring 1 h at 0 °C, the diazonium salt was decomposed by slowly adding the reaction mixture to a boiling solution of H_2SO_4 (20 mL) in 200 mL of water. The solution was cooled to room temperature and then to 0 °C before filtration. Recrystallization from boiling water with decolorizing carbon gave compound **263** as light yellow needles.

Yield: 0.69 g, 69%

MW = 152.15

$C_8H_8O_3$

^{1}H-NMR (400 MHz, $CDCl_3$): δ (ppm) 2.63 (s, 3H, CH_3), 6.77 and 6.87 (2 d, *J* = 8.0 Hz, 1H Ar), 7.35 (t, *J* = 8.0 Hz, 1H Ar), 11.03 (br s, 1H, OH).

Synthesis of benzyl 2-(benzyloxy)-6-methylbenzoate 264

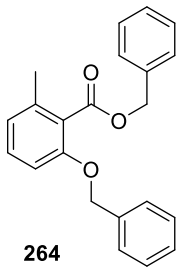

264

A two-phase mixture of compound **263** (2.00 g, 13.14 mmol), NaOH (1.58 g, 39.43 mmol), benzyl bromide (4.69 mL, 39.43 mmol) and tetrabutylammonium bromide (0.42 g, 1.31 mmol) in water (10 mL) and CH_2Cl_2 (10 mL) was stirred at room temperature for 24 h. The

residue was diluted with water and extracted with AcOEt (30 mL x 3). After a column chromatography using PE (bp 40-60 °C)/AcOEt (95:5) as eluent, compound **264** was obtained as a white solid.

Yield: 2.62 g, 60%

MW = 332.29

$C_{22}H_{20}O_3$

^{1}H-NMR (400 MHz, $CDCl_3$): δ (ppm) 2.29 (s, 3H, CH_3), 5.09 and 5.36 (2 s, 2H, CH_2), 6.78-6.81 (m, 2H Ar), 7.20 (t, *J* = 8.0 Hz, 1H Ar), 7.18-7.40 (m, 10H Ar).

Synthesis of 2-(benzyloxy)-6-methylbenzoic acid 265

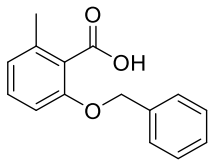

265

A flask containing compound **264** (2.00 g, 6.02 mmol), LiOH (0.43 g, 18.06 mmol) and NaOH (0.72 g, 18.06 mmol) in a mixture of H_2O/THF/MeOH (15:15:15 mL) was stirred at room temperature overnight. Then, the reaction was acidified by addition of few drops of concentrated HCl and extracted with AcOEt (50 mL x 3). The organic phase was dried over Na_2SO_4, filtered and concentrated under reduced pressure. The residue was purified by column chromatography, using cyclohexane/AcOEt as eluent with a gradient elution (6:4 → 1:1), to afford the desired compound as a clear oil.

Yield: 0.58 g, 40%

MW = 242.27

$C_{15}H_{14}O_3$

^{1}H-NMR (400 MHz, $CDCl_3$): δ (ppm) 2.49 (s, 3H, CH_3), 5.18 (s, 2H, CH_2), 6.88-7.00 and 7.26-7.44 (2 m, 8H Ar).

Synthesis of 1-(benzyloxy)-3-methylbenzene 266

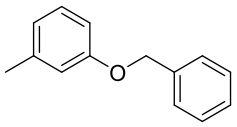

266

To a well-stirred solution of *m*-cresol (1.00 g, 9.25 mmol) dissolved in DMF (8 mL), K_2CO_3 (0.26 g, 18.49 mmol) was added. After 2 h, benzyl bromide (1.65 mL, 13.87 mmol) was added dropwise over a period of 45 minutes and the reaction was stirred at 60 °C for 12 h. The reaction mixture was poured on ice-water (35 mL) and extracted with AcOEt (30 mL x 3). The organic phase was washed with saturated NaCl solution, dried over Na_2SO_4, filtered and concentrated under reduced pressure. After the purification of the crude with a column chromatography, using cyclohexane/AcOEt as eluent with a gradient elution (98:2 → 95:5), compound **266** was obtained as a clear oil.

Yield: 1.56 g, 85%

MW = 198.26

$C_{14}H_{14}O$

^{1}H-NMR (400 MHz, $CDCl_3$): δ (ppm) 2.34 (s, 3H, CH_3), 5.06 (s, 2H, CH_2), 6.78-6.83 (m, 3H Ar), 7.18 (t, *J* = 8.0 Hz, 1H Ar), 7.31-7.46 (m, 5H Ar).

Synthesis of bis(2-(benzyloxy)-6-methylphenyl)methanone 267

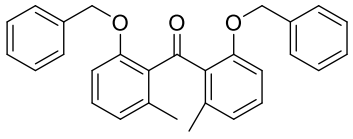

267

To a solution of compound **265** (1.00 g, 4.13 mmol) in ethanol-free $CHCl_3$ (45 mL), compound **266** (2.05 g, 10.32 mmol), TFAA (8.32 mL, 59.85 mmol) and TFA (1.59 mL, 20.64 mmol) were added. The reaction mixture was stirred at reflux under argon overnight. The solvent was removed under vacuum and the residual oil was extracted with Et_2O (50 mL

x 3), washed with diluted aqueous KOH (150 mL) and saturated NaCl solution (150 mL), dried over Na_2SO_4 and concentrated under reduced pressure. The crude was purified by column chromatography, using cyclohexane/AcOEt (9:1) as eluent with a gradient elution (10:0 → 9:1), to obtain compound **267** as clear oil.

Yield: 1.19 g, 68%

MW = 422.51

$C_{29}H_{26}O_3$

^{1}H-NMR (400 MHz, $CDCl_3$): δ (ppm) 2.21 and 2.63 (2 s, 3H, CH_3), 4.95 and 5.10 (2 s, 2H, CH_2), 6.70 (dd, *J* = 8.0 Hz, 1H Ar), 6.78 (d, *J* = 8.0 Hz, 1H Ar), 6.84-6.88, 7.01-7.04, 7.18-7.22 and 7.33-7.44 (4 m, 14H Ar).

Synthesis of bis(2-hydroxy-6-methylphenyl)methanone 268

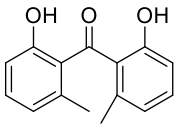

268

A solution of compound **267** (1.00 g, 2.37 mmol) in AcOEt (28 mL) and absolute EtOH (44 mL) was hydrogenated overnight at room temperature and atmospheric pressure over 10% Pd/C (0.19 g, 1.77 mmol). The reaction was filtered over celite and concentrated under reduced pressure, to give the clean product **268** as a brown oil.

Yield: 0.57 g, quantitative

MW = 242.27

$C_{15}H_{14}O_3$

^{1}H-NMR (400 MHz, $CDCl_3$): δ (ppm) 1.90 and 2.41 (2 s, 3H, CH_3), 6.65 and 6.69 (2 d, *J* = 8.0 Hz, 1H Ar), 6.72-6.75 (m, 1H Ar), 6.87 and 7.17 (2 d, *J* = 8.0 Hz, 1H Ar), 7.28-7.30 (m, 1H Ar).

Synthesis of 2,4-dihydroxy-6-methylbenzaldehyde 269

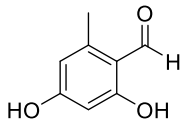

269

To a solution of $POCl_3$ (4.51 mL, 48.33 mmol) in anhydrous DMF (13 mL) a solution of 3,5-dihydroxy toluene (3.00 g, 24.17 mmol) in the same solvent (12 mL) was slowly added. The reaction was stirred at room temperature for 12 h. Then, it was cooled to 0 °C, treated with ice water and then with 10% NaOH to pH ~ 10. The resulting mixture was heated at reflux for 30 minutes and then acidified to pH ~ 3 with concentrated HCl. The precipitate was collected by filtration and washed with water, to get the desired product as a yellow powder.

Yield: 4.41 g, 60%

MW = 152.15

$C_8H_8O_3$

^{1}H-NMR (400 MHz, $CDCl_3$): δ (ppm) 2.46 (s, 3H, CH_3), 6.13 and 6.21 (2 s, 1H Ar), 10.06 (br s, 1H, OH), 10.68 (s, 1H, CHO), 12.06 (br s, 1H, OH).

Synthesis of 2,4-bis(benzyloxy)-6-methylbenzaldehyde 270

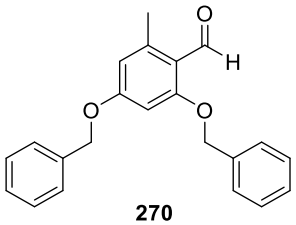

270

To a solution of compound **269** (2.00 g, 13.15 mmol) and benzyl bromide (5.62 g, 32.86 mmol) in acetone (75 mL), K_2CO_3 (7.27 g, 52.58 mmol) was added. The mixture was stirred at reflux for 2.5 h. Then, the reaction was filtered and the solvent evaporated under reduced pressure. The crude was purified by column chromatography using pentane/Et_2O (8:2) as eluent, to obtain the desired compound as a pale green solid.

Yield: 3.54 g, 81%

MW = 332.39

$C_{22}H_{20}O_3$

^{1}H-NMR (400 MHz, $CDCl_3$): 2.60 (s, 3H, CH_3), 5.10 and 5.12 (2 s, 2H, CH_2), 6.42-6.48 and 7.34-7.42 (2 m, 6H Ar), 10.61 (s, 1H, CHO).

Synthesis of 2,4-bis(benzyloxy)-6-methylbenzoic acid 271

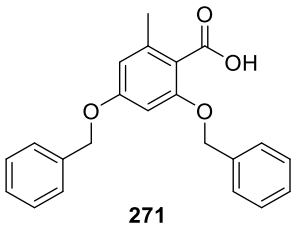

271

A mixture of compound **270** (3.00 g, 9.03 mmol) in *t*-BuOH (112 mL) under nitrogen was sonicated at 40 °C until it was fully dissolved. Subsequently, 2-methyl-2-butene (9.56 mL, 90.30 mmol) and a solution of $NaClO_2$ (1.96 g, 21.66 mmol) and NaH_2PO_4 (6.50 g, 54.15 mmol) in water (30 mL) were added dropwise. The reaction was stirred under nitrogen at room temperature overnight. Then, the mixture was concentrated under vacuum and extracted with CH_2Cl_2 (30 mL x 3) and 10% HCl (30 mL). The organic phase was washed with saturated NaCl solution (90 mL), dried over Na_2SO_4, filtered and concentrated under reduced pressure, to give the pure compound **271** as a light yellow solid.

Yield: 3.15 g, quantitative

MW = 348.39

$C_{22}H_{20}O_4$

NMR (400 MHz, $CDCl_3$): 2.60 (s, 3H, CH_3), 5.09 and 5.15 (2 s, 2H, CH_2), 6.54-6.56 and 7.34-7.41 (2 m, 12H Ar).

Synthesis of 1,3-bis(benzyloxy)-5-methylbenzene 272

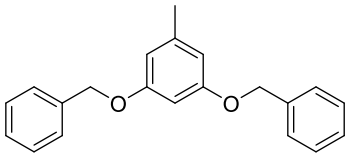

272

To a well-stirred solution of orcinol (1.00 g, 8.06 mmol) in DMF (8 mL), K_2CO_3 (4.45 g, 32.23 mmol) was added. After 2 h, benzyl bromide (2.87 mL, 24.17 mmol) was added dropwise over a period of 45 minutes and the reaction was stirred at 60 °C for 12 h. The reaction mixture was poured on ice-water (100 mL) and extracted with AcOEt (50 mL x 3). The organic phase was washed with saturated NaCl solution, dried over Na_2SO_4, filtered and concentrated under reduced pressure. The crude was purified by column chromatography, using PE (bp 40-60 °C)/AcOEt (98:2) as eluent, to obtain compound **272** as a clear oil.

Yield: 1.47 g, 60%

MW = 304.38

$C_{21}H_{20}O_2$

^{1}H-NMR (400 MHz, $CDCl_3$) 2.31 (s, 3H, CH_3), 5.02 (s, 4H, 2 CH_2), 6.45 (s, 3H Ar), 7.33-7.44 (m, 10H Ar).

Synthesis of bis(2,4-bis(benzyloxy)-6-methylphenyl)methanone 273

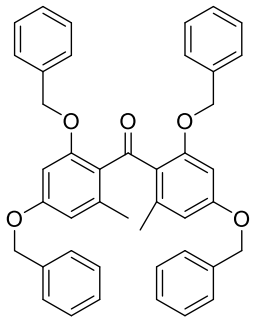

273

To a solution of compound **271** (1.50 g, 4.31 mmol) in ethanol-free $CHCl_3$ (70 mL), compound **272** (3.25 g, 10.68 mmol), TFAA (8.68 mL, 62.43 mmol) and TFA (1.66 mL, 21.53 mmol) were added and the reaction mixture was stirred at reflux under nitrogen overnight. The solvent was removed under vacuum and the residual oil extracted with Et_2O (30 mL x 3), washed with dilute aqueous KOH and saturated NaCl solution (90 mL), dried over Na_2SO_4 and concentrated under reduced pressure. The crude was purified by column chromatography using PE (bp 40-60 °C)/AcOEt (98:2) as eluent, to obtain compound **273** as a yellowish oil.

Yield: 1.42 g, 52%

MW = 634.76

$C_{43}H_{38}O_5$

^{1}H-NMR (400 MHz, $CDCl_3$) 2.26 (s, 6H, 2 CH_3), 5.04 and 5.06 (2 s, 4H, 2 CH_2), 6.45 and 6.48 (2 s, 2H Ar), 7.30-7.41 (m, 20H Ar).

Synthesis of bis(2,4-dihydroxy-6-methylphenyl)methanone 274

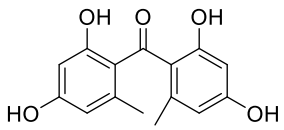

274

A solution of compound **273** (1.00 g, 1.58 mmol) in AcOEt (28 mL) and absolute EtOH (44 mL) was hydrogenated overnight at room temperature and atmospheric pressure over 10% Pd/C (0.38 g, 3.57 mmol). The reaction was filtered over celite and concentrated under reduced pressure to give the clean product **274** as a yellow oil.

Yield: 0.43 g, quantitative

MW = 274.27

$C_{15}H_{14}O_5$

^{1}H-NMR (400 MHz) 2.47 (2 s, 3H, CH_3), 6.30 (s, 4H Ar).

BIBLIOGRAPHY

1. Edwards, R. A., Rower, F. Viral metagenomics. *Nat Rev Microbiol.*, 3 (6), 504-510 (**2005**).
2. Roberts, P. C., Lamb, R. A., Compans, R.W. The M1 and M2 proteins of influenza A virus are important determinants in filamentous particle formation. *Virology*, 240 (1), 127-137 (**1998**).
3. Bourmakina, S. V., García-Sastre A. Reverse genetics studies on the filamentous morphology of influenza A virus. *J Gen Virol*., 84 (3), 517-527 (**2003**).
4. Elleman, C. J., Barclay, W. S. The M1 matrix protein controls the filamentous phenotype of influenza A virus. *Virology*, 30, 321(1), 144-153 (**2004**).
5. Burleigh, L. M., Calder, L. J., Skehel, J. J., Steinhauer, D. A. Influenza a viruses with mutations in the m1 helix six domain display a wide variety of morphological phenotypes. *J Virol*., 79 (2), 1262-1270 (**2005**).
6. Bialas, K. M., Desmet, E. A., Takimoto, T. Specific residues in the 2009 H1N1 swine-origin influenza matrix protein influence virion morphology and efficiency of viral spread in vitro. *PLoS One*, 7 (11), e50595 (**2012**).
7. Campbell, P. J., Kyriakis, C. S., Marshall, N., Suppiah, S., Seladi-Schulman, J., Danzy, S., Lowen, A. C., Steel, J. Residue 41 of the Eurasian avian-like swine influenza a virus matrix protein modulates virion filament length and efficiency of contact transmission. *J Virol*., 88 (13), 7569-7577 (**2014**).
8. Seladi-Schulman, J., Steel, J., Lowen, A. C. Spherical influenza viruses have a fitness advantage in embryonated eggs, while filament-producing strains are selected in vivo. *J Virol*., 87 (24), 13343-13353 (**2013**).
9. Seladi-Schulman, J., Campbell, P. J., Suppiah, S., Steel, J., Lowen, A. C. Filament-producing mutants of influenza A/Puerto Rico/8/1934 (H1N1) virus have higher neuraminidase activities than the spherical wild-type. *PLoS One*, 9 (11), e112462 (**2014**).
10. Baltimore D. Expression of animal virus genomes. *Bacteriol Rev.*, (3), 235-241 (**1971**).
11. Adams, M. J., Lefkowitz, E. J., King, A. M. Q., Harrach, B., Harrison, R. L., Knowles, N. J., Kropinski, A. M., Krupovic, M., Kuhn, J. H., Mushegian, A. R., Nibert, M., Sabanadzovic, S., Sanfaçon, H., Siddell, S. G., Simmonds, P., Varsani, A., Zerbini, F. M., Gorbalenya, A. E., Davison, A. J. Changes to taxonomy and the International Code of

Virus Classification and Nomenclature ratified by the International Committee on Taxonomy of Viruses (2017). *Arch Virol.*, 162 (8), 2505-2538 (**2017**).

12. https://talk.ictvonline.org/.
13. Hause, B. M., Collin, E. A., Liu, R., Huang, B., Sheng, Z., Lu, W., Wang, D., Nelson, E. A., Li, F. Characterization of a novel influenza virus in cattle and Swine: proposal for a new genus in the Orthomyxoviridae family. *MBio.*, 5 (2), e00031-00014 (**2014**).
14. Couch, R. B. Orthomyxoviruses. Baron S, editor. Medical Microbiology. 4th edition. Galveston (TX): University of Texas Medical Branch at Galveston, chapter 58 (**1996**).
15. Fodor, E. The RNA polymerase of influenza a virus: mechanisms of viral transcription and replication. *Acta Virol*., 57 (2), 113-122 (**2013**).
16. Eisfeld, A. J., Neumann, G., Kawaoka, Y. At the centre: influenza A virus ribonucleoproteins. *Nat Rev Microbiol*., 13 (1), 28-41 (**2015**).
17. https://www.cdc.gov/flu/about/viruses/types.htm.
18. Joseph, U., Su, Y. C., Vijaykrishna, D., Smith, G. J. The ecology and adaptive evolution of influenza A interspecies transmission. *Influenza Other Respir Viruses*, 11 (1), 74-84 (**2017**).
19. Stevaert, A., Naesens, L. The Influenza Virus Polymerase Complex: An Update on Its Structure, Functions, and Significance for Antiviral Drug Design. *Med Res Rev*., 36 (6), 1127-1173 (**2016**).
20. https://www.ncbi.nlm.nih.gov/books/NBK459363/.
21. Tong. S., Zhu, X., Li, Y., Shi, M., Zhang, J., Bourgeois, M., Yang, H., Chen, X., Recuenco, S., Gomez, J., Chen, L. M., Johnson, A., Tao, Y., Dreyfus, C., Yu, W., McBride, R., Carney, P. J., Gilbert, A. T., Chang, J., Guo, Z., Davis, C. T., Paulson, J. C., Stevens, J., Rupprecht, C. E., Holmes, E. C., Wilson, I. A., Donis, R. O. New world bats harbor diverse influenza A viruses. *PLoS Pathog*., 9 (10), e1003657 (**2013**).
22. Kilbourne, E. D. Influenza pandemics of the 20th century. *Emerg Infect Dis.*, 12 (1), 9-14 (**2006**).
23. Kumar, B., Asha, K., Khanna, M., Ronsard, L., Meseko, C. A., Sanicas, M. The emerging influenza virus threat: status and new prospects for its therapy and control. *Arch Virol*., 163 (4), 831-844 (**2018**).
24. Ni, F., Kondrashkina, E., Wang, Q. Structural basis for the divergent evolution of influenza B virus hemagglutinin. *Virology*, 446 (1-2), 112-122 (**2013**).

25. Nobusawa, E., Sato, K. Comparison of the mutation rates of human influenza A and B viruses. *J Virol*., 80 (7), 3675-3678 (**2006**).
26. Hay, A. J., Gregory, V., Douglas, A. R., Lin, Y. P. The evolution of human influenza viruses. *Philos Trans R Soc Lond B Biol Sci*., 356 (1416), 1861-1870 (**2001**).
27. Zambon, M. C. Epidemiology and pathogenesis of influenza. *J Antimicrob Chemother*., 44 Suppl B, 3-9 (**1999**).
28. Lapinscki, B., Pereira, L. A., Nogueira, M. B., Vidal, L. R., Riediger, I., Debur, M. C., Presibella, M., Raboni, S. M. Molecular epidemiology of influenza B virus and implications in immunization strategy, Southern Brazil. *Vaccine*, 36 (1), 107-113 (**2018**).
29. Alamgir, A. S., Matsuzaki, Y., Hongo, S., Tsuchiya, E., Sugawara, K., Muraki, Y., Nakamura, K. Phylogenetic analysis of influenza C virus nonstructural (NS) protein genes and identification of the NS2 protein. *J Gen Virol*., 81 (8), 1933-1940 (**2008**).
30. Matsuzaki, Y., Sugawara, K., Mizuta, K., Tsuchiya, E., Muraki, Y., Hongo, S., Suzuki, H., Nakamura, K. Antigenic and genetic characterization of influenza C viruses which caused two outbreaks in Yamagata City, Japan, in 1996 and 1998. *J Clin Microbiol*., 40 (2), 422-429 (**2002**).
31. Matsuzaki, Y., Katsushima, N., Nagai, Y., Shoji, M., Itagaki, T., Sakamoto, M., Kitaoka, S., Mizuta, K., Nishimura, H. Clinical features of influenza C virus infection in children. *J Infect Dis*., 193 (9), 1229-1235 (**2006**).
32. Gouarin, S., Vabret, A., Dina, J., Petitjean, J., Brouard, J., Cuvillon-Nimal, D., Freymuth, F. Study of influenza C virus infection in France. *J Med Virol*., 80 (8), 1441-1446 (**2008**).
33. http://www.who.int/mediacentre/factsheets/fs211/en/.
34. Patrick, G. L. An Introduction to medicinal chemistry, 5th ed. Oxford University Press. EdiSES s.r.l.
35. https://www.fludb.org/brc/home.spg?decorator=influenza
36. Brunotte, L., Flies, J., Bolte, H., Reuther, P., Vreede, F., Schwemmle, M. The nuclear export protein of H5N1 influenza A viruses recruits Matrix 1 (M1) protein to the viral ribonucleoprotein to mediate nuclear export. *J Biol Chem*., 289 (29), 20067-20077 (**2014**).
37. Ma, K., Roy, A. M., Whittaker, G. R. Nuclear export of influenza virus ribonucleoproteins: identification of an export intermediate at the nuclear periphery. *Virology*, 282 (2), 215-220 (**2001**).

38. Elton, D., Simpson-Holley, M., Archer, K., Medcalf, L., Hallam, R., McCauley, J., Digard, P. Interaction of the influenza virus nucleoprotein with the cellular CRM1-mediated nuclear export pathway. *J Virol*., 75 (1), 408-419 (**2001**).
39. Watanabe, K., Takizawa, N., Katoh, M., Hoshida, K., Kobayashi, N., Nagata, K. Inhibition of nuclear export of ribonucleoprotein complexes of influenza virus by leptomycin B. *Virus Res*., 77 (1), 31-42 (**2001**).
40. Martin, K., Helenius, A. Nuclear transport of influenza virus ribonucleoproteins: the viral matrix protein (M1) promotes export and inhibits import. *Cell*., 67 (1), 117-130 (**1991**).
41. Kurokawa, M., Ochiai, H., Nakajima, K., Niwayama, S. Inhibitory effect of protein kinase C inhibitor on the replication of influenza type A virus. *J Gen Virol*., 71 (9), 2149-2155 (**1990**).
42. Bui, M., Wills, E. G., Helenius, A., Whittaker, G. R. Role of the influenza virus M1 protein in nuclear export of viral ribonucleoproteins. *J Virol*., 74 (4), 1781-1786 (**2000**).
43. O'Neill, R. E., Talon, J., Palese, P. The influenza virus NEP (NS2 protein) mediates the nuclear export of viral ribonucleoproteins. *EMBO J*., 17 (1), 288-296 (**1998**).
44. Pleschka, S., Wolff, T., Ehrhardt, C., Hobom, G., Planz, O., Rapp, U. R., Ludwig, S. Influenza virus propagation is impaired by inhibition of the Raf/MEK/ERK signalling cascade. *Nat Cell Biol*., 3 (3), 301-305 (**2001**).
45. Kumar, N., Liang, Y., Parslow, T. G., Liang, Y. Receptor tyrosine kinase inhibitors block multiple steps of influenza a virus replication. *J Virol*., 85 (6), 2818-2827 (**2011**).
46. Alamares-Sapuay, J. G., Martinez-Gil, L., Stertz, S., Miller, M. S., Shaw, M. L., Palese, P. Serum- and glucocorticoid-regulated kinase 1 is required for nuclear export of the ribonucleoprotein of influenza A virus. *J Virol*., 87 (10), 6020-6026 (**2013**).
47. Marjuki, H., Alam, M. I., Ehrhardt, C., Wagner, R., Planz, O., Klenk, H. D., Ludwig, S., Pleschka, S. Membrane accumulation of influenza A virus hemagglutinin triggers nuclear export of the viral genome via protein kinase Calpha-mediated activation of ERK signaling. *J Biol Chem*., 281 (24), 16707-16715 (**2006**).
48. Marjuki, H., Yen, H. L., Franks, J., Webster, R. G., Pleschka, S., Hoffmann, E. Higher polymerase activity of a human influenza virus enhances activation of the hemagglutinin-induced Raf/MEK/ERK signal cascade. *Virol J*., 4, 134 (**2007**).
49. Petri, T., Dimmock, N. J. Phosphorylation of influenza virus nucleoprotein in vivo. *J Gen Virol*., 57 (1), 185-190 (**1981**).

50. Kistner, O., Müller, K., Scholtissek, C. Differential phosphorylation of the nucleoprotein of influenza A viruses. *J Gen Virol*., 70 (9), 2421-2431 (**1989**).
51. Richardson, J. C., Akkina, R. K. NS2 protein of influenza virus is found in purified virus and phosphorylated in infected cells. *Arch Virol*., 116 (1-4), 69-80 (**1991**).
52. Reinhardt, J., Wolff, T. The influenza A virus M1 protein interacts with the cellular receptor of activated C kinase (RACK) 1 and can be phosphorylated by protein kinase C. *Vet Microbiol*., 74 (1-2), 87-100 (**2000**).
53. Hutchinson, E. C., Denham, E. M., Thomas, B., Trudgian, D. C., Hester, S. S., Ridlova, G., York, A., Turrell, L., Fodor, E. Mapping the phosphoproteome of influenza A and B viruses by mass spectrometry. *PLoS Pathog*., 8 (11), e1002993 (**2012**).
54. Momose, F., Kikuchi, Y., Komase, K., Morikawa, Y. Visualization of microtubule-mediated transport of influenza viral progeny ribonucleoprotein. *Microbes Infect*., 9 (12-13), 1422-1433 (**2007**).
55. Amorim, M. J., Bruce, E. A., Read, E. K., Foeglein, A., Mahen, R., Stuart, A. D., Digard, P. A Rab11- and microtubule-dependent mechanism for cytoplasmic transport of influenza A virus viral RNA. *J Virol*., 85 (9), 4143-4156 (**2011**).
56. Momose, F., Sekimoto, T., Ohkura, T., Jo, S., Kawaguchi, A., Nagata, K., Morikawa, Y. Apical transport of influenza A virus ribonucleoprotein requires Rab11-positive recycling endosome. *PLoS One*, 6 (6), e21123 (**2011**).
57. Avilov, S. V., Moisy, D., Naffakh, N., Cusack, S. Influenza A virus progeny vRNP trafficking in live infected cells studied with the virus-encoded fluorescently tagged PB2 protein. *Vaccine*, 30 (51), 7411-7417 (**2012**).
58. Shaw, M. L., Stone, K. L., Colangelo, C. M., Gulcicek, E. E., Palese, P. Cellular proteins in influenza virus particles. *PLoS Pathog*., 4 (6), e1000085 (**2008**).
59. Eisfeld, A. J., Kawakami, E., Watanabe, T., Neumann, G., Kawaoka, Y. RAB11A is essential for transport of the influenza virus genome to the plasma membrane. *J Virol*., 85 (13), 6117-6126 (**2011**).
60. Chou, Y. Y., Heaton, N. S., Gao, Q., Palese, P, Singer, R. H., Lionnet, T. Colocalization of different influenza viral RNA segments in the cytoplasm before viral budding as shown by single-molecule sensitivity FISH analysis. *PLoS Pathog*., 9 (5), e1003358 (**2013**).

61. de Lucas, S., Peredo, J., Marión, R. M., Sánchez, C., Ortín, J. Human Staufen1 protein interacts with influenza virus ribonucleoproteins and is required for efficient virus multiplication. *J Virol*., 84 (15), 7603-7612 (**2010**).
62. Kawaguchi, A., Matsumoto, K., Nagata, K. YB-1 functions as a porter to lead influenza virus ribonucleoprotein complexes to microtubules. *J Virol*., 86 (20), 11086-11095 (**2012**).
63. McCown, M. F., Pekosz, A. The influenza A virus M2 cytoplasmic tail is required for infectious virus production and efficient genome packaging. *J Virol*., 79 (6), 3595-3605 (**2005**).
64. Iwatsuki-Horimoto, K., Horimoto, T., Noda, T., Kiso, M., Maeda, J., Watanabe, S., Muramoto, Y., Fujii, K., Kawaoka, Y. The cytoplasmic tail of the influenza A virus M2 protein plays a role in viral assembly. *J Virol*., 80 (11), 5233-5240 (**2006**).
65. Chen, B. J., Leser, G. P., Jackson, D., Lamb, R. A. The influenza virus M2 protein cytoplasmic tail interacts with the M1 protein and influences virus assembly at the site of virus budding. *J Virol*., 82 (20), 10059-10070 (**2008**).
66. Palese, P., Schulman, J. L. Mapping of the influenza virus genome: identification of the hemagglutinin and the neuraminidase genes. *Proc Natl Acad Sci U S A.*, 73 (6), 2142-2146 (**1976**).
67. Ritchey, M. B., Palese, P., Schulman, J. L. Mapping of the influenza virus genome. III. Identification of genes coding for nucleoprotein, membrane protein, and nonstructural protein. *J Virol*., 20 (1), 307-313 (**1976**).
68. Chen, W,, Calvo, P. A., Malide, D., Gibbs, J., Schubert, U., Bacik, I., Basta, S., O'Neill, R., Schickli, J., Palese, P., Henklein, P., Bennink, J. R., Yewdell, J. W. A novel influenza A virus mitochondrial protein that induces cell death. *Nat Med*., 7 (12), 1306-1312 (**2001**).
69. Wise, H. M., Foeglein, A., Sun, J., Dalton, R. M., Patel, S., Howard, W., Anderson, E. C., Barclay, W. S., Digard, P. A complicated message: Identification of a novel PB1-related protein translated from influenza A virus segment 2 mRNA. *J Virol*., 83 (16), 8021-8031 (**2009**).
70. Jagger, B. W., Wise, H. M., Kash, J. C., Walters, K. A., Wills, N. M., Xiao, Y. L., Dunfee, R. L., Schwartzman, L. M., Ozinsky, A., Bell, G. L., Dalton, R. M., Lo, A., Efstathiou, S., Atkins, J. F., Firth, A. E., Taubenberger, J. K., Digard, P. An overlapping protein-coding region in influenza A virus segment 3 modulates the host response. *Science*, 337 (6091), 199-204 (**2012**).

71. Wise, H. M., Hutchinson, E. C., Jagger, B. W., Stuart, A. D., Kang, Z. H., Robb, N., Schwartzman, L. M., Kash, J. C., Fodor, E., Firth, A. E., Gog, J. R., Taubenberger, J. K., Digard, P. Identification of a novel splice variant form of the influenza A virus M2 ion channel with an antigenically distinct ectodomain. *PLoS Pathog*., 8 (11), e1002998 (**2012**).
72. Selman, M., Dankar, S. K., Forbes, N. E., Jia, J. J., Brown, E. G. Adaptive mutation in influenza A virus non-structural gene is linked to host switching and induces a novel protein by alternative splicing. *Emerg Microbes Infect*, 1 (11), e42 (**2012**).
73. Muramoto, Y., Noda, T., Kawakami, E., Akkina, R., Kawaoka, Y. Identification of novel influenza A virus proteins translated from PA mRNA. *J Virol*., 87 (5), 2455-2462 (**2013**).
74. Yamayoshi, S., Watanabe, M., Goto, H., Kawaoka, Y. Identification of a Novel Viral Protein Expressed from the PB2 Segment of Influenza A Virus. *J Virol*., 90 (1), 444-456 (**2015**).
75. Yang, J., Li, M., Shen, X., Liu, S. Influenza A virus entry inhibitors targeting the hemagglutinin. *Viruses*, 5 (1), 352-373 (**2013**).
76. Wilson, I. A., Skehel, J. J., Wiley, D. C. Structure of the haemagglutinin membrane glycoprotein of influenza virus at 3 A resolution. *Nature*, 289 (5796), 366-373 (**1981**).
77. Xu, R., McBride, R., Paulson, J. C., Basler, C. F., Wilson, I. A. Structure, receptor binding, and antigenicity of influenza virus hemagglutinins from the 1957 H2N2 pandemic. *J Virol*., 84 (4), 1715-1721 (**2010**).
78. Lazniewski, M., Dawson, W. K., Szczepinska, T., Plewczynski, D. The structural variability of the influenza A hemagglutinin receptor-binding site. *Brief Funct Genomics*, 17 (6), 415-427 (**2018**).
79. Ni, F., Kondrashkina, E., Wang, Q. Determinant of receptor-preference switch in influenza hemagglutinin. *Virology*, 513, 98-107 (**2018**).
80. Wu, Y., Wu, Y., Tefsen, B., Shi, Y., Gao, G. F. Bat-derived influenza-like viruses H17N10 and H18N11. *Trends Microbiol*., 22 (4), 183-191 (**2014**).
81. Ma, W., García-Sastre, A., Schwemmle, M. Expected and Unexpected Features of the Newly Discovered Bat Influenza A-like Viruses. *PLoS Pathog*., 11 (6), e1004819 (**2015**).
82. Wang, M., Veit, M. Hemagglutinin-esterase-fusion (HEF) protein of influenza C virus. *Protein Cell*.,7 (1), 28-45 (**2016**).
83. Shtyrya, Y. A., Mochalova, L. V., Bovin, N. V. Influenza virus neuraminidase: structure and function. *Acta Naturae*, 1 (2), 26-32 (**2009**).

84. Byrd-Leotis, L., Cummings, R. D., Steinhauer, D. A. The Interplay between the Host Receptor and Influenza Virus Hemagglutinin and Neuraminidase. *Int J Mol Sci*., 18 (7) (**2017**).
85. Varghese, J. N., Colman, P. M. Three-dimensional structure of the neuraminidase of influenza virus A/Tokyo/3/67 at 2.2 A resolution. *J Mol Biol*., 221 (2), 473-486 (**1991**).
86. Bossart-Whitaker, P., Carson, M., Babu, Y. S., Smith, C. D., Laver, W. G., Air, G. M. Three-dimensional structure of influenza A N9 neuraminidase and its complex with the inhibitor 2-deoxy 2,3-dehydro-N-acetyl neuraminic acid. *J Mol Biol*., 232 (4), 1069-1083 (**1993**).
87. Janakiraman, M. N., White, C. L., Laver, W. G., Air, G. M., Luo, M. Structure of influenza virus neuraminidase B/Lee/40 complexed with sialic acid and a dehydro analog at 1.8-A resolution: implications for the catalytic mechanism. *Biochemistry*, 33 (27), 8172-8179 (**1994**).
88. Varghese, J. N., Colman, P. M., van Donkelaar, A., Blick, T. J., Sahasrabudhe, A., McKimm-Breschkin, J. L. Structural evidence for a second sialic acid binding site in avian influenza virus neuraminidases. *Proc Natl Acad Sci U S A*., 94 (22), 11808-11812 (**1997**).
89. Russell, R. J., Haire, L. F., Stevens, D. J., Collins, P. J., Lin, Y. P., Blackburn, G. M., Hay, A. J., Gamblin, S. J., Skehel, J. J. The structure of H5N1 avian influenza neuraminidase suggests new opportunities for drug design. *Nature*, 443 (7107), 45-49 (**2006**).
90. Lamb, R. A., Choppin, P. W. Identification of a second protein (M2) encoded by RNA segment 7 of influenza virus. *Virology*, 112 (2), 729-737 (**1981**).
91. Ruigrok, R. W., Barge, A., Durrer, P., Brunner, J., Ma, K., Whittaker, G. R. Membrane interaction of influenza virus M1 protein. *Virology*, 267 (2), 289-298 (**2000**).
92. Arzt, S., Baudin, F., Barge, A., Timmins, P., Burmeister, W. P., Ruigrok, R. W. Combined results from solution studies on intact influenza virus M1 protein and from a new crystal form of its N-terminal domain show that M1 is an elongated monomer. *Virology*, 279 (2), 439-446 (**2001**).
93. Hilsch, M., Goldenbogen, B., Sieben, C., Höfer, C. T., Rabe, J. P., Klipp, E., Herrmann, A., Chiantia, S. Influenza A matrix protein M1 multimerizes upon binding to lipid membranes. *Biophys J*., 107 (4), 912-923 (**2014**).

94. Bobone, S., Hilsch, M., Storm, J., Dunsing, V., Herrmann, A., Chiantia, S. Phosphatidylserine Lateral Organization Influences the Interaction of Influenza Virus Matrix Protein 1 with Lipid Membranes. *J Virol*., 91 (12), e00267-17 (**2017**).
95. Elster, C., Larsen, K., Gagnon, J., Ruigrok, R. W., Baudin, F. Influenza virus M1 protein binds to RNA through its nuclear localization signal. *J Gen Virol*., 78 (7), 1589-1596 (**1997**).
96. Zhao, H., Ekström, M., Garoff, H. The M1 and NP proteins of influenza A virus form homo- but not heterooligomeric complexes when coexpressed in BHK-21 cells. *J Gen Virol*., 79 (10), 2435-2446 (**1998**).
97. Ye, Z., Liu, T., Offringa, D. P., McInnis, J., Levandowski, R. A. Association of influenza virus matrix protein with ribonucleoproteins. *J Virol*., 73 (9), 7467-7473 (**1999**).
98. Huang, X., Liu, T., Muller, J., Levandowski, R. A., Ye, Z. Effect of influenza virus matrix protein and viral RNA on ribonucleoprotein formation and nuclear export. *Virology*, 287 (2), 405-416 (**2001**).
99. Noton, S. L., Medcalf, E., Fisher, D., Mullin, A. E., Elton, D., Digard, P. Identification of the domains of the influenza A virus M1 matrix protein required for NP binding, oligomerization and incorporation into virions. *J Gen Virol*., 88 (8), 2280-2290 (**2007**).
100. de Chassey, B., Aublin-Gex, A., Ruggieri, A., Meyniel-Schicklin, L., Pradezynski, F., Davoust, N., Chantier, T., Tafforeau, L., Mangeot, P. E., Ciancia, C., Perrin-Cocon, L., Bartenschlager, R., André, P., Lotteau, V. The interactomes of influenza virus NS1 and NS2 proteins identify new host factors and provide insights for ADAR1 playing a supportive role in virus replication. *PLoS Pathog*., 9 (7), e1003440 (**2013**).
101. Leser, G. P., Lamb, R. A. Lateral Organization of Influenza Virus Proteins in the Budozone Region of the Plasma Membrane. *J Virol*., 91 (9), e02104-e02116 (**2017**).
102. Pielak, R. M., Chou, J. J. Influenza M2 proton channels. *Biochim Biophys Acta*, 1808 (2), 522-529 (**2011**).
103. Holsinger, L. J., Nichani, D., Pinto, L. H., Lamb, R. A. Influenza A virus M2 ion channel protein: a structure-function analysis. *J Virol.*, 68 (3), 1551-1563 (**1994**).
104. Gu, R. X., Liu, L. A., Wei, D. Q., Du, J. G., Liu, L., Liu, H. Free energy calculations on the two drug binding sites in the M2 proton channel. *J Am Chem Soc*., 133 (28), 10817-10825 (**2011**).

105. Yi, M., Cross, T. A., Zhou, H. X. A secondary gate as a mechanism for inhibition of the M2 proton channel by amantadine. *J Phys Chem B.*, 112 (27), 7977-7979 (**2008**).

106. Schnell, J. R., Chou, J. J. Structure and mechanism of the M2 proton channel of influenza A virus. *Nature*, 451 (7178), 591-595 (**2008**).

107. Stouffer, A. L., Acharya, R., Salom, D., Levine, A. S., Di Costanzo, L., Soto, C. S., Tereshko, V., Nanda, V., Stayrook, S., DeGrado, W. F. Structural basis for the function and inhibition of an influenza virus proton channel. *Nature*, 451 (7178), 596-599 (**2008**).

108. Tang, Y., Zaitseva, F., Lamb, R. A., Pinto, L. H. The gate of the influenza virus M2 proton channel is formed by a single tryptophan residue. *J Biol Chem.*, 277 (42), 39880-39886 (**2002**).

109. Venkataraman, P., Lamb, R. A., Pinto, L. H. Chemical rescue of histidine selectivity filter mutants of the M2 ion channel of influenza A virus. *J Biol Chem.*, 280 (22), 21463-21472 (**2005**).

110. Pinto, L. H., Lamb, R. A. The M2 proton channels of influenza A and B viruses. *J Biol Chem.*, 281 (14), 8997-9000 (**2006**).

111. Khurana, E., Dal Peraro, M., DeVane, R., Vemparala, S., DeGrado, W. F., Klein, M. L. Molecular dynamics calculations suggest a conduction mechanism for the M2 proton channel from influenza A virus. *Proc Natl Acad Sci U S A.*, 106 (4), 1069-1074 (**2009**).

112. Acharya, R., Carnevale, V., Fiorin, G., Levine, B. G., Polishchuk, A. L., Balannik, V., Samish, I., Lamb, R. A., Pinto, L. H., DeGrado, W. F., Klein, M. L. Structure and mechanism of proton transport through the transmembrane tetrameric M2 protein bundle of the influenza A virus. *Proc Natl Acad Sci U S A.*, 107 (34), 15075-15080 (**2010**).

113. Hu, F., Luo, W., Hong, M. Mechanisms of proton conduction and gating in influenza M2 proton channels from solid-state NMR. *Science*, 330 (6003), 505-508 (**2010**).

114. Sharma, M., Yi, M., Dong, H., Qin, H., Peterson, E., Busath, D. D., Zhou, H. X., Cross TA. Insight into the mechanism of the influenza A proton channel from a structure in a lipid bilayer. *Science*, 330 (6003), 509-512 (**2010**).

115. Williams, J. K., Zhang, Y., Schmidt-Rohr, K., Hong, M. pH-dependent conformation, dynamics, and aromatic interaction of the gating tryptophan residue of the influenza M2 proton channel from solid-state NMR. *Biophys J.*, 104 (8), 1698-1708 (**2013**).

116. Takeuchi, K., Lamb, R. A. Influenza virus M2 protein ion channel activity stabilizes the native form of fowl plague virus hemagglutinin during intracellular transport. *J Virol*., 68 (2), 911-919 (**1994**).

117. Sakaguchi, T., Leser, G. P., Lamb, R. A. The ion channel activity of the influenza virus M2 protein affects transport through the Golgi apparatus. *J Cell Biol*., 133 (4), 733-747 (**1996**).

118. Su, W. C., Yu, W. Y., Huang, S. H., Lai, M. M. C. Ubiquitination of the Cytoplasmic Domain of Influenza A Virus M2 Protein Is Crucial for Production of Infectious Virus Particles. *J Virol*., 92 (4), e01972-17 (**2018**).

119. Yasuda, J., Nakada, S., Kato, A., Toyoda, T., Ishihama, A. Molecular assembly of influenza virus: association of the NS2 protein with virion matrix. *Virology*, 196 (1), 249-255 (**1993**).

120. Klemm, C., Boergeling, Y., Ludwig, S., Ehrhardt, C. Immunomodulatory Nonstructural Proteins of Influenza A Viruses. *Trends Microbiol*., 26 (7), 624-636 (**2018**).

121. Tan, S. L., Katze, M. G. Biochemical and genetic evidence for complex formation between the influenza A virus NS1 protein and the interferon-induced PKR protein kinase. *J Interferon Cytokine Res*., 18 (9), 757-766 (**1998**).

122. Donelan, N. R., Basler, C. F., García-Sastre, A. A recombinant influenza A virus expressing an RNA-binding-defective NS1 protein induces high levels of beta interferon and is attenuated in mice. *J Virol*., 77 (24), 13257-13266 (**2003**).

123. Li, S., Min, J. Y., Krug, R. M., Sen, G. C. Binding of the influenza A virus NS1 protein to PKR mediates the inhibition of its activation by either PACT or double-stranded RNA. *Virology*, 349 (1), 13-21 (**2006**).

124. Min, J. Y., Li, S., Sen, G. C., Krug, R. M. A site on the influenza A virus NS1 protein mediates both inhibition of PKR activation and temporal regulation of viral RNA synthesis. *Virology*, 363 (1), 236-243 (**2007**).

125. Gack, M. U., Albrecht, R. A., Urano, T., Inn, K. S., Huang, I. C., Carnero, E., Farzan, M., Inoue, S., Jung, J. U., García-Sastre, A. Influenza A virus NS1 targets the ubiquitin ligase TRIM25 to evade recognition by the host viral RNA sensor RIG-I. *Cell Host Microbe*, 5 (5), 439-449 (**2009**).

126. Chen, Z., Li, Y., Krug, R. M. Influenza A virus NS1 protein targets poly(A)-binding protein II of the cellular 3'-end processing machinery. *EMBO J*., 18 (8), 2273-2283 (**1999**).

127. Falcón, A. M., Fortes, P., Marión, R. M., Beloso, A., Ortín, J. Interaction of influenza virus NS1 protein and the human homologue of Staufen in vivo and in vitro. *Nucleic Acids Res*., 27 (11), 2241-2247 (**1999**).

128. Marión, R. M., Fortes, P., Beloso, A., Dotti, C., Ortín, J. A human sequence homologue of Staufen is an RNA-binding protein that is associated with polysomes and localizes to the rough endoplasmic reticulum. *Mol Cell Biol*., 19 (3), 2212-2219 (**1999**).

129. Neumann, G., Hughes, M. T., Kawaoka, Y. Influenza A virus NS2 protein mediates vRNP nuclear export through NES-independent interaction with hCRM1. *EMBO J*., 19 (24), 6751-6758 (**2000**).

130. Robb, N. C., Smith, M., Vreede, F. T., Fodor, E. NS2/NEP protein regulates transcription and replication of the influenza virus RNA genome. *J Gen Virol*., 90 (6), 1398-1407 (**2009**).

131. Pflug, A., Lukarska, M., Resa-Infante, P., Reich, S., Cusack, S. Structural insights into RNA synthesis by the influenza virus transcription-replication machine. *Virus Res*., 234, 103-117 (**2017**).

132. Zhou, Z., Liu, T., Zhang, J., Zhan, P., Liu, X. Influenza A virus polymerase: an attractive target for next-generation anti-influenza therapeutics. *Drug Discov Today*, 23 (3), 503-518 (**2018**).

133. Jones, I. M., Reay, P. A., Philpott, K. L. Nuclear location of all three influenza polymerase proteins and a nuclear signal in polymerase PB2. *EMBO J*., 5 (9), 2371-2376 (**1986**).

134. Akkina, R. K., Chambers, T. M., Londo, D. R., Nayak, D. P. Intracellular localization of the viral polymerase proteins in cells infected with influenza virus and cells expressing PB1 protein from cloned cDNA. *J Virol*., 61 (7), 2217-2224 (**1987**).

135. Smith, G. L., Levin, J. Z., Palese, P., Moss, B. Synthesis and cellular location of the ten influenza polypeptides individually expressed by recombinant vaccinia viruses. *Virology*, 160 (2), 336-345 (**1987**).

136. Nath, S. T., Nayak, D. P. Function of two discrete regions is required for nuclear localization of polymerase basic protein 1 of A/WSN/33 influenza virus (H1 N1). *Mol Cell Biol*., 10 (8), 4139-4145 (**1990**).

137. Mukaigawa, J., Nayak, D. P. Two signals mediate nuclear localization of influenza virus (A/WSN/33) polymerase basic protein 2. *J Virol*., 65 (1), 245-253 (**1991**).

138. Nieto, A., de la Luna, S., Bárcena, J., Portela, A., Valcárcel, J., Melero, J. A., Ortín, J. Nuclear transport of influenza virus polymerase PA protein. *Virus Res.*, 24 (1), 65-75 (**1992**).

139. Nieto, A., de la Luna, S., Bárcena, J., Portela, A., Ortín, J. Complex structure of the nuclear translocation signal of influenza virus polymerase PA subunit. *J Gen Virol.*, 75 (1), 29-36 (**1994**).

140. Fodor, E., Smith, M. The PA subunit is required for efficient nuclear accumulation of the PB1 subunit of the influenza A virus RNA polymerase complex. *J Virol.*, 78 (17), 9144-9153 (**2004**).

141. Naito, T., Momose, F., Kawaguchi, A., Nagata, K. Involvement of Hsp90 in assembly and nuclear import of influenza virus RNA polymerase subunits. *J Virol.*, 81 (3), 1339-1349 (**2007**).

142. Yamashita, M., Krystal, M., Palese, P. Comparison of the three large polymerase proteins of influenza A, B, and C viruses. *Virology*, 171 (2), 458-466 (**1989**).

143. Pflug, A., Guilligay, D., Reich, S., Cusack, S. Structure of influenza A polymerase bound to the viral RNA promoter. *Nature*, 516 (7531), 355-360 (**2012**).

144. Reich, S., Guilligay, D., Pflug, A., Malet, H., Berger, I., Crépin, T., Hart, D., Lunardi, T., Nanao, M., Ruigrok, R. W., Cusack, S. Structural insight into cap-snatching and RNA synthesis by influenza polymerase. *Nature*, 516 (7531), 361-366 (**2014**).

145. Hengrung, N., El Omari, K., Serna Martin, I., Vreede, F. T., Cusack, S., Rambo, R. P., Vonrhein, C., Bricogne, G., Stuart, D. I., Grimes, J. M., Fodor, E. Crystal structure of the RNA-dependent RNA polymerase from influenza C virus. *Nature*, 527 (7576), 114-117 (**2015**).

146. Area, E., Martín-Benito, J., Gastaminza, P., Torreira, E., Valpuesta, J. M., Carrascosa, J. L., Ortín, J. 3D structure of the influenza virus polymerase complex: localization of subunit domains. *Proc Natl Acad Sci U S A.*, 101 (1), 308-313 (**2004**).

147. Poch, O., Sauvaget, I., Delarue, M., Tordo, N. Identification of four conserved motifs among the RNA-dependent polymerase encoding elements. *EMBO J.*, 8 (12), 3867-3874 (**1989**).

148. Biswas, S. K., Nayak, D. P. Mutational analysis of the conserved motifs of influenza A virus polymerase basic protein 1. *J Virol.*, 68 (3), 1819-1826 (**1994**).

149. Dias, A., Bouvier, D., Crépin, T., McCarthy, A. A., Hart, D. J., Baudin, F., Cusack, S., Ruigrok, R. W. The cap-snatching endonuclease of influenza virus polymerase resides in the PA subunit. *Nature*, 458 (7240), 914-918 (**2009**).

150. Yuan, P., Bartlam, M., Lou, Z., Chen, S., Zhou, J., He, X., Lv, Z., Ge, R., Li, X., Deng, T., Fodor, E., Rao, Z., Liu, Y. Crystal structure of an avian influenza polymerase PA(N) reveals an endonuclease active site. *Nature*, 458 (7240), 909-913 (**2009**).

151. DuBois, R. M., Slavish, P. J., Baughman, B. M., Yun, M. K., Bao, J., Webby, R. J., Webb, T. R., White, S. W. Structural and biochemical basis for development of influenza virus inhibitors targeting the PA endonuclease. *PLoS Pathog.*, 8 (8), e1002830 (**2012**).

152. Hara, K., Schmidt, F. I., Crow, M., Brownlee, G. G. Amino acid residues in the N-terminal region of the PA subunit of influenza A virus RNA polymerase play a critical role in protein stability, endonuclease activity, cap binding, and virion RNA promoter binding. *J Virol.*, 80 (16), 7789-7798 (**2006**).

153. Doan, L., Handa, B., Roberts, N. A., Klumpp, K. Metal ion catalysis of RNA cleavage by the influenza virus endonuclease. *Biochemistry*, 38 (17), 5612-5619 (**1999**).

154. Steitz, T. A., Steitz, J. A. A general two-metal-ion mechanism for catalytic RNA. *Proc Natl Acad Sci U S A.*, 90 (14), 6498-6502 (**1993**).

155. Fedor, M. J. The role of metal ions in RNA catalysis. *Curr Opin Struct Biol.*, 12 (3), 289-295 (**2002**).

156. Palermo, G., Cavalli, A., Klein, M. L., Alfonso-Prieto, M., Dal Peraro, M., De Vivo, M. Catalytic metal ions and enzymatic processing of DNA and RNA. *Acc Chem Res.*, 48 (2), 220-228 (**2015**).

157. Kowalinski, E., Zubieta, C., Wolkerstorfer, A., Szolar, O. H., Ruigrok, R. W., Cusack, S. Structural analysis of specific metal chelating inhibitor binding to the endonuclease domain of influenza pH1N1 (2009) polymerase. *PLoS Pathog.*, 8 (8), e1002831 (**2012**).

158. Thierry, E., Guilligay, D., Kosinski, J., Bock, T., Gaudon, S., Round, A., Pflug, A., Hengrung, N., El Omari, K., Baudin, F., Hart, D. J., Beck, M., Cusack, S. Influenza Polymerase Can Adopt an Alternative Configuration Involving a Radical Repacking of PB2 Domains. *Mol Cell.*, 61 (1), 125-137 (**2016**).

159. Stevaert, A., Nurra, S., Pala, N., Carcelli, M., Rogolino, D., Shepard, C., Domaoal, R. A., Kim, B., Alfonso-Prieto, M., Marras, S. A., Sechi, M., Naesens, L. An integrated

biological approach to guide the development of metal-chelating inhibitors of influenzavirus PA endonuclease. *Mol Pharmacol*., 87 (2), 323-337 (**2015**).

160. Xiao, S., Klein, M. L., LeBard, D. N., Levine, B. G., Liang, H., MacDermaid, C. M., Alfonso-Prieto, M. Magnesium-dependent RNA binding to the PA endonuclease domain of the avian influenza polymerase. *J Phys Chem B*., 118 (4), 873-889 (**2014**).
161. Jahnen-Dechent, W., Ketteler, M. Magnesium basics. *Clin Kidney J*., 5 (1), 3-14 (**2012**).
162. Yang, W. Nucleases: diversity of structure, function and mechanism. *Q Rev Biophys*., 44 (1), 1-93 (**2011**).
163. Kotlarek, D., Worch, R. New Insight into Metal Ion-Driven Catalysis of Nucleic Acids by Influenza PA-Nter. *PLoS One*, 11 (6), e0156972 (**2016**).
164. Tarendeau, F., Boudet, J., Guilligay, D., Mas, P. J., Bougault, C. M., Boulo, S., Baudin, F., Ruigrok, R. W., Daigle, N., Ellenberg, J., Cusack, S., Simorre, J. P., Hart, D. J. Structure and nuclear import function of the C-terminal domain of influenza virus polymerase PB2 subunit. *Nat Struct Mol Biol*., 14 (3), 229-233 (**2007**).
165. Guilligay, D., Tarendeau, F., Resa-Infante, P., Coloma, R., Crepin, T., Sehr, P., Lewis, J., Ruigrok, R. W., Ortin, J., Hart, D. J., Cusack, S. The structural basis for cap binding by influenza virus polymerase subunit PB2. *Nat Struct Mol Biol*., 15 (5), 500-506 (**2008**).
166. Shinya, K., Hamm, S., Hatta, M., Ito, H., Ito, T., Kawaoka, Y. PB2 amino acid at position 627 affects replicative efficiency, but not cell tropism, of Hong Kong H5N1 influenza A viruses in mice. *Virology*, 320 (2), 258-266 (**2004**).
167. Steel, J., Lowen, A. C., Mubareka, S., Palese, P. Transmission of influenza virus in a mammalian host is increased by PB2 amino acids 627K or 627E/701N. *PLoS Pathog*., 5 (1), e1000252 (**2009**).
168. Aggarwal, S., Dewhurst, S., Takimoto, T., Kim, B. Biochemical impact of the host adaptation-associated PB2 E627K mutation on the temperature-dependent RNA synthesis kinetics of influenza A virus polymerase complex. *J Biol Chem*., 286 (40), 34504-34513 (**2011**).
169. Ng, A. K., Chan, W. H., Choi, S. T., Lam, M. K., Lau, K. F., Chan, P. K., Au, S. W., Fodor, E., Shaw, P. C. Influenza polymerase activity correlates with the strength of interaction between nucleoprotein and PB2 through the host-specific residue K/E627. *PLoS One*., 7 (5), e36415 (**2012**).

170. Vasin, A. V., Temkina, O. A., Egorov, V. V., Klotchenko, S. A., Plotnikova, M. A., Kiselev, O. I. Molecular mechanisms enhancing the proteome of influenza A viruses: an overview of recently discovered proteins. *Virus Res*., 185, 53-63 (**2014**).

171. Yoshizumi, T., Ichinohe, T., Sasaki, O., Otera, H., Kawabata, S., Mihara, K., Koshiba, T. Influenza A virus protein PB1-F2 translocates into mitochondria via Tom40 channels and impairs innate immunity. *Nat Commun*., 5, 4713 (**2014**).

172. Mazur, I., Anhlan, D., Mitzner, D., Wixler, L., Schubert, U., Ludwig, S. The proapoptotic influenza A virus protein PB1-F2 regulates viral polymerase activity by interaction with the PB1 protein. *Cell Microbiol*., 10 (5), 1140-1152 (**2008**).

173. Chen, C. J., Chen, G. W., Wang, C. H., Huang, C. H., Wang, Y. C., Shih, S. R. Differential localization and function of PB1-F2 derived from different strains of influenza A virus. *J Virol*., 84 (19), 10051-10062 (**2010**).

174. Zamarin, D., García-Sastre, A., Xiao, X., Wang, R., Palese, P. Influenza virus PB1-F2 protein induces cell death through mitochondrial ANT3 and VDAC1. *PLoS Pathog*., 1 (1), e4 (**2005**).

175. Vidic, J., Richard, C. A., Péchoux, C., Da Costa, B., Bertho, N., Mazerat, S., Delmas, B., Chevalier, C. Amyloid Assemblies of Influenza A Virus PB1-F2 Protein Damage Membrane and Induce Cytotoxicity. *J Biol Chem*., 291 (2), 739-751 (**2016**).

176. Ajjaji, D., Richard, C. A., Mazerat, S., Chevalier, C., Vidic, J. N-terminal domain of PB1-F2 protein of influenza A virus can fold into amyloid-like oligomers and damage cholesterol and cardiolipid containing membranes. *Biochem Biophys Res Commun*., 477 (1), 27-32 (**2016**).

177. Kash, J. C., Tumpey, T. M., Proll, S. C., Carter, V., Perwitasari, O., Thomas, M. J., Basler, C. F., Palese, P., Taubenberger, J. K., García-Sastre, A., Swayne, D. E., Katze, M. G. Genomic analysis of increased host immune and cell death responses induced by 1918 influenza virus. *Nature*, 443 (7111), 578-581 (**2006**).

178. Dudek, S. E., Wixler, L., Nordhoff, C., Nordmann, A., Anhlan, D., Wixler, V., Ludwig, S. The influenza virus PB1-F2 protein has interferon antagonistic activity. *Biol Chem*., 392 (12), 1135-1144 (**2011**).

179. Varga, Z. T., Ramos, I., Hai, R., Schmolke, M., García-Sastre, A., Fernandez-Sesma, A., Palese, P. The influenza virus protein PB1-F2 inhibits the induction of type I interferon at the level of the MAVS adaptor protein. *PLoS Pathog*., 7 (6), e1002067 (**2011**).

180. Shin, N., Pyo, C. W., Jung, K. I., Choi, S. Y. Influenza A virus PB1-F2 is involved in regulation of cellular redox state in alveolar epithelial cells. *Biochem Biophys Res Commun*., 459 (4), 699-705 (**2015**).

181. McAuley, J. L., Zhang, K., McCullers, J. A. The effects of influenza A virus PB1-F2 protein on polymerase activity are strain specific and do not impact pathogenesis. *J Virol*., 84 (1), 558-564 (**2010**).

182. McAuley, J. L., Hornung, F., Boyd, K. L., Smith, A. M., McKeon, R., Bennink, J., Yewdell, J. W., McCullers, J. A. Expression of the 1918 influenza A virus PB1-F2 enhances the pathogenesis of viral and secondary bacterial pneumonia. *Cell Host Microbe*, 2 (4), 240-249 (**2007**).

183. Treanor, J. Influenza vaccine--outmaneuvering antigenic shift and drift. *N Engl J Med*., 350 (3), 218-220 (**2004**).

184. Carrat, F., Flahault, A. Influenza vaccine: the challenge of antigenic drift. *Vaccine*, 25 (39-40), 6852-6862 (**2007**).

185. Dos Santos, G., Neumeier, E., Bekkat-Berkani, R. Influenza: Can we cope better with the unpredictable? *Hum Vaccin Immunother*., 12 (3), 699-708 (**2016**).

186. Boktor, S. W., Hafner, J. W. Influenza. *StatPearls Publishing*, (**2018**). Available from: http://www.ncbi.nlm.nih.gov/books/NBK459363/.

187. Fiore, A. E., Bridges, C. B., Cox, N. J. Seasonal Influenza Vaccines. In: Compans R., Orenstein W. (eds) Vaccines for Pandemic Influenza. *Current Topics in Microbiology and Immunology*, 333. Springer, Berlin, Heidelberg (**2009**).

188. Kumar, B., Asha, K., Khanna, M. Ronsard, L., Meseko, C. A., Sanicas, M. The emerging influenza virus threat: status and new prospects for its therapy and control. *Arch Virol*., 163, 831 (**2018**).

189. Shaw, M. L. The next wave of ingluenza drugs. *ACS Infect. Dis*., 3 (10), 691-694 (**2017**).

190. Vichkanova, S. A., Oĭfa, A. I., Goriunova, L. V. Antiviral properties of gossypol in experimental influenza pneumonia. *Antibiotiki*, 15 (12), 1071-1073 (**1970**).

191. Yang, J., Chen, G., Li, L. L., Pan, W., Zhang, F., Yang, J., Wu, S., Tien, P. Synthesis and anti-H5N1 activity of chiral gossypol derivatives and its analogs implicated by a viral entry blocking mechanism. *Bioorg Med Chem Lett*., 23 (9), 2619-2623 (**2013**).

192. Savov, V. M., Galabov, A. S., Tantcheva, L. P., Mileva, M. M., Pavlova, E. L., Stoeva, E. S., Braykova, A. A. Effects of rutin and quercetin on monooxygenase activities in experimental influenza virus infection. *Exp Toxicol Pathol*., 58 (1), 59-64 (**2006**).

193. Eşanu, V., Prahoveanu, E., Crişan, I., Cioca, A. The effect of an aqueous propolis extract, of rutin and of a rutin-quercetin mixture on experimental influenza virus infection in mice. *Virologie*, 32 (3), 213-215 (**1981**).

194. Davis, J. M., Murphy, E. A., McClellan, J. L., Carmichael, M. D., Gangemi, J. D. Quercetin reduces susceptibility to influenza infection following stressful exercise. *Am J Physiol Regul Integr Comp Physiol*., 295 (2), R505-509 (**2008**).

195. Choi, H. J., Song, J. H., Park, K. S., Kwon, D. H. Inhibitory effects of quercetin 3-rhamnoside on influenza A virus replication. *Eur J Pharm Sci*., 37 (3-4), 329-333 (**2009**).

196. Chang, T. T., Sun, M. F., Chen, H. Y., Tsai, F. J., Fisher, M., Lin, J. G., Chen, C. Y. Screening from the world's largest TCM database against H1N1 virus. *J Biomol Struct Dyn*., 28 (5), 773-786 (**2011**).

197. Nakayama, M., Suzuki, K., Toda, M., Okubo, S., Hara, Y., Shimamura, T. Inhibition of the infectivity of influenza virus by tea polyphenols. *Antiviral Res*., 21 (4), 289-299 (**1993**).

198. Zu, M., Yang, F., Zhou, W., Liu, A., Du, G., Zheng, L. In vitro anti-influenza virus and anti-inflammatory activities of theaflavin derivatives. *Antiviral Res*., 94 (3), 217-224 (**2012**).

199. Luo, G., Colonno, R., Krystal, M. Characterization of a hemagglutinin-specific inhibitor of influenza A virus. *Virology*, 226 (1), 66-76 (**1996**).

200. Luo, G., Torri, A., Harte, W. E., Danetz, S., Cianci, C., Tiley, L., Day, S., Mullaney, D., Yu, K. L., Ouellet, C., Dextraze, P., Meanwell, N., Colonno, R., Krystal, M. Molecular mechanism underlying the action of a novel fusion inhibitor of influenza A virus. *J Virol*., 71 (5), 4062-4070 (**1997**).

201. Yoshimoto, J., Kakui, M., Iwasaki, H., Fujiwara, T., Sugimoto, H., Hattori, N. Identification of a novel HA conformational change inhibitor of human influenza virus. *Arch Virol*., 144 (5), 865-878 (**1999**).

202. Rossignol, J. F., La Frazia, S., Chiappa, L., Ciucci, A., Santoro, M. G. Thiazolides, a new class of anti-influenza molecules targeting viral hemagglutinin at the post-translational level. *J Biol Chem*., 284 (43), 29798-29808 (**2009**).

203. Rossignol, J. F. Thiazolides: a new class of antiviral drugs. *Expert Opin Drug Metab Toxicol*., 5 (6), 667-674 (**2009**).

204. Rossignol, J. F. Nitazoxanide: a first-in-class broad-spectrum antiviral agent. *Antiviral Res*., 110, 94-103 (**2014**).

205. Belardo, G., Cenciarelli, O., La Frazia, S., Rossignol, J. F., Santoro, M. G. Synergistic effect of nitazoxanide with neuraminidase inhibitors against influenza A viruses in vitro. *Antimicrob Agents Chemother*., 59 (2), 1061-1069 (**2015**).

206. https://clinicaltrials.gov/ct2/results?cond=&term=nitazoxanide&cntry=&state=&city=&dist=.

207. Koszalka, P., Tilmanis, D., Hurt, A. C. Influenza antivirals currently in late-phase clinical trial. *Influenza Other Respir Viruses*, 11 (3), 240-246 (**2017**).

208. Stachulski, A. V., Santoro, M. G., Piacentini, S., Belardo, G., Frazia, S., Pidathala, C., Row, E. C., Berry, N. G., Iqbal, M., Allman, S. A., Semple, J. E., Eklov, B. M., O'Neill, P. M., Rossignol, J. F.. Second-generation nitazoxanide derivatives: thiazolides are effective inhibitors of the influenza A virus. *Future Med Chem*., 10 (8), 851-862 (**2018**).

209. Liu, S., Li, R., Zhang, R., Chan, C. C., Xi, B., Zhu, Z., Yang, J., Poon, V. K., Zhou, J., Chen, M., Münch, J., Kirchhoff, F., Pleschka, S., Haarmann, T., Dietrich, U., Pan, C., Du, L., Jiang, S., Zheng, B. CL-385319 inhibits H5N1 avian influenza A virus infection by blocking viral entry. *Eur J Pharmacol*., 660 (2-3), 460-467 (**2011**).

210. Waldmann, M., Jirmann, R., Hoelscher, K., Wienke, M., Niemeyer, F. C., Rehders, D., Meyer, B. A nanomolar multivalent ligand as entry inhibitor of the hemagglutinin of avian influenza. *J Am Chem Soc*., 136 (2), 783-788 (**2014**).

211. Dang, Z., Jung, K., Zhu, L., Xie, H., Lee, K. H., Chen, C. H., Huang, L. Phenolic diterpenoid derivatives as anti-influenza a virus agents. *ACS Med Chem Lett*., 6 (3), 355-358 (**2015**).

212. Yu, M., Si, L., Wang, Y., Wu, Y., Yu, F., Jiao, P., Shi, Y., Wang, H., Xiao, S., Fu, G., Tian, K., Wang, Y., Guo, Z., Ye, X., Zhang, L., Zhou, D. Discovery of pentacyclic triterpenoids as potential entry inhibitors of influenza viruses. *J Med Chem*., 57 (23), 10058-10071 (**2014**).

213. Chen, X., Si, L., Liu, D., Proksch, P., Zhang, L., Zhou, D., Lin, W. Neoechinulin B and its analogues as potential entry inhibitors of influenza viruses, targeting viral hemagglutinin. *Eur J Med Chem*., 93, 182-195 (**2015**).

214. Sacramento, C. Q., Martorelli, A., Fintelman-Rodrigues, N., de Freitas, C. S., de Melo, G. R., Rocha, M. E., Kaiser, C. R., Rodrigues, K. F., da Costa, G. L., Alves, C. M., Santos-Filho, O., Barbosa, J. P., Souza, T. M. Aureonitol, a Fungi-Derived Tetrahydrofuran, Inhibits Influenza Replication by Targeting Its Surface Glycoprotein Hemagglutinin. *PLoS One*, 10 (10), e0139236 (**2015**).

215. Chen, T. Y., Chen, D. Y., Wen, H. W., Ou, J. L., Chiou, S. S., Chen, J. M., Wong, M. L., Hsu, W. L. Inhibition of enveloped viruses infectivity by curcumin. *PLoS One*, 8 (5), e62482 (**2013**).

216. Aggarwal, B. B., Deb, L., Prasad, S. Curcumin differs from tetrahydrocurcumin for molecular targets, signaling pathways and cellular responses. *Molecules*, 20 (1), 185-205 (**2014**).

217. Liu, C. L., Hung, H. C., Lo, S. C., Chiang, C. H., Chen, I. J., Hsu, J. T., Hou, M. H. Using mutagenesis to explore conserved residues in the RNA-binding groove of influenza A virus nucleoprotein for antiviral drug development. *Sci Rep*., 6, 21662 (**2016**).

218. Kadam, R. U., Wilson, I. A. Structural basis of influenza virus fusion inhibition by the antiviral drug Arbidol. *Proc Natl Acad Sci U S A*., 114 (2), 206-214 (**2017**).

219. Wright, Z. V. F., Wu, N. C., Kadam, R. U., Wilson, I. A., Wolan, D. W. Structure-based optimization and synthesis of antiviral drug Arbidol analogues with significantly improved affinity to influenza hemagglutinin. *Bioorg Med Chem Lett*., 27 (16), 3744-3748 (**2017**).

220. Sparrow, E., Friede, M., Sheikh, M., Torvaldsen, S., Newall, A. T. Passive immunization for influenza through antibody therapies, a review of the pipeline, challenges and potential applications. *Vaccine*, 34 (45), 5442-5448 (**2016**).

221. Ekiert, D. C., Bhabha, G., Elsliger, M. A., Friesen, R. H., Jongeneelen, M., Throsby, M., Goudsmit, J., Wilson, I. A. Antibody recognition of a highly conserved influenza virus epitope. *Science*, 324 (5924), 246-251 (**2009**).

222. DiLillo, D. J., Tan, G. S., Palese, P., Ravetch, J. V. Broadly neutralizing hemagglutinin stalk-specific antibodies require FcγR interactions for protection against influenza virus in vivo. *Nat Med*., 20 (2), 143-151 (**2014**).

223. Paules, C. I., Lakdawala, S., McAuliffe, J. M., Paskel, M., Vogel, L., Kallewaard, N. L., Zhu, Q., Subbarao, K. The Hemagglutinin A Stem Antibody MEDI8852 Prevents and Controls Disease and Limits Transmission of Pandemic Influenza Viruses. *J Infect Dis*., 216 (3), 356-365 (**2017**).

224. Tharakaraman, K., Subramanian, V., Viswanathan, K., Sloan, S., Yen, H. L., Barnard, D. L., Leung, Y. H., Szretter, K. J., Koch, T. J., Delaney, J. C., Babcock, G. J., Wogan, G. N., Sasisekharan, R., Shriver, Z. A broadly neutralizing human monoclonal antibody is effective against H7N9. *Proc Natl Acad Sci U S A.*, 112 (35), 10890-10895 (**2015**).

225. Baranovich, T., Jones, J. C., Russier, M., Vogel, P., Szretter, K. J., Sloan, S. E., Seiler, P., Trevejo, J. M., Webby, R. J., Govorkova, E. A. The Hemagglutinin Stem-Binding Monoclonal Antibody VIS410 Controls Influenza Virus-Induced Acute Respiratory Distress Syndrome. *Antimicrob Agents Chemother.*, 60 (4), 2118-2131 (**2016**).

226. Wollacott, A. M., Boni, M. F., Szretter, K. J., Sloan, S. E., Yousofshahi, M., Viswanathan, K., Bedard, S., Hay, C. A., Smith, P. F., Shriver, Z., Trevejo, J. M. Safety and Upper Respiratory Pharmacokinetics of the Hemagglutinin Stalk-Binding Antibody VIS410 Support Treatment and Prophylaxis Based on Population Modeling of Seasonal Influenza A Outbreaks. *EBioMedicine*, 5, 147-155 (**2016**).

227. Lim, J. J., Deng, R., Derby, M. A., Larouche, R., Horn, P., Anderson, M., Maia, M., Carrier, S., Pelletier, I., Burgess, T., Kulkarni, P., Newton, E., Tavel, J. A. Two Phase 1, Randomized, Double-Blind, Placebo-Controlled, Single-Ascending-Dose Studies To Investigate the Safety, Tolerability, and Pharmacokinetics of an Anti-Influenza A Virus Monoclonal Antibody, MHAA4549A, in Healthy Volunteers. *Antimicrob Agents Chemother.*, 60 (9), 5437-5444 (**2016**).

228. McBride, J. M., Lim, J. J., Burgess, T., Deng, R., Derby, M. A., Maia, M., Horn, P., Siddiqui, O., Sheinson, D., Chen-Harris, H., Newton, E. M., Fillos, D., Nazzal, D., Rosenberger, C. M., Ohlson, M. B., Lambkin-Williams, R., Fathi, H., Harris, J. M., Tavel, J. A. Phase 2 Randomized Trial of the Safety and Efficacy of MHAA4549A, a Broadly Neutralizing Monoclonal Antibody, in a Human Influenza A Virus Challenge Model. *Antimicrob Agents Chemother.*, 61 (11), e01154-17 (**2017**).

229. Deng, R., Lee, A. P., Maia, M., Lim, J. J., Burgess, T., Horn, P., Derby, M. A., Newton, E., Tavel, J. A., Hanley, W. D. Pharmacokinetics of MHAA4549A, an Anti-Influenza A Monoclonal Antibody, in Healthy Subjects Challenged with Influenza A Virus in a Phase IIa Randomized Trial. *Clin Pharmacokinet.*, 57 (3), 367-377 (**2018**).

230. Wang, J., Wu, Y., Ma, C., Fiorin, G., Wang, J., Pinto, L. H., Lamb, R. A., Klein, M. L., Degrado, W. F. Structure and inhibition of the drug-resistant S31N mutant of the M2 ion channel of influenza A virus. *Proc Natl Acad Sci U S A.*, 110 (4), 1315-1320 (**2013**).

231. Sirohi, D., Kuhn, R. J. Can an FDA-Approved Alzheimer's Drug Be Repurposed for Alleviating Neuronal Symptoms of Zika Virus? *MBio*., 8 (3), e00916-00917 (**2017**).

232. Alves Galvão, M. G., Rocha Crispino Santos, M. A., Alves da Cunha, A. J. Amantadine and rimantadine for influenza A in children and the elderly. *Cochrane Database Syst Rev*., (11), CD002745 (**2014**).

233. Tataridis, D., Fytas, G., Kolocouris, A., Fytas, C., Kolocouris, N., Foscolos, G. B., Padalko, E., Neyts, J., De Clercq, E. Influence of an additional 2-amino substituent of the 1-aminoethyl pharmacophore group on the potency of rimantadine against influenza virus A. *Bioorg Med Chem Lett*., 17 (3), 692-696 (**2007**).

234. Fytas, C., Kolocouris, A., Fytas, G., Zoidis, G., Valmas, C., Basler, C. F. Influence of an additional amino group on the potency of aminoadamantanes against influenza virus A. II - Synthesis of spiropiperazines and in vitro activity against influenza A H3N2 virus. *Bioorg Chem*., 38 (6), 247-251 (**2010**).

235. Du, Q. S., Huang, R. B., Wang, S. Q., Chou, K. C. Designing inhibitors of M2 proton channel against H1N1 swine influenza virus. *PLoS One*, 5 (2), e9388 (**2010**).

236. Wang, J., Ma, C., Wang, J., Jo, H., Canturk, B., Fiorin, G., Pinto, L. H., Lamb, R. A., Klein, M. L., DeGrado, W. F. Discovery of novel dual inhibitors of the wild-type and the most prevalent drug-resistant mutant, S31N, of the M2 proton channel from influenza A virus. *J Med Chem*., 56 (7), 2804-2812 (**2013**).

237. Wu, Y., Canturk, B., Jo, H., Ma, C., Gianti, E., Klein, M. L., Pinto, L. H., Lamb, R. A., Fiorin, G., Wang, J., DeGrado, W. F. Flipping in the pore: discovery of dual inhibitors that bind in different orientations to the wild-type versus the amantadine-resistant S31N mutant of the influenza A virus M2 proton channel. *J Am Chem Soc*., 136 (52), 17987-17995 (**2014**).

238. Rey-Carrizo, M., Torres, E., Ma, C., Barniol-Xicota, M., Wang, J., Wu, Y., Naesens, L., DeGrado, W. F., Lamb, R. A., Pinto, L. H., Vázquez, S. 3-Azatetracyclo[5.2.1.1(5,8).0(1,5)]undecane derivatives: from wild-type inhibitors of the M2 ion channel of influenza A virus to derivatives with potent activity against the V27A mutant. *J Med Chem*., 56 (22), 9265-9274 (**2013**).

239. Rey-Carrizo, M., Barniol-Xicota, M., Ma, C., Frigolé-Vivas, M., Torres, E., Naesens, L., Llabrés, S., Juárez-Jiménez, J., Luque, F. J., DeGrado, W. F., Lamb, R. A., Pinto, L. H., Vázquez, S. Easily accessible polycyclic amines that inhibit the wild-type and amantadine-

resistant mutants of the M2 channel of influenza A virus. *J Med Chem*., 57 (13), 5738-5747 (**2014**).

240. Lin, T. I., Heider, H., Schroeder, C. Different modes of inhibition by adamantine amine derivatives and natural polyamines of the functionally reconstituted influenza virus M2 proton channel protein. *J Gen Virol*., 78 (4), 767-774 (**1997**).
241. Even-Or, O., Samira, S., Rochlin, E., Balasingam, S., Mann, A. J., Lambkin-Williams, R., Spira, J., Goldwaser, I., Ellis, R., Barenholz, Y. Immunogenicity, protective efficacy and mechanism of novel CCS adjuvanted influenza vaccine. *Vaccine*, 28 (39), 6527-6541 (**2010**).
242. Even-Or, O., Joseph, A., Itskovitz-Cooper, N., Samira, S., Rochlin, E., Eliyahu, H., Goldwaser, I., Balasingam, S., Mann, A. J., Lambkin-Williams, R., Kedar, E., Barenholz, Y. A new intranasal influenza vaccine based on a novel polycationic lipid-ceramide carbamoyl-spermine (CCS). II. Studies in mice and ferrets and mechanism of adjuvanticity. *Vaccine*, 29 (13), 2474-2486 (**2011**).
243. Zhao, X., Jie, Y., Rosenberg, M. R., Wan, J., Zeng, S., Cui, W., Xiao, Y., Li, Z., Tu, Z., Casarotto, M. G., Hu, W. Design and synthesis of pinanamine derivatives as anti-influenza A M2 ion channel inhibitors. *Antiviral Res*., 96 (2), 91-99 (**2012**)
244. Ramos, E. L., Mitcham, J. L., Koller, T. D., Bonavia, A., Usner, D. W., Balaratnam, G., Fredlund, P., Swiderek, K. M. Efficacy and safety of treatment with an anti-m2e monoclonal antibody in experimental human influenza. *J Infect Dis*., 211 (7), 1038-1044 (**2015**).
245. Galabov, A. S., Khristova, M. L., Uzunov, S., Wassilewa, L., Bucher, D. J., Kharitonenkov, I. G. Alteration in the antigenic structure of M1 protein of influenza A virus mutant resistant to a new antiviral compound mopyridone. *Acta Virol*., 38 (1), 5-10 (**1994**).
246. Tantcheva, L. P., Rangelova, D. S. Toxicity and enzyme-inducing effect of the antiviral compound mopyridone in mice. *Arzneimittelforschung*, 46 (9), 931-933 (**1996**).
247. Mosier, P. D., Chiang, M. J., Lin, Z., Gao, Y., Althufairi, B., Zhou, Q., Musayev, F., Safo, M. K., Xie, H., Desai, U. R. Broad Spectrum Anti-Influenza Agents by Inhibiting Self-Association of Matrix Protein 1. *Sci Rep*., 6, 32340 (**2016**).

248. Ai, H., Wu, X., Qi, M., Zhang, L., Hu, H., Zhao, Q., Zhao, J., Liu, H. Study on the Mechanisms of Active Compounds in Traditional Chinese Medicine for the Treatment of Influenza Virus by Virtual Screening. *Interdiscip Sci*., 10 (2), 320-328 (**2018**).

249. Palese, P., Schulman, J. L., Bodo, G., Meindl, P. Inhibition of influenza and parainfluenza virus replication in tissue culture by 2-deoxy-2,3-dehydro-N-trifluoroacetylneuraminic acid (FANA). *Virology*, 59 (2), 490-498 (**1974**).

250. Meindl, P., Bodo, G., Lindner, J., Palese, P. Influence of 2-deoxy-2,3-dehydro-N-acetylneuraminic acid on Myxovirus-neuraminidases and the replication of influenza- and Newcastle disease virus. *Z Naturforsch B.*, 26 (8), 792-797 (**1971**).

251. Holzer, C. T., von Itzstein, M., Jin, B., Pegg, M. S., Stewart, W. P., Wu, W. Y. Inhibition of sialidases from viral, bacterial and mammalian sources by analogues of 2-deoxy-2,3-didehydro-N-acetylneuraminic acid modified at the C-4 position. *Glycoconj J.*, 10 (1), 40-44 (**1993**).

252. Varghese, J. N., Epa, V. C., Colman, P. M. Three-dimensional structure of the complex of 4-guanidino-Neu5Ac2en and influenza virus neuraminidase. *Protein Sci.*, 4 (6), 1081-1087 (**1995**).

253. Kim, C. U., Lew, W., Williams, M. A., Liu, H., Zhang, L., Swaminathan, S., Bischofberger, N., Chen, M. S., Mendel, D. B., Tai, C. Y., Laver, W. G., Stevens, R. C. Influenza neuraminidase inhibitors possessing a novel hydrophobic interaction in the enzyme active site: design, synthesis, and structural analysis of carbocyclic sialic acid analogues with potent anti-influenza activity. *J Am Chem Soc*., 119 (4), 681-690 (**1997**).

254. McKimm-Breschkin, J. L. Influenza neuraminidase inhibitors: antiviral action and mechanisms of resistance. *Influenza Other Respir Viruses*, 7 (1), 25-36 (**2013**).

255. Gubareva, L. V., Besselaar, T. G., Daniels, R. S., Fry, A., Gregory, V., Huang, W., Hurt, A. C., Jorquera, P. A., Lackenby, A., Leang, S. K., Lo, J., Pereyaslov, D., Rebelo-de-Andrade, H., Siqueira, M. M., Takashita, E., Odagiri, T., Wang, D., Zhang, W., Meijer, A. Global update on the susceptibility of human influenza viruses to neuraminidase inhibitors, 2015-2016. *Antiviral Res*., 146, 12-20 (**2017**).

256. Bantia, S., Arnold, C. S., Parker, C. D., Upshaw, R., Chand, P. Anti-influenza virus activity of peramivir in mice with single intramuscular injection. *Antiviral Res*., 69 (1), 39-45 (**2006**).

257. Castillo, R., Holland, L. E., Boltz, D. A. Peramivir and its use in H1N1 influenza. *Drugs Today*, 46 (6), 399-408 (**2010**).

258. Mancuso, C. E., Gabay, M. P., Steinke, L. M., Vanosdol, S. J. Peramivir: an intravenous neuraminidase inhibitor for the treatment of 2009 H1N1 influenza. *Ann Pharmacother*., 44 (7-8), 1240-1249 (**2010**).

259. https://www.accessdata.fda.gov/scripts/cder/daf/index.cfm?event=overview.process&aplno=206426.

260. http://www.ema.europa.eu/ema/index.jsp?curl=pages/medicines/pips/EMEA-001856-PIP02-16/pip_001530.jsp&mid=WC0b01ac058001d129.

261. https://clinicaltrials.gov/ct2/results?cond=Peramivir&age_v=&gndr=&type=&rslt=&Search=Apply.

262. Yamashita, M., Tomozawa, T., Kakuta, M., Tokumitsu, A., Nasu, H., Kubo, S. CS-8958, a prodrug of the new neuraminidase inhibitor R-125489, shows long-acting anti-influenza virus activity. *Antimicrob Agents Chemother*., 53 (1),186-192 (**2009**).

263. Watanabe, A., Chang, S. C., Kim, M. J., Chu, D. W., Ohashi, Y; MARVEL Study Group. Long-acting neuraminidase inhibitor laninamivir octanoate versus oseltamivir for treatment of influenza: A double-blind, randomized, noninferiority clinical trial. *Clin Infect Dis*., 51 (10), 1167-1175 (**2010**).

264. Sugaya, N., Ohashi, Y. Long-acting neuraminidase inhibitor laninamivir octanoate (CS-8958) versus oseltamivir as treatment for children with influenza virus infection. *Antimicrob Agents Chemother*., 54 (6), 2575-2582 (**2010**).

265. https://clinicaltrials.gov/ct2/results?cond=&term=CS-8958&cntry=&state=&city=&dist=

266. Ikematsu, H., Kawai, N. Laninamivir octanoate: a new long-acting neuraminidase inhibitor for the treatment of influenza. *Expert Rev Anti Infect Ther*., 9 (10), 851-857 (**2011**).

267. Kati, W. M., Montgomery, D., Carrick, R., Gubareva, L., Maring, C., McDaniel, K., Steffy, K., Molla, A., Hayden, F., Kempf, D., Kohlbrenner, W. In vitro characterization of A-315675, a highly potent inhibitor of A and B strain influenza virus neuraminidases and influenza virus replication. *Antimicrob Agents Chemother*., 46 (4), 1014-1021 (**2002**).

268. Hanessian, S., Wang, J., Montgomery, D., Stoll, V., Stewart, K. D., Kati, W., Maring, C., Kempf, D., Hutchins, C., Laver, W. G. Design, synthesis, and neuraminidase inhibitory

activity of GS-4071 analogues that utilize a novel hydrophobic paradigm. *Bioorg Med Chem Lett*., 12 (23), 3425-3429 (**2002**).

269. Mohan, S., McAtamney, S., Haselhorst, T., von Itzstein, M., Pinto, B. M. Carbocycles related to oseltamivir as influenza virus group-1-specific neuraminidase inhibitors. Binding to N1 enzymes in the context of virus-like particles. *J Med Chem*., 53 (20), 7377-7391 (**2010**).
270. Kerry, P. S., Mohan, S., Russell, R. J., Bance, N., Niikura, M., Pinto, B. M. Structural basis for a class of nanomolar influenza A neuraminidase inhibitors. *Sci Rep*., 3, 2871 (**2013**).
271. Mooney, C. A., Johnson, S. A., 't Hart, P., Quarles van Ufford, L., de Haan, C. A., Moret, E. E., Martin, N. I.. Oseltamivir analogues bearing N-substituted guanidines as potent neuraminidase inhibitors. *J Med Chem*., 57 (7), 3154-3160 (**2014**).
272. Mohan, S., Kerry, P. S., Bance, N., Niikura, M., Pinto, B. M. Serendipitous discovery of a potent influenza virus a neuraminidase inhibitor. *Angew Chem Int Ed Engl*., 53 (4), 1076-1080 (**2014**).
273. Cheng, T. J., Weinheimer, S., Tarbet, E. B., Jan, J. T., Cheng, Y. S., Shie, J. J., Chen, C. L., Chen, C. A., Hsieh, W. C., Huang, P. W., Lin, W. H., Wang, S. Y., Fang, J. M., Hu, O. Y., Wong, C. H. Development of oseltamivir phosphonate congeners as anti-influenza agents. *J Med Chem*., 55 (20), 8657-8670 (**2012**).
274. Kim, J. H., Resende, R., Wennekes, T., Chen, H. M., Bance, N., Buchini, S., Watts, A. G., Pilling, P., Streltsov, V. A., Petric, M., Liggins, R., Barrett, S., McKimm-Breschkin, J. L., Niikura, M., Withers, S. G. Mechanism-based covalent neuraminidase inhibitors with broad-spectrum influenza antiviral activity. *Science*, 340 (6128), 71-75 (**2013**).
275. Schade, D., Kotthaus, J., Riebling, L., Kotthaus, J., Müller-Fielitz, H., Raasch, W., Koch, O., Seidel, N., Schmidtke, M., Clement, B. Development of novel potent orally bioavailable oseltamivir derivatives active against resistant influenza A. *J Med Chem*., 57 (3), 759-769 (**2014**).
276. McKimm-Breschkin, J. L., Colman, P. M., Jin, B., Krippner, G. Y., McDonald, M., Reece, P. A., Tucker, S. P., Waddington, L., Watson, K. G., Wu, W. Y. Tethered neuraminidase inhibitors that bind an influenza virus: a first step towards a diagnostic method for influenza. *Angew Chem Int Ed Engl*., 42 (27), 3118-3121 (**2003**).

277. Watson, K. G., Cameron, R., Fenton, R. J., Gower, D., Hamilton, S., Jin, B., Krippner, G. Y., Luttick, A., McConnell, D., MacDonald, S. J., Mason, A. M., Nguyen, V., Tucker, S. P., Wu, W. Y. Highly potent and long-acting trimeric and tetrameric inhibitors of influenza virus neuraminidase. *Bioorg Med Chem Lett*., 14 (6), 1589-1592 (**2004**).

278. Macdonald, S. J., Cameron, R., Demaine, D. A., Fenton, R. J., Foster, G., Gower, D., Hamblin, J. N., Hamilton, S., Hart, G. J., Hill, A. P., Inglis, G. G., Jin, B., Jones, H. T., McConnell, D. B., McKimm-Breschkin, J., Mills, G., Nguyen, V., Owens, I. J., Parry, N., Shanahan, S. E., Smith, D., Watson, K. G., Wu, W. Y., Tucker, S. P. Dimeric zanamivir conjugates with various linking groups are potent, long-lasting inhibitors of influenza neuraminidase including H5N1 avian influenza. *J Med Chem*., 48 (8), 2964-2971 (**2005**).

279. Tarbet, E. B., Hamilton, S., Vollmer, A. H., Luttick, A., Ng, W. C., Pryor, M., Hurst, B. L., Crawford, S., Smee, D. F., Tucker, S. P. A zanamivir dimer with prophylactic and enhanced therapeutic activity against influenza viruses. *J Antimicrob Chemother*., 69 (8), 2164-2174 (**2014**).

280. Wang, G. T., Chen, Y., Wang, S., Gentles, R., Sowin, T., Kati, W., Muchmore, S., Giranda, V., Stewart, K., Sham, H., Kempf, D., Laver, W. G. Design, synthesis, and structural analysis of influenza neuraminidase inhibitors containing pyrrolidine cores. *J Med Chem*., 44 (8), 1192-1201 (**2001**).

281. Atigadda, V. R., Brouillette, W. J., Duarte, F., Babu, Y. S., Bantia, S., Chand, P., Chu, N., Montgomery, J. A., Walsh, D. A., Sudbeck, E., Finley, J., Air, G. M., Luo, M., Laver, G. W. Hydrophobic benzoic acids as inhibitors of influenza neuraminidase. *Bioorg Med Chem*., 7 (11), 2487-2497 (**1999**).

282. Brouillette, W. J., Bajpai, S. N., Ali, S. M., Velu, S. E., Atigadda, V. R., Lommer, B. S., Finley, J. B., Luo, M., Air, G. M. Pyrrolidinobenzoic acid inhibitors of influenza virus neuraminidase: modifications of essential pyrrolidinone ring substituents. *Bioorg Med Chem*., 11 (13), 2739-2749 (**2003**).

283. Zhang, J., Wang, Q., Fang, H., Xu, W., Liu, A., Du, G. Design, synthesis, inhibitory activity, and SAR studies of hydrophobic p-aminosalicylic acid derivatives as neuraminidase inhibitors. *Bioorg Med Chem*., 16 (7), 3839-3847 (**2008**).

284. Krumbiegel, M., Dimitrov, D. S., Puri, A., Blumenthal, R. Dextran sulfate inhibits fusion of influenza virus and cells expressing influenza hemagglutinin with red blood cells. *Biochim Biophys Acta*, 1110 (2), 158-164 (**1992**).

285. Herrmann, A., Korte, T., Arnold, K., Hillebrecht, B. The influence of dextran sulphate on influenza A virus fusion with erythrocyte membranes. *Antiviral Res*., 19 (4), 295-311 (**1992**).

286. Yamada, H., Moriishi, E., Haredy, A. M., Takenaka, N., Mori, Y., Yamanishi, K., Okamoto, S. Influenza virus neuraminidase contributes to the dextran sulfate-dependent suppressive replication of some influenza A virus strains. *Antiviral Res*., 96 (3), 344-352 (**2012**).

287. Yamada, H., Nagao, C., Haredy, A. M., Mori, Y., Mizuguchi, K., Yamanishi, K., Okamoto, S. Dextran sulfate-resistant A/Puerto Rico/8/34 influenza virus is associated with the emergence of specific mutations in the neuraminidase glycoprotein. *Antiviral Res*., 111, 69-77 (**2014**).

288. Ivachtchenko, A. V., Ivanenkov, Y. A., Mitkin, O. D., Yamanushkin, P. M., Bichko, V. V., Shevkun, N. A., Karapetian, R. N., Leneva, I. A., Borisova, O. V., Veselov, M. S. Novel oral anti-influenza drug candidate AV5080. *J Antimicrob Chemother*., 69 (7), 1892-1902 (**2014**).

289. Miki, K., Nagai, T., Suzuki, K., Tsujimura, R., Koyama, K., Kinoshita, K., Furuhata, K., Yamada, H., Takahashi, K. Anti-influenza virus activity of biflavonoids. *Bioorg Med Chem Lett*., 17 (3), 772-775 (**2007**).

290. Ryu, Y. B., Curtis-Long, M. J., Kim, J. H., Jeong, S. H., Yang, M. S., Lee, K. W., Lee, W. S., Park, K. H. Pterocarpans and flavanones from Sophora flavescens displaying potent neuraminidase inhibition. *Bioorg Med Chem Lett*., 18 (23), 6046-6049 (**2008**).

291. Ryu, Y. B., Curtis-Long, M. J., Lee, J. W., Ryu, H. W., Kim, J. Y., Lee, W. S., Park, K. H. Structural characteristics of flavanones and flavones from Cudrania tricuspidata for neuraminidase inhibition. *Bioorg Med Chem Lett*., 19 (17), 4912-4915 (**2009**).

292. Nagai, T., Miyaichi, Y., Tomimori, T., Suzuki, Y., Yamada, H. In vivo anti-influenza virus activity of plant flavonoids possessing inhibitory activity for influenza virus sialidase. *Antiviral Res*., 19 (3), 207-217 (**1992**).

293. Nagai, T., Suzuki, Y., Tomimori, T., Yamada, H. Antiviral activity of plant flavonoid, 5,7,4'-trihydroxy-8-methoxyflavone, from the roots of Scutellaria baicalensis against influenza A (H3N2) and B viruses. *Biol Pharm Bull*., 18 (2), 295-299 (**1995**).

294. Lee, C. L., Chiang, L. C., Cheng, L. H., Liaw, C. C., Abd El-Razek, M. H., Chang, F. R., Wu, Y. C. Influenza A (H1N1) Antiviral and Cytotoxic Agents from Ferula assa-foetida. *J Nat Prod*., 72 (9), 1568-1572 (**2009**).

295. Palamara, A. T., Nencioni, L., Aquilano, K., De Chiara, G., Hernandez, L., Cozzolino, F., Ciriolo, M. R., Garaci, E. Inhibition of influenza A virus replication by resveratrol. *J Infect Dis*., 191 (10), 1719-1729 (**2005**).

296. Li, C., Fang, J. S., Lian, W. W., Pang, X. C., Liu, A. L., Du, G. H. In vitro antiviral effects and 3D QSAR study of resveratrol derivatives as potent inhibitors of influenza H1N1 neuraminidase. *Chem Biol Drug Des*., 85 (4), 427-438 (**2015**).

297. Ye, Q., Krug, R. M., Tao, Y. J. The mechanism by which influenza A virus nucleoprotein forms oligomers and binds RNA. *Nature*, 444 (7122), 1078-1082 (**2006**).

298. Ye, Q., Guu, T. S., Mata, D. A., Kuo, R. L., Smith, B., Krug, R. M., Tao, Y. J. Biochemical and structural evidence in support of a coherent model for the formation of the double-helical influenza A virus ribonucleoprotein. *MBio*., 4 (1), e00467-12 (**2012**).

299. Kao, R. Y., Yang, D., Lau, L. S., Tsui, W. H., Hu, L., Dai, J., Chan, M. P., Chan, C. M., Wang, P., Zheng, B. J., Sun, J., Huang, J. D., Madar, J., Chen, G., Chen, H., Guan, Y., Yuen, K. Y. Identification of influenza A nucleoprotein as an antiviral target. *Nat Biotechnol*., 28 (6), 600-605 (**2010**).

300. Su, C. Y., Cheng, T. J., Lin, M. I., Wang, S. Y., Huang, W. I., Lin-Chu, S. Y., Chen, Y. H., Wu, C. Y., Lai, M. M., Cheng, W. C., Wu, Y. T., Tsai, M. D., Cheng, Y. S., Wong, C. H. High-throughput identification of compounds targeting influenza RNA-dependent RNA polymerase activity. *Proc Natl Acad Sci U S A*., 107 (45), 19151-19156 (**2010**).

301. Shen, Y. F., Chen, Y. H., Chu, S. Y., Lin, M. I., Hsu, H. T., Wu, P. Y., Wu, C. J., Liu, H. W., Lin, F. Y., Lin, G., Hsu, P. H., Yang, A. S., Cheng, Y. S., Wu, Y. T., Wong, C. H., Tsai, M. D. E339...R416 salt bridge of nucleoprotein as a feasible target for influenza virus inhibitors. *Proc Natl Acad Sci U S A*., 108 (40), 16515-16520 (**2011**).

302. Cheng, H., Wan, J., Lin, M. I., Liu, Y., Lu, X., Liu, J., Xu, Y., Chen, J., Tu, Z., Cheng, Y. S., Ding, K. Design, synthesis, and in vitro biological evaluation of 1H-1,2,3-triazole-4-carboxamide derivatives as new anti-influenza A agents targeting virus nucleoprotein. *J Med Chem*., 55 (5), 2144-2153 (**2012**).

303. Pang, B., Cheung, N. N., Zhang, W., Dai, J., Kao, R. Y., Zhang, H., Hao, Q. Structural Characterization of H1N1 Nucleoprotein-Nucleozin Binding Sites. *Sci Rep*., 6, 29684 (**2016**).

304. Kakisaka, M., Sasaki, Y., Yamada, K., Kondoh, Y., Hikono, H., Osada, H., Tomii, K., Saito, T., Aida, Y. A Novel Antiviral Target Structure Involved in the RNA Binding, Dimerization, and Nuclear Export Functions of the Influenza A Virus Nucleoprotein. *PLoS Pathog*., 11 (7), e1005062 (**2015**).

305. Pons, M. W. The inhibition of influenza virus RNA synthesis by actinomycin D and cycloheximide. *Virology*, 51 (1), 120-128 (**1973**).

306. Lejal, N., Tarus, B., Bouguyon, E., Chenavas, S., Bertho, N., Delmas, B., Ruigrok, R. W., Di Primo, C., Slama-Schwok, A. Structure-based discovery of the novel antiviral properties of naproxen against the nucleoprotein of influenza A virus. *Antimicrob Agents Chemother*., 57 (5), 2231-2242 (**2013**).

307. Shishkina, L. N., Nebol'sin, V. E., Kabanov, A. S., Skarnovich, M. O., Mazurkova, N. A., Sergeev, A. A., Serova, O. A., Stavskiĭ, E. A., Drozdov, I. G. In vitro and in vivo efficacy of Ingavirin against strains of pandemic influenza virus A(H1N1/09)v. *Zh Mikrobiol Epidemiol Immunobiol*., 2, 93-96 (**2011**).

308. Krug, R. M., Yuan, W., Noah, D. L., Latham, A. G. Intracellular warfare between human influenza viruses and human cells: the roles of the viral NS1 protein. *Virology*, 309 (2), 181-189 (**2003**).

309. Yin, C., Khan, J. A., Swapna, G. V., Ertekin, A., Krug, R. M., Tong, L., Montelione, G. T. Conserved surface features form the double-stranded RNA binding site of non-structural protein 1 (NS1) from influenza A and B viruses. *J Biol Chem*., 282 (28), 20584-20592 (**2007**).

310. Hale, B. G., Barclay, W. S., Randall, R. E., Russell, R. J. Structure of an avian influenza A virus NS1 protein effector domain. *Virology*, 378 (1), 1-5 (**2008**).

311. Silverman, R. H. Viral encounters with 2',5'-oligoadenylate synthetase and RNase L during the interferon antiviral response. *J Virol*., 81 (23), 12720-12729 (**2007**).

312. Guo, Z., Chen, L. M., Zeng, H., Gomez, J. A., Plowden, J., Fujita, T., Katz, J. M, Donis, R. O., Sambhara, S. NS1 protein of influenza A virus inhibits the function of intracytoplasmic pathogen sensor, RIG-I. *Am J Respir Cell Mol Biol*., 36 (3), 263-269 (**2007**).

313. Ludwig, S., Wolff, T. Influenza A virus TRIMs the type I interferon response. *Cell Host Microbe*, 5 (5), 420-421 (**2009**).

314. Nemeroff, M. E., Barabino, S. M., Li, Y., Keller, W., Krug, R. M. Influenza virus NS1 protein interacts with the cellular 30 kDa subunit of CPSF and inhibits 3'end formation of cellular pre-mRNAs. *Mol Cell*., 1 (7), 991-1000 (**1998**).

315. Noah, D. L., Twu, K. Y., Krug, R. M. Cellular antiviral responses against influenza A virus are countered at the posttranscriptional level by the viral NS1A protein via its binding to a cellular protein required for the 3' end processing of cellular pre-mRNAS. *Virology*, 307 (2), 386-395 (**2003**).

316. Kochs, G., García-Sastre, A., Martínez-Sobrido, L. Multiple anti-interferon actions of the influenza A virus NS1 protein. *J Virol*., 81 (13), 7011-7021 (**2007**).

317. Twu, K. Y., Noah, D. L., Rao, P., Kuo, R. L., Krug, R. M. The CPSF30 binding site on the NS1A protein of influenza A virus is a potential antiviral target. *J Virol*., 80 (8), 3957-3965 (**2006**).

318. Jablonski, J. J., Basu, D., Engel, D. A., Geysen, H. M. Design, synthesis, and evaluation of novel small molecule inhibitors of the influenza virus protein NS1. *Bioorg Med Chem*., 20 (1), 487-497 (**2012**).

319. Bauman, J. D., Patel, D., Baker, S. F., Vijayan, R. S., Xiang, A., Parhi, A. K., Martínez-Sobrido, L., LaVoie, E. J., Das, K., Arnold, E. Crystallographic fragment screening and structure-based optimization yields a new class of influenza endonuclease inhibitors. *ACS Chem Biol*., 8 (11), 2501-2508 (**2013**).

320. Naesens, L., Stevaert, A., Vanderlinden, E. Antiviral therapies on the horizon for influenza. *Curr Opin Pharmacol*., 30, 106-115 (**2016**).

321. Tomassini, J., Selnick, H., Davies, M. E., Armstrong, M. E., Baldwin, J., Bourgeois, M., Hastings, J., Hazuda, D., Lewis, J., McClements, W., et al. Inhibition of cap (m7GpppXm)-dependent endonuclease of influenza virus by 4-substituted 2,4-dioxobutanoic acid compounds. *Antimicrob Agents Chemother*., 38 (12), 2827-2837 (**1994**).

322. Stevaert, A., Dallocchio, R., Dessì, A., Pala, N., Rogolino, D., Sechi, M., Naesens, L. Mutational analysis of the binding pockets of the diketo acid inhibitor L-742,001 in the influenza virus PA endonuclease. *J Virol*., 87 (19), 10524-10538 (**2013**).

323. Cianci, C., Chung, T. D. Y., Meanwell, N., Putz, H., Hagen, M., J., R., Krystal, M. Identification of N-Hydroxamic Acid and N-Hydroxyimide Compounds that Inhibit the Influenza Virus Polymerase. *Antivir Chem Chemother.*, 7 (6), 353-360 (**1996**).

324. Tomassini, J. E., Davies, M. E., Hastings, J. C., Lingham, R., Mojena, M., Raghoobar, S. L., Singh, S. B., Tkacz, J. S., Goetz, M. A. A novel antiviral agent which inhibits the endonuclease of influenza viruses. *Antimicrob Agents Chemother*., 40 (5), 1189-1193 (**1996**).

325. Singh, S. B., Tomassini, J. E. Synthesis of natural flutimide and analogous fully substituted pyrazine-2,6-diones, endonuclease inhibitors of influenza virus. *J Org Chem*., 66 (16), 5504-5516 (**2001**).

326. Baranov, M. S., Fedyakina, I. T., Shchelkanov, M. Y., Yampolsky, I. V. Ring expanding rearrangement of 2-acyl-5-arylidene-3,5-dihydro-4H-imidazol-4-ones in synthesis of flutimide analogs. *Tetrahedron*, 70 (23), 3712-3719 (**2014**).

327. Parkes, K. E., Ermert, P., Fässler, J., Ives, J., Martin, J. A., Merrett, J. H., Obrecht, D., Williams, G., Klumpp, K. Use of a pharmacophore model to discover a new class of influenza endonuclease inhibitors. *J Med Chem*., 46 (7), 1153-1164 (**2003**).

328. Imanishi, N., Tuji, Y., Katada, Y., Maruhashi, M., Konosu, S., Mantani, N., Terasawa, K., Ochiai, H.. Additional inhibitory effect of tea extract on the growth of influenza A and B viruses in MDCK cells. *Microbiol Immunol*., 46 (7), 491-494 (**2002**).

329. Song, J. M., Lee, K. H., Seong, B. L. Antiviral effect of catechins in green tea on influenza virus. *Antiviral Res*., 68 (2), 66-74 (**2005**).

330. Ling, J. X., Wei, F., Li, N., Li, J. L., Chen, L. J., Liu, Y. Y., Luo, F., Xiong, H. R., Hou, W., Yang, Z. Q. Amelioration of influenza virus-induced reactive oxygen species formation by epigallocatechin gallate derived from green tea. *Acta Pharmacol Sin*., 33 (12), 1533-1541 (**2012**).

331. Kuzuhara, T., Iwai, Y., Takahashi, H., Hatakeyama, D., Echigo, N. Green tea catechins inhibit the endonuclease activity of influenza A virus RNA polymerase. *PLoS Curr*., 1, RRN1052 (**2009**).

332. Iwai, Y., Takahashi, H., Hatakeyama, D., Motoshima, K., Ishikawa, M., Sugita, K., Hashimoto, Y., Harada, Y., Itamura, S., Odagiri, T., Tashiro, M., Sei, Y., Yamaguchi, K., Kuzuhara, T. Anti-influenza activity of phenethylphenylphthalimide analogs derived from thalidomide. *Bioorg Med Chem*., 18 (14), 5379-5390 (**2010**).

333. Iwai, Y., Murakami, K., Gomi, Y., Hashimoto, T., Asakawa, Y., Okuno, Y., Ishikawa, T., Hatakeyama, D., Echigo, N., Kuzuhara, T. Anti-influenza activity of marchantins, macrocyclic bisbibenzyls contained in liverworts. *PLoS One*, 6 (5), e19825 (**2011**).

334. Shoji, M., Takahashi, E., Hatakeyama, D., Iwai, Y., Morita, Y., Shirayama, R., Echigo, N., Kido, H., Nakamura, S., Mashino, T., Okutani, T., Kuzuhara, T. Anti-influenza activity of c60 fullerene derivatives. *PLoS One*, 8 (6), e66337 (**2013**).

335. Parhi, A. K., Xiang, A., Bauman, J. D., Patel, D., Vijayan, R. S, Das, K., Arnold, E., Lavoie, E, J. Phenyl substituted 3-hydroxypyridin-2(1H)-ones: inhibitors of influenza A endonuclease. *Bioorg Med Chem*., 21 (21), 6435-6446 (**2013**).

336. Sagong, H. Y., Parhi, A., Bauman, J. D., Patel, D., Vijayan, R. S., Das, K., Arnold, E., LaVoie, E. J. 3-Hydroxyquinolin-2(1H)-ones As Inhibitors of Influenza A Endonuclease. *ACS Med Chem Lett*., 4 (6), 547-550 (**2013**).

337. Sagong, H. Y., Bauman, J. D., Patel, D., Das, K., Arnold, E., LaVoie, E. J. Phenyl substituted 4-hydroxypyridazin-3(2H)-ones and 5-hydroxypyrimidin-4(3H)-ones: inhibitors of influenza A endonuclease. *J Med Chem*., 57 (19), 8086-8098 (**2014**).

338. Chen, E., Swift, R. V., Alderson, N., Feher, V. A., Feng, G. S., Amaro, R. E. Computation-guided discovery of influenza endonuclease inhibitors. *ACS Med Chem Lett*., 5 (1), 61-64 (**2014**).

339. Carcelli, M., Rogolino, D., Bacchi, A., Rispoli, G., Fisicaro, E., Compari, C., Sechi, M., Stevaert, A., Naesens, L. Metal-chelating 2-hydroxyphenyl amide pharmacophore for inhibition of influenza virus endonuclease. *Mol Pharm*., 11 (1), 304-316 (**2014**).

340. Rogolino, D., Bacchi, A., De Luca, L., Rispoli, G., Sechi, M., Stevaert, A., Naesens, L., Carcelli, M. Investigation of the salicylaldehyde thiosemicarbazone scaffold for inhibition of influenza virus PA endonuclease. *J Biol Inorg Chem*., 20 (7), 1109-1121 (**2015**).

341. Fudo, S., Yamamoto, N., Nukaga, M., Odagiri, T., Tashiro, M., Neya, S., Hoshino, T. Structural and computational study on inhibitory compounds for endonuclease activity of influenza virus polymerase. *Bioorg Med Chem*., 23 (17), 5466-5475 (**2015**).

342. Pala, N., Stevaert, A., Dallocchio, R., Dessì, A., Rogolino, D., Carcelli, M., Sanna, V., Sechi, M., Naesens, L. Virtual Screening and Biological Validation of Novel Influenza Virus PA Endonuclease Inhibitors. *ACS Med Chem Lett*., 6 (8), 866-871 (**2015**).

343. Credille, C. V., Chen, Y., Cohen, S. M. Fragment-Based Identification of Influenza Endonuclease Inhibitors. *J Med Chem*., 59 (13), 6444-6454 (**2016**).

344. Yuan, S., Chu, H., Singh, K., Zhao, H., Zhang, K., Kao, R. Y., Chow, B. K., Zhou, J., Zheng, B. J. A novel small-molecule inhibitor of influenza A virus acts by suppressing PA endonuclease activity of the viral polymerase. *Sci Rep*., 6, 22880 (**2016**).

345. https://clinicaltrials.gov/ct2/results?cond=AL-794&term=&cntry=&state=&city=&dist=.

346. Portsmouth, S., Kawaguchi, K., Arai, M. Tsuchiya, K., Uehara, T. Cap-dependent Endonuclease Inhibitor S-033188 for the Treatment of Influenza: Results from a Phase 3, Randomized, Double-Blind, Placebo- and Active-Controlled Study in Otherwise Healthy Adolescents and Adults with Seasonal Influenza. *Open Forum Infect Dis.*, 4, (1), S734 (**2017**).

347. Sidwell, R. W., Khare, G. P., Allen, L, B., Huffman, J. G., Witkowski, J. T., Simon, L. N., Robins, R. K. In vitro and in vivo effect of 1-beta-D-ribofuranosyl-1,2,4-triazole-3-carboxamide (ribavirin) on types 1 and 3 parainfulenza virus infections. *Chemotherapy*, 21 (3-4), 205-220 (**1975**).

348. Allen, L. B., Boswell, K. H., Khwaja, T. A., Meyer, R. B. Jr, Sidwell, R. W., Witkowski, J. T., Christensen, L. F., Robins, R. K. Synthesis and antiviral acticity of some phosphates of the broad-spectrum antiviral nucleoside, 1-beta-D-ribofuranosyl-1,2,4-triazole-3-carboxamide (ribavirin). *J Med Chem*., 21 (8), 742-746 (**1978**).

349. Goswami, B. B., Borek, E., Sharma, O. K., Fujitaki, J., Smith, R. A. The broad spectrum antiviral agent ribavirin inhibits capping of mRNA. *Biochem Biophys Res Commun*., 89 (3), 830-836 (**1979**).

350. Vanderlinden, E., Vrancken, B., Van Houdt, J., Rajwanshi, V. K., Gillemot, S., Andrei, G., Lemey, P., Naesens, L. Distinct Effects of T-705 (Favipiravir) and Ribavirin on Influenza Virus Replication and Viral RNA Synthesis. *Antimicrob Agents Chemother*., 60 (11), 6679-6691 (**2016**).

351. Furuta, Y., Gowen, B. B., Takahashi, K., Shiraki, K., Smee, D. F., Barnard, D. L. Favipiravir (T-705), a novel viral RNA polymerase inhibitor. *Antiviral Res*., 100 (2), 446-454 (**2013**).

352. https://www.clinicaltrials.gov/ct2/results?cond=Influenza&term=favipiravir&entry=&state=&city=&dist=.

353. Vedula, M. S., Jennepalli, S., Aryasomayajula, R., Rondla, S. R., Musku, M. R., Kura, R. R., Bandi, P. R. Novel nucleosides as potent influenza viral inhibitors. *Bioorg Med Chem*., 18 (17), 6329-6339 (**2010**).

354. Abdel-Magid, A. F. Influenza RNA-Dependent RNA Polymerase (RdRp) Inhibitors: Potential New Therapy for Influenza Treatment. *ACS Med Chem Lett*., 4 (12), 1133-1134 (**2013**).

355. Lin, C., Sun, C., Liu, X., Zhou, Y., Hussain, M., Wan, J., Li, M., Li, X., Jin, R., Tu, Z., Zhang, J. Design, synthesis, and in vitro biological evaluation of novel 6-methyl-7-substituted-7-deaza purine nucleoside analogs as anti-influenza A agents. *Antiviral Res*., 129, 13-20 (**2016**).

356. Kumaki, Y., Day, C. W., Smee, D. F., Morrey, J. D., Barnard, D. L. In vitro and in vivo efficacy of fluorodeoxycytidine analogs against highly pathogenic avian influenza H5N1, seasonal, and pandemic H1N1 virus infections. *Antiviral Res*., 92 (2), 329-340 (**2011**).

357. Ortigoza, M. B., Dibben, O., Maamary, J., Martinez-Gil, L., Leyva-Grado, V. H., Abreu, P. Jr, Ayllon, J., Palese, P., Shaw, M. L. A novel small molecule inhibitor of influenza A viruses that targets polymerase function and indirectly induces interferon. *PLoS Pathog*., 8 (4), e1002668 (**2012**).

358. Pautus, S., Sehr, P., Lewis, J., Fortuné, A., Wolkerstorfer, A., Szolar, O., Guilligay, D., Lunardi, T., Décout, J. L., Cusack, S. New 7-methylguanine derivatives targeting the influenza polymerase PB2 cap-binding domain. *J Med Chem*., 56 (21), 8915-8930 (**2013**).

359. Clark, M. P., Ledeboer, M. W., Davies, I., Byrn, R. A., Jones, S. M., Perola, E., Tsai, A., Jacobs, M., Nti-Addae, K., Bandarage, U. K., Boyd, M. J., Bethiel, R. S., Court, J. J., Deng, H., Duffy, J. P., Dorsch, W. A., Farmer, L. J., Gao, H., Gu, W., Jackson, K., Jacobs, D. H., Kennedy, J. M., Ledford, B., Liang, J., Maltais, F., Murcko, M., Wang, T., Wannamaker, M. W., Bennett, H. B., Leeman, J. R., McNeil, C., Taylor, W. P., Memmott, C., Jiang, M., Rijnbrand, R., Bral, C., Germann, U., Nezami, A., Zhang, Y., Salituro, F. G., Bennani, Y. L., Charifson, P. S. Discovery of a novel, first-in-class, orally bioavailable azaindole inhibitor (VX-787) of influenza PB2. *J Med Chem*., 57 (15), 6668-6678 (**2014**).

360. https://www.clinicaltrials.gov/ct2/results?term=VX787&age_v=&gndr=&type=&rslt=&phase=1&Search=Apply.

361. Byrn, R. A., Jones, S. M., Bennett, H. B., Bral, C., Clark, M. P., Jacobs, M. D., Kwong, A. D., Ledeboer, M. W., Leeman, J. R., McNeil, C. F., Murcko, M. A., Nezami, A., Perola, E., Rijnbrand, R., Saxena, K., Tsai, A. W., Zhou, Y., Charifson, P. S. Preclinical activity of VX-787, a first-in-class, orally bioavailable inhibitor of the influenza virus polymerase PB2 subunit. *Antimicrob Agents Chemother*., 59 (3), 1569-1582 (**2015**).

362. Tsai, A. W., McNeil, C. F., Leeman, J. R., Bennett, H. B., Nti-Addae, K., Huang, C., Germann, U. A., Byrn, R. A., Berlioz-Seux, F., Rijnbrand, R., Clark, M. P., Charifson, P. S., Jones, S. M. Novel Ranking System for Identifying Efficacious Anti-Influenza Virus PB2 Inhibitors. *Antimicrob Agents Chemother*., 59 (10), 6007-6016 (**2015**).

363. Fu, Y., Gaelings, L., Söderholm, S., Belanov, S., Nandania, J., Nyman, T. A., Matikainen, S., Anders, S., Velagapudi, V., Kainov, D. E. JNJ872 inhibits influenza A virus replication without altering cellular antiviral responses. *Antiviral Res*., 133, 23-31 (**2016**).

364. Boyd, M. J., Bandarage, U. K., Bennett, H., Byrn, R. R., Davies, I., Gu, W., Jacobs, M., Ledeboer, M. W., Ledford, B., Leeman, J. R., Perola, E., Wang, T., Bennani, Y., Clark, M. P., Charifson, P. S. Isosteric replacements of the carboxylic acid of drug candidate VX-787: Effect of charge on antiviral potency and kinase activity of azaindole-based influenza PB2 inhibitors. *Bioorg Med Chem Lett*., 25 (9), 1990-1994 (**2015**).

365. Roch, F. F., Hinterkörner, G., Menke, J., Tang, G. Q., Cusack, S., Butzendobler, B., Buschmann, H., Datta, K., Wolkerstorfer, A. An RNA Hybridization Assay for Screening Influenza A Virus Polymerase Inhibitors Using the Entire Ribonucleoprotein Complex. *Assay Drug Dev Technol*., 13 (8), 488-506 (**2015**).

366. Liu, T., Liu, M., Chen, F., Chen, F., Tian, Y., Huang, Q., Liu, S., Yang, J. A Small-Molecule Compound Has Anti-influenza A Virus Activity by Acting as a "PB2 Inhibitor". *Mol Pharm*., 15 (9), 4110-4120 (**2018**).

367. Massari, S., Goracci, L., Desantis, J., Tabarrini, O. Polymerase Acidic Protein-Basic Protein 1 (PA-PB1) Protein-Protein Interaction as a Target for Next-Generation Anti-influenza Therapeutics. *J Med Chem*., 59 (17), 7699-7718 (**2016**).

368. Ghanem, A., Mayer, D., Chase, G., Tegge, W., Frank, R., Kochs, G., García-Sastre, A., Schwemmle, M. Peptide-mediated interference with influenza A virus polymerase. *J Virol*., 81 (14), 7801-7804 (**2007**).

369. Wunderlich, K., Juozapaitis, M., Ranadheera, C., Kessler, U., Martin, A., Eisel, J., Beutling, U., Frank, R., Schwemmle, M. Identification of high-affinity PB1-derived peptides with enhanced affinity to the PA protein of influenza A virus polymerase. *Antimicrob Agents Chemother*., 55 (2), 696-702 (**2011**).

370. Wunderlich, K., Mayer, D., Ranadheera, C., Holler, A. S., Mänz, B., Martin, A., Chase, G., Tegge, W., Frank, R., Kessler, U., Schwemmle, M. Identification of a PA-binding

peptide with inhibitory activity against influenza A and B virus replication. *PLoS One*, 4 (10), e7517 (**2009**).

371. Muratore, G., Mercorelli, B., Goracci, L., Cruciani, G., Digard, P., Palù, G., Loregian, A. Human cytomegalovirus inhibitor AL18 also possesses activity against influenza A and B viruses. *Antimicrob Agents Chemother*., 56 (11), 6009-6013 (**2012**).
372. Fukuoka, M., Minakuchi, M., Kawaguchi, A., Nagata, K., Kamatari, Y. O., Kuwata, K. Structure-based discovery of anti-influenza virus A compounds among medicines. *Biochim Biophys Acta*, 1820 (2), 90-95 (**2012**).
373. Kessler, U., Castagnolo, D., Pagano, M., Deodato, D., Bernardini, M., Pilger, B., Ranadheera, C., Botta, M. Discovery and synthesis of novel benzofurazan derivatives as inhibitors of influenza A virus. *Bioorg Med Chem Lett*., 23 (20), 5575-5577 (**2013**).
374. Pagano, M., Castagnolo, D., Bernardini, M., Fallacara, A. L., Laurenzana, I., Deodato, D., Kessler, U., Pilger, B., Stergiou, L., Strunze, S., Tintori, C., Botta, M. The fight against the influenza A virus H1N1: synthesis, molecular modeling, and biological evaluation of benzofurazan derivatives as viral RNA polymerase inhibitors. *ChemMedChem*., 9 (1), 129-150 (**2014**).
375. Muratore, G., Goracci, L., Mercorelli, B., Foeglein, Á., Digard, P., Cruciani, G., Palù, G., Loregian, A. Small molecule inhibitors of influenza A and B viruses that act by disrupting subunit interactions of the viral polymerase. *Proc Natl Acad Sci U S A*., 109 (16), 6247-6252 (**2012**).
376. Lepri, S., Nannetti, G., Muratore, G., Cruciani, G., Ruzziconi, R., Mercorelli, B., Palù, G., Loregian, A., Goracci, L. Optimization of small-molecule inhibitors of influenza virus polymerase: from thiophene-3-carboxamide to polyamido scaffolds. *J Med Chem*., 57 (10), 4337-4350 (**2014**).
377. Massari, S., Nannetti, G., Goracci, L., Sancineto, L., Muratore, G., Sabatini, S., Manfroni, G., Mercorelli, B., Cecchetti, V., Facchini, M., Palù, G., Cruciani, G., Loregian, A,, Tabarrini, O. Structural investigation of cycloheptathiophene-3-carboxamide derivatives targeting influenza virus polymerase assembly. *J Med Chem*., 56 (24), 10118-10131 (**2013**).
378. Massari, S., Nannetti, G., Desantis, J., Muratore, G., Sabatini, S., Manfroni, G., Mercorelli, B., Cecchetti, V., Palù, G., Cruciani, G., Loregian, A., Goracci, L., Tabarrini, O. A Broad Anti-influenza Hybrid Small Molecule That Potently Disrupts the Interaction

of Polymerase Acidic Protein-Basic Protein 1 (PA-PB1) Subunits. *J Med Chem*., 58 (9), 3830-3842 (**2015**).

379. Yuan, S., Chu, H., Zhao, H., Zhang, K., Singh, K., Chow, B. K., Kao, R. Y., Zhou, J., Zheng, B. J. Identification of a small-molecule inhibitor of influenza virus via disrupting the subunits interaction of the viral polymerase. *Antiviral Res*., 125, 34-42 (**2016**).
380. Takizawa, N., Kimura, T., Watanabe, T., Shibasaki, M. Anti-influenza virus activity of a salcomine derivative mediated by inhibition of viral RNA synthesis. *Arch Virol*., 163 (6), 1607-1614 (**2018**).
381. Presber, H. W., Schroeder, C., Hegenscheid, B., Heider, H., Reefschläger, J., Rosenthal, H. A. Antiviral activity of Norakin (triperiden) and related anticholinergic antiparkinsonism drugs. *Acta Virol*., 28 (6), 501-507 (**1984**).
382. Heider, H., Markushin, S., Schroeder, C., Ghendon, Y. The influence of Norakin on the reproduction of influenza A and B viruses. *Arch Virol*., 86 (3-4), 283-290 (**1985**).
383. Ott, S., Wunderli-Allenspach, H. Effect of the virostatic Norakin (triperiden) on influenza virus activities. *Antiviral Res*., 24 (1), 37-42 (**1994**).
384. Chen, H. W., Cheng, J. X., Liu, M. T., King, K., Peng, J. Y., Zhang, X. Q., Wang, C. H., Shresta, S., Schooley, R. T., Liu, Y. T. Inhibitory and combinatorial effect of diphyllin, a v-ATPase blocker, on influenza viruses. *Antiviral Res*., 99 (3), 371-382 (**2013**).
385. Peterhans, E. Reactive oxygen species and nitric oxide in viral diseases. *Biol Trace Elem Res*., 56 (1), 107-116 (**1997**).
386. Beck, M. A., Handy, J., Levander, O. A. The role of oxidative stress in viral infections. *Ann N Y Acad Sci*., 917, 906-912 (**2000**).
387. Hennet, T., Peterhans, E., Stocker, R. Alterations in antioxidant defences in lung and liver of mice infected with influenza A virus. *J Gen Virol*., 73 (1), 39-46 (**1992**).
388. Mileva, M., Tancheva, L., Bakalova, R., Galabov, A., Savov, V., Ribarov, S.. Effect of vitamin E on lipid peroxidation and liver monooxigenase activity in experimental influenza virus infection. *Toxicol Lett*., 114 (1-3), 39-45 (**2000**).
389. Fraternale, A., Paoletti, M. F., Casabianca, A., Oiry, J., Clayette, P., Vogel, J. U., Cinatl, J. Jr, Palamara, A. T., Sgarbanti, R., Garaci, E., Millo, E., Benatti, U., Magnani, M. Antiviral and immunomodulatory properties of new pro-glutathione (GSH) molecules. *Curr Med Chem*., 13 (15), 1749-1755 (**2006**).

390. Cai, J., Chen, Y., Seth, S., Furukawa, S., Compans, R. W., Jones, D. P. Inhibition of influenza infection by glutathione. *Free Radic Biol Med*., 34 (7), 928-936 (**2003**).

391. Nencioni, L., Iuvara, A., Aquilano, K., Ciriolo, M. R., Cozzolino, F., Rotilio, G., Garaci, E., Palamara, A. T. Influenza A virus replication is dependent on an antioxidant pathway that involves GSH and Bcl-2. *FASEB J*., 17 (6), 758-760 (**2003**).

392. Liu, M., Chen, F., Liu, T., Chen, F., Liu, S., Yang, J. The role of oxidative stress in influenza virus infection. *Microbes Infect*., 19 (12), 580-586 (**2017**).

393. Zhang, X. H., Zhong, X., Zhou, Y. M., Du, H. M., Wang, T. Effect of RRR-alpha-tocopherol succinate on the growth and immunity in broilers. *Poult Sci*., 88 (5), 959-966 (**2009**).

394. Morel, S., Didierlaurent, A., Bourguignon, P., Delhaye, S., Baras, B., Jacob, V., Planty, C., Elouahabi, A., Harvengt, P., Carlsen, H., Kielland, A., Chomez, P., Garçon, N., Van Mechelen, M. Adjuvant System AS03 containing α-tocopherol modulates innate immune response and leads to improved adaptive immunity. *Vaccine*, 29 (13), 2461-2473 (**2011**).

395. Garçon, N., Vaughn, D. W., Didierlaurent, A. M. Development and evaluation of AS03, an Adjuvant System containing α-tocopherol and squalene in an oil-in-water emulsion. *Expert Rev Vaccines*, 11 (3), 349-366 (**2012**).

396. Galabov, A. S., Mileva, M., Simeonova, L., Gegova, G. Combination activity of neuraminidase inhibitor oseltamivir and α-tocopherol in influenza virus A (H3N2) infection in mice. *Antivir Chem Chemother*., 24 (3-4), 83-91 (**2015**).

397. Shoji, M., Arakaki, Y., Esumi, T., Kohnomi, S., Yamamoto, C., Suzuki, Y., Takahashi, E., Konishi, S., Kido, H., Kuzuhara, T. Bakuchiol Is a Phenolic Isoprenoid with Novel Enantiomer-selective Anti-influenza A Virus Activity Involving Nrf2 Activation. *J Biol Chem*., 290 (46), 28001-28017 (**2015**).

398. Michaelis, M., Sithisarn, P., Cinatl, J. Jr. Effects of flavonoid-induced oxidative stress on anti-H5N1 influenza a virus activity exerted by baicalein and biochanin A. *BMC Res Notes*, 7, 384 (**2014**).

399. Selemidis, S., Seow, H. J., Broughton, B. R., Vinh, A., Bozinovski, S., Sobey, C. G., Drummond, G. R., Vlahos, R. Nox1 oxidase suppresses influenza a virus-induced lung inflammation and oxidative stress. *PLoS One*, 8 (4), e60792 (**2013**).

400. Vlahos, R., Selemidis, S. NADPH oxidases as novel pharmacologic targets against influenza A virus infection. *Mol Pharmacol*., 86 (6), 747-759 (**2014**).

401. To, E. E., Vlahos, R., Luong, R., Halls, M. L., Reading, P. C., King, P. T., Chan, C., Drummond, G. R., Sobey, C. G., Broughton, B. R. S., Starkey, M. R., van der Sluis, R., Lewin, S. R., Bozinovski, S., O'Neill, L. A. J., Quach, T., Porter, C. J. H., Brooks, D. A., O'Leary, J. J., Selemidis, S. Endosomal NOX2 oxidase exacerbates virus pathogenicity and is a target for antiviral therapy. *Nat Commun*., 8 (1), 69 (**2017**).

402. Malakhov, M. P., Aschenbrenner, L. M., Smee, D. F., Wandersee, M. K., Sidwell, R. W., Gubareva, L. V., Mishin, V. P., Hayden, F. G., Kim, D. H., Ing, A., Campbell, E. R., Yu, M., Fang, F. Sialidase fusion protein as a novel broad-spectrum inhibitor of influenza virus infection. *Antimicrob Agents Chemother*., 50 (4), 1470-1479 (**2006**).

403. Moss, R. B., Hansen, C., Sanders, R. L., Hawley, S., Li, T., Steigbigel, R. T. A phase II study of DAS181, a novel host directed antiviral for the treatment of influenza infection. *J Infect Dis*., 206 (12), 1844-1851 (**2012**).

404. Zenilman, J. M., Fuchs, E. J., Hendrix, C. W., Radebaugh, C., Jurao, R., Nayak, S. U., Hamilton, R. G., McLeod Griffiss, J. Phase 1 clinical trials of DAS181, an inhaled sialidase, in healthy adults. *Antiviral Res*., 123, 114-119 (**2015**).

405. https://www.drugdevelopment-technology.com/projects/fludase/.

406. Zhirnov, O. P., Klenk, H. D., Wright, P. F. Aprotinin and similar protease inhibitors as drugs against influenza. *Antiviral Res*., 92 (1), 27-36 (**2011**).

407. Laporte, M., Naesens, L. Airway proteases: an emerging drug target for influenza and other respiratory virus infections. *Curr Opin Virol*., 24, 16-24 (**2017**).

408. Haasbach, E., Pauli, E. K., Spranger, R., Mitzner, D., Schubert, U., Kircheis, R., Planz, O. Antiviral activity of the proteasome inhibitor VL-01 against influenza A viruses. *Antiviral Res*., 91 (3), 304-313 (**2011**).

409. Planz, O. Development of cellular signaling pathway inhibitors as new antivirals against influenza. *Antiviral Res*., 98 (3), 457-468 (**2013**).

410. Gibson, S., Widmann, C., Johnson, G. L. Differential involvement of MEK kinase 1 (MEKK1) in the induction of apoptosis in response to microtubule-targeted drugs versus DNA damaging agents. *J Biol Chem*., 274 (16), 10916-10922 (**1999**).

411. Ludwig, S., Wolff, T., Ehrhardt, C., Wurzer, W. J., Reinhardt, J., Planz, O., Pleschka, S. MEK inhibition impairs influenza B virus propagation without emergence of resistant variants. *FEBS Lett*., 561 (1-3), 37-43 (**2004**).

412. Hsieh, H. P., Hsu, J. T. Strategies of development of antiviral agents directed against influenza virus replication. *Curr Pharm Des*., 13 (34), 3531-3542 (**2007**).

413. Haasbach, E., Müller, C., Ehrhardt, C., Schreiber, A., Pleschka, S., Ludwig, S., Planz, O. The MEK-inhibitor CI-1040 displays a broad anti-influenza virus activity in vitro and provides a prolonged treatment window compared to standard of care in vivo. *Antiviral Res*., 142, 178-184 (**2017**).

414. Pahl, H. L. Activators and target genes of Rel/NF-kappaB transcription factors. *Oncogene*, 18 (49), 6853-6866 (**1999**).

415. Kumar, N., Xin, Z. T., Liang, Y., Ly, H., Liang, Y. NF-kappaB signaling differentially regulates influenza virus RNA synthesis. *J Virol*., 82 (20), 9880-9889 (**2008**).

416. Leban, J., Baierl, M., Mies, J., Trentinaglia, V., Rath, S., Kronthaler, K., Wolf, K., Gotschlich, A., Seifert, M. H. A novel class of potent NF-kappaB signaling inhibitors. *Bioorg Med Chem Lett*., 17 (21), 5858-5862 (**2007**).

417. Mazur, I., Wurzer, W. J., Ehrhardt, C., Pleschka, S., Puthavathana, P., Silberzahn, T., Wolff, T., Planz, O., Ludwig, S. Acetylsalicylic acid (ASA) blocks influenza virus propagation via its NF-kappaB-inhibiting activity. *Cell Microbiol*., 9 (7), 1683-1694 (**2007**).

418. Droebner, K., Haasbach, E., Dudek, S. E., Scheuch, G., Nocker, K., Canisius, S., Ehrhardt, C., von Degenfeld, G., Ludwig, S., Planz, O. Pharmacodynamics, Pharmacokinetics, and Antiviral Activity of BAY 81-8781, a Novel NF-κB Inhibiting Anti-influenza Drug. *Front Microbiol*., 8, 2130 (**2017**).

419. Haasbach, E., Reiling, S. J., Ehrhardt, C., Droebner, K., Rückle, A., Hrincius, E. R., Leban, J., Strobl, S., Vitt, D., Ludwig, S., Planz, O. The NF-kappaB inhibitor SC75741 protects mice against highly pathogenic avian influenza A virus. *Antiviral Res*., 99 (3), 336-344 (**2013**).

420. Ehrhardt, C., Rückle, A., Hrincius, E. R., Haasbach, E., Anhlan, D., Ahmann, K., Banning, C., Reiling, S. J., Kühn, J., Strobl, S., Vitt, D., Leban, J., Planz, O., Ludwig, S. The NF-κB inhibitor SC75741 efficiently blocks influenza virus propagation and confers a high barrier for development of viral resistance. *Cell Microbiol*., 15 (7), 1198-1211 (**2013**).

421. Dudek, S. E., Luig, C., Pauli, E. K., Schubert, U., Ludwig, S. The clinically approved proteasome inhibitor PS-341 efficiently blocks influenza A virus and vesicular stomatitis virus propagation by establishing an antiviral state. *J Virol*., 84 (18), 9439-9451 (**2010**).

422. Song, J. H., Choi, H. J. Silymarin efficacy against influenza A virus replication. *Phytomedicine*, 18 (10), 832-835 (**2011**).

423. Dai, J. P., Wu, L. Q., Li, R., Zhao, X. F., Wan, Q. Y., Chen, X. X., Li, W. Z., Wang, G. F., Li, K. S. Identification of 23-(s)-2-amino-3-phenylpropanoyl-silybin as an antiviral agent for influenza A virus infection in vitro and in vivo. *Antimicrob Agents Chemother*., 57 (9), 4433-4443 (**2013**).

424. Liu, S., Wang, W., Jiang, L., Wan, S., Zhang, L., Yu, R., Jiang, T. 2-Pyridinyl-4(3H)-quinazolinone: a scaffold for anti-influenza A virus compounds. *Chem Biol Drug Des*., 86 (5), 1221-1125 (**2015**).

425. Ehrhardt, C., Marjuki, H., Wolff, T., Nürnberg, B., Planz, O., Pleschka, S., Ludwig, S. Bivalent role of the phosphatidylinositol-3-kinase (PI3K) during influenza virus infection and host cell defence. *Cell Microbiol*., 8 (8), 1336-1348 (**2006**).

426. Shin, Y. K., Liu, Q., Tikoo, S. K., Babiuk, L. A., Zhou, Y. Effect of the phosphatidylinositol 3-kinase/Akt pathway on influenza A virus propagation. *J Gen Virol*., 88 (3), 942-950 (**2007**).

427. Zhirnov, O. P., Klenk, H. D. Control of apoptosis in influenza virus-infected cells by up-regulation of Akt and p53 signaling. *Apoptosis*, 12 (8), 1419-1432 (**2007**).

428. Murray, J. L., McDonald, N. J., Sheng, J., Shaw, M. W., Hodge, T. W., Rubin, D. H., O'Brien, W. A., Smee, D. F. Inhibition of influenza A virus replication by antagonism of a PI3K-AKT-mTOR pathway member identified by gene-trap insertional mutagenesis. *Antivir Chem Chemother*., 22 (5), 205-215 (**2012**).

429. Alsuwaidi, A. R., George, J. A., Almarzooqi, S., Hartwig, S. M., Varga, S. M., Souid, A. K. Sirolimus alters lung pathology and viral load following influenza A virus infection. *Respir Res*., 18 (1), 136 (**2017**).

430. Huang, C. T., Hung, C. Y., Chen, T. C., Lin, C. Y., Lin, Y. C., Chang, C. S., He, Y. C., Huang, Y. L., Dutta, A. Rapamycin adjuvant and exacerbation of severe influenza in an experimental mouse model. *Sci Rep*., 7 (1), 4136 (**2017**).

431. Hoffmann, H. H., Palese, P., Shaw, M. L. Modulation of influenza virus replication by alteration of sodium ion transport and protein kinase C activity. *Antiviral Res*., 80 (2),124-134 (**2008**).

432. Gaelings, L., Söderholm, S., Bugai, A., Fu, Y., Nandania, J., Schepens, B., Lorey, M. B., Tynell, J., Vande Ginste, L., Le Goffic, R., Miller, M. S., Kuisma, M., Marjomäki, V., De

Brabander, J., Matikainen, S., Nyman, T. A., Bamford, D. H., Saelens, X., Julkunen, I., Paavilainen, H., Hukkanen, V., Velagapudi, V., Kainov, D. E.. Regulation of kynurenine biosynthesis during influenza virus infection. *FEBS J.*, 284 (2), 222-236 (**2017**).

433. Boergeling, Y., Ludwig, S. Targeting a metabolic pathway to fight the flu. *FEBS J.*, 284 (2), 218-221 (**2017**).
434. Haasbach, E., Hartmayer, C., Planz, O. Combination of MEK inhibitors and oseltamivir leads to synergistic antiviral effects after influenza A virus infection in vitro. Antiviral Res., 98 (2), 319-324 (**2013**).
435. Selvy, P. E., Lavieri, R. R., Lindsley, C. W., Brown, H. A. Phospholipase D: enzymology, functionality, and chemical modulation. *Chem Rev.*, 111 (10), 6064-6119 (**2011**).
436. Oguin, T. H. 3rd, Sharma, S., Stuart, A. D., Duan, S., Scott, S. A., Jones, C. K., Daniels, J. S., Lindsley, C. W., Thomas, P. G., Brown, H. A. Phospholipase D facilitates efficient entry of influenza virus, allowing escape from innate immune inhibition. *J Biol Chem.*, 289 (37), 25405-25417 (**2014**).
437. O'Reilly, M. C., Oguin, T. H. 3rd, Scott, S. A., Thomas, P. G., Locuson, C. W., Morrison, R. D., Daniels, J. S., Brown, H. A., Lindsley, C. W. Discovery of a highly selective PLD2 inhibitor (ML395): a new probe with improved physiochemical properties and broad-spectrum antiviral activity against influenza strains. *ChemMedChem.*, 9 (12), 2633-2637 (**2014**).
438. Boulo, S., Akarsu, H., Ruigrok, R. W., Baudin, F. Nuclear traffic of influenza virus proteins and ribonucleoprotein complexes. *Virus Res.*, 124 (1-2), 12-21 (**2007**).
439. Paterson, D., Fodor, E. Emerging roles for the influenza A virus nuclear export protein (NEP). *PLoS Pathog.*, 8 (12), e1003019 (**2012**).
440. Perwitasari, O., Johnson, S., Yan, X., Howerth, E., Shacham, S., Landesman, Y., Baloglu, E., McCauley, D., Tamir, S., Tompkins, S. M., Tripp, R. A. Verdinexor, a novel selective inhibitor of nuclear export, reduces influenza a virus replication in vitro and in vivo. *J Virol.*, 88 (17), 10228-10243 (**2014**).
441. Perwitasari, O., Johnson, S., Yan, X., Register, E., Crabtree, J., Gabbard, J., Howerth, E., Shacham, S., Carlson, R., Tamir, S., Tripp, R. A. Antiviral Efficacy of Verdinexor In Vivo in Two Animal Models of Influenza A Virus Infection. *PLoS One*, 11 (11), e0167221 (**2016**).

442. Khanna, M., Saxena, L., Rajput, R., Kumar, B., Prasad, R. Gene silencing: a therapeutic approach to combat influenza virus infections. *Future Microbiol*., 10 (1), 131-140 (**2015**).

443. Ge, Q., Filip, L., Bai, A., Nguyen, T., Eisen, H. N., Chen, J. Inhibition of influenza virus production in virus-infected mice by RNA interference. *Proc Natl Acad Sci U S A*., 101 (23), 8676-8681 (**2004**).

444. Seth, S., Templin, M. V., Severson, G., Baturevych, O. A potential therapeutic for pandemic influenza using RNA interference. *Methods Mol Biol*., 623, 397-422 (**2010**).

445. Betáková, T., Svančarová, P. Role and application of RNA interference in replication of influenza viruses. *Acta Virol*., 57 (2), 97-104 (**2013**).

446. Winterling, C., Koch, M., Koeppel, M., Garcia-Alcalde, F., Karlas, A., Meyer, T. F. Evidence for a crucial role of a host non-coding RNA in influenza A virus replication. *RNA Biol*., 11 (1), 66-75 (**2014**).

447. Ouyang, J., Zhu, X., Chen, Y., Wei, H., Chen, Q., Chi, X., Qi, B., Zhang, L., Zhao, Y., Gao, G. F., Wang, G., Chen, J. L. NRAV, a long noncoding RNA, modulates antiviral responses through suppression of interferon-stimulated gene transcription. *Cell Host Microbe*, 16 (5), 616-626 (**2014**).

448. Utsunomiya, T., Kobayashi, M., Pollard, R. B., Suzuki, F. Glycyrrhizin, an active component of licorice roots, reduces morbidity and mortality of mice infected with lethal doses of influenza virus. *Antimicrob Agents Chemother*., 41 (3), 551-556 (**1997**).

449. Fiore, C., Eisenhut, M., Krausse, R., Ragazzi, E., Pellati, D., Armanini, D., Bielenberg, J. Antiviral effects of Glycyrrhiza species. *Phytother Res*., 22 (2), 141-148 (**2008**).

450. Wolkerstorfer, A., Kurz, H., Bachhofner, N., Szolar, O. H.. Glycyrrhizin inhibits influenza A virus uptake into the cell. *Antiviral Res*., 83 (2), 171-178 (**2009**).

451. Michaelis, M., Geiler, J., Naczk, P., Sithisarn, P., Ogbomo, H., Altenbrandt, B., Leutz, A., Doerr, H. W., Cinatl, J. Jr. Glycyrrhizin inhibits highly pathogenic H5N1 influenza A virus-induced pro-inflammatory cytokine and chemokine expression in human macrophages. *Med Microbiol Immunol*., 199 (4), 291-297 (**2010**).

452. de Jong, M. D., Simmons, C. P., Thanh, T. T., Hien, V. M., Smith, G. J., Chau, T. N., Hoang, D. M., Chau, N. V., Khanh, T. H., Dong, V. C., Qui, P. T., Cam, B. V., Ha do, Q., Guan, Y., Peiris, J. S., Chinh, N. T., Hien, T. T., Farrar, J. Fatal outcome of human influenza A (H5N1) is associated with high viral load and hypercytokinemia. *Nat Med*., 12 (10), 1203-1207 (**2006**).

453. Carter, M. J. A rationale for using steroids in the treatment of severe cases of H5N1 avian influenza. *J Med Microbiol*., 56 (7), 875-883 (**2007**).

454. Zhou, J., Wang, D., Gao, R., Zhao, B., Song, J., Qi, X., Zhang, Y., Shi, Y., Yang, L., Zhu, W., Bai, T., Qin, K., Lan, Y., Zou, S., Guo, J., Dong, J., Dong, L., Zhang, Y., Wei, H., Li, X., Lu, J., Liu, L., Zhao, X., Li, X., Huang, W., Wen, L., Bo, H., Xin, L., Chen, Y., Xu, C., Pei, Y., Yang, Y., Zhang, X., Wang, S., Feng, Z., Han, J., Yang, W., Gao, G. F., Wu, G., Li, D., Wang, Y., Shu, Y. Biological features of novel avian influenza A (H7N9) virus. *Nature*, 499 (7459), 500-503 (**2013**).

455. Linko, R., Pettilä, V., Ruokonen, E., Varpula, T., Karlsson, S., Tenhunen, J., Reinikainen, M., Saarinen, K., Perttilä, J., Parviainen, I., Ala-Kokko, T., FINNH1N1-STUDY GROUP. Corticosteroid therapy in intensive care unit patients with PCR-confirmed influenza A(H1N1) infection in Finland. *Acta Anaesthesiol Scand*., 55 (8), 971-979 (**2011**).

456. Kudo, K., Takasaki, J., Manabe, T., Uryu, H., Yamada, R., Kuroda, E., Kobayashi, N., Matsushita, T. Systemic corticosteroids and early administration of antiviral agents for pneumonia with acute wheezing due to influenza A(H1N1)pdm09 in Japan. *PLoS One*, 7 (2), e32280 (**2012**).

457. Diaz, E., Martin-Loeches, I., Canadell, L., Vidaur, L., Suarez, D., Socias, L., Estella, A., Gil Rueda, B., Guerrero, J. E., Valverdú-Vidal, M., Vergara, J. C., López-Pueyo, M. J., Magret, M., Recio, T., López, D., Rello, J., Rodriguez, A, H1N1 SEMICYUC-CIBERES-REIPI Working Group (GETGAG). Corticosteroid therapy in patients with primary viral pneumonia due to pandemic (H1N1) 2009 influenza. *J Infect*., 64 (3), 311-318 (**2012**).

458. Brun-Buisson, C., Richard, J. C., Mercat, A., Thiébaut, A. C., Brochard, L., REVA-SRLF A/H1N1v 2009 Registry Group. Early corticosteroids in severe influenza A/H1N1 pneumonia and acute respiratory distress syndrome. *Am J Respir Crit Care Med*., 183 (9), 1200-1206 (**2011**).

459. Kim, S. H., Hong, S. B., Yun, S. C., Choi, W. I., Ahn, J. J., Lee, Y. J., Lee, H. B., Lim, C. M., Koh, Y., Korean Society of Critical Care Medicine H1N1 Collaborative. Corticosteroid treatment in critically ill patients with pandemic influenza A/H1N1 2009 infection: analytic strategy using propensity scores. *Am J Respir Crit Care Med*., 183 (9), 1207-1214 (**2011**).

460. Han, K., Ma, H., An, X., Su, Y., Chen, J., Lian, Z., Zhao, J., Zhu, B. P., Fontaine, R. E., Feng, Z., Zeng, G. Early use of glucocorticoids was a risk factor for critical disease and death from pH1N1 infection. *Clin Infect Dis*., 53 (4), 326-333 (**2011**).

461. Martín-Loeches, I., Bermejo-Martin, J. F., Vallés, J., Granada, R., Vidaur, L., Vergara-Serrano, J. C., Martín, M., Figueira, J. C., Sirvent, J. M., Blanquer, J., Suarez, D., Artigas, A., Torres, A., Diaz, E., Rodriguez, A., SEMICYUC/REIPI/CIBERES H1N1 Working Group. Macrolide-based regimens in absence of bacterial co-infection in critically ill H1N1 patients with primary viral pneumonia. *Intensive Care Med*., 39 (4), 693-702 (**2013**).

462. Lee, N., Leo, Y. S., Cao, B., Chan, P. K., Kyaw, W. M., Uyeki, T. M., Tam, W. W., Cheung, C. S., Yung, I. M., Li, H., Gu, L., Liu, Y., Liu, Z., Qu, J., Hui, D. S. Neuraminidase inhibitors, superinfection and corticosteroids affect survival of influenza patients. *Eur Respir J*., 45 (6), 1642-1652 (**2015**).

463. Hui, D. S., Lee, N., Chan, P. K., Beigel, J. H. The role of adjuvant immunomodulatory agents for treatment of severe influenza. *Antiviral Res*., 150, 202-216 (**2018**).

464. Weitz-Schmidt, G., Welzenbach, K., Brinkmann, V., Kamata, T., Kallen, J., Bruns, C., Cottens, S., Takada, Y., Hommel, U. Statins selectively inhibit leukocyte function antigen-1 by binding to a novel regulatory integrin site. *Nat Med*., 7 (6), 687-692 (**2001**).

465. Jain, M. K., Ridker, P. M. Anti-inflammatory effects of statins: clinical evidence and basic mechanisms. *Nat Rev Drug Discov*., 4 (12), 977-987 (**2005**).

466. Fedson, D. S. Confronting the next influenza pandemic with anti-inflammatory and immunomodulatory agents: why they are needed and how they might work. *Influenza Other Respir Viruses*, 3 (4), 129-142 (**2009**).

467. Yeganeh, B., Ghavami, S., Kroeker, A. L., Mahood, T. H., Stelmack, G. L., Klonisch, T., Coombs, K. M., Halayko, A. J. Suppression of influenza A virus replication in human lung epithelial cells by noncytotoxic concentrations bafilomycin A1. *Am J Physiol Lung Cell Mol Physiol*., 308 (3), 270-286 (**2015**).

468. Guinea, R., Carrasco, L. Concanamycin A blocks influenza virus entry into cells under acidic conditions. *FEBS Lett*., 349 (3), 327-330 (**1994**).

469. Calkin, A. C., Cooper, M. E., Jandeleit-Dahm, K. A., Allen, T. J. Gemfibrozil decreases atherosclerosis in experimental diabetes in association with a reduction in oxidative stress and inflammation. *Diabetologia*, 49 (4), 766-774 (**2006**).

470. Budd, A., Alleva, L., Alsharifi, M., Koskinen, A., Smythe, V., Müllbacher, A., Wood, J., Clark, I. Increased survival after gemfibrozil treatment of severe mouse influenza. *Antimicrob Agents Chemother*., 51 (8), 2965-2968 (**2007**).

471. Aldridge, J. R. Jr, Moseley, C. E., Boltz, D. A., Negovetich, N. J., Reynolds, C., Franks, J., Brown, S. A., Doherty, P. C., Webster, R. G., Thomas, P, G. TNF/iNOS-producing dendritic cells are the necessary evil of lethal influenza virus infection. *Proc Natl Acad Sci U S A.*, 106 (13), 5306-5311 (**2009**).

472. Bauer, C. M., Zavitz, C. C., Botelho, F. M., Lambert, K. N., Brown, E. G., Mossman, K. L., Taylor, J. D., Stämpfli, M. R. Treating viral exacerbations of chronic obstructive pulmonary disease: insights from a mouse model of cigarette smoke and H1N1 influenza infection. *PLoS One*, 5 (10), e13251 (**2010**).

473. Zheng, J., Wu, W. L., Liu, Y., Xiang, Z., Liu, M., Chan, K. H., Lau, S. Y., Lam, K. T., To, K. K., Chan, J. F., Li, L., Chen, H., Lau, Y. L., Yuen, K. Y., Tu, W. The Therapeutic Effect of Pamidronate on Lethal Avian Influenza A H7N9 Virus Infected Humanized Mice. *PLoS One*, 10 (8), e0135999 (**2015**).

474. Villarroel, M. C., Hidalgo, M., Jimeno, A. Mycophenolate mofetil: An update. *Drugs Today*, 45 (7), 521-532 (**2009**).

475. Volkmann, E. R., Tashkin, D. P., Li, N., Roth, M. D., Khanna, D., Hoffmann-Vold, A. M., Kim, G., Goldin, J., Clements, P. J., Furst, D. E., Elashoff, R. M. Mycophenolate Mofetil Versus Placebo for Systemic Sclerosis-Related Interstitial Lung Disease: An Analysis of Scleroderma Lung Studies I and II. *Arthritis Rheumatol*., 69 (7), 1451-1460 (**2017**).

476. To, K. K., Mok, K. Y., Chan, A. S., Cheung, N. N., Wang, P., Lui, Y. M., Chan, J. F., Chen, H., Chan, K. H., Kao, R. Y., Yuen, K. Y. Mycophenolic acid, an immunomodulator, has potent and broad-spectrum in vitro antiviral activity against pandemic, seasonal and avian influenza viruses affecting humans. *J Gen Virol*., 97 (8), 1807-1817 (**2016**).

477. Cho, J., Yi, H., Jang, E. Y., Lee, M. S., Lee, J. Y., Kang, C., Lee, C. H., Kim, K. Mycophenolic mofetil, an alternative antiviral and immunomodulator for the highly pathogenic avian influenza H5N1 virus infection. *Biochem Biophys Res Commun*., 494 (1-2), 298-304 (**2017**).

478. Hsu, A. C., Parsons, K., Barr, I., Lowther, S., Middleton, D., Hansbro, P. M., Wark, P. A. Critical role of constitutive type I interferon response in bronchial epithelial cell to influenza infection. *PLoS One*, 7 (3), e32947 (**2012**).

479. Durbin, R. K., Kotenko, S. V., Durbin, J. E. Interferon induction and function at the mucosal surface. *Immunol Rev*., 255 (1), 25-39 (**2013**).

480. Arimori, Y., Nakamura, R., Yamada, H., Shibata, K., Maeda, N., Kase, T., Yoshikai, Y. Type I interferon limits influenza virus-induced acute lung injury by regulation of excessive inflammation in mice. *Antiviral Res*., 99 (3), 230-237 (**2013**).

481. Haasbach, E., Droebner, K., Vogel, A. B., Planz, O. Low-dose interferon Type I treatment is effective against H5N1 and swine-origin H1N1 influenza A viruses in vitro and in vivo. *J Interferon Cytokine Res*., 31 (6), 515-525 (**2011**).

482. Ilyushina, N. A., Donnelly, R. P. In vitro anti-influenza A activity of interferon (IFN)-λ1 combined with IFN-β or oseltamivir carboxylate. *Antiviral Res*., 111, 112-120 (**2014**).

483. D'Agostino, I., Giacchello, I., Nannetti, G., Fallacara, A. L., Deodato, D., Musumeci, F., Grossi, G., Palù, G., Cau, Y., Trist, I. M., Loregian, A., Schenone, S., Botta, M. Synthesis and biological evaluation of a library of hybrid derivatives as inhibitors of influenza virus PA-PB1 interaction. *Eur J Med Chem*., 157, 743-758 (**2018**).

484. He, X., Zhou, J., Bartlam, M., Zhang, R., Ma, J., Lou, Z., Li, X., Li, J., Joachimiak, A., Zeng, Z., Ge, R., Rao, Z., Liu, Y. Crystal structure of the polymerase PA(C)-PB1(N) complex from an avian influenza H5N1 virus. *Nature*, 454 (7208), 1123-1126 (**2008**).

485. Obayashi, E., Yoshida, H., Kawai, F., Shibayama, N., Kawaguchi, A., Nagata, K., Tame, J. R., Park, S. Y. The structural basis for an essential subunit interaction in influenza virus RNA polymerase. *Nature*, 454 (7208), 1127-1131 (**2008**).

486. Moen, S. O., Abendroth, J., Fairman, J. W., Baydo, R. O., Bullen, J., Kirkwood, J. L., Barnes, S. R., Raymond, A. C., Begley, D. W., Henkel, G., McCormack, K., Tam, V. C., Phan, I., Staker, B. L., Stacy, R., Myler, P. J., Lorimer, D., Edwards, T. E. Structural analysis of H1N1 and H7N9 influenza A virus PA in the absence of PB1. *Sci Rep*., 4, 5944 (**2014**).

487. Liu, H., Yao, X. Molecular basis of the interaction for an essential subunit PA-PB1 in influenza virus RNA polymerase: insights from molecular dynamics simulation and free energy calculation. *Mol Pharm*., 7 (1), 75-85 (**2010**).

488. Verdonk, M. L., Cole, J. C., Hartshorn MJ, Murray CW, Taylor RD. Improved protein-ligand docking using GOLD. *Proteins*, 52 (4), 609-623 (**2003**).

489. Chase, G., Wunderlich, K., Reuther, P., Schwemmle, M. Identification of influenza virus inhibitors which disrupt of viral polymerase protein-protein interactions. *Methods*, 55 (2), 188-191 (**2011**).

490. Tintori, C., Laurenzana, I., Fallacara, A. L., Kessler, U., Pilger, B., Stergiou, L., Botta, M. High-throughput docking for the identification of new influenza A virus polymerase inhibitors targeting the PA-PB1 protein-protein interaction. *Bioorg Med Chem Lett*. 24 (1), 280-282 (**2014**).

491. Trist, I. M., Nannetti, G., Tintori, C., Fallacara, A. L., Deodato, D., Mercorelli, B., Palù, G., Wijtmans, M., Gospodova, T., Edink, E., Verheij, M., de Esch, I., Viteva, L., Loregian, A., Botta, M. 4,6-Diphenylpyridines as Promising Novel Anti-Influenza Agents Targeting the PA-PB1 Protein-Protein Interaction: Structure-Activity Relationships Exploration with the Aid of Molecular Modeling. *J Med Chem*., 59 (6), 2688-2703 (**2016**).

492. Yang, N. J., Hinner, M. J. Getting across the cell membrane: an overview for small molecules, peptides, and proteins. *Methods Mol Biol*., 1266, 29-53 (**2015**).

493. Beaumont, K., Webster, R., Gardner, I., Dack, K.. Design of ester prodrugs to enhance oral absorption of poorly permeable compounds: challenges to the discovery scientist. *Curr Drug Metab*., 4 (6), 461-485 (**2003**).

494. Montes-Avila, J., Díaz-Camacho, S. P., Sicairos-Félix, J., Delgado-Vargas, F., Rivero, I. A. Solution-phase parallel synthesis of substituted chalcones and their antiparasitary activity against Giardia lamblia. *Bioorg Med Chem*., 17 (18), 6780-6785 (**2009**).

495. Choudhary, A. N., Juyal, V. Synthesis of chalcone and their derivatives as antimicrobial agents. *Int. J. Pharm. Pharmaceut. Sci*., 3 (3), 125-128 (**2011**).

496. Hayat, F., Salahuddin, A., Umar, S., Azam, A. Synthesis, characterization, antiamoebic activity and cytotoxicity of novel series of pyrazoline derivatives bearing quinoline tail. *Eur J Med Chem*., 45 (10), 4669-4675 (**2010**).

497. Attia, A. M., Elgemeie, G. H. A new class of dihydropyridine thioglycosides via piperidinium salts. *Synth. Commun*., 33, 2243-2255 (**2003**).

498. Zhu, X. Q., Zhao, B. J., Cheng, J. P. Mechanisms of the oxidations of NAD(P)H model Hantzsch 1,4-dihydropyridines by nitric oxide and its donor N-methyl-N-nitrosotoluene-p-sulfonamide. *J Org Chem*., 65 (24), 8158-8163 (**2000**).

499. Windridge, G. C., Jorgensen, E. C. 1-Hydroxybenzotriazole as a racemization-suppressing reagent for the incorporation of im-benzyl-L-histidine into peptides. *J Am Chem Soc*., 93 (23), 6318-6319 (**1971**).

500. Sidwell, R. W., Huffman, J. H., Khare, G. P., Allen, L. B., Witkowski, J. T., Robins, R. K. Broad-spectrum antiviral activity of Virazole: 1-beta-D-ribofuranosyl-1,2,4-triazole-3-carboxamide. *Science*, 177 (4050), 705-706 (**1972**).

501. Jones, G., Willett, P., Glen, R. C., Leach, A. R., Taylor, R. Development and validation of a genetic algorithm for flexible docking. *J Mol Biol*., 267 (3), 727-748 (**1997**).

502. Cau, Y., Mori, M., Supuran, C. T., Botta, M. Mycobacterial carbonic anhydrase inhibition with phenolic acids and esters: kinetic and computational investigations. *Org Biomol Chem*., 14 (35), 8322-8330 (**2016**).

503. Cau, Y., Fiorillo, A., Mori, M., Ilari, A., Botta, M., Lalle, M. Molecular Dynamics Simulations and Structural Analysis of Giardia duodenalis 14-3-3 Protein-Protein Interactions. *J Chem Inf Model*., 55 (12), 2611-2622 (**2015**).

504. Schomaker, J. M., Delia, T. J. Arylation of halogenated pyrimidines via a Suzuki coupling reaction. *J Org Chem*., 66 (21), 7125-7128 (**2011**).

505. Peng, Z. H., Journet, M., Humphrey, G. A highly regioselective amination of 6-aryl-2,4-dichloropyrimidine. *Org Lett*., 8 (3), 395-398 (**2006**).

506. Jacobson, K. A., Gao, Z. G. Adenosine receptors as therapeutic targets. *Nat Rev Drug Discov*., 5 (3), 247-264 (**2006**).

507. Fredholm, B. B. Adenosine, an endogenous distress signal, modulates tissue damage and repair. *Cell Death Differ*., 14 (7), 1315-1323 (**2007**).

508. Ballarín, M., Fredholm, B. B., Ambrosio, S., Mahy, N. Extracellular levels of adenosine and its metabolites in the striatum of awake rats: inhibition of uptake and metabolism. *Acta Physiol Scand*., 142 (1), 97-103 (**1991**).

509. King, A. E., Ackley, M. A., Cass, C. E., Young, J. D., Baldwin, S. A. Nucleoside transporters: from scavengers to novel therapeutic targets. *Trends Pharmacol Sci*., 27 (8), 416-425 (**2006**).

510. MacDonald, P. E., Braun, M., Galvanovskis, J., Rorsman, P. Release of small transmitters through kiss-and-run fusion pores in rat pancreatic beta cells. *Cell Metab*., 4 (4), 283-290 (**2006**).

511. Zhang, Z., Chen, G., Zhou, W., Song, A., Xu, T., Luo, Q., Wang, W., Gu, X. S., Duan, S. Regulated ATP release from astrocytes through lysosome exocytosis. *Nat Cell Biol*., 9 (8), 945-953 (**2007**).

512. Chen, J. F., Eltzschig, H. K., Fredholm, B. B. Adenosine receptors as drug targets--what are the challenges? *Nat Rev Drug Discov*., 12 (4), 265-286 (**2013**).

513. Enjyoji, K., Sévigny, J., Lin, Y., Frenette, P. S., Christie, P. D., Esch, J. S. 2nd, Imai, M., Edelberg, J. M., Rayburn, H., Lech, M., Beeler, D. L., Csizmadia, E., Wagner, D. D., Robson, S. C., Rosenberg, R. D. Targeted disruption of cd39/ATP diphosphohydrolase results indisordered hemostasis and thromboregulation. *Nat Med*., 5 (9), 1010-1017 (**1999**).

514. Sun, D., Samuelson, L. C., Yang, T., Huang, Y., Paliege, A., Saunders, T., Briggs, J., Schnermann, J. Mediation of tubuloglomerular feedback by adenosine: evidence from mice lacking adenosine 1 receptors. *Proc Natl Acad Sci U S A*., 98 (17), 9983-9988 (**2001**).

515. Eltzschig, H. K., Ibla, J. C., Furuta, G. T., Leonard, M. O., Jacobson, K. A., Enjyoji, K., Robson, S. C., Colgan, S. P. Coordinated adenine nucleotide phosphohydrolysis and nucleoside signaling in posthypoxic endothelium: role of ectonucleotidases and adenosine A2B receptors. *J Exp Med*., 198 (5), 783-796 (**2003**).

516. Thompson, L. F., Eltzschig, H. K., Ibla, J. C., Van De Wiele, C. J., Resta, R., Morote-Garcia, J. C., Colgan, S. P. Crucial role for ecto-5'-nucleotidase (CD73) in vascular leakage during hypoxia. *J Exp Med*., 200 (11), 1395-1405 (**2004**).

517. Fedele, D. E., Li, T., Lan, J. Q., Fredholm, B. B., Boison, D.. Adenosine A1 receptors are crucial in keeping an epileptic focus localized. *Exp Neurol*., 200 (1), 184-190 (**2006**).

518. Schenone, S., Brullo, C., Musumeci, F., Bruno, O., Botta, M. A1 receptors ligands: past, present and future trends. *Curr Top Med Chem*., 10 (9), 878-901 (**2010**).

519. Fredholm, B. B., Arslan, G., Halldner, L., Kull, B., Schulte, G., Wasserman, W. Structure and function of adenosine receptors and their genes. *Naunyn Schmiedebergs Arch Pharmacol*., 362 (4-5), 364-374 (**2000**).

520. Vannucci, S. J., Klim, C. M., Martin, L. F., LaNoue, K. F. A1-adenosine receptor-mediated inhibition of adipocyte adenylate cyclase and lipolysis in Zucker rats. *Am J Physiol*., 257 (6), 871-888 (**1989**).

521. Vallon, V., Mühlbauer, B., Osswald, H. Adenosine and kidney function. *Physiol Rev*., 86 (3), 901-940 (**2006**).

522. Boison D. Adenosine as a neuromodulator in neurological diseases. *Curr Opin Pharmacol*., 8 (1), 2-7 (**2008**).

523. Ponnoth, D. S., Nadeem, A., Tilley, S., Mustafa, S. J. Involvement of A1 adenosine receptors in altered vascular responses and inflammation in an allergic mouse model of asthma. *Am J Physiol Heart Circ Physiol*., 299 (1), 81-87 (**2010**).

524. Camaioni, E., Costanzi, S., Vittori, S., Volpini, R., Klotz, K. N., Cristalli, G. New substituted 9-alkylpurines as adenosine receptor ligands. *Bioorg Med Chem*., 6 (5), 523-533 (**1998**).

525. Lohse, M. J., Klotz, K. N., Lindenborn-Fotinos, J., Reddington, M., Schwabe, U., Olsson, R. A. 8-Cyclopentyl-1,3-dipropylxanthine (DPCPX) a selective high affinity antagonist radioligand for A1 adenosine receptors. *Naunyn Schmiedebergs Arch Pharmacol*., 336 (2), 204-210 (**1987**).

526. Holschbach, M. H., Olsson, R. A., Bier, D., Wutz, W., Sihver, W., Schüller, M., Palm, B., Coenen, H. H. Synthesis and evaluation of no-carrier-added 8-cyclopentyl-3-(3-[(18)F]fluoropropyl)-1-propylxanthine ([(18)F]CPFPX): a potent and selective A(1)-adenosine receptor antagonist for in vivo imaging. *J Med Chem*., 45 (23), 5150-5156 (**2002**).

527. Ilas, J., Pecar, S., Hockemeyer, J., Euler, H., Kirfel, A., Müller, C. E. Development of spin-labeled probes for adenosine receptors. *J Med Chem*., 48 (6), 2108-2114 (**2005**).

528. Gottlieb, S. S., Brater, D. C., Thomas, I., Havranek, E., Bourge, R., Goldman, S., Dyer, F., Gomez, M., Bennett, D., Ticho, B., Beckman, E., Abraham, W. T. BG9719 (CVT-124), an A1 adenosine receptor antagonist, protects against the decline in renal function observed with diuretic therapy. *Circulation*, 105 (11), 1348-1353 (**2002**).

529. Kiesman, W. F., Zhao, J., Conlon, P. R., Petter, R. C., Jin, X., Smits, G., Lutterodt, F., Sullivan, G. W., Linden, J. Norbornyllactone-substituted xanthines as adenosine A(1) receptor antagonists. *Bioorg Med Chem*., 14 (11), 3654-3661 (**2006**).

530. Slawsky, M. T., Givertz, M. M. Rolofylline: a selective adenosine 1 receptor antagonist for the treatment of heart failure. *Expert Opin Pharmacother*., 10 (2), 311-322 (**2009**).

531. Voors, A. A., Dittrich, H. C., Massie, B. M., DeLucca, P., Mansoor, G. A., Metra, M., Cotter, G., Weatherley, B. D., Ponikowski, P., Teerlink, J. R., Cleland, J. G., O'Connor, C. M., Givertz, M. M. Effects of the adenosine A1 receptor antagonist rolofylline on renal function in patients with acute heart failure and renal dysfunction: results from PROTECT

(Placebo-Controlled Randomized Study of the Selective Adenosine A1 Receptor Antagonist Rolofylline for Patients Hospitalized with Acute Decompensated Heart Failure and Volume Overload to Assess Treatment Effect on Congestion and Renal Function). *J Am Coll Cardiol*., 57 (19), 1899-1907 (**2011**).

532. Weyler, S., Fülle, F., Diekmann, M., Schumacher, B., Hinz, S., Klotz, K. N., Müller, C. E. Improving potency, selectivity, and water solubility of adenosine A1 receptor antagonists: xanthines modified at position 3 and related pyrimido[1,2,3-cd]purinediones. *ChemMedChem*., 1 (8), 891-902 (**2006**).
533. Kiesman, W. F., Zhao, J., Conlon, P. R., Dowling, J. E., Petter, R. C., Lutterodt, F., Jin, X., Smits, G., Fure, M., Jayaraj, A., Kim, J., Sullivan, G., Linden, J. Potent and orally bioavailable 8-bicyclo[2.2.2]octylxanthines as adenosine A1 receptor antagonists. *J Med Chem*., 49 (24), 7119-7131 (**2006**).
534. Marti, C., Cole, R., Kalogeropoulos, A,, Georgiopoulou, V., Butler, J. Medical therapy for acute decompensated heart failure: what recent clinical trials have taught us about diuretics and vasodilators. *Curr Heart Fail Rep*., 9 (1), 1-7 (**2012**).
535. Drabczyńska, A., Müller, C. E., Karolak-Wojciechowska, J., Schumacher, B., Schiedel, A., Yuzlenko, O., Kieć-Kononowicz, K. N9-benzyl-substituted 1,3-dimethyl- and 1,3-dipropyl-pyrimido[2,1-f]purinediones: synthesis and structure-activity relationships at adenosine A1 and A2A receptors. *Bioorg Med Chem*., 15 (14), 5003-5017 (**2007**).
536. Novellino, E., Abignente, E., Cosimelli, B., Greco, G., Iadanza, M., Laneri, S., Lavecchia, A., Rimoli, M. G., Settimo, F. D., Primofiore, G., Tuscano, D., Trincavelli, L., Martini, C. Design, synthesis and biological evaluation of novel N-alkyl- and N-acyl-(7-substituted-2-phenylimidazo[1,2-a][1,3,5]triazin-4-yl)amines (ITAs) as novel A(1) adenosine receptor antagonists. *J Med Chem*., 45 (23), 5030-5036 (**2002**).
537. Biagi, G., Giorgi, I., Leonardi, M., Livi, O., Pacchini, F., Scartoni, V., Costa, B., Lucacchini, A. New N6- or N(9)-hydroxyalkyl substituted 8-azaadenines or adenines as effective A1 adenosine receptor ligands. *Eur J Med Chem*., 38 (9), 801-810 (**2003**).
538. Chang, L. C., Spanjersberg, R. F., von Frijtag Drabbe Künzel, J. K., Mulder-Krieger, T., Brussee, J., Ijzerman, A. P. 2,6-disubstituted and 2,6,8-trisubstituted purines as adenosine receptor antagonists. *J Med Chem*., 49 (10), 2861-2867 (**2006**).

539. Chang, L. C., von Frijtag Drabbe Künzel, J. K., Mulder-Krieger, T., Westerhout, J., Spangenberg, T., Brussee, J., Ijzerman, A. P. 2,6,8-trisubstituted 1-deazapurines as adenosine receptor antagonists. *J Med Chem.*, 50 (4), 828-834 (**2007**).

540. http://clinicaltrials.gov/ct2/show/NCT00160134.

541. http://clinicaltrials.gov/ct2/show/NCT00744341.

542. Maemoto, T., Tada, M., Mihara, T., Ueyama, N., Matsuoka, H., Harada, K., Yamaji, T., Shirakawa, K., Kuroda, S., Akahane, A., Iwashita, A., Matsuoka, N., Mutoh, S. Pharmacological characterization of FR194921, a new potent, selective, and orally active antagonist for central adenosine A1 receptors. *J Pharmacol Sci.*, 96 (1), 42-52 (**2004**).

543. Matsuya, T., Takamatsu, H., Murakami, Y., Noda, A., Ichise, R., Awaga, Y., Nishimura, S. Synthesis and evaluation of [11C]FR194921 as a nonxanthine-type PET tracer for adenosine A1 receptors in the brain. *Nucl Med Biol.*, 32 (8), 837-844 (**2005**).

544. Ferguson, G. N., Valant, C., Horne, J., Figler, H., Flynn, B. L., Linden, J., Chalmers, D. K., Sexton, P. M., Christopoulos, A., Scammells, P. J. 2-aminothienopyridazines as novel adenosine A1 receptor allosteric modulators and antagonists. *J Med Chem.*, 51 (19), 6165-6172 (**2008**).

545. Müller, C. E., Grahner, B., Heber, D. Amino-substituted 1,8-naphthyridines and pyrido[2,3-d]pyrimidines: new compounds with affinity for A1- and A2-adenosine receptors. *Pharmazie*, 49 (12), 878-880 (**1994**).

546. Ferrarini, P. L., Mori, C., Manera, C., Martinelli, A., Mori, F., Saccomanni, G., Barili, P. L., Betti, L., Giannaccini, G., Trincavelli, L., Lucacchini, A. A novel class of highly potent and selective A1 adenosine antagonists: structure-affinity profile of a series of 1,8-naphthyridine derivatives. *J Med Chem.*, 43 (15), 2814-2823 (**2000**).

547. Ferrarini, P. L., Betti, L., Cavallini, T., Giannaccini, G., Lucacchini, A., Manera, C., Martinelli, A., Ortore, G., Saccomanni, G., Tuccinardi, T. Study on affinity profile toward native human and bovine adenosine receptors of a series of 1,8-naphthyridine derivatives. *J Med Chem.*, 47 (12), 3019-3031 (**2004**).

548. Hess, S., Müller, C. E., Frobenius, W., Reith, U., Klotz, K. N., Eger, K. 7-Deazaadenines bearing polar substituents: structure-activity relationships of new A(1) and A(3) adenosine receptor antagonists. *J Med Chem.*, 43 (24), 4636-4646 (**2000**).

549. Da Settimo, F., Primofiore, G., Taliani, S., Marini, A. M., La Motta, C., Novellino, E., Greco, G., Lavecchia, A., Trincavelli, L., Martini, C. 3-Aryl[1,2,4]triazino[4,3-

a]benzimidazol-4(10H)-ones: a new class of selective A1 adenosine receptor antagonists. *J Med Chem*., 44 (3), 316-327 (**2001**).

550. Colotta, V., Catarzi, D., Varano, F., Filacchioni, G., Martini, C., Trincavelli, L., Lucacchini, A., Colotta, V. Synthesis and structure-activity relationships of 4-cycloalkylamino-1, 2, 4-triazolo[4, 3-a]quinoxalin-1- one derivatives as A1 and A3 adenosine receptor antagonists. *Arch Pharm (Weinheim)*, 337 (1), 35-41 (**2004**).
551. Vu, C. B., Kiesman, W. F., Conlon, P. R., Lin, K. C., Tam, M., Petter, R. C., Smits, G., Lutterodt, F., Jin, X., Chen, L., Zhang, J. Tricyclic imidazoline derivatives as potent and selective adenosine A1 receptor antagonists. *J Med Chem*., 49 (24), 7132-7139 (**2006**).
552. Shook, B. C., Rassnick, S., Hall, D., Rupert, K. C., Heintzelman, G. R., Hansen, K., Chakravarty, D., Bullington, J. L., Scannevin, R. H., Magliaro, B., Westover, L., Carroll, K., Lampron, L., Russell, R., Branum, S., Wells, K., Damon, S., Youells, S., Li, X., Osbourne, M., Demarest, K., Tang, Y., Rhodes, K., Jackson, P. F. Methylene amine substituted arylindenopyrimidines as potent adenosine A(2A)/A(1) antagonists. *Bioorg Med Chem Lett*., 20 (9), 2864-2867 (**2010**).
553. Shook, B. C., Rassnick, S., Chakravarty, D., Wallace, N., Ault, M., Crooke, J., Barbay, J. K., Wang, A., Leonard, K., Powell, M. T., Alford, V., Hall, D., Rupert, K. C., Heintzelman, G. R., Hansen, K., Bullington, J. L., Scannevin, R. H., Carroll, K., Lampron, L., Westover, L., Russell, R., Branum, S., Wells, K., Damon, S., Youells, S., Beauchamp, D., Li, X., Rhodes, K., Jackson, P. F. Optimization of arylindenopyrimidines as potent adenosine A(2A)/A(1) antagonists. *Bioorg Med Chem Lett*., 20 (9), 2868-2871 (**2010**).
554. Jackson, P. Shook, B. Arylindenopyrimidines with reduces hERG channel binding. *US20113112956* (**2011**).
555. Jackson, P. Shook, B. Arylindenopyrimidines for treating neurodegenerative and movement disorders while minimizing cardiac toxicity. *WO2011159302* (**2011**).
556. van Muijlwijk-Koezen, J. E., Timmerman, H., Vollinga, R. C., Frijtag von Drabbe Künzel, J., de Groote, M., Visser, S., IJzerman, A. P. Thiazole and thiadiazole analogues as a novel class of adenosine receptor antagonists. *J Med Chem*., 44 (5), 749-762 (**2001**).
557. van Tilburg, E. W., van der Klein, P. A., de Groote, M., Beukers, M. W., IJzerman, A. P. Substituted 4-phenyl-2-(phenylcarboxamido)-1,3-thiazole derivatives as antagonists for the adenosine A(1) receptor. *Bioorg Med Chem Lett*., 11 (15), 2017-2019 (**2001**).

558. Gonzales, L. L., Camacho-Gomez, J. A. New compounds as adenosine A1 receptor antagonists. *WO2009044250* (**2009**).

559. Chang, L. C., Spanjersberg, R. F., von Frijtag Drabbe Künzel, J. K., Mulder-Krieger, T., van den Hout, G., Beukers, M. W., Brussee, J., Ijzerman, A. P. 2,4,6-trisubstituted pyrimidines as a new class of selective adenosine A1 receptor antagonists. *J Med Chem*., 47 (26), 6529-6540 (**2004**).

560. Schenone, S., Bruno, O., Fossa, P., Ranise, A., Menozzi, G., Mosti, L., Bondavalli, F., Martini, C., Trincavelli, L. Synthesis and biological data of 4-amino-1-(2-chloro-2-phenylethyl)-1H-pyrazolo[3,4-b]pyridine-5-carboxylic acid ethyl esters, a new series of A1-adenosine receptor (A1AR) ligands. *Bioorg Med Chem Lett*., 11 (18), 2529-2531 (**2001**).

561. Bondavalli, F., Botta, M., Bruno, O., Ciacci, A., Corelli, F., Fossa, P., Lucacchini, A., Manetti, F., Martini, C., Menozzi, G., Mosti, L., Ranise, A., Schenone, S., Tafi, A., Trincavelli, M. L. Synthesis, molecular modeling studies, and pharmacological activity of selective A(1) receptor antagonists. *J Med Chem*., 45 (22), 4875-4887 (**2002**).

562. Manetti, F., Schenone, S., Bondavalli, F., Brullo, C., Bruno, O., Ranise, A., Mosti, L., Menozzi, G., Fossa, P., Trincavelli, M. L., Martini, C., Martinelli, A., Tintori, C., Botta, M. Synthesis and 3D QSAR of new pyrazolo[3,4-b]pyridines: potent and selective inhibitors of A1 adenosine receptors. *J Med Chem*., 48 (23), 7172-7185 (**2005**).

563. Tuccinardi, T., Schenone, S., Bondavalli, F., Brullo, C., Bruno, O., Mosti, L., Zizzari, A. T., Tintori, C., Manetti, F., Ciampi, O., Trincavelli, M. L., Martini, C., Martinelli, A., Botta, M. Substituted pyrazolo[3,4-b]pyridines as potent A1 adenosine antagonists: synthesis, biological evaluation, and development of an A1 bovine receptor model. *ChemMedChem*., 3 (6), 898-913 (**2008**).

564. Okada, T., Fujiyoshi, Y., Silow, M., Navarro, J., Landau, E. M., Shichida, Y. Functional role of internal water molecules in rhodopsin revealed by X-ray crystallography. *Proc Natl Acad Sci U S A*., 99 (9), 5982-5987 (**2002**).

565. Martinelli, A., Tuccinardi, T. An overview of recent developments in GPCR modelling: methods and validation. *Expert Opin Drug Discov*., 1 (5), 459-476 (**2006**).

566. Fiser, A., Do, R. K., Sali, A. Modeling of loops in protein structures. *Protein Sci*., 9 (9), 1753-1773 (**2000**).

567. Martinelli, A., Tuccinardi, T. Molecular modeling of adenosine receptors: new results and trends. *Med Res Rev*., 28 (2), 247-277 (**2008**).

568. Gever G. Hydrazinoalkanols. *J. Am. Chem. Soc.*, 76, 1283-1285 (**1954**).

569. Cheng, Y., Prusoff, W. H. Relationship between the inhibition constant (K1) and the concentration of inhibitor which causes 50 per cent inhibition (I50) of an enzymatic reaction. *Biochem Pharmacol*., 22 (23), 3099-3108 (**1973**).

570. Holstein, P. M., Vogler, M., Larini, P., Pillet, G., Clot, E., Baudoin, O. Efficient Pd^0-Catalyzed Asymmetric Activation of Primary and Secondary C−H B onds Enabled by Modular Binepine Ligands and Carbonate Bases. *ACS Catal*., 5, 4300-4308 (**2015**).

571. Nakanishi, M., Katayev, D., Besnard, C., Kündig, E. P. Fused indolines by palladium-catalyzed asymmetric C-C coupling involving an unactivated methylene group. *Angew Chem Int Ed Engl*., 50 (32), 7438-7441 (**2011**).

572. Anas, S., Cordi, A., Kagan, H. B. Enantioselective synthesis of 2-methyl indolines by palladium catalysed asymmetric C(sp3)-H activation/cyclisation. *Chem Commun (Camb)*., 47 (41), 11483-11485 (**2011**).

573. Saget, T., Lemouzy, S. J., Cramer, N. Chiral monodentate phosphines and bulky carboxylic acids: cooperative effects in palladium-catalyzed enantioselective C(sp3)-H functionalization. *Angew Chem Int Ed Engl*., 51 (9), 2238-2242 (**2012**).

574. Saget, T., Cramer, N. Palladium(0)-catalyzed enantioselective C-H arylation of cyclopropanes: efficient access to functionalized tetrahydroquinolines. *Angew Chem Int Ed Engl*., 51 (51), 12842-12845 (**2012**).

575. Martin, N., Pierre, C., Davi, M., Jazzar, R., Baudoin, O. Diastereo- and enantioselective intramolecular C(sp3)-H arylation for the synthesis of fused cyclopentanes. *Chemistry*, 18 (15), 4480-4484 (**2012**).

576. Albicker, M. R., Cramer, N. Enantioselective palladium-catalyzed direct arylations at ambient temperature: access to indanes with quaternary stereocenters. *Angew Chem Int Ed Engl*., 48 (48), 9139-9142 (**2009**).

577. Liu, L., Zhang, A. A., Wang, Y., Zhang, F., Zuo, Z., Zhao, W. X., Feng, C. L., Ma, W. Asymmetric Synthesis of P-Stereogenic Phosphinic Amides via Pd(0)-Catalyzed Enantioselective Intramolecular C-H Arylation. *Org Lett*., 17 (9), 2046-2049 (**2015**).

578. Lin, Z. Q., Wang, W. Z., Yan, S. B., Duan, W. L. Palladium-catalyzed enantioselective C-H arylation for the synthesis of P-stereogenic compounds. *Angew Chem Int Ed Engl*., 54 (21), 6265-6269 (**2015**).

579. He, C., Hou, M., Zhu, Z., Gu, Z. Enantioselective Synthesis of Indole-Based Biaryl Atropisomers via Palladium-Catalyzed Dynamic Kinetic Intramolecular C−H Cyclization. *ACS Catal.*, 7, 5316-5320 (**2017**).

580. Grosheva, D., Cramer, N. Ketene Aminal Phosphates: Competent Substrates for Enantioselective Pd(0)-Catalyzed C-H Functionalizations. *ACS Catal*., 7 (11), 7417-7420 (**2017**).

581. Grosheva, D., Cramer, N. Enantioselective Access to 1H-Isoindoles with Quaternary Stereogenic Centers by Palladium(0)-Catalyzed C-H Functionalization. *Angew Chem Int Ed Engl*., 57 (41), 13644-13647 (**2018**).

582. Rousseaux, S., Davi, M., Sofack-Kreutzer, J., Pierre, C., Kefalidis, C. E., Clot, E., Fagnou, K., Baudoin, O. Intramolecular palladium-catalyzed alkane C-H arylation from aryl chlorides. *J Am Chem Soc*., 132 (31), 10706-10716 (**2010**).

583. Yang, L., Neuburger, M., Baudoin, O. Chiral Bifunctional Phosphine-Carboxylate Ligands for Palladium(0)-Catalyzed Enantioselective C-H Arylation. *Angew Chem Int Ed Engl*., 57 (5), 1394-1398 (**2018**).

584. Mack, J., Vogel, P., Jones, D., Kaval, N., Sutton, A. The development of corannulene-based blue emitters. *Org Biomol Chem*., 5 (15), 2448-2452 (**2007**).

585. Xiao, W., Passerone, D., Ruffieux, P., Aït-Mansour, K., Gröning, O., Tosatti, E., Siegel, J. S., Fasel, R. C60/corannulene on Cu(110): a surface-supported bistablebuckybowl-buckyball host-guest system. *J Am Chem Soc*., 130 (14), 4767-4771 (**2008**).

586. Uozumi, Y., Kawatsura, M., Hayashi, T. (R)-2-Diphenylphosphino-2′-Methoxy-1,1′-Binaphthyl. *Organic Synthesis*, 78, 1 (**2002**).

587. Stokker, G. E., Alberts, A. W., Gilfillan, J. L., Huff, J. W., Smith, R. L. 3-Hydroxy-3-methylglutaryl-coenzyme A reductase inhibitors. 5. 6-(Fluoren-9-yl)- and 6-(fluoren-9-ylidenyl)-3,5-dihydroxyhexanoic acids and their lactone derivatives. *J Med Chem*., 29 (5), 852-855 (**1986**).

588. Tze-Lock, C., Mak, t. C. W., Poon, C. D., Wong, H. N. C., Jia, J. H., Wang, L. L. A stable derivative of cyclooctatrienyne: Synthesis and crystal structures of 1,4,7,10-

tetramethyl-5,6-didehydrodibenzo[*a,e*]cyclooctene and 1,4,7,10-tetramethyldibenzo[*a,e*] cyclooctene. *Tetrahedron*, 42 (2) 655-661 (**1986**).

589. Pakusch, J., Rüchardt, C. A Sterically Hindered Bridgehead System: 13-Substituted 1,4,5,8,9,12-Hexamethyltriptycenes. *Chemische Berichte*, 123 (11), 2147-2151 (**1990**).
590. Caspar, M. L., Stothers, J. B., Wilson, N. K. ^{13}C-Nuclear Magnetic Resonance Studies of Methylated Anthracenes. *Can. J. Chem*., 53, 1958-1969 (**1975**).
591. Seidel, J. L., Epstein, W. W., Davidson, D. W. Neotropical ant gardens: I. Chemical constituents. *J Chem Ecol*., 16 (6), 1791-1816 (**1990**).
592. Rewcastle, G. W., Atwell, G. J., Baguley, B. C., Calveley, S. B., Denny, W. A. Potential antitumor agents. 58. Synthesis and structure-activity relationships of substituted xanthenone-4-acetic acids active against the colon 38 tumor in vivo. *J Med Chem*., 32 (4), 793-799 (**1789**).
593. Chakraborti, A. K., Chankeshwara, S. V. Counterattack mode differential acetylative deprotection of phenylmethyl ethers: applications to solid phase organic reactions. *J Org Chem*., 74 (3), 1367-1370 (**2009**).
594. Ojida, A., Nonaka, H., Miyahara, Y., Tamaru, S., Sada, K., Hamachi, I. Bis(Dpa-Zn(II)) appended xanthone: excitation ratiometric chemosensor for phosphate anions. *Angew Chem Int Ed Engl*., 45 (33), 5518-5521 (**2006**).